THE UNIVERSITY
of EDINBURGH

Investigating the Synthesis of Ettringite and Monosulfate Analogue Phases and Their Use as Waste Remediation Materials

Rebecca Rae

THE UNIVERSITY *of* EDINBURGH

A thesis submitted for the degree of Doctor of Philosophy

The University of Edinburgh

2021

DECLARATION

I declare that this thesis is an original report of my research, has been written by me and has not been submitted for any previous degree. The experimental work is almost entirely my own work; the collaborative contributions have been indicated clearly and acknowledged. Due references have been provided on all supporting literatures and resources.

I declare that this thesis was composed by myself, that the work contained herein is my own except where explicitly stated otherwise in the text, and that this work has not been submitted for any other degree or professional qualification.

Rebecca Rae

April 2021

ABSTRACT

Pollution from industrial sources into freshwater supplies is a growing global problem with 80 % of all wastewater produced being released into the environment with no treatment. This poses a risk to both human and animal health, as well as affecting the environment and economy. This research will focus on non-organic pollutants, which cannot simply be destroyed and are not biodegradable. The main way these types of wastes are dealt with are by stabilisation and solidification processes where the contaminants are either converted to non-hazardous forms or encapsulated in solid materials to reduce their mobility.

The work presented in this thesis will focus on using the mineral ettringite ($Ca_6[Al(OH)_6]_2(SO_4)_3.26H_2O$) to solidify hazardous waste ions. Ettringite is an important hydration product of Portland cement and also occurs naturally, first being discovered in 1874. It has a well characterised structure crystallising in the space group P31c. The structure consists of cation columns with composition $Ca_3[Al(OH)_6.12H_2O]^{3+}$, that run parallel to the *c* axis, with the sulfate anions and remaining water molecules in channels running parallel to these columns. The crystal structure of ettringite has been shown to accommodate other cations, including Fe^{3+} and Cr^{3+}, on the Al^{3+} sites, and other oxyanions, including CO_3^{2-} and NO_3^-, in place of the SO_4^{2-} in the channels.

The ability of the structure to accommodate a range of different ions, gives it the potential for use as a waste remediation material. To test its viability, the synthesis of analogue phases was investigated, along with the time dependence of the formation of these phases.

Ettringite analogue phases containing chromate and selenate ($Ca_6[Al(OH)_6]_2(XO_4)_3.26H_2O$, X=$Cr^{6+}$, Se^{6+}) were successfully synthesised using the saccharate method. These particular phases were targeted as hexavalent chromium and selenium are hazardous pollutants which affect public freshwater as a result of

industrial runoff. With successful syntheses of the chromate and selenate ettringite analogue phases confirmed, a reaction was set up to emulate the remediation process of removing selenium or chromium from solutions, by incorporation into an ettringite analogue phase. The time dependence of the reaction was studied by taking samples at different time points to follow the evolution of the reaction products and removal of the pollutant ions from the solution.

Tricalcium aluminate ($Ca_3Al_2O_6$, C3A) was chosen as the start material and was added to solutions of varying concentrations of chromate or selenate. For chromate containing solutions, the chromate ettringite analogue phase was only formed in concentrated conditions (0.2 M K_2CrO_4 solution), with weaker solutions (0.01 – 0.1 M K_2CrO_4 solutions) producing a related phase known as monochromate ($Ca_4Al_2O_6(CrO_4).xH_2O$). All tests resulted in the successful removal of hexavalent chromium from solution and solidification of it into the solid phase.

For selenate containing solutions, the selenate ettringite analogue phase was formed in all concentrations of solutions (0.02 – 0.2 M Na_2SeO_4 solutions) when the reaction time was less than 24 hours, with conversion of these phases to the related monoselenate phase ($Ca_4Al_2O_6(SeO_4).xH_2O$) at reaction times greater than this. The end result was that selenium was removed from solution and stabilised in a solid phase for all tested concentrations.

Solid solution behaviour between the ettringite end member and analogue phase end members was investigated to determine the level of incorporation of the hazardous ions CrO_4^{2-} and SeO_4^{2-} when in the presence of SO_4^{2-}. The chromate-sulfate ettringite series ($Ca_6[Al(OH)_6]_2(CrO_4)_x(SO_4)_{3-x}.26H_2O$) was found to only exhibit solid solution behaviour when $x < 0.44$, and any attempts to incorporate more chromate resulted in the production of the two end members. The selenate-sulfate ettringite series ($Ca_6[Al(OH)_6]_2(SeO_4)_x(SO_4)_{3-x}.26H_2O$) was found to behave as a complete solid solution for a full range of compositions $0 < x < 3$. The solid solution investigation results can inform future remediation strategies if competing sulfur is present in the waste system.

Ettringite analogue phases containing iron and gallium ($Ca_6[X(OH)_6]_2(SO_4)_3.26H_2O$, X=Fe, Ga) were successfully synthesised and the ideal conditions for their formation were investigated. The inclusion of sugar in the synthesis was found to be necessary to produce an ettringite phase with no secondary impurity phases present. The gallium analogue phase could form in 10 minutes, with the iron analogue phase requiring a 24 hour reaction time. The solid solution behaviour between aluminium ettringite and gallium ettringite end members ($Ca_6[Al_xGa_{1-x}(OH)_6]_2(SO_4)_3.26H_2O$, x = 0, 0.1, 0.2, 0.3, 0.4, 0.5, 0.6, 0.7, 0.8, 0.9, 1.0) was investigated and the series was found to form completely. These results demonstrated that gallium could be partially incorporated into the ettringite structure with aluminium also present.

From the research presented and discussed in this thesis, the overall conclusions were that the precipitation of ettringite analogue phases and other related materials could be used to remove hazardous ions from water and stabilise them in a solid phase.

LAY SUMMARY

One of the problems the world faces today is pollution of freshwater sources that communities rely on for drinking water. Often this pollution comes from industry, as a by-product of their processes. When dangerous and toxic substances are released without first being treated, they can travel through groundwater, or rivers, and end up accumulating in areas of freshwater. This study is concerned with the release of toxic and carcinogenic chemical elements, in particular chromium and selenium. Both of these elements have the potential to harm river wildlife and endanger human health.

A common way to remove pollution of this kind is by a process called “stabilisation and solidification”. This means the dangerous particles are captured by a solid substance, which can then be removed from the water, leaving clean freshwater behind. There are many different things that can be dangerous to humans in polluted water, so there needs to be different techniques and materials designed to remove the pollutants in a quick and safe manner. This thesis describes a new method for solidifying toxic elements, which has been developed using minerals used in the cement industry and inspired by the processes that occur when cement is mixed and is setting.

A single material, known as tricalcium aluminate, was added to solutions containing either chromium or selenium. Samples were taken, of the solid and liquid, at different time points to track how much of the toxic element was removed from the solution and how the chemical structure of the solid was changing. The results of this study show that the method tested was effective and that the toxic elements were removed from solution. They were identified as being inside the solid and the structure of the solid was found to be different depending on how long the solution was left to react with the tricalcium aluminate material. The solid products formed were identified as structural analogues of either the mineral ettringite

($Ca_6[Al(OH)_6]_2(SO_4)_3.26H_2O$) or the mineral monosulfate ($3CaO.Al_2O_3.CaSO_4.14H_2O$). The structure of the products that were formed during this study were investigated in detail. The results of this work have been used to find ways to develop this method, in order to take it forward and use it to remove pollution from the environment.

ACKNOWLEDGEMENTS

Nothing is achieved alone, and this thesis would never have been completed without the help and support of all the amazing people I have met and known over the course of this project. Firstly, the biggest thanks of all must go to my incredible supervisor, Dr Caroline Kirk. Thank you for giving me the opportunity to work on this project and for all the support you have given me. You have taught me so many new skills and encouraged me to have more confidence in my ideas. I couldn't have asked for a better supervisor, and I owe you a very large caipirinha to say thank you. Along with this, I would like to also thank the University of Edinburgh for providing the funding for my project and giving me the chance to do my PhD in the beautiful City of Edinburgh.

Thanks also go to the past and present members of the Kirk group (the Kirkettes): Kurt, Kiran, Paul, Loda, Cameron, Shane, Roma, Ewan, Rheanna, and especially Fi and William. Fi, you are the other half of Fibecca and my PhD would not have been the same without you. I'll never forget exploring Japan with you, drinking chilled red wine and winning Moomins. William (AKA oor Wullie), you were there at the creation of the beamline dance and helped me make sense of Topas as the start of my PhD, for which I am very grateful.

To all the members of Office 82: Adam, Akachai, Angela, Ellie, Emily, Hannah, Hayleigh, Imogen, Karl, Lisette, Nisa, Rowan, Scott, Stuart, Sumit, and Xiaojiao, thank you for welcoming me to Edinburgh Chemistry and for all the help you gave me when I had just started my project and didn't know where to find deionised water or a vacuum pump. And thanks for all the memorable games nights, viva celebrations, and dinners at Wings and Pataka. I also need to say thank you to my chemistry friends from outside the office, Hannah, you kept me sane with fancy coffee trips, and Padraig, the stress of demonstrating Chem4p will never leave me but you at least halved that stress.

I would also like to thank the wonderful academics I have worked with in Edinburgh and beyond over the course of my project. Thanks go to Professor Paul Attfield, for all your support on my project, Professor Margaret Graham, for welcoming me and including me as an honorary member of your group, Dr Gary Nichol, for your help with the D2, D8 and with a very fussy TGA, Dr Nicola Cayzer, for helping me to collect such beautiful SEM images, Dr Lorna Eades, for training me to use the ICP-OES and for always being willing to answer my questions and come to the rescue when I couldn't remember which button to press next, Professor Donald MacPhee, for your interest in my project and for your advice about all things ettringite, and all the amazing beamline scientists who supported my beamtime at Diamond Light Source and ISIS Neutron Source: Dr Claire Murray, Dr Sarah Day, Dr Phil Chater, Dr Stephen Thompson, Dr Ron Smith, and Professor Chiu Tang.

My final thanks go to my friends and family, you have always been there for me throughout these last 4 years. Jennie, Kara, Kirstie, Kirsty, Catherine, Kiara and Mairi, you have all been the best friends, supported me, and most importantly forced me to get fresh air and go on walks, which definitely helped the writing process. Thanks to the whole Rae-Angus-Robertson-Scott fam! The zoom quizzes kept me going through lockdown and I am forever thankful and so lucky to have such a brilliant and loving family. To Mum, Dad, Scott, Gran, and Grandma, your love and support means more to me than I can put into words and this thesis is for you all.

TABLE OF CONTENTS

CHAPTER 1 INTRODUCTION

Ettringite is a mineral with composition $Ca_6[Al(OH)_6]_2(SO_4)_3.26H_2O$. It is an important mineral in the fields of materials chemistry, cement chemistry and environmental chemistry. This project aims to investigate the synthesis of ettringite and a selection of its structural analogue phases. This will be done with an overall aim of using these phases for removal of hazardous waste ions from the environment, specifically focussed on water pollution.

1.1 HISTORY AND CRYSTAL STRUCTURE DETERMINATION OF ETTRINGITE

Ettringite ($Ca_6[Al(OH)_6]_2(SO_4)_3.26H_2O$) was first discovered occurring naturally in Germany, at the Ettringen Bellerberg in 1874. Chemical analysis was carried out by J. Lehmann on the small crystals which he collected from the limestone enclosures[1]. This allowed Lehmann to determine that it was a calcium sulfoaluminate mineral. They had originally assumed it was gypsum ($CaSO_4.2H_2O$) so the presence of aluminium in the chemical analysis confirmed that this was a new mineral discovery.

Fragments of ettringite were collected by Professor C. E. Tilley from Scawt Hill, Co. Antrim, Northern Ireland in 1936[2]. There he found it occurring alongside the other minerals afwillite ($Ca_3(SiO_3OH)_2.2H_2O$), portlandite ($Ca(OH)_2$) and hydrocalumite ($Ca_2Al(OH)_6[Cl_{1-x}(OH)_x].3H_2O$). Bannister, Hey and Bernal[3] managed to separate the ettringite sufficiently so that they could compare this sample to the crystals from Germany by chemical analysis. Their chemical analysis results agreed with Lehman's data so the Scawt Hill sample was confirmed to be ettringite. One of the crystals collected was large enough to be analysed by X-ray diffraction and from these single crystal X-ray diffraction data, Bannister concluded that ettringite had a hexagonal unit cell in the space group $P6_3/mmc$, Z=2, with a= 11.26 Å, c= 21.48 Å. They also

suggested that the structure was based on chains of Ca^{2+} and $Al(OH)_6^{3-}$ ions, with SO_4^{2-} ions and H_2O molecules between the chains.

Moore and Taylor (1968) also analysed single crystal samples from Scawt Hill[4]. Their single crystal X-ray diffraction results showed the same systematic absences as Bannisters study, however, the symmetry was found to be trigonal, not hexagonal. This meant that the space group was *P*31*c* or *P*-31*c.* They attributed the apparent hexagonal symmetry of some of the crystals to twinning. Moore and Taylor reported that the structure of ettringite was based on columns of $(Ca_3[Al(OH)_6].12H_2O)^{3+}$ running parallel to the *c* axis with SO_4^{2-} ions and H_2O molecules in between in the channels. They published this crystal structure in 1970[5]. It was also thought that the hexagonal symmetry observed previously could have been due to disorder of the species in the channels.

In 2006, F. Goetz-Neunhoeffer and J. Neubauer published a refined structure for ettringite[6]. They synthesised powder samples and analysed the samples using a Siemens D5000 powder X-ray diffractometer. They carried out Rietveld refinement of the data using the software suite TOPAS, using the fundamental parameters approach[7]. The refinement was carried out in space group *P*31*c*, and the refined unit cell parameters were: *a* = 11.229(1) Å, *c* = 21.478(3) Å and volume = 2345.46(6) $Å^3$. This crystal structure is in the International Centre for Diffraction Data: Powder Diffraction File (PDF) entry number 41-1451. A diagram of this structural model was produced using the crystal structure drawing package VESTA (Copyright (C) 2006-2018, Koichi Momma and Fujio Izumi) and is shown below (Figure 1.1, Figure 1.2):

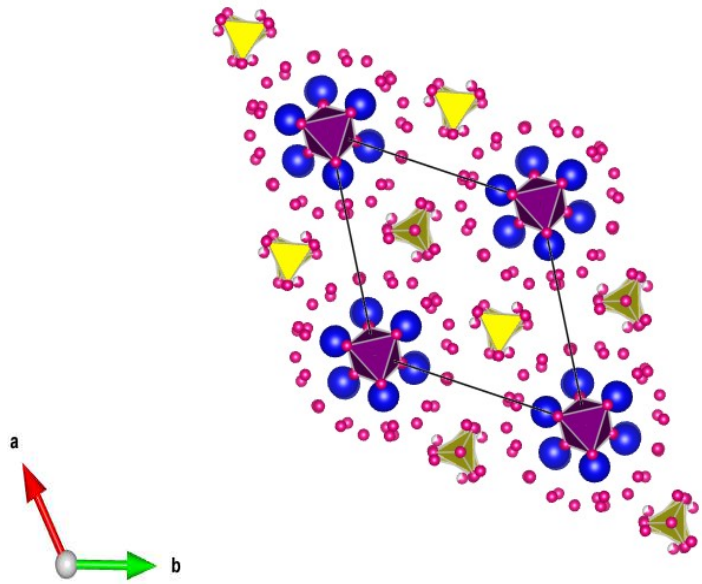

*Figure 1.1: **ab** projection of the ettringite structure: $Al(OH)_6$ purple, SO_4^{2-} yellow, Ca blue, O pink*

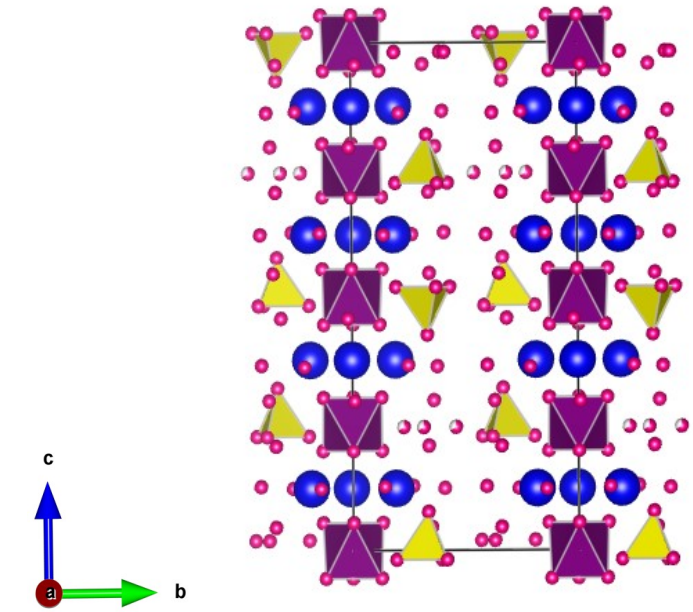

*Figure 1.2: [11-20] projection of ettringite with the **c** axis vertical: $Al(OH)_6$ purple, SO_4^{2-} yellow, Ca blue, O pink*

When crystals of ettringite occur naturally, they usually take the form of hexagonal prismatic crystals or long needles[5] and form through acicular crystal growth[8]. They are transparent to yellow in colour, if the crystals are white/ opaque in colour partial

dehydration has occurred. As well as Germany (Figure 1.3) and Northern Ireland, ettringite has been located in South Africa in the N'Chwaning Mine[9] (Figure 1.4), and as a weathering crust on the mineral larnite in the Hatrurium Formation, Israel[10,11].

Figure 1.3: Photograph of ettringite crystals from the Casper Quarry, Ettringen, Germany. Photo © Stephen Wolfsried 3/2007

Figure 1.4: Photograph of ettringite crystal form N'Chwaning II Mine, South Africa. Photo © Rob Lavinsky

1.2 Synthesis of Ettringite and Its Analogue Phases

As well as occurring naturally in mineral form, ettringite can be synthesised in powder form. Ettringite has been successfully synthesised by various different methods. In cement systems ettringite is formed by the reaction of tricalcium aluminate ($Ca_3Al_2O_6$, C3A) with gypsum ($CaSO_4.2H_2O$)[12,13] and early investigations into the laboratory synthesis of ettringite adapted this reaction.

In 1989 Odler and Abdul-Maula employed three different methods to synthesise ettringite[14]. Two were similar to a cement system in that they involved mixing tricalcium aluminate with gypsum. The difference between the two methods was the amount of water included, with one having only a small amount of water present resulting in a paste which was stored before the solid ettringite product was ground and dried (this method was called Ettr-I). The other method used excess water and the mixture was agitated before isolation of the ettringite by filtration (Ettr–II). For the third method (Ettr–III) a suspension containing calcium hydroxide and aluminium sulfate hydrate in water was agitated before isolating the ettringite produced by filtration. All three methods resulted in the production of crystalline ettringite.

Pollmann, Kuzel and Wenda synthesised ettringite and a variety of analogue phases in 1989[15,16]. They used two main methods for ettringite synthesis: the paste method and the saccharate method. The paste method used was based on that of Buhlert (1971)[17] and used all calcium salts ($CaO.Al_2O_3$ + CaO + $CaSO_4.2H_2O$) shaken in polyethylene bottles with excess water for long periods of time. When using this method, the storage containers had lime soda in them to inhibit the absorption of carbon dioxide from the air into the ettringite structure. The saccharate method used the combination of a calcium oxide/ sugar solution, sodium aluminate and sodium sulfate in a supersaturated solution to form the ettringite structure.

This method is known as the saccharate method due to its inclusion of sugar in the reaction mixture. The sugar increases the solubility of calcium oxide in water with this effect being discovered by Carlson and Berman in 1960[18]. They were attempting to

synthesise a calcium aluminate carbonate hydrate salt ($3CaO.Al_2O_3.3CaCO_3.32H_2O$) from solutions of calcium aluminate, calcium oxide and sodium carbonate. They found that there were always small amounts of calcite ($CaCO_3$) present in the product so needed to find a way to inhibit its formation. They found that adding sugar allowed them to have a higher concentration of CaO dissolved in solution, and also inhibited the formation of the calcite.

When the saccharate method is used for ettringite synthesis the sugar binds to the calcium oxide and forms compounds with approximate composition $C_{12}H_{22}O_{11}$.1-3CaO, and this increases the solubility of calcium oxide in water over 200 times. The calcium oxide is only weakly bound and as such the sugar can be easily removed during the ettringite crystallisation process.

The saccharate method was also used by Norman *et al* in 2013[19], they used a calcium oxide/ sugar solution but directly combined this with an aluminium sulfate solution to synthesise ettringite. This method is more similar to Odler and Abdul-Maula's Ettr-III method but with the addition of sugar to assist with calcium solubility.

More recently, mechanochemical synthesis methods have been successfully implemented for ettringite[20,21]. Zhong *et al.* (2016) used a mechanochemically prepared precursor (C3A + gypsum) and added it to water before stirring to produce ettringite[20]. Stroh *et al.* (2019) employed a two-step mechanochemical method of first combining reagents stoichiometrically ($Al(OH)_3$, $CaSO_4.2H_2O$, $Ca(OH)_2$) in a vibration ball mill and grinding together before the stoichiometric amount of water was added to the grinding jar and combined with the rest of the reagents to produce ettringite[21].

This study is particularly concerned with synthesising structurally analogous phases of ettringite, as it is known the ettringite crystal structure is flexible and can accommodate a variety of cations and anions[15]. In the case of ettringite structural analogues, these are phases where one of the ions present in ettringite ($Ca_6[Al(OH)_6]_2(SO_4)_3.26H_2O$) has been replaced with a different ion. Often, the ions chosen will have similar charge, size and shape to that that they are replacing.

Structural analogues of ettringite have been synthesised with replacement of the aluminium or sulfate ions. For example, using the general formula $Ca_6[M(OH)_6]_2(X)_3.26H_2O$, analogue phases have been synthesised where M = Fe, Si[15], Cr[22]; X = $B(OH)_4^-$, CrO_4^{2-} [16]. Analogue phases where there is complete substitution of particular crystallographic sites are known as “end member phases” but there can also be partial substitution and these phases are known as “solid solution phases”. There are a number of naturally known ettringite analogue phases that have been discovered and identified and it is more common to find the partially substituted “solid solution” ettringite phases in nature. This study will focus on optimising the saccharate method used by Norman *et al.* for synthesis of ettringite and some of its related analogue phases containing iron, gallium, chromium and selenium. Chromium and selenium are potentially toxic elements (PTEs) and reacting C3A ($Ca_3Al_2O_6$) with solutions containing these PTEs will be investigated. The process of forming ettringite-type phases from this reaction will be monitored and hence its potential as a remediation material will be assessed.

1.2.1 Naturally Occurring Analogues of the Ettringite Structure

Several analogues of the ettringite structure have been identified occurring naturally. Details of these are given in Table 1.1.

Table 1.1: Minerals in the ettringite group and their localities

Mineral	Formula	Locality	Reference
Bentorite	$Ca_6(Cr^{3+},Al)_2(OH)_{12}(SO_4)_3.26H_2O$	Hatrurium Formation, Israel	Gross (1980)[23,24] Seryotkin (2018)[25]
Charlesite	$Ca_6(Al,Si)_2(SO_4)_3[B(OH)_4](OH,O)_{12}.26H_2O$	Franklin Mine, New Jersey, USA	Peacor (1983)[26]
Siwaqaite	$Ca_6Al_2(OH)_{12}(CrO_4)_3.26H_2O$	North Siwaqa Complex, Jordan	Juroszek (2020)[27]
Sturmanite	$Ca_6(Fe^{3+},Al,Mn^{3+})_2(OH)_{12}(SO_4)_2[B(OH)_4].25H_2O$	Black Rock Mine, South Africa	Peacor (1983)[28]

The mineral phases bentorite, charlesite and sturmanite all crystallise with the ettringite structure, but the aluminium site is partially occupied by chromium, silicon, and iron/ manganese respectively. Sturmanite also has $B(OH)_4$ partially occupying the SO_4^{2-} sites. These examples show the problem with referring to phases simply as their mineral name, as one mineral name, for example bentorite, encompasses a series of phases where the occupancy of the aluminium site is variable and as such different chemical compositions are grouped under this name. Chemical formulae should be given when referring to specific compositions.

1.2.2 Synthetic Analogues of the Ettringite Structure

There have been many studies where analogue phases of the ettringite structure are synthesised[15,19,29–33]. This is a topic of interest as formation of these analogue phases could be used to remediate waste, through incorporation of PTEs and as such there is research into which ions can be hosted in the ettringite structure.

One set of investigations focusses on the total or partial replacement of the Al^{3+} cation with other cations. Wieczorek-Ciurowa *et al.*[22] (2001) synthesised a chromium analogue of the ettringite structure where the Cr^{3+} was in the place of the aluminium and they showed that an alkaline pH was needed for the analogue to form with no impurities.

Norman, *et al*[19] (2013) synthesised analogues of the ettringite structure where the aluminium cation was replaced by other metal cations. These cations included: iron, gallium, manganese, and tin. Synchrotron PXRD studies were carried out at the Diamond Light Source synchrotron facility and accurate unit cell parameters along with the structural models were refined for these analogue phases. They found that the analogues containing manganese and tin actually crystallised with a thaumasite-type structure that was different but related to that of ettringite. The mineral thaumasite ($Ca_3Si(OH)_6(CO_3)(SO_4).12H_2O$) crystallises in the hexagonal space group $P6_3$ with unit cell parameters, a= 11.04 Å, c= 10.39 Å. It is composed of cation columns, $[Ca_3Si(OH)_6.12H_2O]^{4+}$, isostructural to those in ettringite ($[Ca_3Al(OH_6).12H_2O]^{3+}$), but the inclusion of carbonate and sulfate in the intercolumnar space results in the space group being approximately half the length in the *c* direction. Due to the similarities in the structures and the fact that both can form during the hydration of cement through reaction with calcium sulfate hydrate (gypsum), it is important to consider the potential for thaumasite analogue phases to form while studying the synthesis of ettringite analogue phases.

There are also several studies into the formation of an ettringite solid solution where the occupancy of the aluminium sites was varied between aluminium and iron

($Ca_6[Al_{1-x}Fe_x(OH)_6]_2(SO_4)_3.26H_2O$). Odler and Abdul-Maula (1984) used equimolar amounts of aluminium (III) sulfate hydrate and iron (III) sulfate hydrate along with calcium hydroxide in water to target the ettringite phase $Ca_6[Al_{0.5}Fe_{0.5}(OH)_6]_2(SO_4)_3.26H_2O$. They formed an ettringite type phase containing both aluminium and iron in the crystalline lattice with a composition $Ca_6[Al_{0.53}Fe_{0.47}(OH)_6]_2(SO_4)_3.26H_2O$)[14]. Möschner and Lothenbach (2009) used a similar method, mixing calcium oxide, aluminium sulfate hydrate, and iron sulfate hydrate in a potassium hydroxide solution. However, unlike Odler and Abdul-Maula, they synthesised compounds where the ratio of aluminium: iron was varied[34] to produce a range of compositions, $Ca_6[Al_{1-x}Fe_x(OH)_6]_2(SO_4)_3.26H_2O$) where x = 0.1, 0.2, 0.7, 0.8, 0.9.

There are also a series of investigations where the occupancy of the sulfur sites of ettringite are altered, creating analogue phases and solid solutions containing anions other than sulfate. These have the general formula $Ca_6[Al(OH)_6]_2(SO_4)_{3-x}(X)_x.26H_2O$, where X can be a range of different anions. Some examples will now be discussed.

Pöllmann *et al.*[15] (1989) synthesised end member analogues of the ettringite structure where there was complete substitution of the sulfate sites with different anions. These included: nitrate, borate, hydroxide, and carbonate. Chemical analysis along with IR and PXRD were carried out to confirm the phases formed were ettringite-type phases.

Wang *et al.* (2017) investigated solid solution formation between sulfate and arsenate in ettringite[32]. Their results indicated that arsenate could incorporate into the ettringite structure as $HAsO_4^{2-}$ in place of the sulfate ions and synthesised samples with measured compositions $Ca_6[Al(OH)_6]_2(SO_4)_{3-x}(HAsO_4)_x.26H_2O$, x = 0, 0.04, 0.09, 0.12, 0.30, 0.53, 0.65, 1.

Kumarathasan *et al.* (1990) successfully synthesised analogues where selenate had completely replaced the sulfate ($Ca_6[Al(OH)_6]_2(SeO_4)_3.26H_2O$) and synthesised analogues where arsenate, borate and vanadate had partially replaced the sulfate[31]. They were not able to give definitive compositions for the partially substituted phases

but confirmed the incorporation of the arsenate, borate and vanadate by FTIR spectroscopy and EDXRF. Pöllmann *et al.* (1993) synthesised solid solutions of the ettringite with borate and chromate partially substituting for the sulfate[16]. For both of these series ($Ca_6[Al(OH)_6]_2(SO_4)_{3-x}(CrO_4)_x.26H_2O$ and $Ca_6[Al(OH)_6]_2(SO_4)_{3-3x}(OH)_{2x}B(OH)_4)_{4x}.26H_2O$) they confirmed synthesis of a variety of compositions across the whole range $0 < x < 3$.

Guo, Sasaki and Hirajima published a series of studies in 2017 all related to a selenate ettringite analogue phase[35–37]. They also compared uptake of selenate (SeO_4^{2-}) and selenite (SeO_3^{2-}) into ettringite as dopant ions with an aim of assessing the immobilisation potential of this process[36]. They confirmed, through use of EXAFS, FTIR and TG, that the selenate occupied the sulfate positions in the channels of the ettringite crystal structure and proposed that selenite would form complexes with the calcium hydroxides in the columns of the structure.

A number of other studies also investigated the formation of chromate ettringite, selenate ettringite, and solid solutions of these end members and ettringite. These included: Hassett and McCarthy (1990)[30], Perkins and Palmer (2000)[29] and Leisinger and Lothenbach (2010)[38]. Specific details of these studies will be discussed in Chapter 5 of this study where chromate-sulfate, and selenate-sulfate ettringite solid solution series will be fully investigated.

All of the above studies show the wide potential for analogue formation of the ettringite structure. Many of the studies use different synthesis methods, have different experimental parameters, and have varying results for the compositions they are able to synthesise. This study will aim to substitute either the aluminium cation or sulfate anion of the ettringite crystal structure and optimise the experimental conditions for forming each structural analogue found. Substituting ions will include: Fe^{3+}, Ga^{3+}, CrO_4^{2-}, and SeO_4^{2-}, with some of these being PTEs, critical elements or industrially important products. Finding ideal conditions for analogue formation is important if intending to use the formation of analogue phases for

removal of PTEs and other wastes from the environment in a waste remediation process.

1.3 Presence of Ettringite in Cement Systems

Ettringite is also a known hydration product of ordinary portland cement (OPC), forming in the early stages of the cement hydration process. OPC is a widely used material in construction and one of the most important materials in the world. The United States Geological Survey 2020 estimated that in 2019 4.1 billion tonnes of the cement clinker (dry cement start material) was produced, with the USA producing 88.5 million tonnes total cement, and 97 % of this production being OPC[39]. OPC is made by heating limestone and clay to a temperature of around 1450 ^{o}C to produce cement clinker[12]. The cement clinker can vary based on the specific materials used but typically has a composition around 67 % CaO, 22% SiO_2, 5% Al_2O_3, 3% Fe_2O_3 and 3% other components. The four major phases that make up the clinker are called alite (Ca_3SiO_5), belite (Ca_2SiO_4), aluminate ($Ca_3Al_2O_6$) and ferrite (Ca_2AlFeO_5). The hydration reactions between these components, water, and gypsum ($CaSO_4.2H_2O$) result in the hardening and strength of cement.

This project is particularly concerned with the reaction of the aluminate phase. The aluminate phase of OPC is tricalcium aluminate (C3A, $Ca_3Al_2O_6$) and during the hydration of cement it reacts quickly causing too rapid a setting unless another reagent is added. The reagent used to stop this 'flash setting' is gypsum (calcium sulfate hydrate, $CaSO_4.2H_2O$). When C3A hydrates in the presence of gypsum, ettringite is formed in the cement matrix[40,41]. This hydration mechanism has been studied by many different groups using different techniques including using *in-situ* neutron diffraction[42–44].

The presence of ettringite in the early stages of cement hydration can be beneficial to the early strength of the cement[45]. In most ordinary portland cement, being used

at normal temperatures, the ettringite can be detected by XRD within a few hours and will reach a maximum amount usually at around 24 hours. After this time, and when all of the gypsum has been consumed, any ettringite that has formed will react with more C3A to convert to a phase known as AFm or monosulfate (calcium aluminate monosulfate hydrate). The AFm phase is usually identified as being poorly crystalline with broad XRD peaks.

If any ettringite reforms after the cement has hardened and set this can have a damaging effect on the cement as the growth of new ettringite crystals is expansive and this expansion can cause the cement to crack[46,47]. This process is called delayed ettringite formation (DEF)[48]. DEF often occurs when there is an excess of sulfate present in the cement which can react with other components of the hydrated cement to form more ettringite.

This project will aim to use the hydration of C3A in the presence of oxyanions other than sulfate to form ettringite analogue phases. This should follow a similar pathway to the hydration of C3A in the presence of sulfate ions to form ettringite which occurs in cement. As such, there is a possibility that some AFm analogue phases will also form.

The AFm or monosulfate phase ($3CaO.Al_2O_3.CaSO_4.14H_2O$) has a hexagonal crystal structure made up of layers of $[Ca_3Al(OH)_6]_2^{2-}$ with 1 SO_4^{2-} and 6 H_2O in the interlayer. A projection of the crystal structure is shown in Figure 1.5 and is generated from the crystallographic information determined by Allmann in 1977[49]. Its crystals take the form of thin hexagonal platelets[50]. The interlayer (sulfate) site can accommodate other ions[51], for example carbonate, which can be readily incorporated[12]. The interlayer water content has also been shown to be able to change reversibly giving a range of different compositions[52].

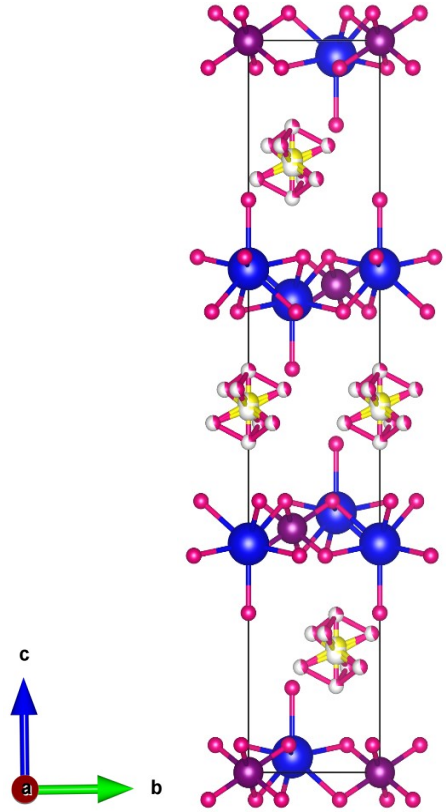

*Figure 1.5: Projection of the AFm (monosulfate) crystal structure with the **c** axis vertical: AL purple, S^{-}* yellow, Ca blue, O pink

Analogue phases of the AFm structure are known and include Friedel's salt which is a monochloride phase ($3CaO.Al_2O_3.CaCl_2.10H_2O$)[53]. There have also been studies which have synthesised chromate analogue phases[54–58] and selenate analogue phases[59] of the AFm structure ($3CaO.Al_2O_3.CaXO_4.nH_2O$, X = Cr, Se). It is, therefore, very possible that these analogue phases may be produced alongside ettringite analogue phases during the hydration of C3A in the presence of chromate or selenate, as will be investigated here. AFm analogue phases have even been tested as waste remediation materials themselves with Friedel's salt being used to remove arsenic and selenate from solutions[60,61].

1.4 Global Water Pollution: Problems and Solutions

This project aims to use ettringite analogue phases and other related phases to remove PTEs from polluted water. Waste remediation is the process of removing waste from contaminated sites in the environment and a remediation material is the specific material that is used to remove the waste particles.

1.4.1 Global Water Pollution

According to the Food and Agriculture Organisation of the United Nations' (FAO) database on the global use of water (AQUASTAT) 3928 km^3 of freshwater was used globally in 2010 with 2212 km^3 of wastewater being produced[62]. This freshwater was used in different ways as shown in Figure 1.6, which shows the fate of the total freshwater withdrawn. It shows that around 44 % of the freshwater removed from ground or surface water sources is fully consumed by agriculture, industry and municipal water systems. The remainder of the freshwater taken from the environment ends up being rereleased back into the environment as wastewater.

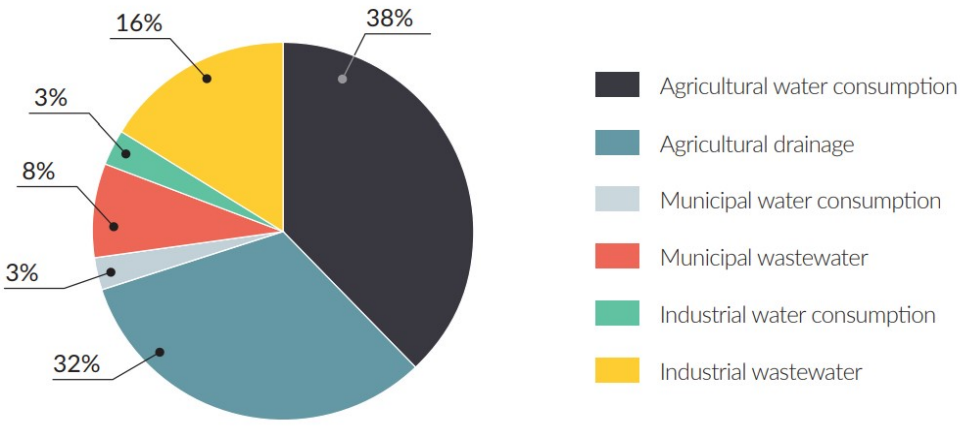

Figure 1.6: Fate of global freshwater withdrawals in 2010. Figure from UNESCO 2017 WWAP[62], with data from the AQUASTAT database analysed by Mateo-Sagasta et al.[63] and Shiklomanov[64]

Globally, over 80 % of all wastewater produced is released into the environment with no treatment whatsoever[62]. The term wastewater can be defined in many different ways and as such there is no one universally accepted definition. A comprehensive definition, however, was provided by Raschid-Sally and Jayakody in 2008[65]:

"Wastewater is regarded as a combination of one or more of: domestic effluent consisting of blackwater (excreta, urine and faecal sludge) and greywater (used water from washing and bathing); water from commercial establishments and institutions, including hospitals; industrial effluent, stormwater and other urban runoff; and agricultural, horticultural and aquaculture runoff."

Figure 1.7 shows where wastewater enters the water cycle either through surface water or groundwater and how both of these routes lead to the ocean. It also shows how wastewater treatment plants (WWTP) can be used to take untreated wastewater from industry, agriculture and residential sources as well as urban runoff and process it into treated wastewater that can either be reused or emitted into the environment safely. Water treatment plants (WTP) then take this treated wastewater (along with raw groundwater) and make it useable for industry and agriculture.

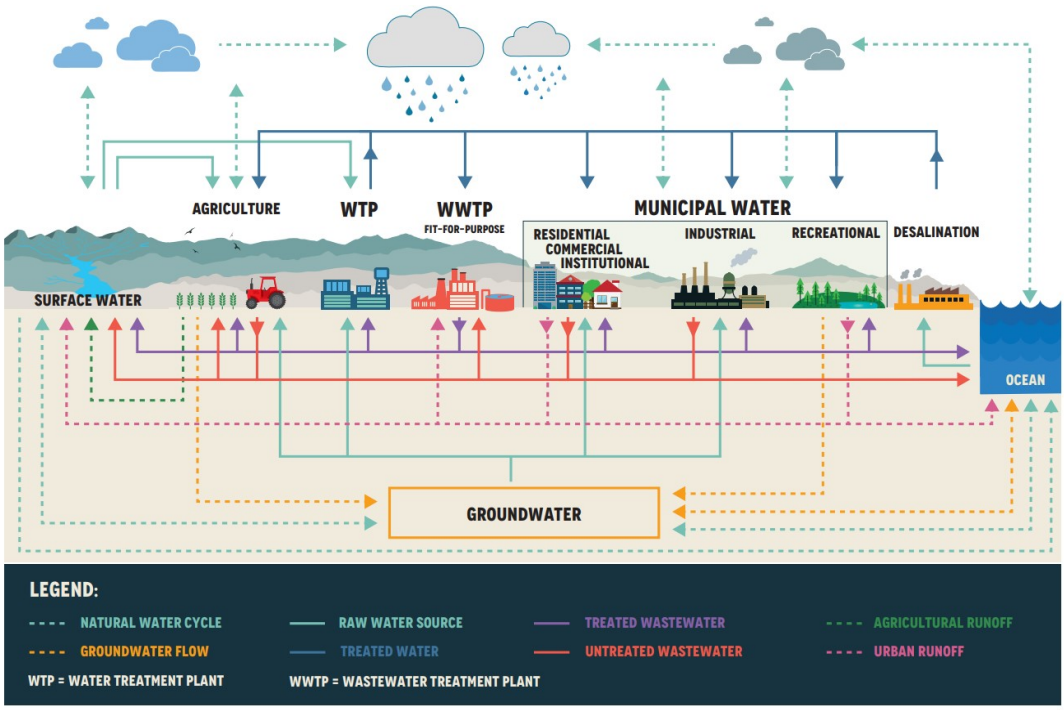

Figure 1.7: Schematic showing how wastewater fits into the water cycle (figure from UNESCO 2017 WWAP)[62]

If untreated wastewater is discharged into the environment, it can affect freshwater supplies and its eventual destination will be the ocean where it can affect the marine ecosystem. The release of untreated wastewater has the ability to have huge knock-on effects to society as it can impact both human and animal health with the former causing a reduction in global productivity and the latter impacting global agriculture and food production. Another knock-on effect to the economy is the wider implications for the tourism and housing markets that are based around bodies of water that end up polluted. So, there are economic as well as public health incentives to effectively treat wastewater.

This project will focus on wastes that are produced by industry. The volume of industrial wastewater produced is only expected to increase as the global population increases. The 2017 UN report states that by 2030 the global demand for energy is expected to increase by 40 % and the global demand for water is expected to increase by 50 %[62]. With this, the volumes of industrial wastewater is expected to be double

their 2007 values by 2025[66] and as such, the market for industrial water treatment technologies is predicted to grow significantly[67].

Along with the health, environmental, and economic benefits of treating wastewater, finding ways to reuse the treated wastewater could solve a wide range of problems. For example, many countries are already facing water scarcity and this problem will only get worse as the population increases and global warming affects the planet even more significantly. Treating wastewater could allow it to be used for agricultural and industrial uses, reducing the need for more freshwater.

This project is focussed on testing a new method for treating the potentially toxic elements (PTEs) chromium and selenium, which are constituents of industrial wastewater. The waste remediation method tested will be precipitation of ettringite analogue phases that contain these PTEs.

1.4.2 Industrial Waste Remediation Methods

As previously stated, wastewater is a huge and growing global problem with many different sources, such as industrial, agricultural, and public waste. This project will be focussed on waste produced by industry and specifically polluted water containing PTEs. These inorganic pollutants are different from organic contaminants as they are not biodegradable, cannot be destroyed and can be toxic or carcinogenic, posing significant risk to life[68]. Heavy metals are the main pollutants found in European soils and groundwater[69]. The two main ways to deal with heavy metal and other inorganic wastes are referred to as stabilisation and solidification.

Stabilisation involves chemically changing the pollutant into a different form which is non-hazardous, either by conversion to a non-toxic form, or reducing the ions mobility by forming insoluble compounds e.g. chemical precipitation[33]. The chemical precipitation method is the most commonly used in industry[70]. This is because it is an easy to implement, simple process where a remediation material is added to

wastewater and a chemical reaction occurs between it and the contaminants to produce an insoluble precipitate which can be easily separated from the water.

Solidification involves reducing the contaminants mobility by physically encapsulating it in a material which will not allow it to leach out. The most common way to 'solidify' a contaminant is by encapsulation into a cement matrix. Cement is used worldwide to encapsulate and dispose of radioactive and hazardous wastes as it both solidifies and stabilises the waste and prevents any future leaching of the hazardous material back into the environment[71]. One of the problems of stabilising waste in a cement matrix is the high pH environment of cement. By first solidifying and encapsulating the waste in cement minerals, as this project aims to do, this problem can be avoided.

1.4.3 Ettringite as a Waste Remediation Material

Ettringite is a particular material of interest for stabilising hazardous waste ions as it has been previously shown to accommodate a wide range of different ions (Section 1.2). It can undergo ionic substitution of the Ca^{2+}, Al^{3+}, and SO_4^{2-} sites meaning this single material could be used to remediate many different PTEs from waste streams. A further advantage to using ettringite as a stabilisation system for hazardous ions is that the materials used to synthesise ettringite and its analogues are readily and cheaply available as they are industrial by-products and used in the production of cement.

One particular waste product is fly ash, which is one of the waste residues produced in the combustion of coal[72]. The exact composition of fly ash will differ but can, and often will, contain the toxic elements: arsenic, chromium, selenium, and molybdenum among others. These elements are usually present as oxyanions which means that they will be highly mobile and able to make their way into water. Hexavalent selenium (Se^{6+}) is present in waste sources related to fly ash and is a

highly toxic pollutant, particularly to aquatic wildlife, as it can bio accumulate in rivers[73]. This has led to situations where fish and other wildlife have been negatively impacted due to exposure to selenium pollution[74]. In California, fish were found to have spinal deformities due to consumption of selenium and the effects were worsening due to the ability of the selenium to accumulate and be passed between mother and juvenile[75].

Ettringite has been shown to form analogue phases with selenate oxyanions on the sulfur sites[30] and therefore this analogue formation could be used to remove hexavalent selenium waste from the environment. Initial studies have been done to test the viability of this method and have been successful[31,72,76].

Another metal ion of concern, that this study will investigate, is hexavalent chromium. Compounds containing hexavalent chromium are genotoxic carcinogens, which means they can damage DNA and cause cancer and other mutagenic damage[77], and as such pose a threat to human health and life[78]. Chromium is most often present as a pollutant in wastewater as a result of untreated industry waste runoff[79] where it can enter the groundwater[80]. The industrial activities that can result in the release of hexavalent chromium include metal (chrome) plating, textile preservation and tanning[81]. There have been several high-profile cases of hexavalent chromium pollution with perhaps the best known being the Hinkley, USA case. In Hinkley, hexavalent chromium was found to be present in drinking water because the Pacific Gas and Electric compressor station near the town had used hexavalent chromium to prevent corrosion of the cooling stacks. Any wastewater produced was dumped, untreated, into ponds where it eventually entered the groundwater[82]. This case was brought to widespread public attention by the movie Erin Brockovich[83].

The Polmadie Burn in Glasgow, Scotland, is another site which has been polluted with hexavalent chromium. The pollution in this burn originated from historic industrial plants which disposed of chromite ore processing residue (COPR) to landfill where the hexavalent chromium was able to release to the groundwater[84,85]. This is a

problem that remains to this day (2021) with efforts to remediate the waste ongoing[86].

Hexavalent chromium is often present in water as the chromate (CrO_4^{2-}) oxyanion, and ettringite has been shown to form analogue phases with chromate on the sulfur sites of its crystal structure[16,29,38]. Ettringite precipitation could therefore be used to remove hexavalent chromium from wastewater. There have been some previous studies using ettringite formation as a method to remove Cr(VI) from water[31,87,88] which have found that this could be a promising method of remediation.

There have been other studies into using ettringite as a waste remediation material for a variety of other waste ions. These include arsenic[89,90,91], aluminium[92], lead[93], boron[76,94], and sulfate[91,95,96]. This project will investigate a new method of precipitating selenate ettringite and chromate ettringite phases as a means to remediate selenium and chromium containing waste streams.

1.5 AIMS AND OUTLINE OF RESEARCH

Pollution from industrial sources into wastewater is a growing global problem. This research aims to explore how the mineral ettringite can be used to remove waste ions from aqueous sources. In order to do this, analogue phase formation, solid solution behaviour and the reaction pathway of tricalcium aluminate with target waste ions needs to be investigated. Therefore, the objectives of the project are:

- Optimise a synthesis method based on the "saccharate method" for the synthesis of ettringite and ettringite analogue phases containing the oxyanions chromate or selenate ($Ca_6[Al(OH)_6]_2(XO_4)_3.26H_2O$, X = Cr^{6+}, Se^{6+}). Confirm the synthesis of analogue phases using powder X-ray diffraction (PXRD) and fourier transform infrared spectroscopy (FTIR). (Chapter 3)

- Investigate the reaction between tricalcium aluminate and solutions containing hexavalent chromium or selenium and asses the viability of this method for waste remediation. Fully investigate the reaction by altering the concentration of the solutions and the reaction time. Characterise solid samples, taken at various reaction times, using PXRD and FTIR to determine what phases have formed. Measure the amount of chromium or selenium present in the solid using inductively coupled plasma – optical emission spectroscopy (ICP-OES). (Chapter 4)

- Investigate the solid solution series' of chromate-sulfate and selenate-sulfate ettringite ($Ca_6[Al(OH)_6]_2(SO_4)_{3-x}(X)_x.26H_2O$, X = CrO_4^{2-}, SeO_4^{2-}). Knowledge about these series' is important for waste remediation purposes as the maximum content of waste ions that can be incorporated into the ettringite structure must be determined. PXRD was used to find any differences in the crystal structure/ unit cell parameters of phases with different compositions. (Chapter 5)

- Investigate the formation of ettringite analogue phases containing trivalent iron or gallium ($Ca_6[X(OH)_6]_2(SO_4)_3.26H_2O$, X = Fe, Ga). Determine the optimum conditions by analysing the products of different synthesis methods using PXRD and FTIR. Investigate the gallium-aluminium ettringite solid solution series ($Ca_6[Al_xGa_{1-x}(OH)_6]_2(SO_4)_3.26H_2O$) and refine the unit cell parameters of the members using PXRD data. (Chapter 6)

1.6 REFERENCES

1 J. Lehmann, *Neues Jahrb. für Mineral. Geol. und Palaontologie*, 1874, **6**, 273–275.

2 C. E. Tilley and H. F. Harwood, *Mineral. Mag.*, 1931, **22**, 439–468.

3 F. A. Bannister, M. H. Hey and J. D. Bernal, *Mineral. Mag.*, 1936, **24**, 324–329.

4 A. E. Moore and H. F. W. Taylor, *Nature*, 1968, **218**, 1048–1049.

5 A. E. Moore and H. F. W. Taylor, *Acta Crystallogr. Sect. B Struct. Crystallogr. Cryst. Chem.*, 1970, **26**, 386–393.

6 F. Goetz-Neunhoeffer and J. Neubauer, *Powder Diffr.*, 2006, **21**, 4–11.

7 A. A. Kern and A. A. Coelho, *A new fundamental parameters approach in profile analysis of powder data*, Allied Publishers, New Delhi, 1998.

8 R. Komatsu, N. Mizukoshi, K. Makida and K. Tsukamoto, *J. Cryst. Growth*, 2009, **311**, 1005–1008.

9 B. Cairncross and 1959- Dixon Roger, *Minerals of South Africa*, Geological Society of South Africa, Linden, Republic of South Africa, 1995.

10 S. Gross, *Geol. Surv. Isr. Bull.*, 1977, **70**, 1–80.

11 E. V. Galuskin, F. Gfeller, T. Armbruster, I. O. Galuskina, Y. Vapnik, M. Dulski, M. Murashko, P. Dzierżanowski, V. V. Sharygin, S. V. Krivovichev and R. Wirth, *Eur. J. Mineral.*, 2015, **27**, 123–136.

12 H. F. W. Taylor, *Cement chemistry 2nd Edition*, Thomas Telford, London, 2nd edn., 1997.

13 H. N. Stein, *J. Appl. Chem.*, 2007, **15**, 314–325.

14 I. Odler and S. Abdul-Maula, *Cem. Concr. Res.*, 1984, **14**, 133–141.

15 H. Pöllmann, H. J. Kuzel and R. Wenda, *Neues Jahrb. Miner. Abh.*, 1989, **160**,

133–158.

16 H. Pöllmann, S. Auer, H.-J. Kuzel and R. Wenda, *Cem. Concr. Res.*, 1993, **23**, 422–430.

17 R. Buhlert and H. J. Kuzel, *Zement-kalk-gips*, 1971, **2**, 83–85.

18 E. T. Carlson and H. A. Berman, *J. Res. Natl. Bur. Stand. - A Phys. Chem.*, 1960, **64A**, 333–341.

19 R. L. Norman, S. E. Dann, S. C. Hogg and C. A. Kirk, *Solid State Sci.*, 2013, **25**, 110–117.

20 L. Zhong, J. Qu, X. Li, X. He and Q. Zhang, *RSC Adv.*, 2016, **6**, 35203–35209.

21 J. Stroh, N. Z. Ali, C. Maierhofer and F. Emmerling, *ACS Omega*, 2019, **4**, 7734–7737.

22 K. Wieczorek-Ciurowa, K. Fela and A. J. Kozak, *J. Therm. Anal. Calorim.*, 2001, **65**, 655–660.

23 M. Fleischer and L. C. Cabri, *Am. Mineral.*, 1981, **66**, 637.

24 S. Gross, *Isr. J. Earth Sci.*, 1980, **29**, 81–84.

25 Y. V. Seryotkin, E. V. Sokol, S. N. Kokh and M. N. Murashko, *Phys. Chem. Miner.*, 2018, **45**, 279–292.

26 P. J. Dunn, D. R. Peacor, P. B. Leavens and J. L. Baum, *Am. Mineral.*, 1983, **68**, 1033–1037.

27 R. Juroszek, B. Krüger, I. Galuskina, H. Krüger, Y. Vapnik and E. Galuskin, *Am. Mineral.*, 2020, **105**, 409–421.

28 D. R. Peacor, P. J. Dunn and M. Duggan, *Can. Mineral.*, 1983, **21**, 705–709.

29 R. B. Perkins and C. D. Palmer, *Appl. Geochemistry*, 2000, **15**, 1203–1218.

30 D. J. Hassett, G. J. McCarthy, P. Kumarathasan and D. Pflughoeft-Hassett, *Mater. Res. Bull.*, 1990, **25**, 1347–1354.

31 P. Kumarathasan, G. J. McCarthy, D. J. Hassett and D. F. Pflughoeft-Hassett, *Mater. Res. Soc. Symp. Proc.*, 1990, **178**, 83–104.

32 W. Wang, Y. Shao, H. Hou and M. Zhou, *PLoS One*, 2017, **12**, e0182160.

33 W. Klemm, *Ettringite & oxyanion-substituted ettringites - their characterization and applications in the fixation of heavy metals : a synthesis of the literature*, Portland Cement Association, Skokie Ill., 1998.

34 G. Möschner, B. Lothenbach, F. Winnefeld, A. Ulrich, R. Figi and R. Kretzschmar, *Cem. Concr. Res.*, 2009, **39**, 482–489.

35 B. Guo, K. Sasaki and T. Hirajima, *RSC Adv.*, 2017, **7**, 42407.

36 B. Guo, K. Sasaki and T. Hirajima, *Cem. Concr. Res.*, 2017, **100**, 166–175.

37 B. Guo, K. Sasaki and T. Hirajima, *Cem. Concr. Res.*, 2017, **99**, 30–37.

38 S. M. Leisinger, B. Lothenbach, G. Le Saout, R. Kägi, B. Wehrli and C. A. Johnson, *Environ. Sci. Technol.*, 2010, **44**, 8983–8988.

39 USGS National Minerals Information Center, *US Geological Survey, Mineral Commodity Summaries 2020*, 2020.

40 J. E. Bailey, C. J. Hampson and J. Bensted, *Philos. Trans. R. Soc. London. Ser. A, Math. Phys. Sci.*, 1983, **310**, 105–111.

41 C. J. Hampson and J. E. Bailey, *J. Mater. Sci.*, 1983, **18**, 402–410.

42 A. N. Christensen, H. Fjellvag and M. S. Lehmann, *Acta Chem. Scand. A*, 1985, 593–604.

43 A. N. Christensen, T. R. Jensen and J. C. Hanson, *J. Solid State Chem.*, 2004, **177**, 1944–1951.

44 M. R. Hartman and R. Berliner, *J. Solid State Chem.*, 2005, **178**, 3256–3264.

45 F. P. Glasser, *Cem. Concr. Compos.*, 1996, **18**, 187–193.

46 S. Diamond, *Cem. Concr. Compos.*, 1996, **18**, 205–215.

47 C. Evju and S. Hansen, *Cem. Concr. Res.*, 2001, **31**, 257–261.

48 H. Y. Ghorab, in *International RILEM TC 186-ISA Workshop on Internal Sulfate Attack and Delayed Ettringite Formation*, 2002, pp. 65–81.

49 R. Allmann, *Neues Jahrb.Mineral. Monatsh.*, 1977, **3**, 136–144.

50 P. C. Hewlett and M. Liska, *Lea's chemistry of cement and concrete*, Elsevier Science & Technology, Saint Louis, Fifth., 2019.

51 S. Stöber and H. Pöllmann, in *Cementitious Materials*, ed. H. Pöllmann, De Gruyter, Berlin, Boston, 2017, pp. 191–250.

52 R. Fischer and H. J. Kuzel, *Cem. Concr. Res.*, 1982, **12**, 517–526.

53 G. Renaudin, F. Kubel, J.-P. Rivera and M. Francois, *Cem. Concr. Res.*, 1999, **29**, 1937–1942.

54 J. Göske, U. König and H. Pöllmann, *Mater. Sci. Forum*, 2004, **443**–**444**, 299–302.

55 H. Pöllmann and J. Goske, *Minerals as Advanced Materials II*, Springer Berlin Heidelberg, Berlin, Heidelberg, 2012.

56 S. M. Leisinger, B. Lothenbach, G. Le Saout and C. A. Johnson, *Cem. Concr. Res.*, 2012, **42**, 158–165.

57 H. Pöllmann and S. Auer, *J. Solid State Chem.*, 2012, **185**, 82–88.

58 M. Zhang and E. J. Reardon, *Sci. China, Ser. C Life Sci.*, 2004, **48**, 165–173.

59 L. Nedyalkova, B. Lothenbach, G. Renaudin, U. Mäder and J. Tits, *Cem. Concr. Res.*, 2019, **123**, 105803.

60 D. Zhang, Y. Jia, J. Ma and Z. Li, *J. Hazard. Mater.*, 2011, **195**, 398–404.

61 Y. Wu, Y. Chi, H. Bai, G. Qian, Y. Cao, J. Zhou, Y. Xu, Q. Liu, Z. P. Xu and S. Qiao, *J. Hazard. Mater.*, 2010, **176**, 193–198.

62 WWAP (United Nations World Water Assessment Programme), *The United*

Nations world water development report, 2017: Wastewater: the untapped resource, Paris, 2017.

63 J. Mateo-Sagasta, L. Raschid-Sally and A. Thebo, in *Wastewater: Economic Asset in an Urbanizing World*, Springer Netherlands, 2015, pp. 15–39.

64 I. A. Shiklomanov, *World water resources and their use a joint SHI/UNESCO product. Database.*, 1999.

65 L. Raschid-Sally and P. Jayakody, *Drivers and characteristics of wastewater agriculture in developing countries: results from a global assessment*, 2008.

66 UNEP FI (United Nations Environment Programme Finance Initiative), *Half Full or Half Empty? A Set of Indicative Guidelines for Water-Related Risks and an Overview of Emerging Opportunities for Financial Institutions.*, Geneva, 2007, vol. 29.

67 GWI (Global Water Intelligence), *Industrial Water Technology Markets 2015*, Oxford, 2015.

68 F. Fu and Q. Wang, *J. Environ. Manage.*, 2011, 92, 407–418.

69 P. Panagos, M. Van Liedekerke, Y. Yigini and L. Montanarella, *J. Environ. Public Health*, , DOI:10.1155/2013/158764.

70 Y. Ku and I.-L. Jung, *Water Res.*, 2001, **35**, 135–142.

71 M. L. D. Gougar, B. E. Scheetz and D. M. Roy, *Waste Manag.*, 1996, **16**, 295–303.

72 M. Zhang and E. J. Reardon, *Environ. Sci. Technol.*, 2003, **37**, 2947–2952.

73 A. D. Lemly, *Ecotoxicol. Environ. Saf.*, 2004, **59**, 44–56.

74 A. D. Lemly, *Aquat. Toxicol.*, 2002, **57**, 39–49.

75 R. C. Johnson, A. R. Stewart, K. E. Limburg, R. Huang, D. Cocherell and F. Feyrer, *Environ. Sci. Technol.*, 2020, **54**, 2892–2901.

76 D. J. Hassett, in *Society of Petroleum Engineers 37910*, 1997, pp. 219–221.

77 K. Salnikow and A. Zhitkovich, , DOI:10.1021/tx700198a.

78 A. Zhitkovich, *Chem. Res. Toxicol.*, 2011, **24**, 1617–1629.

79 C. Pellerin and S. M. Booker, *Environ. Health Perspect.*, 2000, 108, 402–407.

80 D. Rai, L. E. Eary and J. M. Zachara, *Sci. Total Environ.*, 1989, **86**, 15–23.

81 A. Broadway, M. R. Cave, J. Wragg, F. M. Fordyce, R. J. F. Bewley, M. C. Graham, B. T. Ngwenya and J. G. Farmer, *Sci. Total Environ.*, 2010, **409**, 267–277.

82 J. A. Izbicki and K. Groover, *Natural and man-made hexavalent chromium, Cr(VI), in groundwater near a mapped plume, Hinkley, California- study progress as of May 2017, and a summative-scale approach to estimate background Cr(VI) concentrations*, 2018.

83 S. Soderbergh, *Erin Brockovich*, 2000.

84 C. Whalley, A. Hursthouse, S. Rowlatt, P. Iqbal-Zahid, H. Vaughan and R. Durant, *Water, Air Soil Pollut.*, 1999, **112**, 389–405.

85 J. G. Farmer, R. P. Thomas, M. C. Graham, J. S. Geelhoed, D. G. Lumsdon and E. Paterson, *J. Environ. Monit.*, 2002, **4**, 235–243.

86 M. C. Graham, J. G. Farmer, P. Anderson, E. Paterson, S. Hillier, D. G. Lumsdon and R. J. F. Bewley, *Sci. Total Environ.*, 2006, **364**, 32–44.

87 G. J. Mccarthy, D. J. Hassett and J. A. Bender, *Mater. Res. Soc. Symp. Proc.*, 1992, **245**, 129–140.

88 H. He and H. Suito, *ISIJ Int.*, 2002, **42**, 139–145.

89 S. C. B. Myneni, S. J. Traina, T. J. Logan and G. A. Waychunas, *Environ. Sci. Technol.*, 1997, **31**, 1761–1768.

90 W.-H. Choi, J.-H. Shim, P. A. Ghorpade and J.-Y. Park, *Desalin. Water Treat.*, 2014, **52**, 712–718.

91 E.-T. Tolonen, T. Hu, J. Rämö and U. Lassi, *J. Environ. Manage.*, 2016, **181**, 856–862.

92 E. Álvarez-Ayuso and H. W. Nugteren, *Water Res.*, 2005, **39**, 65–72.

93 L. Xiang, H. Zhu and R. Zhou, *Adv. Civ. Eng.*, 2018, **2018**, 1–8.

94 J. K. Solem-Tishmack, G. J. McCarthy, B. Docktor, K. E. Eylands, J. S. Thompson and D. J. Hassett, *Cem. Concr. Res.*, 1995, **25**, 658–670.

95 I. Kabdaşli, A. Bilgin and O. Tünay, *Environ. Technol.*, 2016, **37**, 446–451.

96 W. Dou, Z. Zhou, L. M. Jiang, A. Jiang, R. Huang, X. Tian, W. Zhang and D. Chen, *J. Environ. Manage.*, 2017, **196**, 518–526.

CHAPTER 2 EXPERIMENTAL TECHNIQUES AND METHODS

2.1 SYNTHESIS METHODS

2.1.1 Synthesis of Anion Substituted Ettringite Phases and Monosulfate Phases (Chapter 3)

2.1.1.1 Synthesis of Anion Substituted Ettringite Phases

Ettringite ($Ca_6[Al(OH)_6]_2(SO_4)_3.26H_2O$) was prepared using the following method. Calcium oxide (CaO, Acros Organics, 96 %, 0.3224 g, 5.75 mmol), which had been heated overnight at 1000 °C in a furnace, was added to a 10 wt% sugar (white granulated, Tate and Lyle) in deionised water solution (25 cm^3, 2.5 g sugar). A solution containing aluminium sulfate hexadecahydrate ($Al_2(SO_4)_3.16H_2O$, Vickers Labs, pure grade, 0.6039 g, 0.958 mmol**)** in deionised water (25 cm^3) was prepared then this was mixed with the calcium oxide solution. The resulting solution was stirred for 24 hours, covered in Parafilm M, at room temperature before the solid products were isolated by vacuum filtration.

Ettringite analogue phases with the formulae $Ca_6[Al(OH)_6]_2(XO_4)_3.26H_2O$, X = Cr, Se, were prepared using the following method. Calcium oxide (0.3224 g, 5.75 mmol) was added to a 10 wt% sugar solution (25 cm^3, 2.5 g sugar) and stirred until the calcium oxide had dissolved. A second solution was prepared containing sodium aluminate ($NaAlO_2$¸ Sigma-Aldrich, technical grade, 0.1571 g, 1.916 mmol) and either potassium chromate (K_2CrO_4, Honeywell Fluka, 99%, 0.5583 g, 2.875 mmol) or sodium selenate (Na_2SeO_4, Alfa Aesar, 99.8%, 0.5432 g, 2.875 mmol) in 25 cm^3 deionised water. The two solutions were combined, and the resulting mixture was sealed in an HDPE bottle

and agitated on a roller mixer for 24 hours before the solid products were isolated by vacuum filtration.

2.1.1.2 Preparation of C3A

Tricalcium aluminate ($Ca_3Al_2O_6$, C3A) was prepared by grinding calcium carbonate ($CaCO_3$, Acros Organics, 99%, 3.3338 g, 33.3 mmol) and aluminium oxide (Al_2O_3, Acros Organics, 99.7%, 1.1224 g, 11.1 mmol) together in a mortar and pestle, before transferring to a furnace at 800 ^oC for 12 hours. The sample was then reground before being transferred to a furnace at 1300 ^oC for 48 hours. This grinding and heating of the sample at 1300 ^oC was repeated until the product (C3A) was obtained and determined to be pure by Powder X-ray Diffraction (PXRD).

2.1.1.3 Synthesis of a Monochromate Phase

A monochromate phase with the formula $3CaO.Al_2O_3.CaCrO_4.14H_2O$ was prepared by addition of C3A ($Ca_3Al_2O_6$, 0.25 g, 0.925 mmol) to a solution of potassium chromate (K_2CrO_4, 25 cm^3, 0.2 M). The resulting mixture was agitated on a roller mixer in a sealed HDPE bottle for 1 month before the solid product was separated by vacuum filtration.

2.1.2 Time Resolved Investigations into Removal of Hexavalent Chromium or Selenium from Solution using C3A ($Ca_3Al_2O_6$) (Chapter 4)

Prepared C3A (0.25 g, 0.925 mmol) was added to solutions (25 cm^3) of either potassium chromate or sodium selenate. The concentrations of the solutions were varied. The resulting mixture was agitated on a roller mixer in a HDPE bottle. The

agitation time was varied and after the allotted time period any solid products were separated by vacuum filtration.

2.1.3 Synthesis of Solid Solutions of the Ettringite Structure (Chapter 5)

2.1.3.1 Synthesis of a Chromate-Sulfate Ettringite Solid Solution ($Ca_6[Al(OH)_6]_2(CrO_4)_x(SO_4)_{3-x}.26H_2O$)

A solid solution series with the general formula $Ca_6[Al(OH)_6]_2(CrO_4)_x(SO_4)_{3-x}.26H_2O$ and x = 0, 0.3, 0.6, 0.9, 1.2, 1.5, 1.8, 2.1, 2.4, 2.7 and 3.0 was synthesised using the following precipitation method. The value of x here refers to the reagent ratio used in the synthesis. That may not reflect the actual ratio of anions incorporated in the solid, elemental analysis was carried out to determine the actual anion ratio.

Calcium oxide (CaO, 0.1612 g, 2.875 mmol) was added to a 10 % sugar in deionised water solution (1.3 g sugar in 13 cm^3 water). The resulting mixture was stirred until the CaO had dissolved. A second solution was prepared by adding sodium aluminate ($NaAlO_2$, 0.0786 g, 0.9583 mmol) along with varying stoichiometric amounts of potassium chromate (K_2CrO_4) and sodium sulfate (Na_2SO_4, Fisher Chemical, >95%) (1.4375 mmol in total) to 13 cm^3 deionised water to give different molar ratios of CrO_4^{2-}:SO_4^{2-}.

The two solutions were combined, and the resulting mixtures were sealed in HDPE bottles and agitated on a roller mixer at ambient conditions for either 24 hours or 7 days. The solid products were separated from solution using vacuum filtration with Whatman Grade 50 quantitative filter paper and dried in air.

2.1.3.2 Synthesis of a Selenate-Sulfate Ettringite Solid Solution ($Ca_6[Al(OH)_6]_2(SeO_4)_x(SO_4)_{3-x}.26H_2O$)

A second solid solution series with general formula $Ca_6[Al(OH)_6]_2(SeO_4)_x(SO_4)_{3-x}.26H_2O$ and x = 0, 0.3, 0.6, 0.9, 1.2, 1.5, 1.8, 2.1, 2.4, 2.7 and 3.0 was synthesised using the method described above in 2.1.3.1 but with sodium selenate (Na_2SeO_4) substituted for potassium chromate. The same synthesis times of 1 day and 7 days were used. Again, the values of x given here refer to the reagent ratio used in the synthesis. That may not reflect the actual ratio of anions incorporated in the solid and elemental analysis was carried out to determine the actual anion ratio.

2.1.4 Synthesis of Cation Substituted Ettringite Analogue Phases (Chapter 6)

Powder samples of ettringite and its structural analogues with various metal cations ($Ca_6[X(OH)_6]_2(SO_4)_3.26H_2O$, X = Al, Ga, Fe) were prepared using a general precipitation method called the saccharate method. Calcium oxide (CaO, Acros Organics, 96 %, 0.3224 g, 5.75 mmol) which had been heated overnight at 1000 °C in a furnace, was added to a 10 wt% sugar in deionised water solution (25 cm^3). A solution containing either a metal sulfate (0.958 mmol) in deionised water (25 cm^3), then this was mixed with the calcium oxide solution. The resulting solution was stirred for a varied amount of time, covered in Parafilm M, at room temperature before the solid products were isolated by vacuum filtration. Details of the metal sulfates and sodium salts used are shown in Table 2.1. A variation of this method was implemented where the second solution (25 cm^3) contained sodium aluminate (0.1571 g, 1.916 mmol) and sodium sulfate (0.4083 g, 2.875 mmol) instead of a metal sulfate.

Table 2.1: Metal sulfates and sodium salts used in the synthesis of ettringite and aluminium substituted ettringite analogue phases

Metal Sulfate	Formula	Supplier	Purity	Mass
Aluminium sulfate hexadecahydrate	$Al_2(SO_4)_3.16H_2O$	Vickers Labs	Pure grade	0.6039 g
Gallium sulfate hydrate	$Ga_2(SO_4)_3.13H_2O$	Sigma-Aldrich	99.99 %	0.6340 g
Iron sulfate pentahydrate	$Fe_2(SO_4)_3.5H_2O$	Acros Organics	97 %	0.4690 g

2.1.4.1 Synthesis of a solid solution series between aluminium ettringite and gallium ettringite ($Ca_6[Al_xGa_{1-x}(OH)_6]_2(SO_4)_3.26H_2O$)

A solid solution series with the general formula $Ca_6[Al_xGa_{1-x}(OH)_6]_2(SO_4)_3.26H_2O$ and x= 0, 0.1, 0.2, 0.3, 0.4, 0.5, 0.6, 0.7, 0.8, 0.9 and 1.0 was synthesised using the previously described saccharate method. A solution (13 cm^3), containing both aluminium sulfate and gallium sulfate (0.479 mmol in total) was added to the calcium oxide / sugar solution (13 cm^3,). The ratio of aluminium sulfate to gallium sulfate was varied to produce the different members of the solid solution series. Solutions were mixed for 24 hours before the solid products were isolated by vacuum filtration. The values of x given in the formula refer to the ratio of reagents used in the synthesis. They may not reflect the actual ratio of cations incorporated in the solid.

2.2 Characterisation Methods

2.2.1 Powder X-ray Diffraction (PXRD)

Powder X-ray diffraction (PXRD) was used to identify the crystalline phases present in the samples. In addition to phase identification it can also provide information

about the crystal structure of the phases present. In this study different refinement methods were employed to extract information about the crystal structure of phases from PXRD data. Refinement of PXRD data was carried out using the Topas Academic V6 software suite. Refinement using the Pawley method[1] uses a known space group and unit cell parameters to generate peak positions. The intensities of any reflections at these positions are only assumed and are allowed to vary to any values while the refinement is taking place. Therefore, no information is obtained from the reflection intensities when refining using the Pawley method. The unit cell parameters are refined to give the best fit to the data, so this method was used for phase identification and to obtain the unit cell parameters of phases formed in this study.

Refinement using the Rietveld method[2,3] differs from the Pawley method as the peak intensities are calculated using the structure factors from the full crystal structure model. Using the Rietveld method requires the full model structure to be known and allows refinement of the atomic positions, site occupancies and thermal parameters. Refinement of PXRD data using the Rietveld method was used in this study to assess the stoichiometry of solid solution phases by refining the site occupancy and to perform bond valence analysis using calculated bond lengths.

2.2.1.1 Powder X-ray Diffraction (PXRD) using Laboratory Sources

The PXRD data were collected on two different X-ray powder diffractometers at the University of Edinburgh and the details of each is given below:

- Bruker D2 Phaser- this instrument operates in reflection mode (Bragg-Brentano geometry) using Cu Kα radiation (λ = 1.5418 Å). A LynxEye position sensitive detector was used to collect data over the 2θ range 6-60 ^{o} or 6-72 ^{o} with an internal silicon standard added. Data were collected for either 15 or 30 minutes. Sample preparation for analysis using the D2 involved grinding

powder samples, mixing with acetone then depositing a thin layer onto a zero-background silicon (911) substrate.

- Bruker D8 Advanced- this instrument operates in transmission mode (Debye-Scherrer geometry) using Cu $K\alpha_1$ radiation (λ = 1.5406 Å) with a Ge (111) monochromator. A LynxEye detector was used to collect data over the 2θ range 5-60 ^{o} and the data collection time was 120 minutes. Sample preparation for the D8 involved grinding the powder sample before loading into a 0.5 mm diameter borosilicate glass capillary which was attached and secured to the goniometer head with wax. The capillary was then aligned manually before attaching to the main goniometer.

Analysis of the data (including Pawley and Rietveld refinements) was carried out using the software suite TOPAS-Academic, Version 6. Phase identification was carried out by comparison of data from the Inorganic Crystal Structure Database (ICSD). This provides crystallographic information files (.cif files) for published inorganic crystal structures.

2.2.1.2 High Resolution Powder X-ray Diffraction at a Synchrotron Light Source

For targeted samples, high resolution PXRD synchrotron studies were carried out. A synchrotron light source produces a beam which is millions of times brighter than the laboratory sources (D2 and D8) and is highly collimated. This means that extremely high resolution data could be collected quickly. This allows more accurate determination and refinement of unit cell parameters and so is invaluable when working with solid solution phases where the unit cell parameters are only changing by small increments between each sample. It also allows detection of impurity phases which are present in such small amounts that cannot be picked up on the laboratory diffractometers.

Synchrotron X-ray powder diffraction data were collected at the Diamond Light Source on beamline I11 (High Resolution Powder Diffraction) with a fixed wavelength of 0.82661 Å. The formed phases were loaded into 0.5 mm diameter capillaries and data were collected over the 2θ range 2-92 ^{o} using the Mythen 2 position sensitive detector (PSD) mounted on the δ circle. 10 second snapshots were collected for each sample.

2.2.2 Powder Neutron Diffraction (PND)

Powder neutron diffraction was carried out on a sample of C3A ($Ca_3Al_2O_6$) in order to refine the atomic positions and compare the refined crystal structure to the one refined using synchrotron X-ray powder diffraction data. The data was collected at the ISIS Neutron and Muon Source using the Polaris time-of-flight powder neutron diffractometer. Polaris is a high intensity, medium resolution powder diffractometer with five ZnS scintillator based detector banks covering a range $6^{o} \leq 2\theta \leq 168^{o}$. The data were collected at room temperature for ~110 minutes (350 μAh). The data collected on Bank 4 was used for Rietveld refinement of the structure of C3A.

2.2.3 Fourier Transform Infrared Spectroscopy (FTIR)

Infrared spectroscopy can be used to identify the functional groups present in solid products. FTIR spectra were collected using a Perkin Elmer Spectrum Two with an ATR (attenuated total reflectance) attachment. Samples were ground into fine powders before analysis. The absorption of the samples was measured between 4000-450 cm^{-1}. A resolution of 2 cm^{-1} and a data interval of 0.5 cm^{-1} was used. The characteristic bands of the phases produced in this work are detailed in Table 2.2.

Table 2.2: Infrared bands relating to the functional groups of ettringite and related phases[4,5]

Functional Group	**Wavenumber (cm^{-1})**
Water stretch $\tilde{\nu}_1$	3200-3570 (broad)[6]
Water bend $\tilde{\nu}_2$	1600-1650[6]
Sulfate $\tilde{\nu}_3$	1105[7]
Carbonate $\tilde{\nu}_2$	873[4]
Chromate $\tilde{\nu}_3$	863[9]
Selenate $\tilde{\nu}_3$	856[7,9]
Carbonate $\tilde{\nu}_4$	706[4]
Sulfate $\tilde{\nu}_4$	611[4]

2.2.4 Inductively Coupled Plasma- Optical Emission Spectrometry (ICP-OES)

ICP-OES was used to analyse the elemental composition of solid products. This was especially useful for the solid solution phases, where reagent ratios were altered to target specific compositions in a series. In these cases, ICP-OES was used to measure the true composition of the products.

For each sample being analysed by ICP-OES, a fraction of the solid product (0.01 g) was dissolved in 75% HNO_3 (5 cm^3) in a volumetric flask. These were then diluted 25x using 2% HNO_3 before ICP-OES measurements were taken.

The concentration of elements remaining in solutions was also measured by ICP-OES. For these samples, the solutions were diluted x20 using 2% HNO_3 before ICP-OES measurements were taken.

The diluted samples were analysed by ICP-OES using a Perkin Elmer Optima 8300 DV employing an RF forward power of (1500 W), with argon gas flows of 10, 0.2, and 0.6 $Lmin^{-1}$) for plasma, auxiliary, and nebuliser flows, respectively. Using a peristaltic pump, sample solutions were taken up into a Gem Tip Cross-Flow nebuliser and Scotts spray chamber at a rate of 1.30 mL min^{-1}.

The instrument was operated in axial mode for all elements. The recommended wavelengths for each element were selected and analysed by peak area (defined by three points per unit wavelength). Three replicate measurements per sample were employed.

A range of calibration standards for each element were prepared using: ICP multi element standard solution IV (Merck CertiPUR®) (containing aluminium and calcium at 1000 mg/l), along with single element selenium, chromium and sulfur (all 1000 mg/l) diluted with 2 % v/v HNO_3.

For all of the calibration lines, the correlation coefficients for either the linear regression or weighted linear regression were 0.99814 or better. Initially several wavelengths were selected for each element. After the analysis was completed the following wavelengths were selected for reporting results based on the shape of the peaks at that wavelength, background interferences, wavelength sensitivity and linearity of the calibration lines: Al- 308.215 nm, Ca- 317.933 nm, Cr- 205.560 nm, S- 181.975 nm, and Se- 196.026 nm.

The results reported are the concentrations of each element present in the sample in mg/l.

2.2.5 Scanning Electron Microscopy (SEM) and Energy Dispersive X-ray Spectroscopy (EDS)

A scanning electron microscope was used to acquire images of some of the synthesised phases. This was to allow information on the morphology and microstructure of the phases to be determined. EDS was also carried out simultaneously using the same instrument to get information on what chemical elements were present in the solid phases at specific chosen points on the crystals.

A Carl Zeiss SIGMA HD VP Field Emission SEM was used to carry out the analysis for this project. The accelerating voltage used was 15 kV with a pressure of 1 $x10^{-6}$ mbar

and a working distance of 7 mm. Sample preparation for this technique involved attaching a double sided carbon sticker to the top of an aluminium stub. Powder samples were sprinkled onto the sticky carbon surface and any excess was blown off using compressed air. The sample was then coated with either a thin gold coating or a carbon coating before analysis took place. Oxford Instruments AZtec software was used to carry out the EDS analysis.

2.3 REFERENCES

1 G. S. Pawley, *J. Appl. Crystallogr.*, 1981, **14**, 357–361.

2 H. M. Rietveld, *Acta Crystallogr.*, 1967, **22**, 151–152.

3 H. M. Rietveld, *J. Appl. Crystallogr.*, 1969, **2**, 65–71.

4 K. Nakamoto, *Infrared and Raman Spectra of Inorganic and Coordination Compounds Part A : Theory and Applications*, 1978.

5 J. Coates, in *Encyclopedia of Analytical Chemistry*, 2006, pp. 1–23.

6 G. E. Walrafen, *J. Chem. Phys.*, 1964, **40**, 3249–3256.

7 Landolt-Bornstein, *Physikalisch-chemische Tabellen Vol 2*, Springer, Berlin, 1951.

8 S. Bhagavantam and T. Venkatarayudu, *Proc. Indian Acad. Sci. - Sect. A*, 1939, **9**, 224–258.

9 M. Malchos and M. Jansen, *Z. Naturforsch*, 1998, **53b**, 704.

CHAPTER 3 INVESTIGATING THE SYNTHESIS OF ETTRINGITE ANALOGUE PHASES AND MONOSULFATE ANALOGUE PHASES CONTAINING SULFUR, CHROMIUM, AND SELENIUM

3.1 INTRODUCTION

This study is focussed on investigating the synthesis of ettringite analogue phases containing chromate or selenate ($Ca_6[Al(OH)_6]_2(XO_4)_3.26H_2O$, X = Cr, Se). These analogue phases crystallise with the same structure as ettringite ($Ca_6[Al(OH)_6]_2(SO_4)_3.26H_2O$) but with chromium or selenium on the sulfur sites of the crystal structure. This is possible because chromate and selenate ions have radii similar to the sulfate ion (sulfate = 2.18 Å, chromate = 2.29 Å and selenate = 2.29 Å)[1,2].

Chromate ettringite has been previously synthesised by Pöllmann and Wenda (1993)[3] and Perkins and Palmer (2000)[4]. In the study by Pöllmann and Wenda, they used the saccharate method to synthesise chromate ettringite and reported the phase crystallised with unit cell parameters *a* = 11.39 Å, *c* = 21.47 Å which they refined using a least squares method. The study by Perkins and Palmer used a modified version of Odler and Abdul-Maula's paste method[5] and after analysing their sample by PXRD they indexed the pattern with refined unit cell parameters of *a* = 11.41 Å, *c* = 21.44 Å.

Selenate ettringite has been synthesised previously by Hassett *et al.* (1990)[6] and Guo *et al.* (2017)[7,8]. Hassett's study used the saccharate synthesis method and a least squares method to refine the unit cell parameters to *a* = 11.387 Å, *c* = 21.46 Å. The study by Guo did not use the saccharate method and selenate ettringite was synthesised using a different solution precipitation method where sodium selenate

was mixed with calcium hydroxide and aluminium chloride. They found that pure selenate ettringite had refined unit cell parameters *a* = 11.40 Å, *c* = 21.48 Å.

The various processes that ettringite undergoes in a cement system have been outlined in Chapter 1.3. After ettringite is formed from the reaction of C3A ($Ca_3Al_2O_6$) with gypsum ($CaSO_4.2H_2O$), it can go on to react with more C3A to form monosulfate ($3CaO.Al_2O_3.CaSO_4.14H_2O$)[9,10]. Analogue phases of monosulfate have been reported, including a series of chromium containing structural analogues known as monochromate ($3CaO.Al_2O_3.CaCrO_4.nH_2O$, n = 9-14)[11–14]. Like the monosulfate phase they are classed as layered double hydroxides (LDH) and can be described as consisting of positively charged layers, $[Ca_2Al(OH)_62H_2O]^+$, with the interlayer containing chromate anions along with water. The slight difference in size between the sulfate and chromate ions means that monochromate has a different distance between the positively charged layers to monosulfate[11]. Monosulfate crystallises in the space group R-3, with reported unit cell parameters *a* = 5.76 Å, *c* = 26.8 Å and an interlayer distance of 8.6 Å[15]. However, there is no universally agreed upon crystal structure for the monochromate phases, with various studies into the structure of monochromate reporting different stacking sequences/ arrangement of the layers, along with different levels of hydration. This results in the reported monochromate phases being refined into different space groups with different unit cell parameters. The structural information for the monochromate phases produced by various studies is summarised in Table 3.1.

Table 3.1: Summary of the different unit cell parameters for monochromate ($3CaO.Al_2O_3.CaCrO_4.nH_2O$) found in the literature

Study	Hydration level (nH_2O)	*a* parameter (Å)	*c* parameter (Å)	Interlayer distance (Å)	Space group
Leisinger and Lothenbach (2012)[11]	12	5.74	30.72	10.2	R-3
Göske *et al* (2004)[12]	14	5.75	30.73	10.2	P-3
Göske *et al* (2004)[12]	12	5.75	29.22	9.7	R-3
Rapin (2001)[13]	12	5.75	19.42	9.7	P3
Segni (2005)[14]	13	5.75	20.16	10.1	P-3

The different reported structures are likely due to the variety of synthesis methods used, causing the chromate ions to be in a range of crystallographic positions in the interlayer. This means that the various reported structures of monochromate phases have different stacking sequences and therefore distinct structures. Crystal structure projections for the models of monosulfate proposed by Allmann and monochromate proposed by Segni are shown in Figure 3.1 a) and b). These diagrams show the disorder and uncertainty in the structural models. In both models, the sulfur and chromium sites are partially occupied, indicating the disorder of these anions. There is also uncertainty of where the free water is positioned in the layers. These issues with the models demonstrate how challenging it is to refine layered structures like

these using powder X-ray diffraction. This study has synthesised a sample of monochromate, and comparisons of refined unit cell parameters and structure to structural data reported on these phases in literature have been made to determine if there were similarities to any of the previous studies.

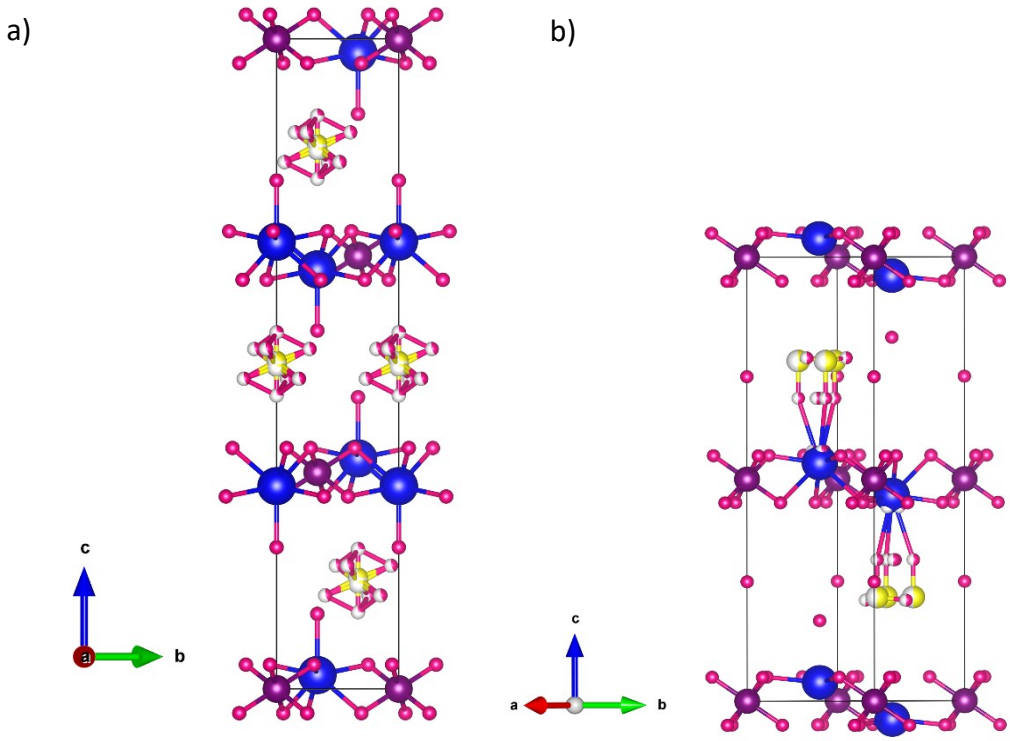

Figure 3.1 a) and b): Structural models of a) the monosulfate structure proposed by Allmann[15] b) the monochromate structure proposed by Segni[14]. Blue = calcium, purple = aluminium, pink = oxygen, yellow in a) = sulfur and in b) = chromium

3.2 AIMS

The aims of this study were to synthesise ettringite and its chromate and selenate analogue phases ($Ca_6[Al(OH)_6]_2(XO_4)_3.26H_2O$, X = S, Cr, Se) using the saccharate method. The crystal structure and morphology of the synthesised phases were investigated using PXRD, FTIR and SEM/EDS and any similarities or differences were discussed. The structure of monochromate ($3CaO.Al_2O_3.CaCrO_4.14H_2O$) was investigated through analysis and refinement of high resolution synchrotron X-ray powder diffraction data, and a model of the structure was produced.

3.3 SYNTHESIS OF ETTRINGITE AND ITS CHROMIUM AND SELENIUM CONTAINING ANALOGUE PHASES

Samples of ettringite and its chromium and selenium containing analogue phases ($Ca_6[Al(OH)_6]_2(XO_4)_3.26H_2O$, X = S, Cr, Se) were synthesised using the saccharate method (as described in Section 2.1.1.1). High resolution PXRD data were collected on the samples on the beamline I11 at the Diamond Light Source synchrotron. Rietveld refinement was carried out in Topas to refine the unit cell parameters along with atomic positions and thermal parameters. Stable refinements were able to be obtained for the data collected on the samples of sulfate ettringite and chromate ettringite. There were issues with the refinement of the PXRD data collected on the sample of selenate ettringite. The results of refining this data using the Pawley method are presented here and future work is needed to improve the Rietveld refinement of the selenate ettringite structure. The observed, calculated and difference profiles obtained from the refinements are shown in Figure 3.2, Figure 3.3 and Figure 3.4 along with the tick marks which show the reflection positions.

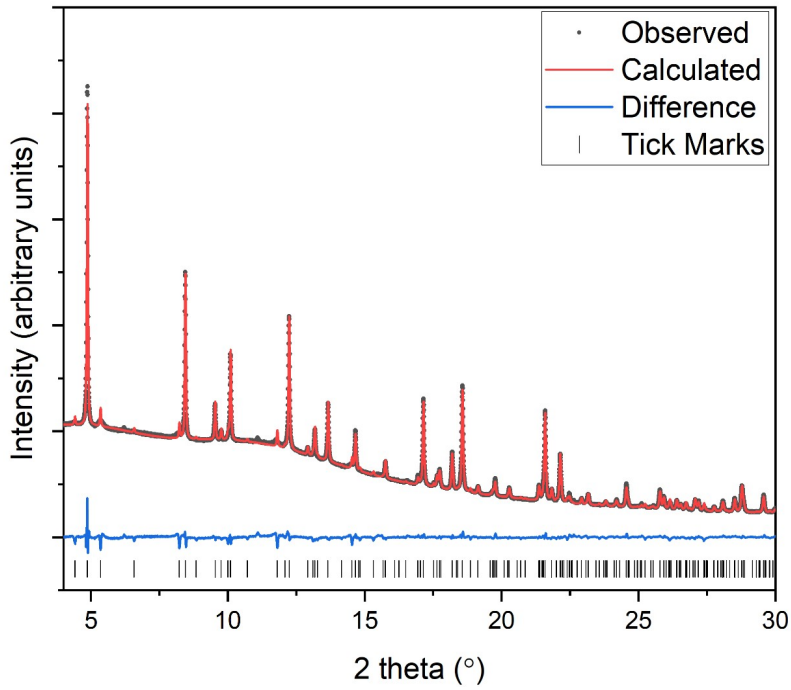

Figure 3.2: Observed-calculated-difference profiles for the data collected on an ettringite sample synthesised using the saccharate method and a synthesis time of 24 hours (data collected on I11 at the Diamond Light Source Synchrotron, λ = 0.82661 Å) and refined using the Rietveld method against ICSD structure 251756

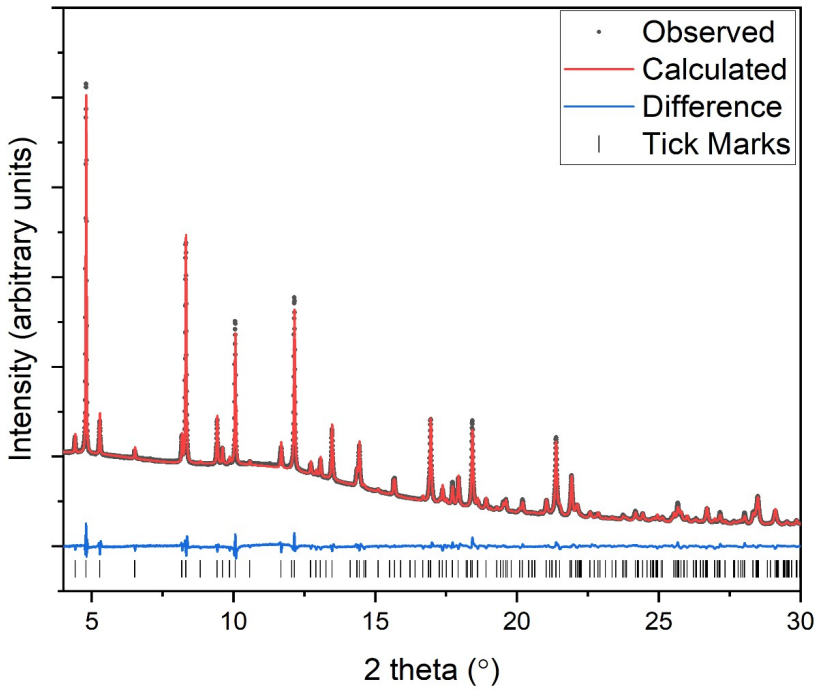

Figure 3.3: Observed-calculated-difference profiles for the data collected on a chromate-ettringite sample synthesised using the saccharate method and a synthesis time of 24 hours (data collected on I11 at the Diamond Light Source Synchrotron, λ = 0.82661 Å) and refined using the Rietveld method against a modified version of ICSD structure 251756

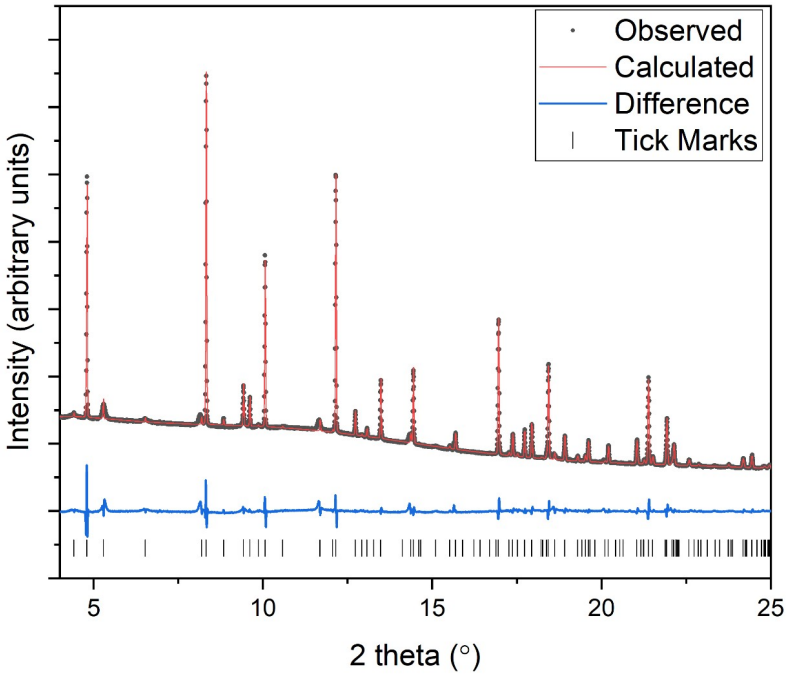

Figure 3.4: Observed-calculated-difference profiles for the data collected on a selenate-ettringite sample synthesised using the saccharate method and a synthesis time of 24 hours (data collected on I11 at the Diamond Light Source Synchrotron, λ = 0.82661 Å) and refined using the Pawley method against a modified version of ICSD structure 251756

The unit cell parameters for the sulfate ettringite and chromate ettringite samples were refined using the Rietveld method in the space group P31c and are presented in Table 3.2, along with the literature parameters for sulfate ettringite refined by Norman *et al.*[16]. The unit cell parameters for the selenate ettringite sample were refined using the Pawley method and they are also presented in Table 3.2.

The refinement strategy for the synthesised sample of sulfate ettringite was as follows: the background was modelled using a Chebychev function and the peak shapes using the modified Thomson-Cox-Hasting pseudo Voigt function. The simple axial model was used to model the asymmetry of low angle peaks. The unit cell parameters were allowed to refine, along with the background and peak shape. After the refinement of these parameters had converged, the atomic positions from the published ettringite structural model (ICSD structure 251756)[16] were allowed to refine along with the thermal parameters. The thermal parameters of the sites were constrained in the following sets in order to give stable refinements, O1–O4 (oxygen

sites coordinated to aluminium sites), O5-O12 (oxygen sites coordinated to calcium sites), O13-O18 (oxygen sites coordinated to sulfur sites) and S1-S3 (sulfur sites coordinated to oxygen sites). The positional parameters for Ca1, O3, O19 and the sulfate anions were fixed to those of the structural model in order to give reasonable bond lengths and Beq thermal parameters. Certain positional and thermal parameters need to be constrained when refining ettringite samples analysed using PXRD data. This is because calcium has the greatest number of electrons in the material, and as such has the strongest scattering. This makes refinement of the lighter elements sulfur and oxygen more challenging. Transmission geometry was used when collecting the PXRD data on the sample contained in a capillary, and this creates issues with absorption of the X-rays which can impact the quality of the refinement. There are also a lot of oxygen sites which are held loosely in the hydrous structure of ettringite, and the sulfur sites can often exhibit disorder as they are held in the channels in between the columns of the structure.

The refinement strategy for chromate ettringite was the same as for sulfate ettringite, but the model from ICSD structure 251756 was modified to include chromium sites instead of sulfur sites and the unit cell parameters were set to a = 11.3978 Å, c = 21.4721 Å (obtained from Pawley refinement of the data) before Rietveld refinement. The thermal parameters were constrained in the same sets, but to obtain a stable refinement with reasonable calculated bond lengths, the positional parameters for O1-O4 (oxygen sites coordinated to aluminium sites), O13-O15 (oxygen sites coordinated to Cr), O19 (the oxygen site of the unbound water molecule) and Cr1-Cr3 were fixed.

Table 3.2: Unit cell parameters, refined using the Rietveld and Pawley methods, for synthesised samples of ettringite, chromate ettringite and selenate ettringite ($Ca_6[Al(OH)_6]_2(XO_4)_3.26H_2O$, X = S, Cr, Se), compared to literature ettringite unit cell parameters

	Literature sulfate ettringite[16]	**Sulfate ettringite**	**Chromate ettringite**	**Selenate ettringite**
***a* (Å)**	11.22335 (8)	11.22430 (8)	11.39761 (7)	11.38696 (8)
***c* (Å)**	21.4541 (2)	21.4565 (2)	21.4713 (2)	21.4530 (2)
Volume (Å^3)	2340.35	2341.03 (4)	2415.56 (4)	2408.99 (4)
R_{wp} value		2.005	1.941	2.757

Comparing the refined unit cell parameters for chromate ettringite and selenate ettringite to those of sulfate ettringite, the *a* parameter is found to be the most affected by changing the sulfate ions to chromate or selenate. This is due to the XO_4^{2-} anions being located in the channels in between the columns of the crystal structure (Figure 3.5). In the *c* direction there is enough space between the oxyanions that the change in size from a sulfate ion (2.18 Å) to a chromate ion (2.29 Å) or a selenate ion (2.29 Å)[1,2] does not affect the overall unit cell size in this direction, and this can be seen highlighted by the vertical arrows on the projection (Figure 3.5). The average X-X distance in the *c* direction is 5.23 Å (X1-X2 = 4.4 Å, X2-X3 = 3.8 Å, X1-X3 = 7.5 Å). However, in the *a* direction the XO_4^{2-} tetrahedra are closer to one another (the distance between X1 and X3 highlighted by the horizontal arrow on the projection is 3.88 Å) and so the change in size from sulfate to chromate or selenate causes the overall unit cell to expand in the *a* direction from 11.2243 Å to 11.3976 Å for chromate and to 11.3870 Å for selenate. The refined *a* unit cell parameter for chromate ettringite and selenate ettringite are very similar as chromate and selenate anions have the same ionic radii.

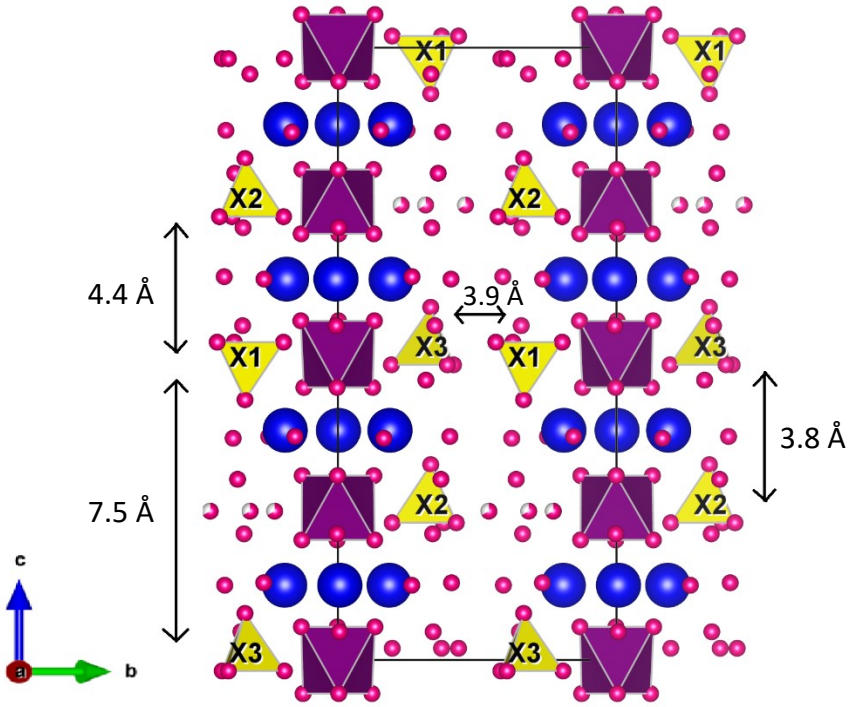

Figure 3.5: [11-20] projection of the ettringite crystal structure parallel to the c axis. Yellow tetrahedra = XO_4^{2-}, X = S, Cr or Se. Arrows highlight the proximity of the XO_4^{2-} anions in different directions

The calculated bond lengths are given in Table 3.3 along with the atomic valences, calculated using bond valence sum analysis. The refined atomic positions and Beq thermal parameters are given in Appendix 1. The strategies used resulted in stable refinements with low Rwp numbers and reasonable calculated bond lengths. The Cr-O bond lengths were found to be longer than the S-O bonds but this is expected from literature[17,18]. The distances between the sites that make up the columns (Al-O and Ca-O) don't vary considerably from the literature sulfate ettringite values when the sulfate anion is changed to chromate. This complements the unit cell parameter analysis as the *c* unit cell parameter doesn't change greatly and so the columns remain largely unchanged in the ettringite structure. The atomic valences, calculated using bond valence sum analysis, for the sulfate ettringite sample were all reasonably close to what would be expected, indicating that the model used in the refinement was stable. The model used for the chromate ettringite model was less reliable and this is shown in the valences of the chromium sites being varied. Cr1 had a calculated

valence close to 6 but Cr 2 and 3 were significantly lower as the Cr-O bonds were longer and the sites were underbonded. Al1 was also underbonded compared to Al2, suggesting Al2 is the favoured aluminium site.

Table 3.3: Bond lengths and atomic valences, calculated using the Rietveld refinement method, for synthesised samples of ettringite, chromate ettringite and selenate ettringite ($Ca_6[Al(OH)_6]_2(XO_4)_3.26H_2O$, X = S, Cr, Se), compared to literature ettringite values

Bonds to O	Literature sulfate ettringite (X = S)[16]	Bond lengths for sulfate ettringite (X = S) (Å)	Atomic valence for sulfate ettringite	Bond lengths for chromate ettringite (X = Cr) (Å)	Atomic valence for chromate ettringite
Al1-O1	1.95 x3	2.13 x3	3.17	2.03 x3	2.65
Al1-O2	1.85 x3	1.70 x3		1.84 x3	
Al2-O3	2.02 x3	1.74 x3	3.30	1.75 x3	3.13
Al2-O4	1.81 x3	1.98 x3		2.02 x3	
Ca1-O1	2.40	2.45	1.70	2.30	1.78
Ca1-O1	2.50	2.48		2.50	
Ca1-O3	2.34	2.42		2.39	
Ca1-O3	2.54	2.45		2.44	
Ca1-O6	2.51	2.60		2.52	
Ca1-O8	2.38	2.52		2.70	
Ca1-O10	2.58	2.78		2.83	
Ca1-O12	2.51	2.83		2.92	
Ca2-O2	2.46	2.39	2.07	2.40	2.04
Ca2-O2	2.49	2.43		2.51	
Ca2-O4	2.45	2.50		2.43	
Ca2-O4	2.46	2.51		2.55	
Ca2-O5	2.60	2.29		2.37	
Ca2-O7	2.45	2.69		2.66	
Ca2-O9	2.71	2.46		2.47	

Ca2-O11	2.76	2.61		2.46	
X1-O13	1.72	1.44	5.84	1.65	6.28
X1-O16	1.58 x3	1.50 x3		1.62 x3	
X2-O14	1.42	1.46	5.87	1.67	3.98
X2-O17	1.86 x3	1.49 x3		1.85 x3	
X3-O15	1.59	1.44	5.84	1.74	4.03
X3-O18	1.41 x3	1.50 x3		1.81 x3	

FTIR was used to identify the functional groups present in the samples to further confirm successful synthesis of ettringite. The spectra are shown below in Figure 3.6 a) b) and c) and the functional groups present are tabulated with the wavenumber of their bands in Table 3.4.

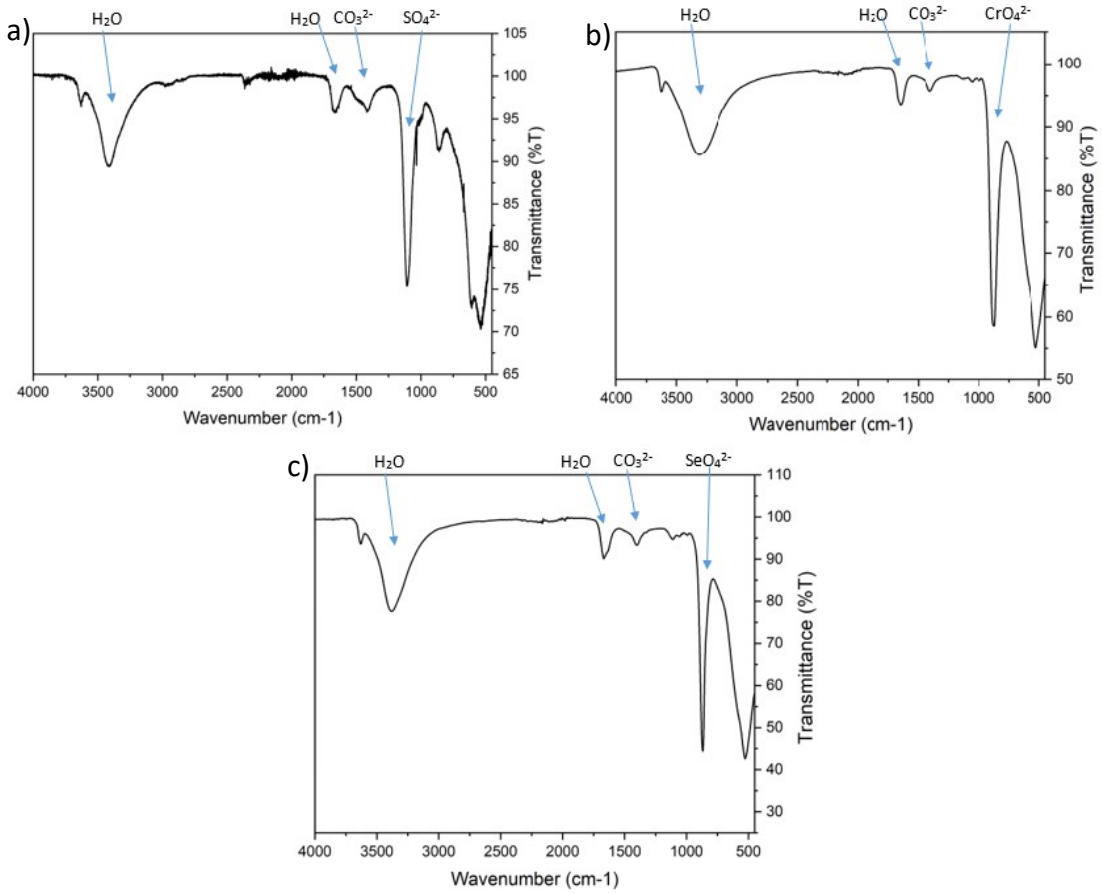

Figure 3.6 a) b) and c): FTIR data for synthesised a) sulfate ettringite, b) chromate ettringite, and c) selenate ettringite samples, with bands for key functional groups indicated by arrows and labels

Table 3.4: FTIR bands related to functional groups present in spectra for sulfate, chromate and selenate ettringite samples

Functional Group	**Wavenumber (cm^{-1})**
Water stretch $\tilde{\nu}_1$	3200-3570 (broad)
Water bend $\tilde{\nu}_2$	1600-1650
Carbonate $\tilde{\nu}_3$	1429-1492
Sulfate $\tilde{\nu}_3$	1105
Carbonate $\tilde{\nu}_2$	873
Chromate $\tilde{\nu}_3$	863
Selenate $\tilde{\nu}_3$	856
Carbonate $\tilde{\nu}_4$	706
Sulfate $\tilde{\nu}_4$	611

The spectra from all three samples are very similar, with all containing the bands associated to water, and the bands for sulfate, chromate and selenate are each present respectively. The presence of the carbonate bands (1429 cm^{-1} and 873 cm^{-1}) in all of the spectra is notable, as the presence of carbonate in these ettringite structures ($Ca_6[Al(OH)_6]_2(XO_4)_3.26H_2O$, X = S, Cr, Se) is not expected and we do not observe the contraction in the *c* unit cell parameter which usually occurs when carbonate is incorporated into ettringite. From the PXRD data, reflections at ~ 15.65 ° 2θ in the patterns for chromate ettringite and selenate ettringite can be assigned to calcite ($CaCO_3$). Although they are very small intensity reflections, the presence of carbonate in the FTIR spectra can be attributed to the impurity phase, calcite. Calcite can form during the synthesis of ettringite phases when air is not excluded from the reaction vessel, as the calcium containing reagent can react with carbon dioxide absorbed from the air. Reflections assigned to calcite are not present in the PXRD pattern for sulfate ettringite, but the FTIR spectrum contains the bands for carbonate at both 1430 cm^{-1} and 873 cm^{-1}. Calcite could be present in this sample in amounts too low to be observed by PXRD or it could be incorporating into the ettringite structures in small amounts.

SEM images were acquired on the samples of sulfate ettringite, chromate ettringite and selenate ettringite synthesised using reaction times of 7 days. The previous PXRD and FTIR data in this chapter was collected on samples synthesised with a reaction time of 1 day. This was due to the availability of synchrotron experimental time, so, high resolution PXRD data were not collected on samples synthesised with a 7 day reaction time. However, the SEM images were acquired on 7 day reaction time samples, as these samples were made up of larger crystallites which were more separated, and made observing the morphology easier. The 7 day samples were confirmed by laboratory PXRD to have the same diffraction patterns as the 1 day samples and the diffraction patterns for the 7 day samples are included in Appendix 1. The SEM images are presented in Figure 3.7 a) b) and c) below and allow the morphology of the ettringite analogue phases to be compared.

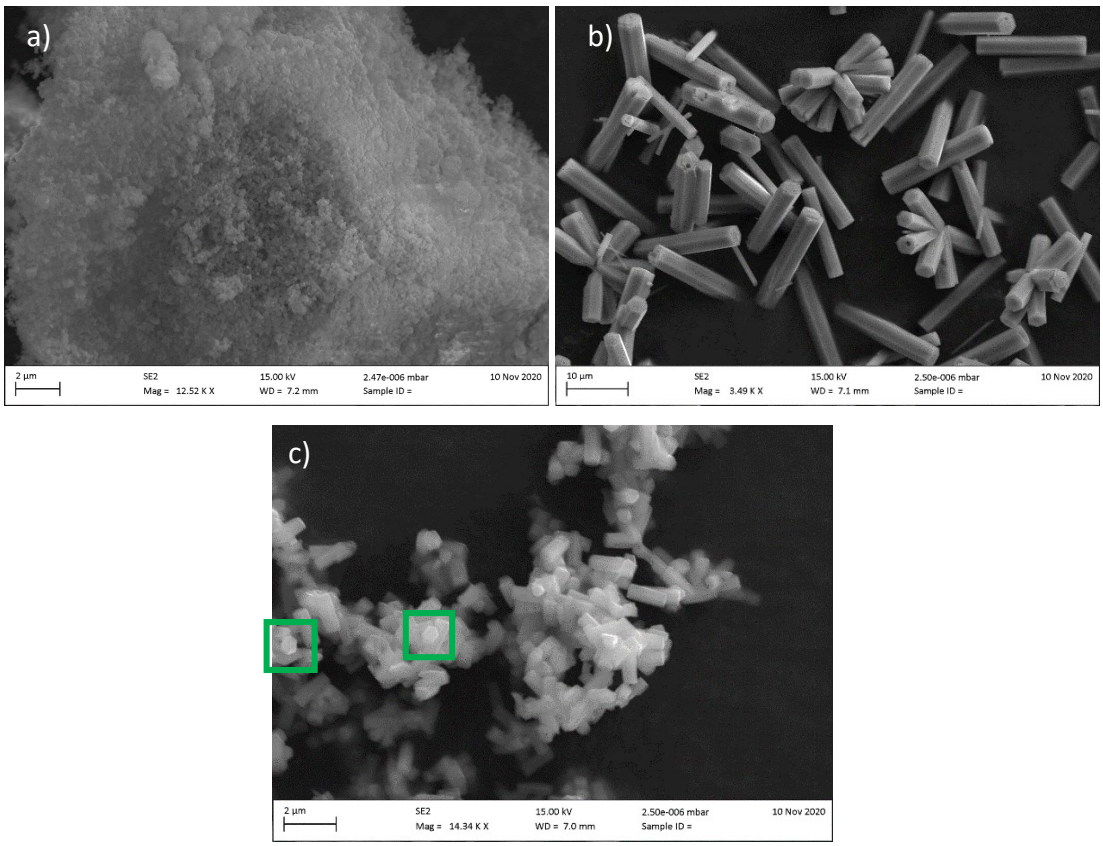

Figure 3.7 a) b) and c) SEM images of a) sulfate ettringite, b) chromate ettringite and c) selenate ettringite synthesised using the saccharate method with synthesis times of 7 days. (hexagonal faces highlighted using green boxes in c))

It is important to note that the SEM images presented in Figure 3.7 a) b) and c) have different magnifications. The images of the samples of sulfate ettringite and selenate ettringite (a and c) have approximately the same scale but image b) of the sample of chromate ettringite has a magnification 3x lower. The images presented used the magnification that gave the clearest picture of the crystallites for each sample.

Ettringite has been previously reported to crystallise with a hexagonal prismatic morphology[19] and this is what can be observed for the synthesised samples of chromate ettringite and selenate ettringite (Figure 3.7 b and c). The SEM image of the chromate ettringite sample revealed that it is made up of large and well defined hexagonal prismatic crystallites. Most of the crystallites are similarly sized (~20 µm in length) with a smaller number of crystallites that are thinner, suggesting different stages of growth. EDS analysis (EDS spectra included in Appendix 1) on various points, both faces and edges, of the crystallites showed the presence of calcium, aluminium, chromium, and oxygen. The SEM image of selenate ettringite showed that the sample is also made up of hexagonal prismatic crystallites. They are smaller in length (~ 1 µm) than the chromate ettringite crystallites. Even with their small size the hexagonal faces on the ends of the crystallites can be clearly seen (examples are identified with green boxes on Figure 3.7 c). The image of the selenate ettringite is less sharply focussed on the crystallites than the other two and the reason for this is the extremely small size of the crystallites. The synthesised sample was a very fine powder made up of the tiny crystallites which meant some had sunk into the carbon substrate on the SEM stub. This made focussing on the crystallites difficult. EDS analysis of the crystallites was performed, and the EDS spectra are shown in Appendix 1. The spectra contained peaks for calcium, aluminium, selenium, and oxygen.

The SEM image of sulfate ettringite (Figure 3.7 a) showed that the sample was comprised of large (> 20 µm) agglomerates, which were made up of very small crystallites. Whether or not the smaller crystallites that make up these agglomerates were hexagonal prisms was not able to be observed/ resolved with the SEM. The SEM image does not reveal the characteristic hexagonal prismatic morphology for samples of sulfate ettringite synthesised with this method.

This study has shown that sulfate ettringite and its chromium and selenium containing analogue phases $Ca_6[Al(OH)_6]_2(XO_4)_3.26H_2O$, X = S, Cr, Se) can be synthesised successfully and with a relatively short reaction time (24 hours). This means that formation of these phases could potentially be used to remediate hexavalent chromium or selenium containing wastes. The viability of this will be tested in the following chapters using a precipitation/ solidification method.

3.4 Structure Solution of a Synthesised Sample of Monochromate

Monochromate ($3CaO.Al_2O_3.CaCrO_4.14H_2O$) is an analogue of monosulfate ($3CaO.Al_2O_3.CaSO_4.14H_2O$) and as monosulfate is a phase produced in cement as part of the same hydration process that produces ettringite, its analogues will also be investigated in this study. As described in the introduction, monochromate phases have been reported but there is currently no consensus on crystal structure. A sample of monochromate was synthesised using the method described in Section 2.1.1.3. The PXRD data for this sample were collected on the high resolution beamline I11 at the Diamond Light Source synchrotron which means the data quality are high, which may allow full structural refinement of the data to be carried out. The PXRD pattern is shown in Figure 3.8 and the reflections assigned to monochromate were indexed. Pawley refinements were performed using the published unit cell parameters for monochromate (Table 3.1). Pawley refinement of the data using the published models with *c* parameters ~30 Å, gave very poor fits to the data, with some reflections present in the data not taken into account by the model. Refining using the parameters published by Segni[14] and Rapin[13] gave better fits but using the model published by Segni to carry out Rietveld refinement of the data gave unstable refinements. For this reason, it was decided to perform a full index of the pattern using Topas. The results of the indexing assigned the space group P3c1 the highest goodness of fit (GOF) with unit cell parameters a = 5.7669 Å, c = 20.2762 Å. This was

a different space group than was found by any of the previous studies but with comparable unit cell parameters to the structures described by Segni[14] and Rapin[13].

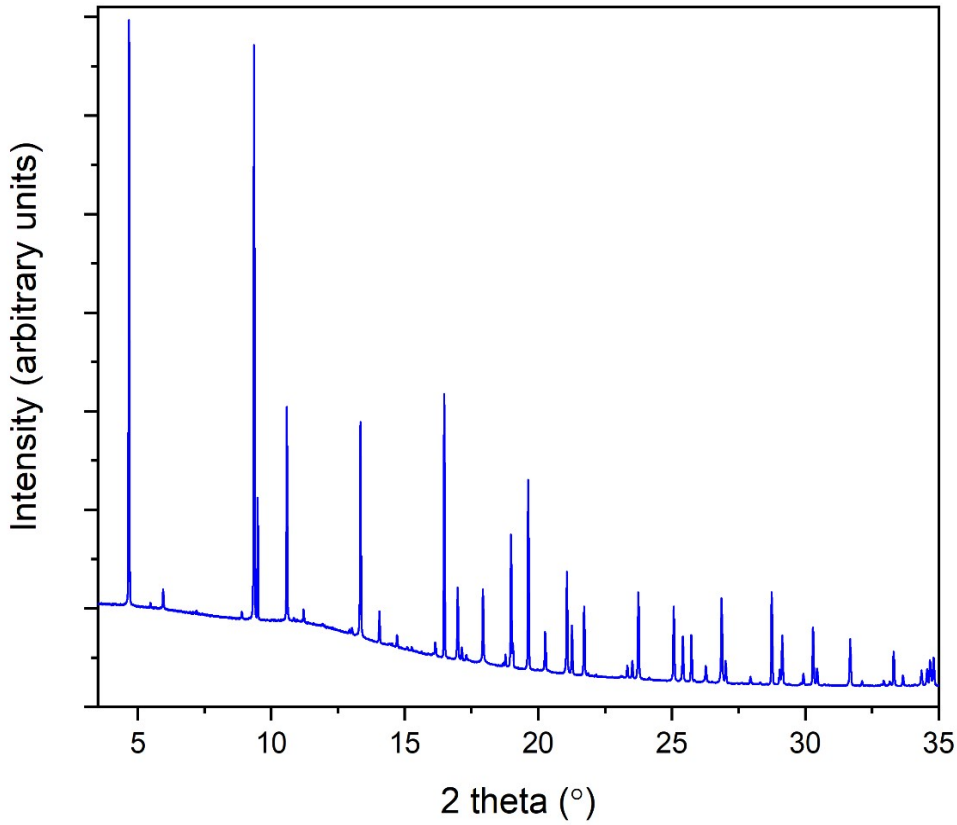

Figure 3.8: PXRD pattern for the monochromate phase "0.2 M K_2CrO_4 1 month sample" (data collected on I11 at the Diamond Light Source Synchrotron, λ = 0.82661 Å)

A search of literature of the crystal structures of layered double hydroxide minerals found none crystallising in the space group P3c1. However, the layered double hydroxide phase known as "binitroaluminate" ($3CaO.Al_2O_3.Ca(NO_3)_2.10H_2O$) crystallised in the space group P-3c1 with unit cell parameters a = 5.7445 Å, c = 17.2350 Å. The structural model was published by Renaudin and Francois in 1999[20] and the published atomic positions, thermal parameters and occupancies are given in Table 3.5. The structural model for binitroaluminate is shown in Figure 3.9 and the PXRD pattern that this model generates is shown in Figure 3.10. From the occupancies of the nitro groups shown in Table 3.5, we can see that there is a level

of disorder between the layers of this structure, which has been seen previously for the structural models of monosulfate and the monochromate model proposed by Segni (Figure 3.1).

Table 3.5: Published atomic positions, thermal parameters and occupancies for binitroaluminate (ICSD structure 280171)

Site	Multiplicity	x	y	z	Thermal Parameter	Occupancy
Al1	2b	0	0	0	0	1
Ca1	4d	0	1/3	2/3	0	1
O1	12g	0.3070	0.0572	0.05807	0.02	1
O2	4d	1/3	2/3	0.1765	0	0.5
O3	12g	0.287	0.579	0.1741	0.072	1/6
N1	12g	0.428	0.745	0.2254	0.052	1/6
O4	12g	0.394	0.680	0.2965	0.044	1/6
O5	12g	0.619	0.974	0.2061	0.106	1/6
O6	12g	1.045	0.908	0.264	0.128	1/6

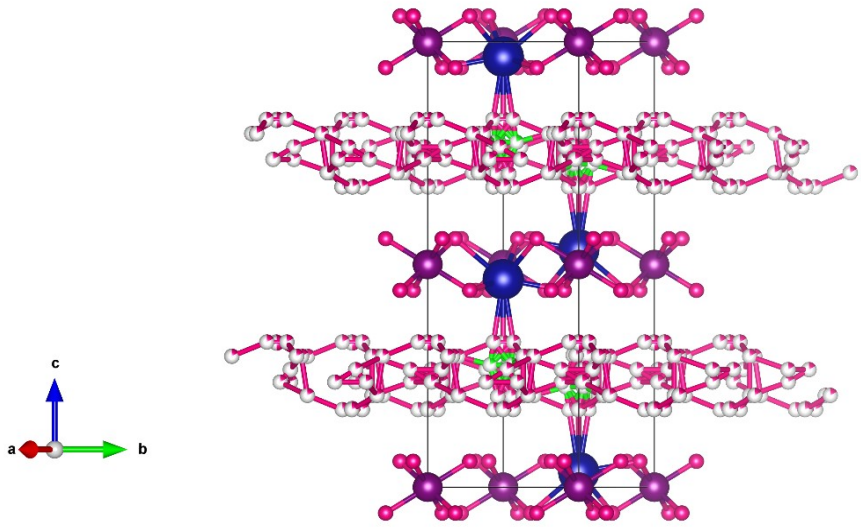

Figure 3.9: Projection of the binitroaluminate crystal structure (generated from ICSD structure 280171) Blue = calcium, purple = aluminium, pink = oxygen, green = nitrogen

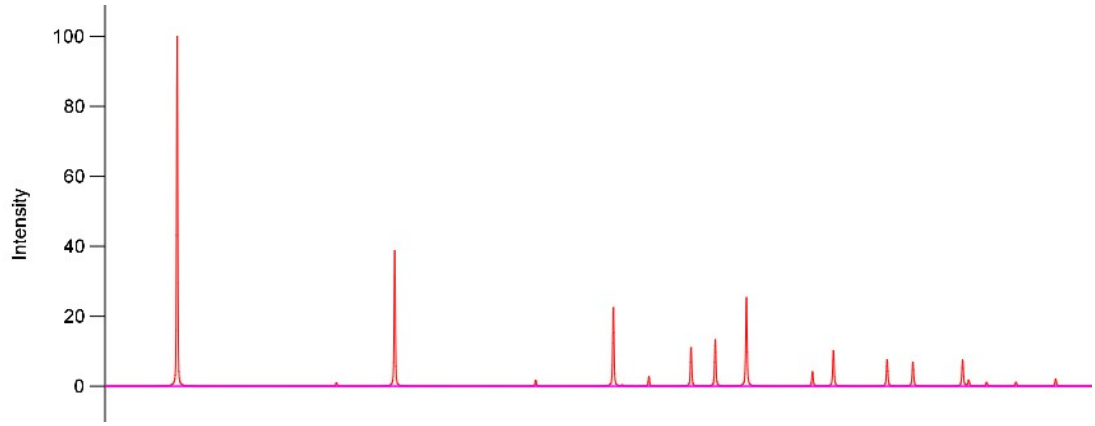

Figure 3.10: Theoretical PXRD pattern generated from the binitroaluminate crystal structure model (using synchrotron wavelength, λ = 0.82661 Å)

This theoretical PXRD pattern does not match well with the data acquired on the monochromate phase (Figure 3.8), however the crystallographic information could be adapted to generate a starting model for analysis of the data. Using the International Tables for Crystallography the binitroaluminate structural model was converted from space group P-3c1 to the space group P3c1 by comparison of the special and general positions of both space groups. The unit cell parameters were changed to those calculated from indexing the data (a = 5.7669 Å, c = 20.2762 Å), and the nitrogen sites were changed to chromium sites with the occupancy halved in order to correct for the differing stoichiometry. The modified structural model is given in Table 3.6. A projection of the crystal structure model is shown in Figure 3.11 and the theoretical PXRD pattern is shown in Figure 3.12 along with the PXRD pattern collected on the synthesised sample to allow comparison.

Table 3.6: Atomic site positions and other crystallographic information for the predicted monochromate crystal structure

Site	Multiplicity	x	y	z	Thermal Parameter (Beq Å²)	Occupancy
Al1	2a	0	0	0.5	1	1
Ca1	2b	1/3	2/3	0.03345	1	1
Ca2	2c	2/3	1/3	0.96655	1	1
O1A	6d	0.307	0.0572	0.05807	1	1
O1B	6d	0.693	0.9428	0.94193	1	1
O2A	2b	1/3	2/3	0.1765	1	1/2
O2B	2c	2/3	1/3	0.8235	1	1/2
O3A	6d	0.287	0.579	0.1741	1	1/6
O3B	6d	0.713	0.421	0.8259	1	1/6
Cr1	6d	0.428	0.745	0.2254	1	1/12
Cr2	6d	0.572	0.255	0.745	1	1/12
O4A	6d	0.394	0.68	0.2965	1	1/6
O4B	6d	0.606	0.32	0.7035	1	1/6
O5A	6d	0.619	0.974	0.2061	1	1/6
O5B	6d	0.381	0.026	0.7939	1	1/6
O6A	6d	0.045	0.908	0.264	1	1/6
O6B	6d	0.955	0.092	0.736	1	1/6

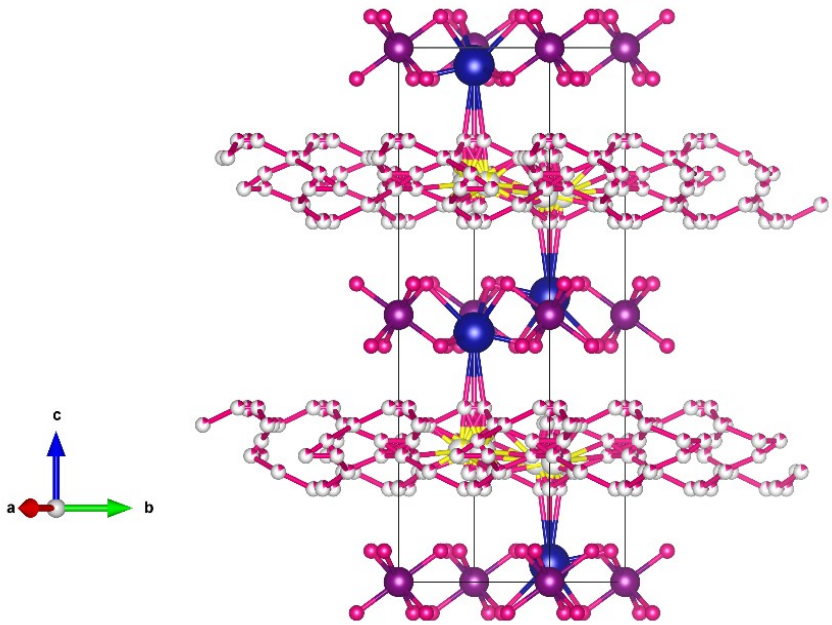

Figure 3.11: Projection of the predicted monochromate crystal structure. Blue = calcium, purple = aluminium, pink = oxygen, yellow = chromium

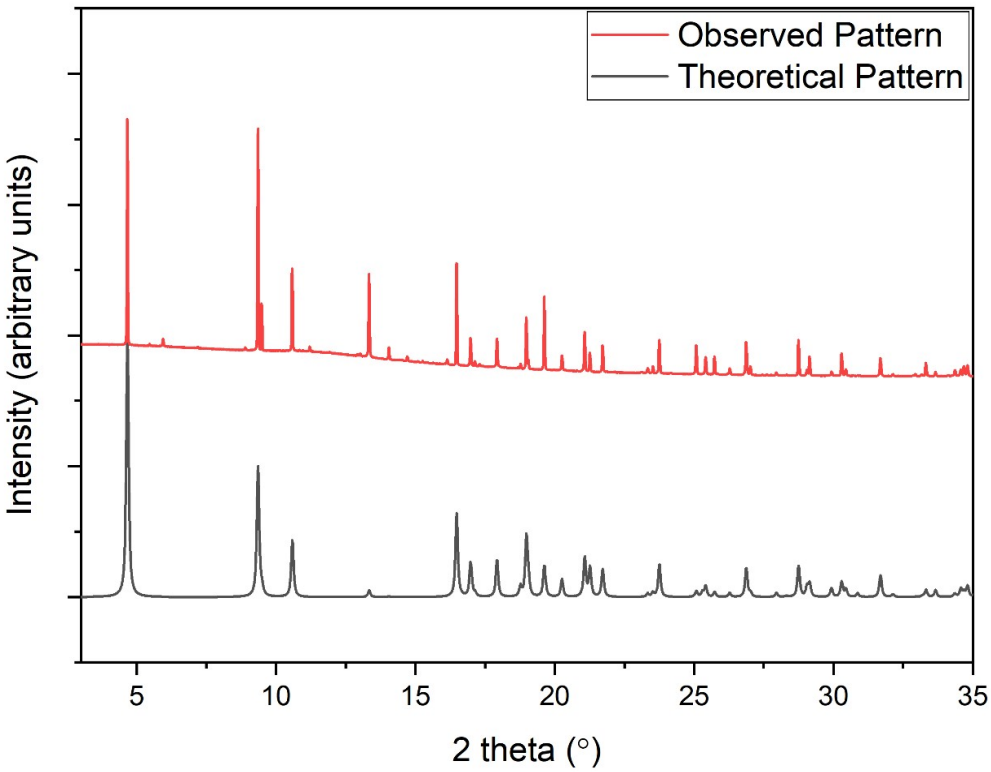

Figure 3.12: Theoretical PXRD pattern generated from the predicted monochromate crystal structure model (Table 3.6) compared to the PXRD pattern collected on the synthesised sample of monochromate (synchrotron wavelength used, λ = 0.82661 Å)

This theoretical PXRD pattern matched more closely with the data collected on the synthesised sample, suggesting that this model more closely represents the structure of the monochromate sample. However, there are issues with the positions of the chromium sites between the layers. To determine the positions of the chromium sites a difference Fourier map was generated. A difference Fourier map shows areas where electron density has been measured in the PXRD data but has not been taken into account by the current model. It is calculated using the differences between the structure factor amplitudes observed from the PXRD data and the structure factor amplitudes that are calculated from the model being used, these being called the Fourier coefficients.

As it is the positions of the chromate anions between the layers that are uncertain, an adapted model where only the layers were included (sites Al1, Ca1, Ca2, O1A, and O1B) was created (Figure 3.13 a)). Rietveld refinement of the PXRD data was carried out using this model, and the Fourier coefficients were extracted from this process. A difference Fourier map was plotted in VESTA using the information from this process and is shown in Figure 3.13 b).

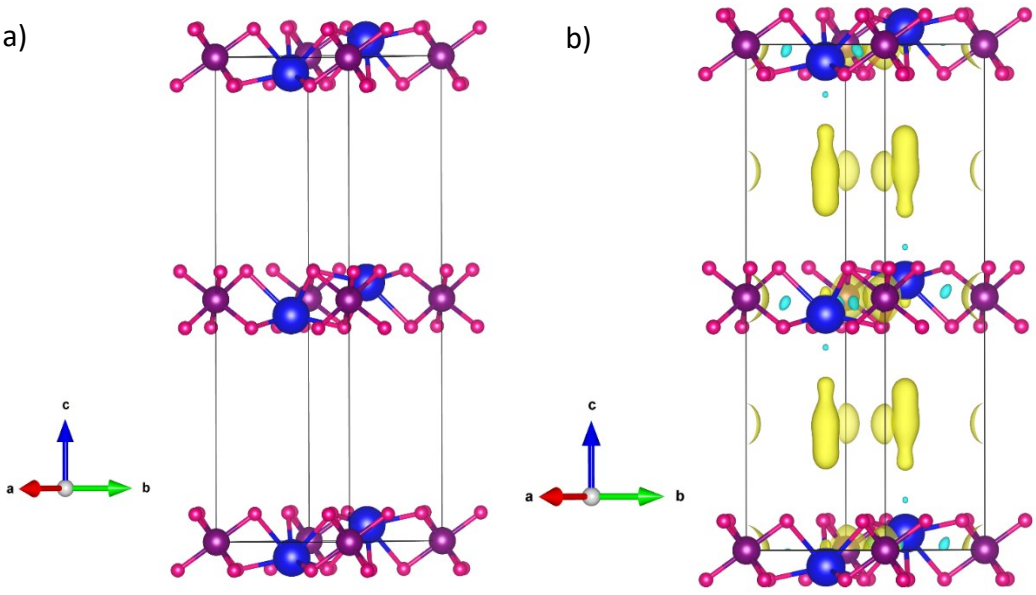

Figure 3.13 a) and b): a) Projection of the layer structure of the monochromate structure. Blue = calcium, purple = aluminium, pink = oxygen. b) Difference fourier map generated from PXRD data collected on a synthesised monochromate sample. Blue = calcium, purple = aluminium, pink = oxygen

The areas of electron density which are not taken into account by the model are shown by the yellow isosurfaces on the difference Fourier map in Figure 3.13 b). From this map, it can be observed that there are areas of electron density centred on sites at (1/3, 2/3, z) and (2/3, 1/3, z). It can be assumed that these sites are where the chromate anions are positioned in the unit cell. There are also spheres of unaccounted for electron density on the edges of the unit cell at z = 1/4 and 3/4. A new model was proposed with chromium located on all of these positions. For the new chromium sites inside the unit cell, z was set to 1/4 and 3/4 (e.g. (1/3, 2/3, 3/4) and (2/3, 1/3, 1/4) and allowed to refine as the area of electron density shown on the map was not spherical or situated on these exact positions.

Rietveld refinement of the PXRD data was performed using this new model and the observed, calculated and difference profiles are shown in Figure 3.14. The refinement strategy involved modelling the background using a Chebychev function and the peak shapes using the modified Thomson-Cox-Hasting pseudo Voigt function. The simple axial model was used to model the asymmetry of low angle peaks. The unit cell parameters were allowed to refine, along with the background and peak shape. After the refinement of these parameters had converged, the thermal parameters were constrained in sets of atom types and all were allowed to refine, except for the thermal parameter of the Al site which had to be fixed. The site occupancies were allowed to refine, and this resulted in some of the oxygen sites refining to zero occupancy and being removed from the model. Finally, the *z* positional parameters of sites Cr1, Cr2 were allowed to refine, along with the positional parameters of site O6. Using this model gave a good fit to the data, with an R_{wp} = 4.75, and the unit cell parameters refined in the space group P3c1 to *a* = 5.76706 (4) Å and *c* = 20.2748 (3) Å. A projection of the structure after refinement is shown in Figure 3.15 and the refined positions, occupancies and thermal parameters of the final model are given in Table 3.7.

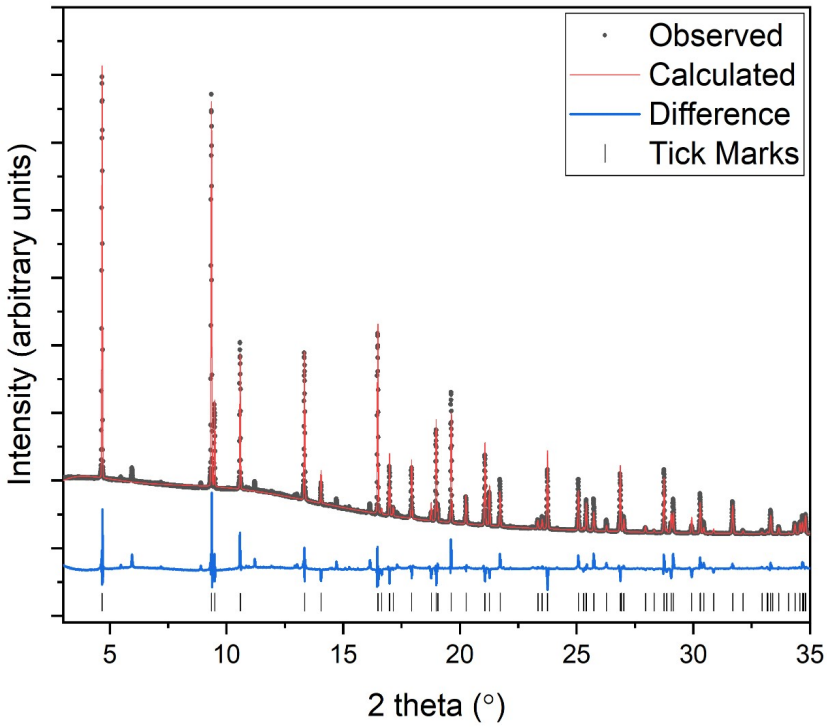

Figure 3.14: Observed-calculated-difference profiles for data collected on the synthesised monochromate sample (data collected on I11 at the Diamond Light Source Synchrotron, λ = 0.82661 Å) and refined using the Rietveld method against the new model

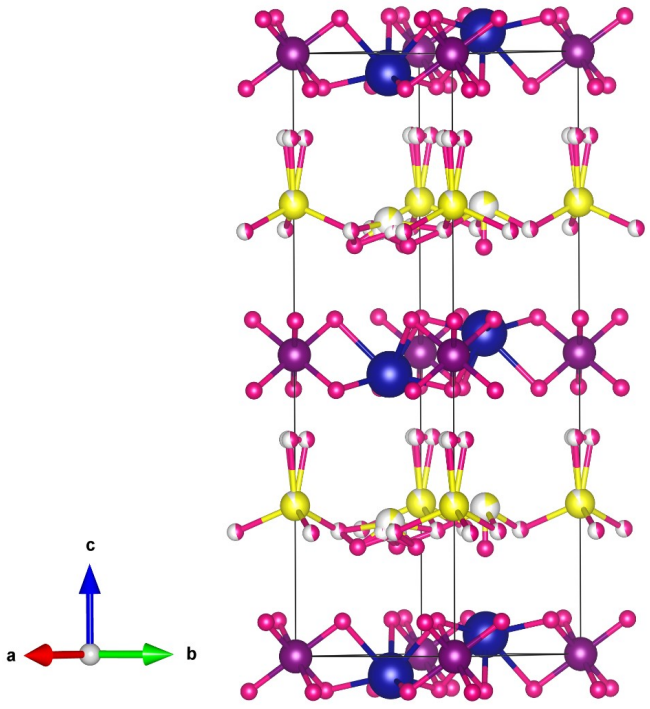

Figure 3.15: Structural model of the monochromate crystal structure with Cr sites on positions suggested by the difference Fourier map, after Rietveld refinement of the PXRD data. Blue = calcium, purple = aluminium, pink = oxygen, yellow = chromium

Table 3.7: Atomic site positions and other crystallographic information for the monochromate crystal structure after Rietveld refinement

Site	Multiplicity	x	y	z	Occupancy	Thermal Parameter (Beq Å^2)
Al1	2a	0	0	0.5	1	1
Ca1	2b	1/3	2/3	0.0335	1	2.66
Ca2	2c	2/3	1/3	0.9666	1	2.66
O1A	6d	0.307	0.0572	0.0581	1	2.52
O1B	6d	0.693	0.9428	0.9419	1	2.52
O2A	2b	1/3	2/3	0.1765	1.12	2.52
O5A	6d	0.619	0.974	0.2061	0.40	2.52
O6A	6d	-0.083	0.937	0.3558	0.40	2.52
O6B	6d	0.771	0.166	0.6907	0.89	2.52
Cr1	2c	2/3	1/3	0.1677	0.30	10.21
Cr2	2b	1/3	2/3	0.7504	0.19	10.21
Cr3	2a	0	0	0.75	0.90	10.21

By using the information gained from the difference Fourier map, the fit to the collected PXRD data has improved, suggesting that the model produced is a good approximation for the structure of monochromate ($3CaO.Al_2O_3.CaCrO_4.14H_2O$). There are clearly some issues with the oxygen positions and chromium site occupancies, but as this experiment used powder X-ray diffraction data collected using transmission geometry, it would be very difficult to fully resolve these. Furthermore, the hydrous nature of the monochromate product, where units of water can be added or removed readily[12] and are held loosely by hydrogen bonds in the interlayer, means that the interlayer arrangement of the water molecules is likely to be highly disordered. It can also be assumed that due to the disordered nature of the interlayer, the synthesis method can influence the structure, and that samples produced under different reaction conditions could have different interlayer

arrangements. This could explain why there is no consensus in the literature on the exact structure of this compound. The model produced in this study is a good approximation of the structure and can be used in future work to confirm the presence of monochromate in products and carry out phase quantification analysis. Further work using different techniques such as low temperature neutron diffraction would be needed to accurately refine the oxygen positions.

3.5 CONCLUSIONS

A pure sample of ettringite ($Ca_6[Al(OH)_6]_2(SO_4)_3.26H_2O$) was synthesised using the saccharate method. The unit cell parameters were refined using the Rietveld method in the space group P31c to *a* = 11.2243 (7) Å, *c* = 21.456 (2) Å, confirming that ettringite had been successfully synthesised. This study also successfully synthesised chromate and selenate ettringite analogue phases ($Ca_6[Al(OH)_6]_2(XO_4)_3.26H_2O$, X = Cr, Se) using the saccharate method. The unit cell parameters were refined and the unit cells were found to be larger in the *a* direction for the chromium and selenium containing analogues compared to the sulfur containing ettringite phase.

Structural studies, including indexing the PXRD data, of a synthesised sample of monochromate ($3CaO.Al_2O_3.CaCrO_4.14H_2O$) led to the conclusion that the sample produced in this study crystallised in the space group P3c1. An approximate model was created and the theoretical PXRD pattern closely matched the observed PXRD data, with Rietveld refinement of the data giving an Rwp of 4.75. However, accurate chromium and oxygen positions could not be determined from this study alone. Further work is needed, and low temperature neutron diffraction studies would be necessary to confirm the oxygen positions. It is likely that due to the disordered interlayer structure, the use of different synthesis conditions results in different interlayer structures forming. This is observed in the variety of different structures for monochromate that have been proposed in other published studies.

3.6 REFERENCES

1 M. C. Simoes, K. J. Hughes, D. B. Ingham, L. Ma and M. Pourkashanian, *Inorg. Chem.*, 2017, **56**, 7566–7573.

2 H. K. Roobottom, H. Donald, B. Jenkins, J. Passmore and L. Glasser, *Thermochemical Radii of Complex Ions*, 1999, vol. 76.

3 H. Pöllmann, S. Auer, H.-J. Kuzel and R. Wenda, *Cem. Concr. Res.*, 1993, **23**, 422–430.

4 R. B. Perkins and C. D. Palmer, *Appl. Geochemistry*, 2000, **15**, 1203–1218.

5 I. Odler and S. Abdul-Maula, *Cem. Concr. Res.*, 1984, **14**, 133–141.

6 D. J. Hassett, G. J. McCarthy, P. Kumarathasan and D. Pflughoeft-Hassett, *Mater. Res. Bull.*, 1990, **25**, 1347–1354.

7 B. Guo, K. Sasaki and T. Hirajima, *Cem. Concr. Res.*, 2017, **99**, 30–37.

8 B. Guo, K. Sasaki and T. Hirajima, *Cem. Concr. Res.*, 2017, **100**, 166–175.

9 H. F. W. Taylor, *Cement chemistry 2nd Edition*, Thomas Telford, London, 2nd edn., 1997.

10 H. J. Kuzel, *Cem. Concr. Compos.*, 1996, **18**, 195–203.

11 S. M. Leisinger, B. Lothenbach, G. Le Saout and C. A. Johnson, *Cem. Concr. Res.*, 2012, **42**, 158–165.

12 J. Göske, U. König and H. Pöllmann, *Mater. Sci. Forum*, 2004, **443–444**, 299–302.

13 J.-P. Rapin, Universite Henri Poincare, 2001.

14 R. Segni, Universite Blaise Pascal, 2005.

15 R. Allmann, *Neues Jahrb.Mineral. Monatsh.*, 1977, **3**, 136–144.

16 R. L. Norman, S. E. Dann, S. C. Hogg and C. A. Kirk, *Solid State Sci.*, 2013, **25**, 110–117.

17 S. J. Louisnathan, R. J. Hill and G. V. Gibbs, *Phys. Chem. Miner.*, 1977, **1**, 53–69.

18 T. J. Dines and S. Inglis, *Phys. Chem. Chem. Phys.*, 2003, **5**, 1320–1328.

19 A. E. Moore and H. F. W. Taylor, *Acta Crystallogr. Sect. B Struct. Crystallogr. Cryst. Chem.*, 1970, **26**, 386–393.

20 G. Renaudin and M. François, *Acta Crystallogr. Sect. C Cryst. Struct. Commun.*, 1999, **55**, 835–838.

CHAPTER 4 INVESTIGATING THE USE OF C3A TO REMOVE HEXAVALENT CHROMIUM AND SELENIUM FROM SOLUTION

4.1 INTRODUCTION

This study is focussed on using the precipitation of ettringite type phases as a method for the remediation of hexavalent chromium and selenium. Chapter 3 investigated the synthesis of ettringite analogue phases containing chromate or selenate ($Ca_6[Al(OH)_6]_2(XO_4)_3.26H_2O$, X = Cr, Se). The synthesis of these phases was successful.

As has been described in Chapter 1.4, hexavalent chromium and selenium are hazardous elements that are produced by industry and can be found polluting public water sources[1–4]. To remediate solutions containing chromate or selenate a start material was chosen that, when added to the solution, could result in the precipitation of chromate ettringite or selenate ettringite. By encapsulating the ions in a solid phase they can be easily filtered out, thus remediating the water. For this study, tricalcium aluminate (C3A, $Ca_3Al_2O_6$) was chosen as it provides a source of both calcium and aluminium. Also, it is a phase present in cement clinkers and during the process of cement hydration it forms ettringite ($Ca_6[Al(OH)_6]_2(SO_4)_3.26H_2O$) by reaction with the gypsum ($CaSO_4.2H_2O$), which is added to control the setting. It is this behaviour that was exploited to form ettringite analogue phases in solutions containing chromate or selenate. In order for a remediation method to be feasible for implementation in a real-world scenario, the process should be as simple as possible and having a single starting material is advantageous as it simplifies the process. The various processes that C3A undergoes during cement hydration have been outlined in Chapter 1 and are summarised in Equations (1) and (2). (1) C3A reacts with gypsum ($CaSO_4.2H_2O$) to produce ettringite, then (2) ettringite reacts with more C3A to form monosulfate ($3CaO.Al_2O_3.CaSO_4.14H_2O$)[5,6].

(1) $Ca_3Al_2O_6 + 3(CaSO_4.2H_2O) + 26H_2O \rightarrow Ca_6[Al(OH)_6]_2(SO_4)_3.26H_2O$

(2) $Ca_6[Al(OH)_6]_2(SO_4)_3.26H_2O + 2Ca_3Al_2O_6 + 10H_2O \rightarrow 3(3CaO.Al_2O_3.CaSO_4.14H_2O)$

Equations (1) and (2): Reactions of C3A during cement hydration that produce ettringite and monosulfate

In this study, C3A was added to solutions containing either chromate or selenate anions. If the C3A is in excess of the chromate or selenate ions present in solution then it is likely, based on the reactions that occur in cement, that an ettringite analogue phase will form initially and subsequently undergo further reaction with unreacted C3A in the system, forming a monosulfate analogue phase (e.g. monochromate or monoselenate). As both an ettringite analogue phase and a monosulfate analogue phase contain encapsulated waste ions, both were acceptable end products.

In Chapter 3, examples of the monochromate crystal structure ($3CaO.Al_2O_3.CaCrO_4.nH_2O$), reported in literature were discussed[7–10] and the crystal structure of a synthesised sample of monochromate ($3CaO.Al_2O_3.CaCrO_4.14H_2O$) was determined from synchrotron PXRD data. It is reported that mono phases can have different hydration levels e.g. $3CaO.Al_2O_3.CaCrO_4.nH_2O$, n = 9, 12, 14. A study by Göske, König and Pöllmann (2004) used thermogravimetric analysis and powder X-ray diffraction to assign the peak position of the (002) reflection for monochromate phases to different hydration levels[8]. The d spacing of the (002) reflections and the hydration levels are presented in Table 4.1.

Table 4.1: d spacing of the (002) reflection of monochromate phases determined by Goske et al.

Hydration Level (n in $3CaO.Al_2O_3.CaCrO_4.nH_2O$)	d spacing of (002) reflection (Å)
9	8.402
12	9.742
14	10.238

The information presented in Table 4.1 was used to identify the mono phases and their hydration levels during the time resolved experiment in this chapter, with the monoselenate phases assumed to be structurally analogous to monochromate, as is the case for selenate ettringite and chromate ettringite.

The overall viability of this method for remediation of chromium and selenium was assessed by measuring the amount of waste ions in the solid products. The specific phases that the waste ion is encapsulated in were monitored at various time points as the reaction progressed. Knowing which phases form at different times during the reaction of C3A with Cr or Se is important for planning a waste remediation strategy where it may be more desirable to target one specific product.

4.2 AIMS

The formation of chromate and selenate ettringite ($Ca_6[Al(OH)_6]_2(XO_4)_3.26H_2O$, X = Cr, Se) phases was investigated in this study as a method for the removal of hexavalent chromium and selenium, which are waste ions present in some contaminated waters. Tricalcium aluminate ($Ca_3Al_2O_6$, C3A) was added to aqueous solutions with varying concentrations of either CrO_4^{2-} or SeO_4^{2-}. The solid phases formed at various reaction times were separated and analysed using PXRD, FTIR, SEM and ICP-OES to determine what structures had formed and to what extent the chromium/ selenium had been incorporated into the solid phase. The results of this investigation will be used to determine whether this method is viable for use in waste remediation.

4.3 THE STRUCTURE OF TRICALCIUM ALUMINATE (C3A)

The previous chapter has shown the successful synthesis of ettringite analogue phases containing hexavalent chromium or selenium. This chapter tests out a potential waste remediation strategy for these ions. C3A ($Ca_3Al_2O_6$) was added to a solution containing either hexavalent chromium or selenium. Cubic C3A was synthesised using a high temperature solid state method described in Section 2.1.1.2. An orthorhombic polymorph of C3A also exists and is the major form in cement systems when there is a moderate sodium content[11]. The sodium dopes the C3A ($Na_{2x}Ca_{3-x}Al_2O_6$) and when the sodium content is $0.16 \leq x \leq 0.20$ the orthorhombic polymorph is stabilised. For this study, there was no sodium present during the synthesis of C3A, resulting in production of the cubic form of C3A. Its structure was studied in detail, with both powder X-ray diffraction (PXRD) and powder neutron diffraction (PND) data collected on samples. Images of the powder sample were also acquired using SEM.

4.3.1 Rietveld Refinement of the Structure of C3A from Synchrotron PXRD Data

The powder X-ray diffraction pattern of a sample of C3A was measured on the high resolution powder diffraction beamline, I11, at the Diamond Light Source synchrotron. The unit cell parameters, atomic positions and thermal parameters of the crystal structure were refined using the Rietveld method against the ICSD structure 1841 for C3A[12]. The refinement strategy involved modelling the background using a Chebychev function and the peak shapes using the modified Thomson-Cox-Hasting pseudo Voigt function. The simple axial model was used to model the asymmetry of low angle peaks. The unit cell parameters were allowed to refine, along with the background and peak shape. After the refinement of these parameters had converged, the atomic positions from the published C3A structural model were allowed to refine. The thermal parameters of the Ca and Al sites were refined but the

thermal parameters for the O sites had to be constrained in order to give a stable refinement.

The observed, calculated and difference profiles from the refinement are shown in Figure 4.1, and the refined atomic positions and thermal parameters are tabulated in Table 4.2. The unit cell parameters refined in the space group Pa3 to a = 15.2670 (1) Å, which compares well to the published values reported by Mondal and Jeffrey, a = 15.263 Å.[12]

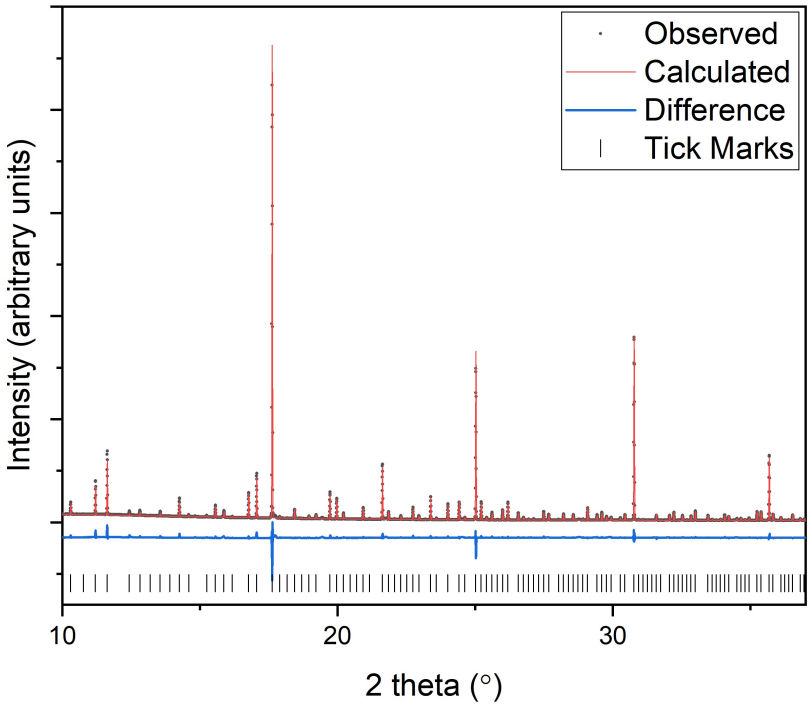

Figure 4.1: Observed-calculated-difference profiles from data collected on a sample of C3A on the I11 beamline at the Diamond Light Source synchrotron (λ = 0.82661 Å) and refined using the Rietveld method against the ICSD structure 1841

Table 4.2: Refined atomic positions and thermal parameters for a synthesised sample of C3A, synchrotron x-ray diffraction data refined using the Rietveld method against ICSD structure 1841

Atomic Position	**x**	**y**	**z**	**Thermal parameter (Beq Å^2)**
Ca1	0	0	0	0.2 (1)
Ca2	0.5	0	0	0.04 (9)
Ca3	0.2561	0.2561	0.2561	0.1 (1)
Ca4	0.3750	0.3750	0.3750	0.76 (8)
Ca5	0.1399 (1)	0.3766 (1)	0.1271 (2)	0.58 (6)
Ca6	0.3802 (2)	0.3844 (1)	0.1210 (1)	0.08 (6)
Al1	0.2534 (2)	0.0153 (2)	0.0206 (2)	0.42 (8)
Al2	0.2437 (2)	0.2327 (2)	0.0059 (2)	0.13 (9)
O1	0.2798 (3)	0.1240 (5)	0.0095 (3)	0.01
O2	0.4828 (4)	0.1328 (5)	0.2528 (3)	0.01
O3	0.2663 (4)	0.2835 (4)	0.1043 (4)	0.01
O4	0.2351 (4)	0.4048 (4)	0.2949 (4)	0.01
O5	0.3495 (4)	-0.0409 (4)	-0.0174 (4)	0.01
O6	0.1484 (4)	-0.0115 (4)	-0.0249 (4)	0.01

Although the refined unit cell parameters were consistent with literature data, the thermal parameters for the oxygen sites had to be constrained to stop them consistently refining to negative values. For this reason, it was decided to analyse a sample of synthesised C3A using powder neutron diffraction as this technique can often give more accurate refinement of oxygen positions.

4.3.2 Rietveld Refinement of the Structure of C3A from Neutron Diffraction Data

A sample of C3A was also analysed on the POLARIS beamline at the ISIS Neutron and Muon Source. The POLARIS beamline is a high intensity, medium resolution powder diffractometer. The unit cell parameters, atomic positions and thermal parameters of the crystal structure were refined using the Rietveld method on the data collected from Bank 4. The same strategy for Rietveld refinement was used as before with the powder X-ray diffraction data. The unit cell parameters were fixed to those obtained from refinement of the PXRD data, a = 15.267 (4) Å (literature value, a = 15.236 Å)[12] and the zero point was refined to obtain a stable refinement. The observed, calculated and difference profiles obtained from the Rietveld refinement are shown in Figure 4.2 and the refined atomic positions and thermal parameters are displayed in Table 4.3.

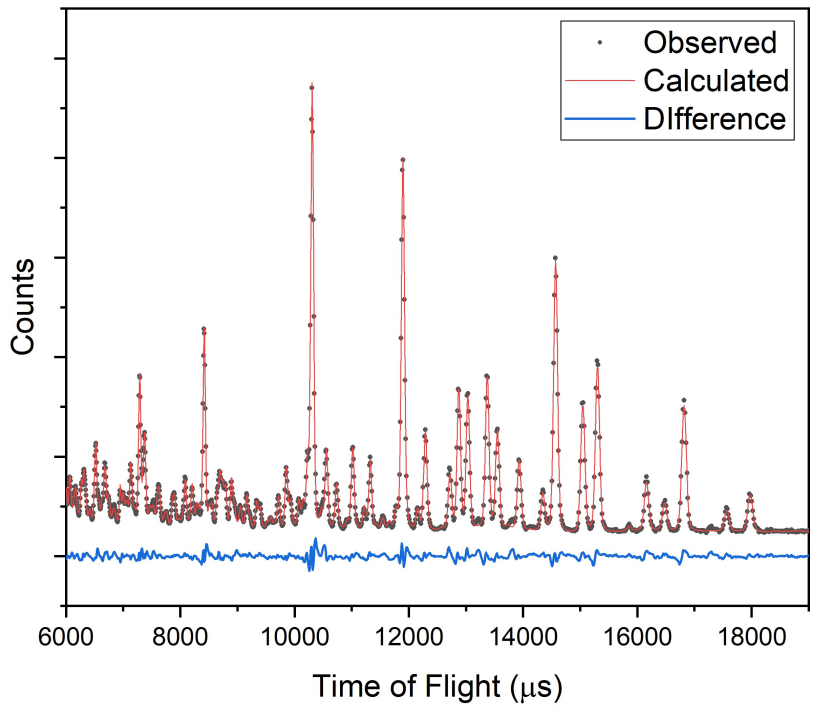

Figure 4.2: Observed-calculated-difference profiles from Time of Flight Neutron Diffraction data collected by bank 4 on a sample of C3A at the POLARIS beamline at ISIS Neutron and Muon Source and refined using the Rietveld method against the ICSD structure 1841

Table 4.3: Refined atomic positions and thermal parameters for a synthesised sample of C3A, neutron diffraction data refined using the Rietveld method against ICSD structure 1841

Atomic Position	x	y	z	Thermal parameter (Beq Å^2)
Ca1	0	0	0	1.3 (4)
Ca2	0.5	0	0	0.4 (3)
Ca3	0.2561	0.2561	0.2561	0.4 (3)
Ca4	0.3750	0.3750	0.3750	1.8 (3)
Ca5	0.1367 (5)	0.3757 (5)	0.1260 (6)	1.2 (1)
Ca6	0.3799 (5)	0.3843 (4)	0.1198 (4)	0.3 (1)
Al1	0.2538 (6)	0.0149 (7)	0.0195 (6)	0.6 (1)
Al2	0.2427 (6)	0.2329 (7)	0.0057 (6)	0.5 (2)
O1	0.2780 (3)	0.1237 (5)	0.0099 (3)	0.8 (1)
O2	0.4822 (3)	0.1314 (5)	0.2545 (3)	1.1 (1)
O3	0.2664 (3)	0.2836 (4)	0.1044 (4)	0.47 (9)
O4	0.2336 (4)	0.4042 (4)	0.2938 (4)	1.8 (1)
O5	0.3505 (4)	-0.0366 (4)	-0.0170 (3)	0.8 (1)
O6	0.1515 (4)	-0.0107 (3)	-0.0241 (3)	0.9 (1)

Refinement of the PND data, using the unit cell parameters obtained from refinement of the PXRD data, gave reliable atomic positions and the thermal parameters of the oxygen sites refined to positive values. The bond lengths from both refinements are given in Appendix 2 and both refinements gave reasonable values confirming the correct coordination of the calcium and aluminium. A projection of the C3A structure is shown in Figure 4.3 and shows that the tetrahedrally coordinated AlO_4 corner share to form 6-fold rings. The CaO_6 octahedra edge share with other CaO_6 octahedra and corner share with the AlO_4 to form the 3D network that makes up the crystal structure. Both powder diffraction methods confirm that the synthesised C3A starting material is cubic and that there are no impurity phases present.

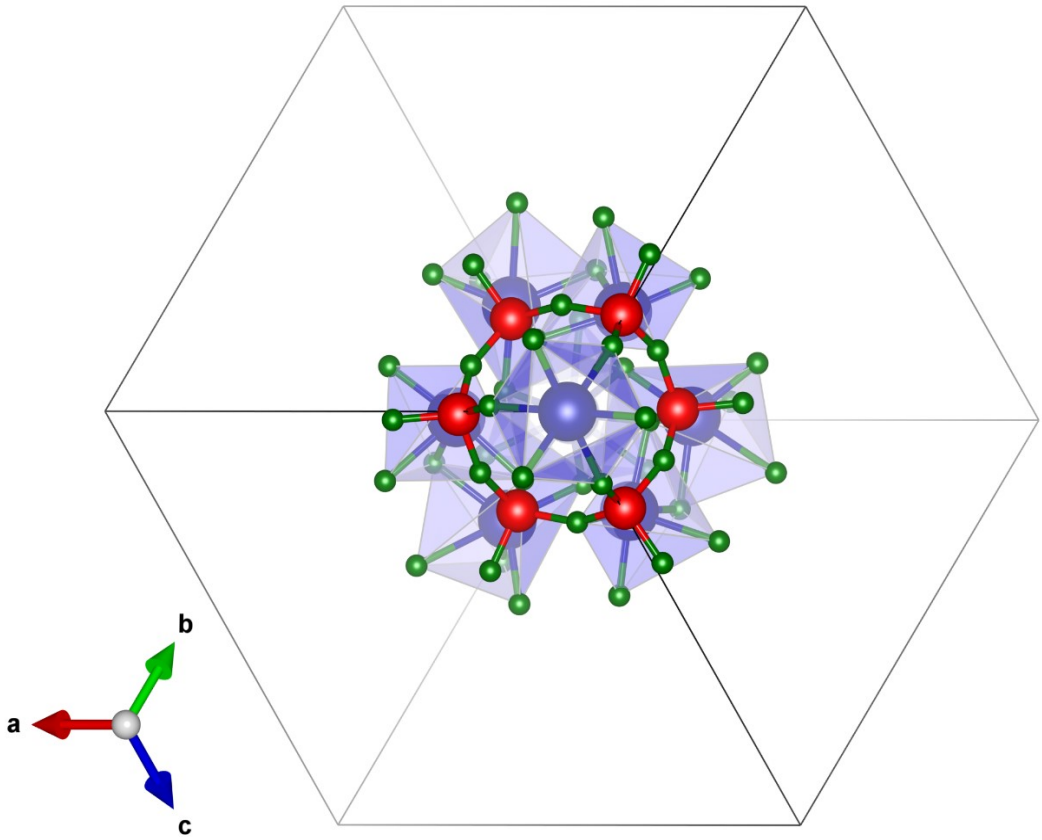

Figure 4.3: Projection of part of the C3A crystal structure, illustrating the coordination of calcium (blue) to oxygen (green), and aluminium (red) to oxygen

4.3.3 SEM Analysis of C3A

An image of the morphology of the C3A crystallites was obtained using SEM and is shown in Figure 4.4. It was observed that the sample of C3A comprised smooth agglomerates ranging in size but with approximate average diameters of ~30 µm.

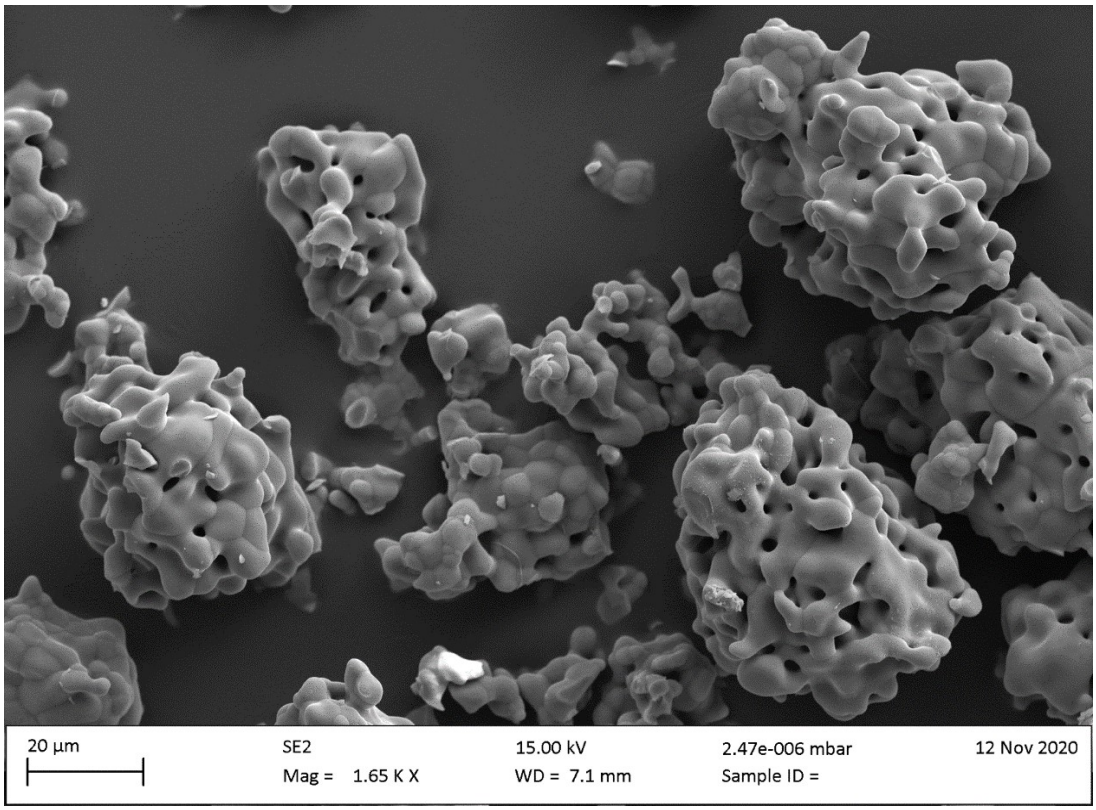

Figure 4.4: SEM image of a sample of synthesised C3A

4.4 Removal of Hexavalent Chromium from Solution Using C3A

For all of the work discussed in this chapter, the following naming convention will apply: "X M source, time" where X is the concentration of the solution, "source" is the material the solution is made from, and "time" is the reaction time when the sample was separated from the solution. For example, "0.2 M K_2CrO_4, 1 hour" is the name of the sample formed when C3A was added to a 0.2 M solution of potassium chromate with a reaction time of 1 hour.

The following time resolved experiments were carried out according to the experimental procedure described in Section 2.1.2. All solid samples were analysed using powder X-ray diffraction (PXRD), fourier transform infrared spectroscopy (FTIR) and elemental analysis using inductively coupled plasma- optical emission spectroscopy (ICP-OES).

4.4.1 Reaction of C3A with a 0.2 M K_2CrO_4 Solution

The first experiment was performed by adding C3A to a more concentrated (0.2 M) solution of potassium chromate. The reaction times at which solid samples were isolated from the solution and the phases identified by PXRD are summarised in Table 4.4. The powder diffraction patterns (collected on beamline I11 at the Diamond Light Source synchrotron) are plotted in Figure 4.5 and reflections assigned to the various identified phases are designated with symbols. The chemical formulae of the phases identified in this experiment are:

- C3A: $Ca_3Al_2O_6$
- Chromate ettringite: $Ca_6[Al(OH)_6]_2(CrO_4)_3.26H_2O$
- Monochromate $14H_2O$: $3CaO.Al_2O_3.CaCrO_4.14H_2O$
- Gypsum analogue: $CaCrO_4.2H_2O$

The above abbreviations will be used throughout the discussion of the results in this section instead of including the full chemical formulae.

Table 4.4: Summary of reaction times and phases identified by PXRD in the solid products from the experiment "0.2 M K_2CrO_4"

Time from C3A Addition	**Phases Identified by PXRD**
1 hour	C3A, monochromate $14H_2O$, chromate ettringite
3 hours	C3A, monochromate $14H_2O$, chromate ettringite
6 hours	C3A, monochromate $14H_2O$, chromate ettringite
24 hours	C3A, monochromate $14H_2O$, chromate ettringite
1 week	monochromate $14H_2O$, gypsum analogue
1 month	monochromate $14H_2O$, gypsum analogue

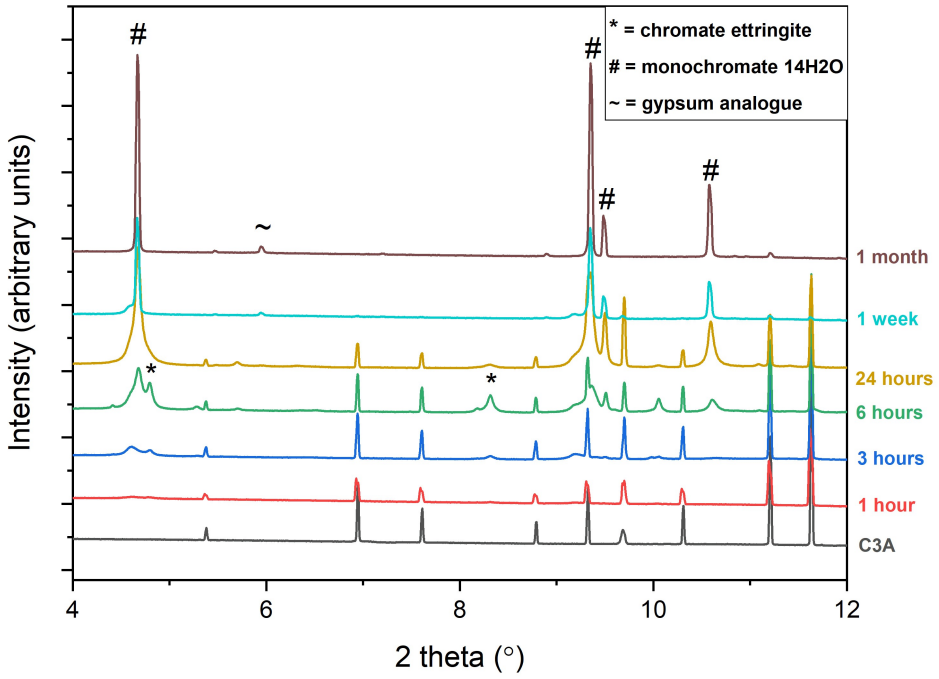

Figure 4.5: Powder X-ray diffraction patterns of the solid samples collected at various time points during the experiment "0.2 M K_2CrO_4" (data collected on I11 at the Diamond Light Source Synchrotron, λ = 0.82661 Å)

From these PXRD data the phases present in the solid at different reaction times have been identified and therefore the reaction pathway can be determined. After 1 hour, unreacted C3A is the major phase present with only low intensity reflections at 4.6 and 4.8 ° 2θ present which are assigned to chromate ettringite and monochromate $14H_2O$. These reflections grow in intensity after 6 hours of reaction but after 24 hours there are no longer any reflections which can be assigned to chromate ettringite in the PXRD data. The samples reacted for 1 week and 1 month, show monochromate $14H_2O$ as the main phase present, and there is no longer any evidence for the presence of the C3A starting material. A gypsum analogue phase ($CaCrO_4.2H_2O$) is also identified as present in these samples.

Multiphase Rietveld refinement was carried out on the collected PXRD data of these samples. This allowed Quantitative Phase Analysis (QPA) to be carried out. The QPA results, in terms of percentage of phases present as a function of time are shown in

Figure 4.6. The refinement strategy involved modelling the background using a Chebychev function and structural models for each of the identified phases were added to the refinement. The structural models used are given in Table 4.5.

Table 4.5: Table of structural models used for QPA analysis by Rietveld refinement of "0.2 M K_2CrO_4" samples

Phase	**Structural Model used**
C3A	ICSD card 1841
Chromate ettringite	Adapted from ICSD card 251756 (ettringite)
Monochromate 14H_2O	Model developed in Chapter 3.4
Gypsum analogue	Adapted from ICSD card 2058 (gypsum)

Unit cell parameters of the phases were allowed to refine first then atomic positions were allowed to refine. The peak shapes were modelled separately for each phase using modified Thomson-Cox-Hasting pseudo-Voigt functions. Likewise, separate simple axial models were used to model the asymmetry of low angle peaks.

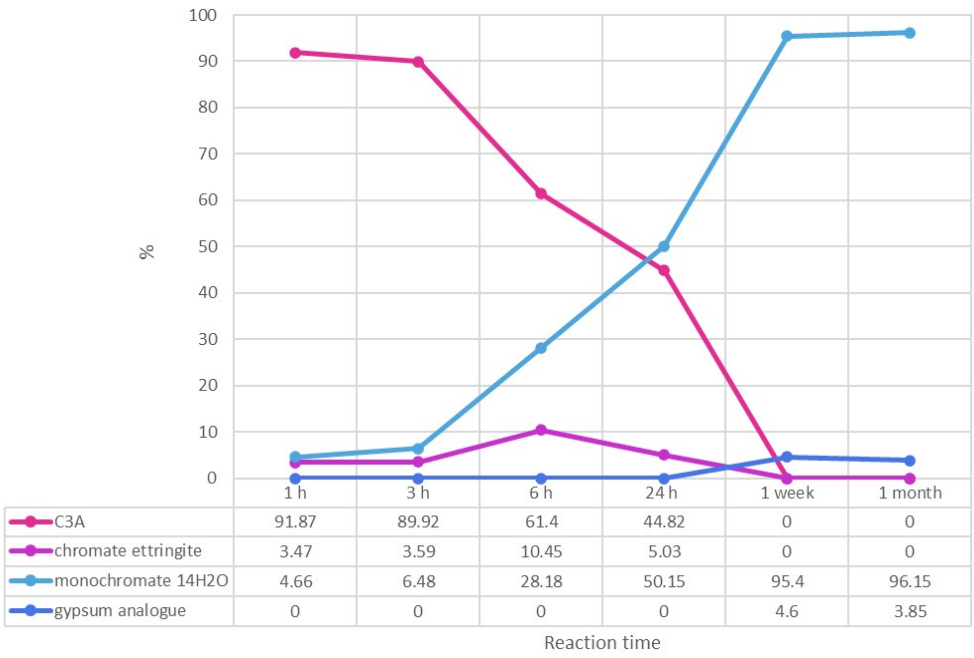

Figure 4.6: Proportions of phases identified as present by quantitative phase analysis by Rietveld refinement of "0.2 M K_2CrO_4" PXRD data

The phase quantification results clearly show that the two major phases identified by PXRD are the starting material, C3A, and the monochromate $14H_2O$ product. As the C3A content decreases it is mostly converting to the monochromate phase with only a small proportion of the solid phase (10.45 %) forming chromate ettringite at a reaction time of 6 hours. Monochromate $14H_2O$ is present in larger quantities than the starting material after a reaction time of 24 hours and after 1 week, only monochromate $14H_2O$ and ~4 % of $CaCrO_4.2H_2O$ are present.

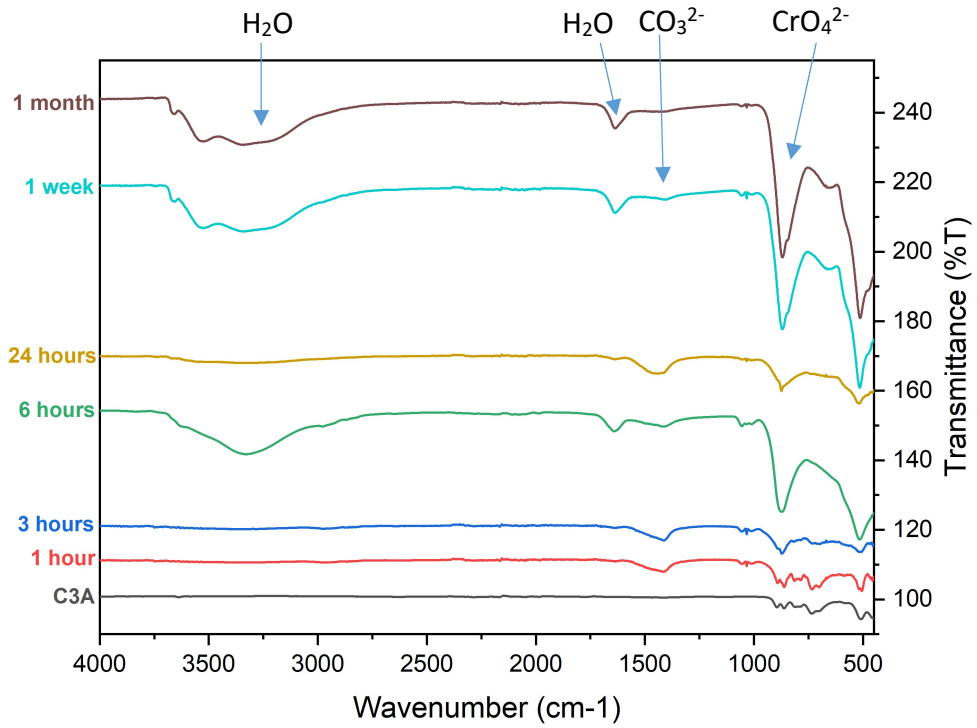

Figure 4.7: FTIR spectra of the solid samples collected at various time points during the experiment "0.2 M K_2CrO_4", with bands for key functional groups indicated by arrows and labels

FTIR spectra were also recorded on these samples (Figure 4.7) and these can be used in conjunction with the PXRD data to confirm the phases identified. The 3 hour sample has the band for chromate which supports the PXRD analysis and shows that some chromate has been removed from solution and is now in the solid phase. A carbonate stretch is observed, suggesting the presence of a carbonate containing

phase, which is not accounted for in the PXRD analysis. The carbonate stretch is also observed in all the later spectra up to a reaction time of 1 month. Monocarbonate ($3CaO.Al_2O_3.CaCO_3.nH_2O$) and hemicarbonate ($3CaO.Al_2O_3.½CaCO_3.½Ca(OH)_2.nH_2O$) phases with similar layered structures to the expected monochromate are known to exist in cement systems where there has been exposure to air[6]. In these layered "mono" phases the chromate and carbonate are positioned between the calcium alumino layers and therefore can easily exchange with other ions. So, most likely, a carbonate containing precursor (monocarbonate/ hemicarbonate) is forming and then the chromate ions exchange into the structure forming the monochromate $14H_2O$ final product. As the carbonate stretch is not present in the IR spectrum for the 1 month sample, it can be deduced that the excess of chromate in the solution has exchanged with and replaced any carbonate that had initially been absorbed from the air into the mono phase.

Combining the results from the PXRD and FTIR analysis shows that the reaction pathway is as follows:

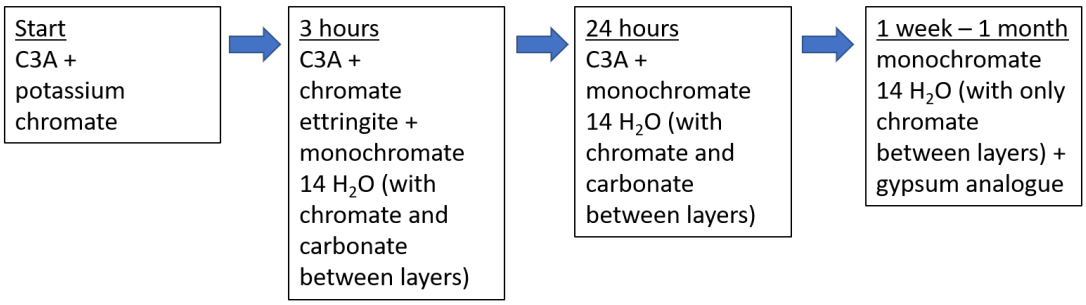

The exact mechanism of the hydration of C3A in the presence of sulfate is still debated in the literature but all now agree that ettringite forms on the surface of C3A from the slow dissolution of C3A, and when all the sulfate has depleted, the ettringite recrystallises as monosulfate[11,13]. In this analogous system, we are observing the chromate ettringite and mono phases forming simultaneously. This early monochromate formation could be due to the influence of the absorbed carbonate,

forming monocarbonate phases preferentially, which allows for the easy exchange of chromate into its layered structure.

Elemental analysis was carried out on the solid samples using ICP-OES. The solid samples were dissolved in nitric acid and diluted according to the procedure outlined in Section 2.2.4. Calcium, aluminium and chromium were measured using this technique. For each sample, the concentrations of these elements in mol/l were measured and summed together to give the total Ca, Al, Cr content. Then a relative % content was calculated for each element using the following example formula:

$$\%\ Cr = \frac{Cr\ concentration}{total\ concentration\ of\ Cr+Al+Ca}.$$

As such the results presented here do not give the absolute composition of the solid products but are indicative and can be used to confirm conclusions formed from analysis of the PXRD and FTIR data. The relative percentages of Ca, Al and Cr are presented in Figure 4.8. The raw concentration values obtained from the ICP-OES spectrometer are presented in Appendix 2.

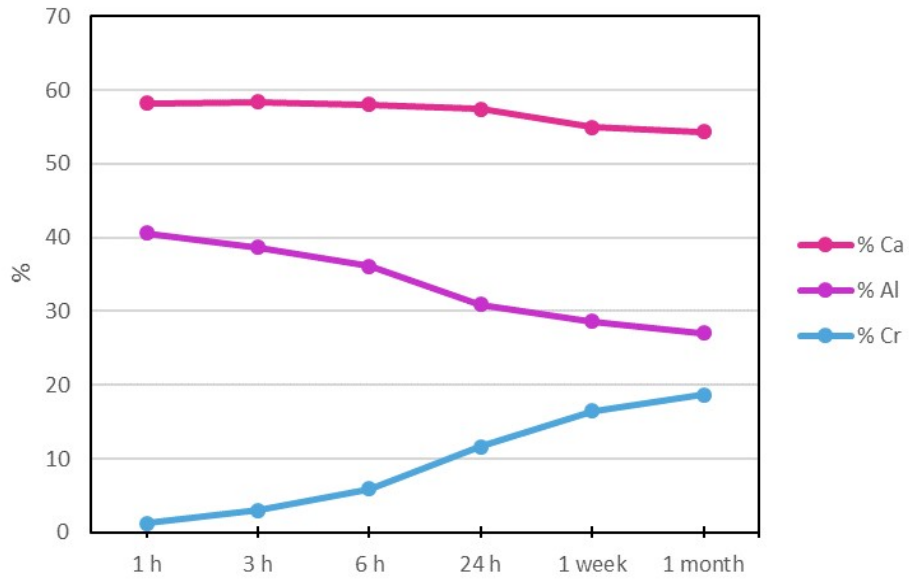

Figure 4.8: ICP-OES results for the solid samples collected at various time points during the experiment "0.2 M K_2CrO_4" expressed as relative percentages of the Ca, Al, Cr content

The elemental analysis clearly shows that the amount of chromium encapsulated in the solid phase increases as the reaction time increases. The relative calcium content stays approximately constant with the relative aluminium content decreasing as the chromium is removed from the solution into the solid phase. The 1 month sample has a relative elemental composition of 54 % calcium, 27 % aluminium and 19 % chromium which is almost equivalent to what would be expected from a pure sample of monochromate $14H_2O$ as the ideal composition of $Ca_4Al_2O_6(CrO_4).14H_2O$ expressed as the same relative percentages of Ca, Al, and Cr is 57 % calcium, 29 % aluminium, 14 % chromium. Therefore, these data can be used to confirm the PXRD results.

Ultimately, the presence of chromium in the solid phase is the most important factor for showing a viability for waste remediation as it shows that this method can be used to remove the chromium from the solution and encapsulate it into a solid phase. Identifying what crystal structure the solid phases have at certain reaction times is also important as they will all have different susceptibilities to Cr leaching.

ICP-OES analysis was also carried out on the liquid filtrate separated from the 1 month reaction time solid sample. The concentration of chromium in the solution was measured and this allows us to calculate how much chromium had been removed from the solution after 1 month of reaction with C3A. The concentration of chromium in the initial solution and the solution after 1 month is presented in Figure 4.9. The ICP-OES results show that around half of the chromium initially present in the solution has been removed and is now stabilised in the solid phase. This experiment used a 0.2 M potassium chromate solution which has a very high concentration of chromium. The chromium is in excess to the C3A added and so total removal of chromium was not possible. But a large amount was removed over 1 months reaction and this proves that this method can successfully remove chromium from solution.

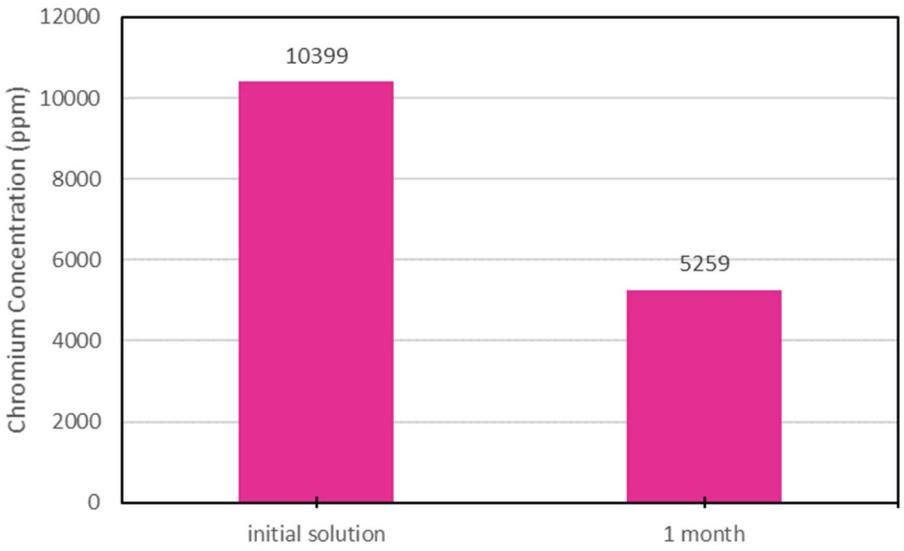

Figure 4.9: Chromium concentrations of the initial 0.2 M solution of K_2CrO_4 and the same solution after 1 month reaction with C3A

SEM images were acquired for two of the 0.2 M K_2CrO_4 samples, the 3 hour sample where there was a mixture of phases present (Figure 4.10 a)), and the 1 month sample where it presented as an almost pure monochromate phase from analysis of the PXRD data (Figure 4.10 b)). The SEM images will show the morphology of the samples and EDS analysis will identify what elements are present on specific crystallites.

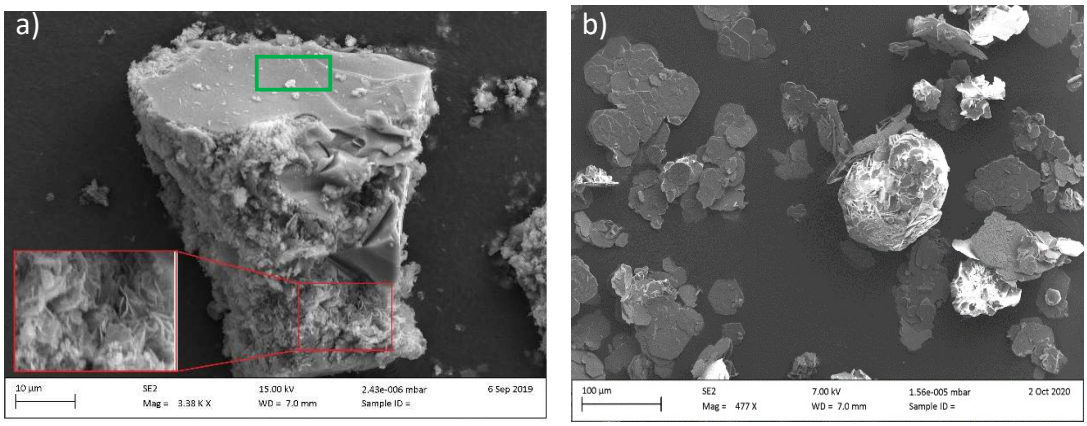

Figure 4.10 a) and b): SEM images of the 0.2 M K_2CrO_4 a) 3 hour sample (boxes and inset added to highlight areas for EDS analysis) and b) 1 month sample

Figure 4.10 a) shows that the sample after 3 hours reaction time is made up of large (~50 µm width) smooth crystallites, with smaller crystallites which appear to be "growing" on the side and are either needles or plates (highlighted in the inset). Qualitative EDS analysis was performed on specific sites and the spectra are provided in Appendix 2. The site highlighted by the red box on the figure contained calcium, aluminium, oxygen and chromium, whereas the site highlighted by the green box contained only calcium, aluminium and oxygen. This means that the image is showing a grain of C3A (the smooth large crystallite) with the chromate ettringite (needles) and monochromate (plates) phases, as observed in the PXRD for this sample, growing on the surface (the fine structured areas).

The 1 month sample was shown to have formed monochromate $14H_2O$, with a small impurity phase ($Ca_2CrO_4.2H_2O$) present by PXRD analysis. The SEM image shows us the morphology of the monochromate phase. It forms as hexagonal plates with ~40 µm diameter which can be observed on Figure 4.10 b), with some of the plates combining into larger agglomerates. Crystals shaped as hexagonal platelets have been previously reported for the mono phases which have hexagonal layered crystal structures[7]. EDS analysis (spectra provided in Appendix 2) of a variety of different points of the plates and agglomerates all gave the same result, identification of calcium, aluminium, oxygen and chromium.

These SEM images support the hypothesis that chromate ettringite is growing from the surface of the C3A grains but in this case, it appears to be at the same time as monochromate is forming which is different to literature reports for the sulfate system[11,13]. A further, more detailed SEM study including lower reaction time samples would need to be performed to fully track the morphological changes as the reaction proceeds.

4.4.2 Reaction of C3A with Solutions of K_2CrO_4 with Lower Concentrations

The solution concentration was lowered to 0.1 M, 0.02 M, and 0.01 M but the same experimental procedures as the 0.2 M K_2CrO_4 experiment were used. This section will determine differences in reaction pathways as the solutions become less concentrated and therefore closer to realistic waste-water concentrations.

4.4.2.1 PXRD

The phases identified from the PXRD analysis (collected on a laboratory D8 diffractometer) are summarised in Table 4.6. The chemical formulae for all the phases identified in this experiment are:

- C3A: $Ca_3Al_2O_6$
- Monochromate $14H_2O$: $3CaO.Al_2O_3.CaCrO_4.14H_2O$
- Monochromate $12H_2O$: $3CaO.Al_2O_3.CaCrO_4.12H_2O$
- C3AH6: $Ca_3Al_2O_6.6H_2O$ (hydrated C3A)
- Monochromate $9H_2O$: $3CaO.Al_2O_3.CaCrO_4.9H_2O$
- Monocarbonate: $3CaO.Al_2O_3.CaCO_3.11H_2O$

Throughout this section, the above names for compounds will be used in place of their chemical formulae.

Samples were taken at different reaction times for each experiment. As the aim of the experiment was to remove chromium from the solutions, samples were taken at reaction times up to 1 month, or until there was evidence that all the chromium had been removed from the solutions. Therefore, some experiments have samples taken at time points that were not necessary in others. The PXRD patterns are plotted in Figure 4.11 a), b) and c) (note, larger diagrams are presented in Appendix 2). No reliable QPA was carried out on these samples as the data were collected on a laboratory diffractometer.

Table 4.6: Summary of phases identified in the solid products from the experiments: "0.1 M K_2CrO_4", "0.02 M K_2CrO_4", "0.01 M K_2CrO_4"

Time from C3A Addition	**Phases Identified by PXRD "0.1 M"**	**Phases Identified by PXRD "0.02 M"**	**Phases Identified by PXRD "0.01 M"**
1 hour	C3A	C3A	
3 hours	C3A	C3A, monochromate $14H_2O$, amorphous content	
6 hours	C3A, monochromate $14H_2O$, amorphous content	C3A, monochromate $14H_2O$, C3AH6, amorphous content	
24 hours	C3A, monochromate $14H_2O$, amorphous content	C3A, monochromate $14H_2O$, C3AH6, amorphous content	C3A, monochromate $14H_2O$, monochromate $12H_2O$, amorphous content
3 days		C3A, monochromate $14H_2O$, C3AH6, amorphous content	monochromate $14H_2O$, monochromate $12H_2O$, monocarbonate, amorphous content
5 days			monochromate $14H_2O$, monochromate $12H_2O$, monocarbonate, amorphous content
1 week	monochromate $14H_2O$, monochromate $12H_2O$, amorphous content	monochromate 14 H_2O, monochromate 12 H_2O, C3AH6, amorphous content	monochromate $14H_2O$, monochromate $12H_2O$, monocarbonate, amorphous content
1 month	monochromate $14H_2O$, monochromate $12H_2O$, amorphous content	monochromate $14H_2O$, monochromate $12H_2O$, monochromate $9H_2O$, amorphous content	

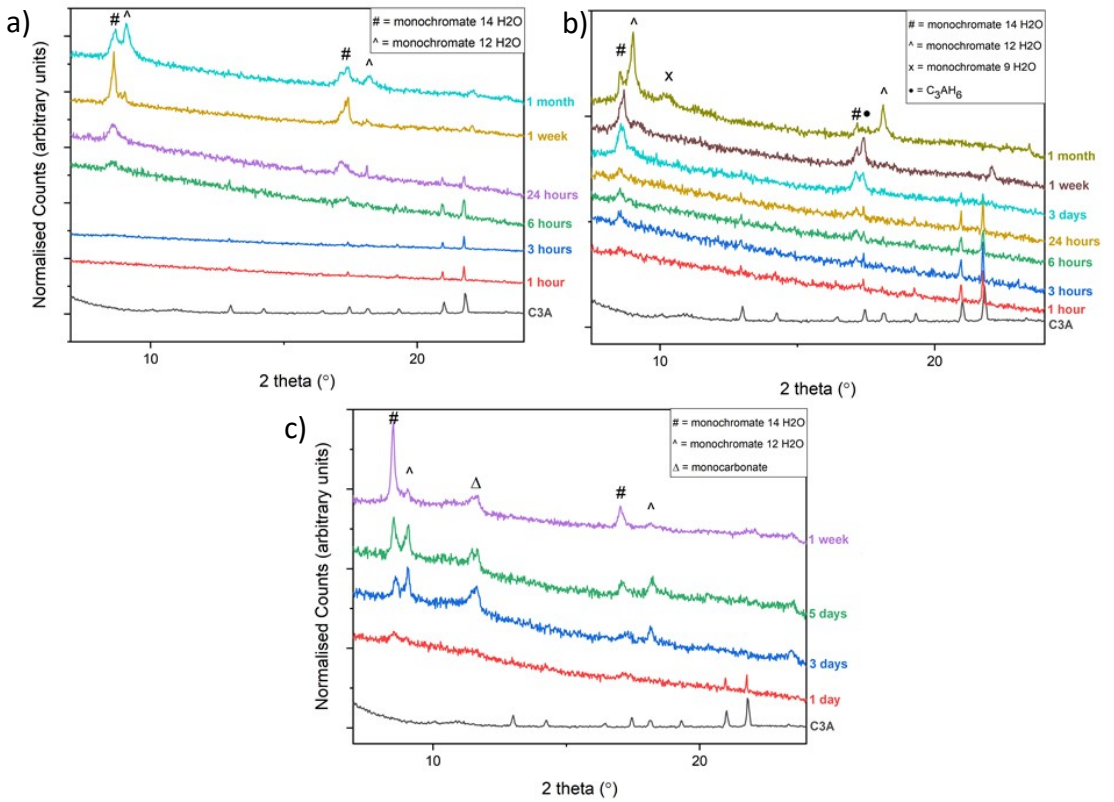

Figure 4.11 a) b) and c): Powder X-ray diffraction patterns of the solid samples collected at various time points during the experiments a) "0.1 M K_2CrO_4", b) "0.02 M K_2CrO_4", and c) "0.01 M K_2CrO_4" (all data collected on laboratory Bruker D8, λ = 1.5406 Å, transmission geometry)

The main difference we can note between the 0.2M K_2CrO_4 experiment and these experiments with a lower solution concentration is that chromate ettringite is not observed in any of the PXRD data and the chromium containing phases identified are monochromate ($3CaO.Al_2O_3.CaCrO_4.nH_2O$, n=9-14) phases. The reason that no ettringite is able to form in these lower concentration experiments is due to the stoichiometric differences in the formulae of ettringite ($Ca_6[Al(OH)_6]_2(CrO_4)_3.26H_2O$) and of monochromate ($3CaO.Al_2O_3.CaCrO_4.nH_2O$, n=9-14). Ettringite requires 3 formula units of chromate compared to 1 formula unit required for monochromate and as there is only a 2.5:1 molar ratio of chromate:C3A in this solution, it is more thermodynamically favourable for monochromate to be formed. This process occurs in cement systems, where ettringite will form from reaction of C3A and calcium sulfate hydrate until all the sulfate has been consumed, then the ettringite will react with more C3A to form monosulfate[5]. In this case, the lack of chromate means the

monochromate is forming directly from the reaction of the C3A with the chromate in solution.

In the 0.1M experiment, only the starting material, C3A, is identified until 6 hours of reaction time when the 14 H_2O form of monochromate can also be identified. After 1 week of reaction the phases present are monochromate $14H_2O$ and $12H_2O$. These are phases where the only difference is the amount of interlayer water which causes the layer spacing reflection (8.6 ° 2θ for $14H_2O$ and 9.1 ° 2θ for $12H_2O$) to shift, as a decrease in the water content of the interlayer causes the d spacing of the layers to be smaller and so the reflection appears at a higher 2θ position on the diffraction pattern. There are no phase pure products identified in this experiment as the 6 and 24 hour samples are poorly crystalline and the 1 week and 1 month samples contain a mixture of two monochromate phases with different hydration levels.

When the concentration of the solutions is lowered further for the 0.02 M and 0.01 M experiments, different hydration levels of the monochromate phases are the main products but there are also phases identified that contain no chromium. For the 0.02 M experiment C3AH6 is the hydrated form of the starting material C3A and can be identified by its (112) reflection at 17.3 º 2θ. This phase can be identified in all patterns with a reaction time of more than 6 hours. With the C3A now in excess (~2:1 molar ratio C3A:chromate) the excess C3A has hydrated as there are not enough available chromate ions in solution to react with. A similar reaction occurs in the 0.01 M experiment where the excess C3A (now ~4:1 molar ratio C3A:chromate) is not simply hydrating but reacting with carbonate absorbed from the air in the reaction vessel and forming monocarbonate. It was identified in samples with a reaction time of 3 days or greater by the presence of its (011) layer reflection at 11.5 º 2θ and its presence will be confirmed by the FTIR data. Monocarbonate has a layered crystal structure similar to the monochromate phases but with carbonate ions between the calcium aluminate layers and a smaller interlayer distance. It is possible that there may also be impurity phases present that cannot be identified from these diffraction patterns as these were measured on a laboratory diffractometer which has a lower

intensity, flux and resolution than the synchrotron beamline used for the 0.2 M samples.

4.4.2.2 FTIR

FTIR spectra were measured to confirm that even though no ettringite phases were forming, chromate was still present in the solid phases produced. The spectra are plotted in Figure 4.12 a) b) and c).

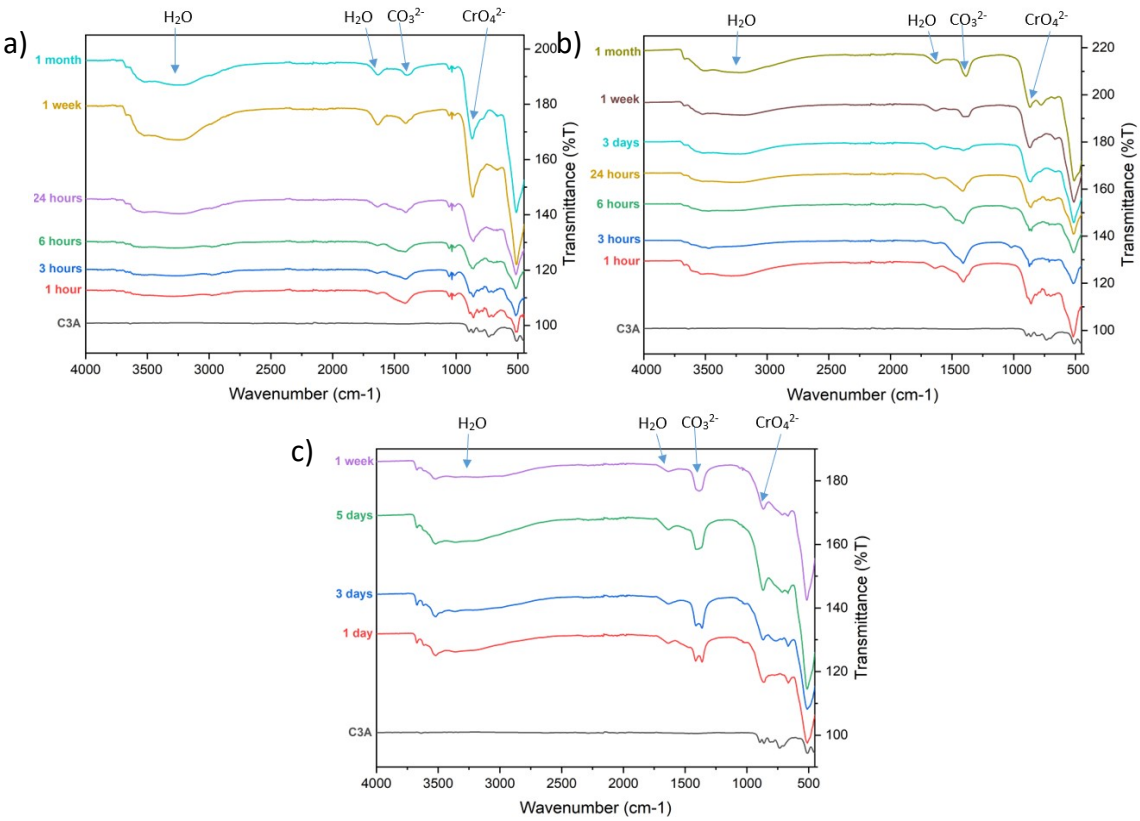

Figure 4.12 a) b) and c): FTIR spectra of the solid samples collected at various time points during the experiments a) "0.1 M K_2CrO_4", b) "0.02 M K_2CrO_4", and c) "0.01 M K_2CrO_4" with bands for key functional groups indicated by arrows and labels

The spectra for each of the samples in the 0.1 M and 0.02 M experiments contain the bands for chromate and carbonate. The PXRD patterns for the 1 hour samples (and the 3 hour sample for 0.1 M) do not show any crystalline chromate-containing phases. This suggests that carbonate and chromate may be absorbing onto the surface of the C3A, forming amorphous phases initially, or the amount of chromate-containing phases present is less than that detectable by these PXRD methods (~3-5 wt%). The carbonate bands are significant for all samples and this indicates that the monochromate phases identified have some carbonate also incorporated into the structure through absorption from the air. The carbonate stretch is still present in the spectra for the final samples, collected after 1 month of reaction. This is because there is an insufficient amount of chromate ions in these solutions, and as such they cannot replace the carbonate to produce any pure monochromate phases. It was the case with the "0.2 M K_2CrO_4 1 month" samples, that all the carbonate was replaced with chromate.

All spectra for the 0.01 M samples also show the presence of significant carbonate bands, which can be attributed to the presence of a monocarbonate phase, identified by PXRD, in the samples with reaction times of over 1 day. However, the carbonate band is prominent in the 1 day sample, which didn't have any strong reflections observed by PXRD which could be assigned to a monocarbonate phase. This suggests that monocarbonate formation had already begun at short times, but the product was either poorly crystalline, amorphous or present in quantities less than that detectable by these PXRD methods (~3-5 wt%). The carbonate band present in the spectra at ~1450 cm^{-1} also shows peak splitting which indicates that there are two different carbonate environments in the samples. This fits with the identification from PXRD that there are both monocarbonate phases and monochromate phases with some carbonate incorporated.

Overall, these results show that the absorption of carbonate is a major contributor to the products forming in these experiments where the chromium concentration is lower. As real wastewater will have a very low concentration of chromium the

absorption of carbonate should be considered in any future experiments to remediate chromium using these materials.

4.4.2.3 ICP-OES

ICP-OES was used to quantify how much chromium was in each solid sample and the elemental percentages of calcium, aluminium and chromium (relative to total Ca, Al, Cr content) are plotted in Figure 4.13 a) b) and c). The raw concentration data is given in Appendix 2.

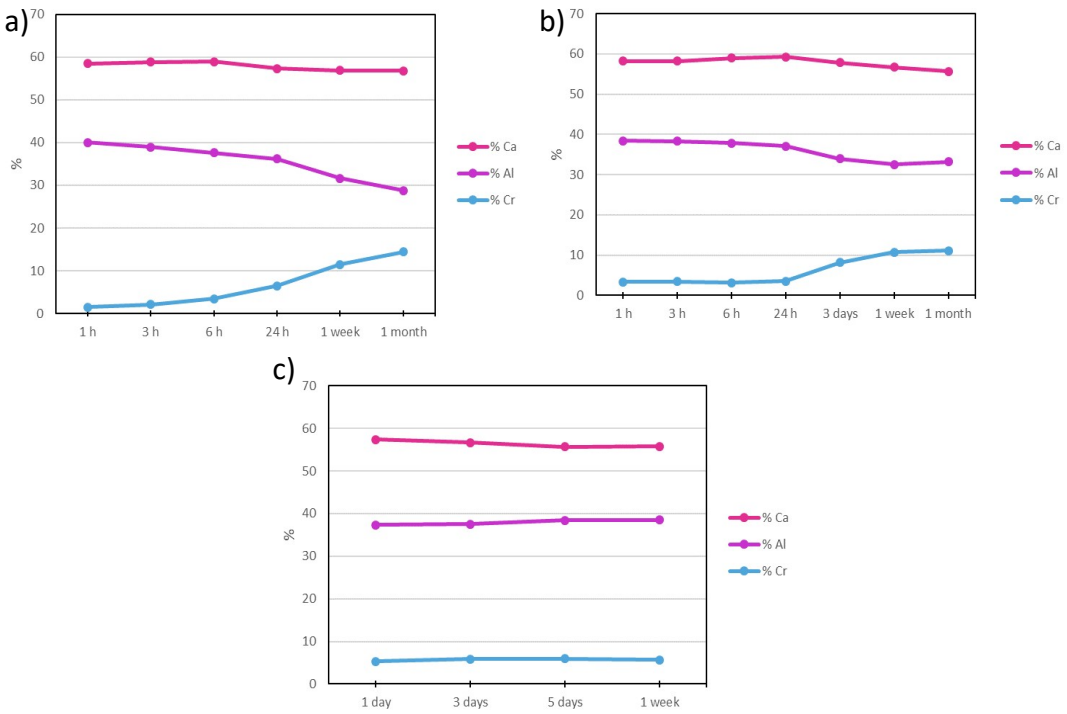

Figure 4.13 a) b) and c): ICP-OES results for the solid samples collected at various time points during the experiments a) "0.1 M K_2CrO_4" b) "0.02 M K_2CrO_4" and c) "0.01 M K_2CrO_4" expressed as relative percentages (% Ca = pink, % Al = purple, % Cr = blue)

The results obtained from ICP-OES analysis shows that chromium has been taken up from solution into the solid products after 1 hour reaction time. For the 0.1 M

experiment the measured chromium content increases with reaction time and the major uptake of chromium from the solution into the solid phase occurs after 6 hours of reaction time. This is the point in the reaction when the monochromate phases start to form in large enough quantities to be observed on the powder diffraction patterns. For the 0.02 M and 0.01 M experiments the relative % Cr plateaus and stops increasing after a point (1 week reaction for 0.02 M and 1 day reaction time for 0.01 M). This suggests that these samples have taken in the maximum amount of chromium for this system. This assumption can be further confirmed by the colour of the filtrate. The initial solutions of potassium chromate are vibrant yellow in colour, but the filtrates of the 1 week and 1 month samples for 0.02 M solutions and the 3, 5 and 7 day samples for 0.01 M solutions are colourless. As it is the presence of hexavalent chromium that is responsible for the yellow colour, the process of adding C3A to the solution has removed potentially all of the chromium at these reaction times. The final % Cr present decreases in the solid samples as the solution concentration is lowered with 14.4 % for 0.1 M 1 month, 11.1 % for 0.02 M 1 month and 5.7 % for 0.01 M 1 week. This is because there is less chromium available in the starting solution and the same starting mass of C3A used meaning the relative % content of Ca and Al will be higher than the maximum possible % Cr content for the experiments with lower solution concentrations.

It is difficult to determine if the amount of chromium measured by the ICP-OES to be in these samples is equivalent to all the chromium in the starting solution. This is because a portion of the total solid is dissolved for the ICP-OES analysis and the total solid mass cannot be accurately measured due to potential sample loss during filtration and transfer. In addition to this, as the solid samples are comprised of a mixture of phases, its exact composition is not accurately known. To confirm if all the chromium had been removed from the solutions that were colourless, ICP-OES elemental analysis was carried out on these solutions after the solid products had been separated from them. The measured chromium concentrations of the solutions after reaction with C3A for various times are presented in Figure 4.14.

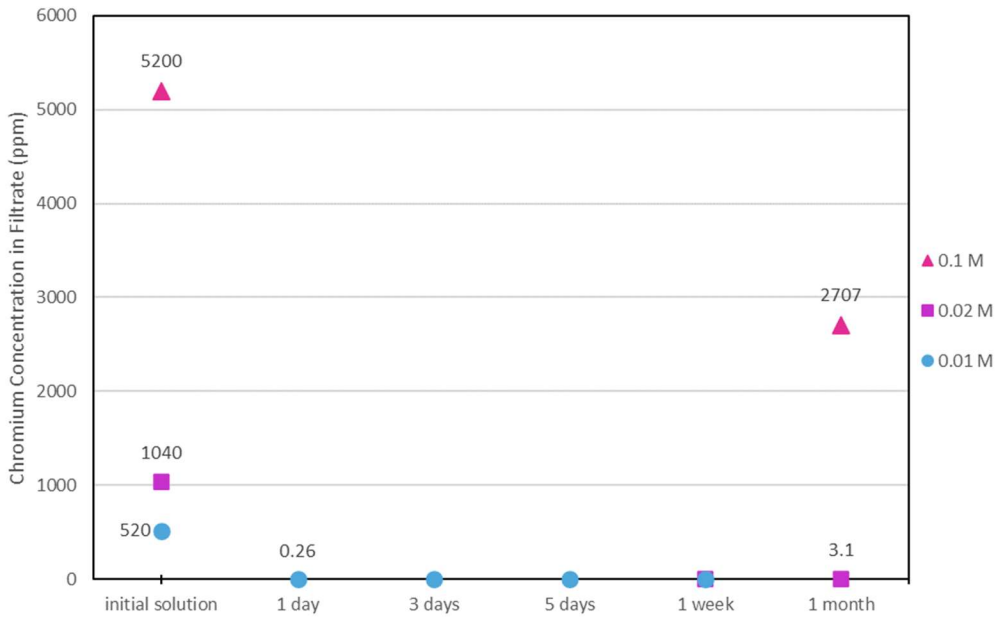

Figure 4.14: Chromium concentrations of the solutions after solid products separated, measured by ICP-OES

Elemental analysis of the solutions after reaction shows that significant amounts of chromium are being removed by this process. For the 0.1 M experiment, around half of the chromium is removed, leaving the solution with a chromium concentration of 2707 ppm. But the lower concentration experiments have successfully removed practically all of the chromium, within error, with the 0.02 M experiment starting with a solution concentration of 1040 ppm and ending with 3.1 ppm after 1 week of reaction with C3A. The 0.01 M experiment started with a chromium concentration of 520 ppm and after only 1 day this reduced to 0.26 ppm. This experimental procedure has been proven to be extremely efficient at removing chromium from solution, which makes it very promising for implementation to real waste remediation situations.

This study into removing hexavalent chromium using C3A as a starting material has proven that this method results in successful removal of chromium from solution and its encapsulation in a solid phase. Differences that occur when lower concentration chromium solutions are used have been identified, with monochromate phases found to be the dominant products, not the chromate containing ettringite analogue

phase. Carbonate was found to easily incorporate into the solid products of these reactions, with this being more pronounced at lower solution concentrations. These are all important factors to consider when further developing this as a waste remediation process.

4.5 Removal of Hexavalent Selenium from Solution Using C3A

The time resolved ion removal experiments were also carried out for hexavalent selenium. C3A was again used as the single starting material, added to the solutions of sodium selenate (Na_2SeO_4) to encapsulate selenate ions into a solid product. The same experimental procedures as used for the chromium removal experiments were repeated here and the same solution concentrations and reaction times were used to allow comparison of the experimental results.

4.5.1 Reaction of C3A with a 0.2 M Na_2SeO_4 Solution

The concentration of the solution for this set of experiments was 0.2 M. The phases identified from the PXRD analysis (collected on beamline I11 at the Diamond Light Source synchrotron) are summarised in Table 4.7 and the powder diffraction patterns are plotted in Figure 4.15 with reflections assigned to the identified phases using symbols. The chemical formulae of the phases identified in this experiment are:

- C3A: $Ca_3Al_2O_6$
- Selenate ettringite: $Ca_6[Al(OH)_6]_2(SeO_4)_3.26H_2O$
- Gypsum analogue: $CaSeO_4.2H_2O$
- Monoselenate $14H_2O$: $3CaO.Al_2O_3.CaSeO_4.14H_2O$
- Monoselenate $9H_2O$: $3CaO.Al_2O_3.CaSeO_4.9H_2O$

The above names of the phases will be used in the analysis rather than stating the full chemical formulae throughout.

Table 4.7: Summary of reaction times and phases identified in the solid products by PXRD from the experiment "0.2 M Na_2SeO_4"

Time from C3A Addition	Phases Identified by PXRD
1 hour	C3A, selenate ettringite
3 hours	C3A, selenate ettringite
6 hours	C3A, selenate ettringite, gypsum analogue,
24 hours	C3A, selenate ettringite, gypsum analogue, monoselenate $14H_2O$, monoselenate $9H_2O$
1 week	selenate ettringite, monoselenate $14H_2O$, monoselenate $9H_2O$
1 month	monoselenate $14H_2O$, monoselenate $9H_2O$

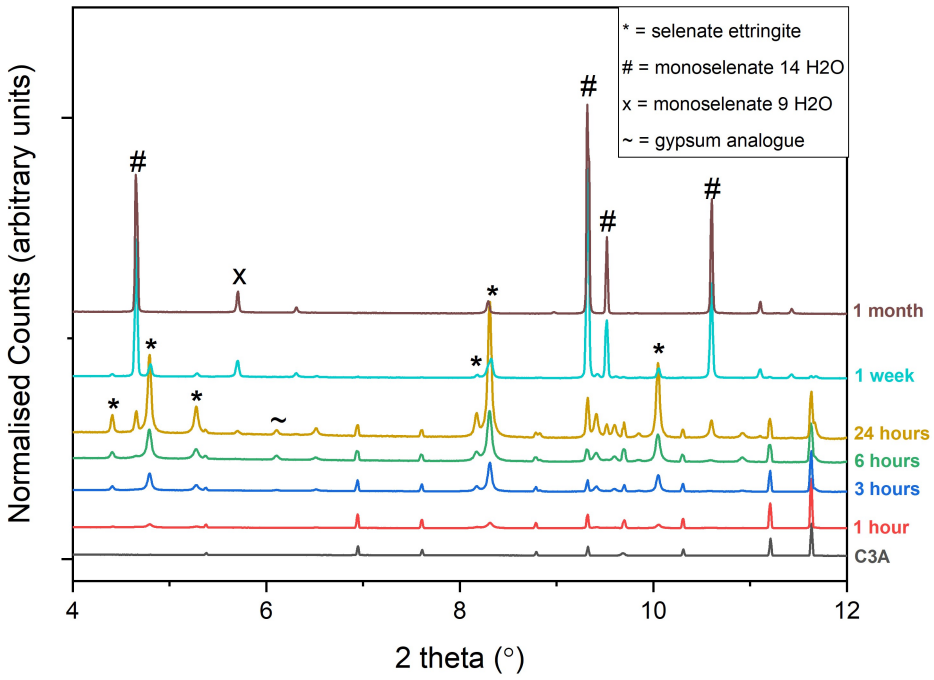

Figure 4.15: Powder X-ray diffraction patterns of the solid samples collected at various time points during the experiment "0.2 M Na_2SeO_4" (data collected on I11 at the Diamond Light Source Synchrotron, λ = 0.82661 Å)

Selenate ettringite is identified by PXRD in the samples from reaction times as early as 1 hour by presence of the reflections at 4.8 and 8.3 º 2θ. This indicates that selenium is being removed from solution after only 1 hour. Selenate ettringite ($Ca_6[Al(OH)_6]_2(SeO_4)_3.26H_2O$) continues to be the main product up to a reaction time of 24 hours when reflections assigned to a second phase, monoselenate $14H_2O$ ($3CaO.Al_2O_3.CaSeO_4.14H_2O$), begin to appear in the PXRD patterns. This phase coexists with selenate ettringite at reaction times of 1-7 days but the sample synthesised with a reaction time of 1 month contains only reflections for monoselenate phases of different hydration levels. This phenomenon is the same as was observed for the 0.2 M K_2CrO_4 samples where ettringite formed initially but eventually converted completely to a "mono" phase and is a process that mirrors the one that occurs in cement systems with sulfate containing phases. Multiphase Rietveld refinement was carried out on the collected PXRD data and allowed quantitative phase analysis (QPA). The QPA results are plotted as a function of time in Figure 4.16. The refinement strategy was the same as described in section 4.4.1 for the "0.2 M K_2CrO_4" experiment, but with the models adapted to contain selenium instead of chromium.

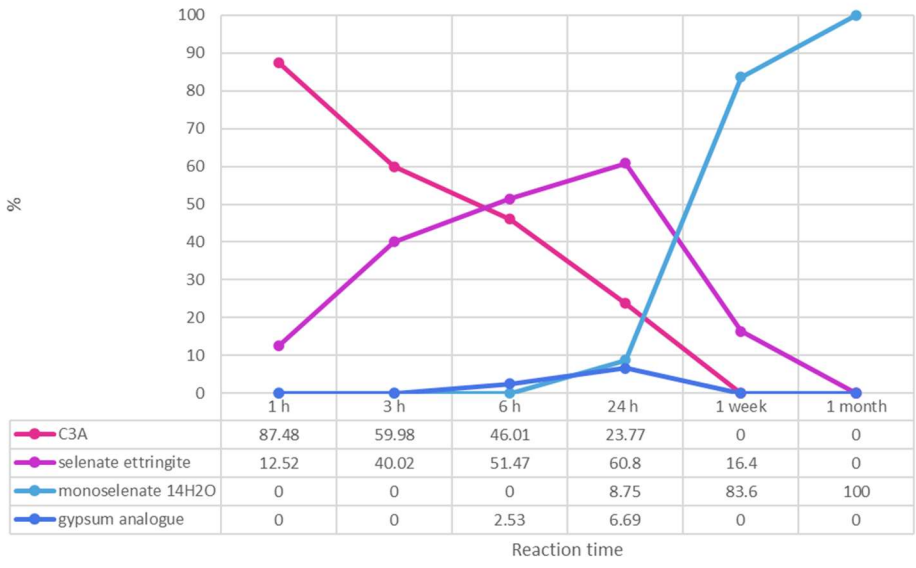

Figure 4.16: Proportions of phases identified as present by quantitative phase analysis (QPA) by Rietveld refinement of "0.2 M Na_2SeO_4" PXRD data

The QPA results show the C3A content decreasing as the reaction proceeds. Initially, selenate ettringite is the major product up to reaction times of 24 hours, and after that the conversion to monoselenate can be observed as it becomes over 80 % of the solid content at reaction times of over 1 week. It is important to note that the 100 % assigned to monoselenate $14H_2O$ for the 1 month reaction time sample represents that the samples composition is 100 % monoselenate nH_2O and that both the $14H_2O$ and $9H_2O$ hydration levels of monoselenate were identified as present in the PXRD data. The $9H_2O$ hydration level product is identified by the presence of its main (002) reflection at 5.64 ° 2θ, but as there is not a full crystal known model for monoselenate $9H_2O$, Rietveld refinement cannot be carried out to quantify the phase. The reaction pathway observed here is similar to that observed for solutions of potassium chromate but with larger amounts of the ettringite analogue phase being formed. The selenate ettringite is reacting more slowly with the remaining dissolved C3A to finally form monoselenate. From this, we can assume that selenate ettringite is a more stable product than chromate ettringite under these reaction conditions.

The FTIR spectra (Figure 4.17) show the presence of the selenate stretch for all samples. The band assigned to carbonate is present in the spectra for some samples, but the intensities are low in all cases, which indicates that there has been only a small amount of CO_2 absorbed from the air into the samples. This could be why more selenate ettringite is formed in this experiment than chromate ettringite was. The potassium chromate solution absorbed more carbonate, and this led to the formation of monochromate phases containing carbonate being favoured over the formation of chromate ettringite. The sodium selenate solution does not appear to have absorbed as much carbonate from the air and as a result, carbonate containing mono phases are not forming initially and selenate ettringite is the favoured product at early reaction times. The profile of the water stretch at ~3500 cm^{-1} changes for the samples where the main phase present is monoselenate (1 week and 1 month) instead of selenate ettringite (3 hours, 6 hours and 24 hours). This is caused by the different ways that water molecules are bound / free in the ettringite and monoselenate structures.

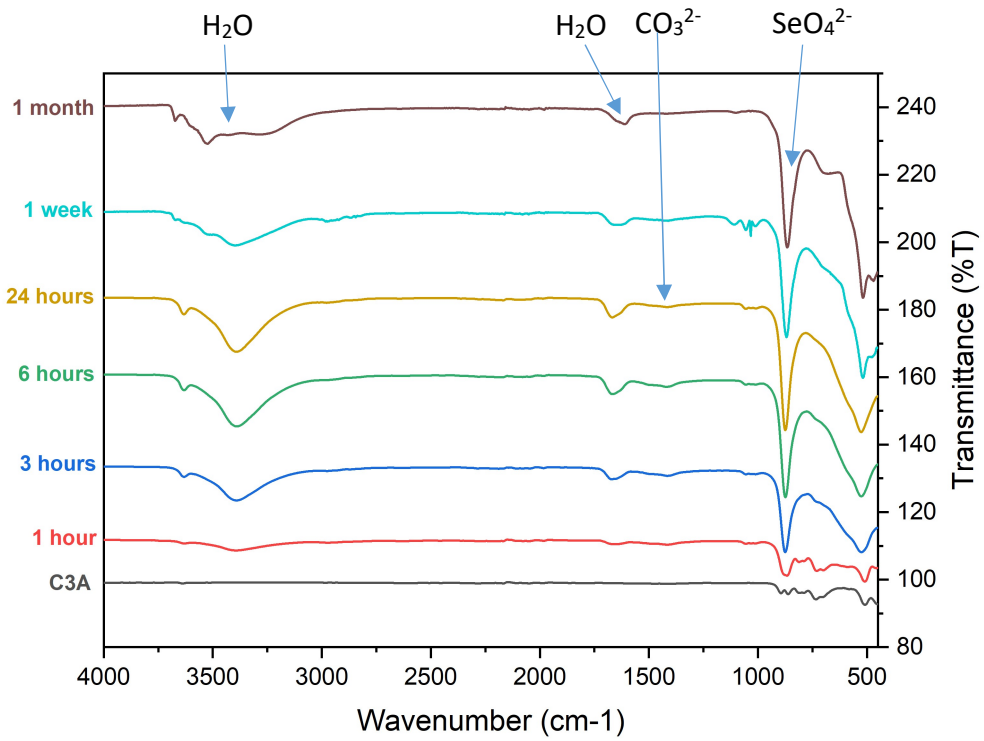

Figure 4.17: FTIR spectra of the solid samples collected at various time points during the experiment "0.2 M Na_2SeO_4", with bands for key functional groups indicated by arrows and labels

Elemental analysis using ICP-OES was performed to measure the selenium content of the solid samples along with the calcium and aluminium content, and the % content of each element, relative to a total Ca, Al, Se content of each sample, are displayed graphically in Figure 4.18 (the raw concentration results are given in Appendix 2). The results confirm that selenium is present in the solid phase from 1 hour of reaction time and the selenium content increases steadily as the reaction time increases. The relative composition of the 1 month sample (assigned as majority monoselenate $14H_2O$ by PXRD) is 56 % calcium, 27 % aluminium and 17 % selenium, which is comparable to what would be expected for a pure sample of monoselenate $14H_2O$ (ideal content of $Ca_4Al_2O_6(SeO_4).14H_2O$ = 57 % calcium, 29 % aluminium, 14 % selenium using the same relative composition calculation).

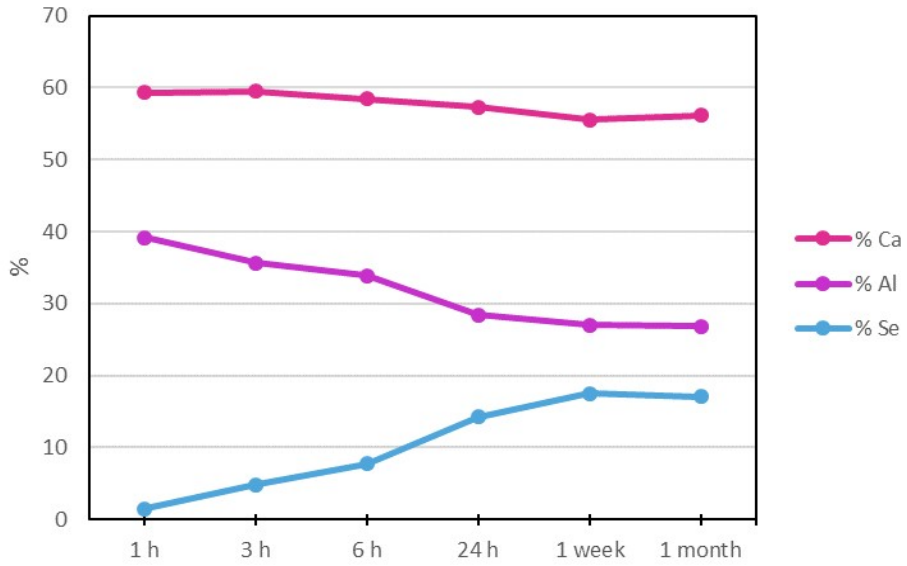

Figure 4.18: ICP-OES results for the solid samples collected at various time points during the experiment "0.2 M Na_2SeO_4" expressed as relative percentages

ICP-OES analysis was also carried out on the solution after the 1 month solid product had been separated from it by filtration. The concentration of selenium in the solution was measured to allow comparison to the initial solution prepared. The concentration of selenium in the initial solution and the solution after 1 month is presented in Figure 4.19. Analysis of the solution after 1 month of reaction with C3A shows that the selenium concentration has decreased from 15792 ppm to 10118 ppm, a reduction of around 1/3 of the selenium content. This shows that the method is effective at removing selenium from solution.

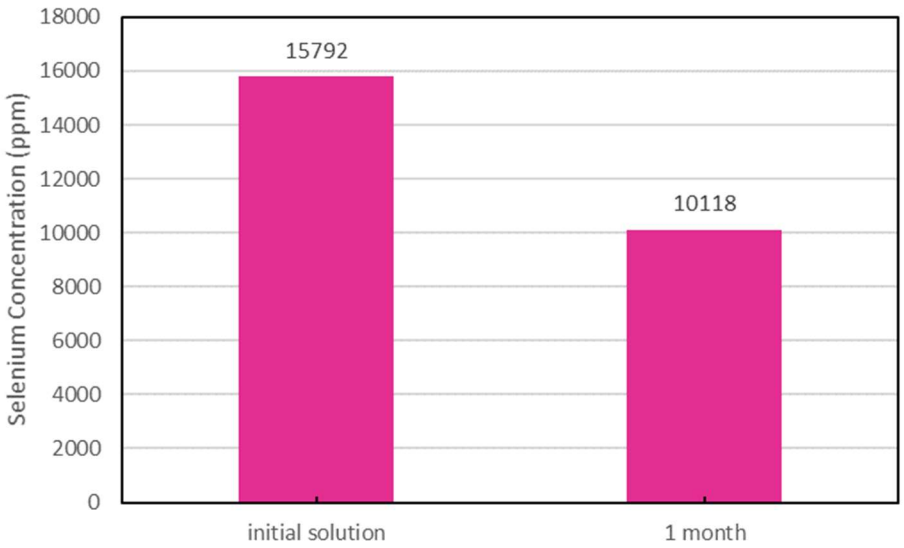

Figure 4.19: Selenium concentrations of the initial 0.2 M solution of Na_2SeO_4 and the same solution after 1 month reaction with C3A

SEM images were acquired for two of the 0.2 M Na_2SeO_4 samples, the 3 hour sample where selenate ettringite and the starting material C3A were present, and the 1 month sample which was comprised of monoselenate phases and no C3A remained. The SEM images show the morphology of the samples and EDS analysis identifies what elements are present on specific crystallites. The SEM images for the 3 hour and 1 month samples are shown in Figure 4.20 a) and b) respectively.

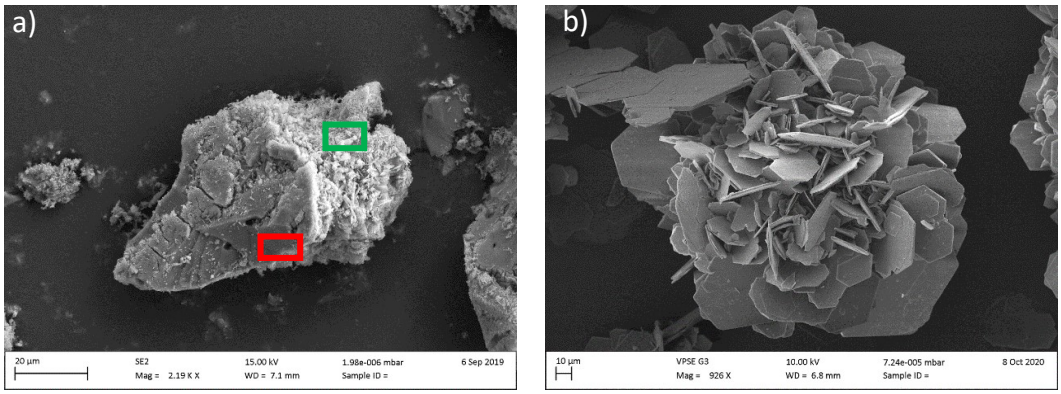

Figure 4.20 a) and b): SEM image of the 0.2 M Na_2SeO_4 a) 3 hour sample (boxes added to highlight areas for EDS analysis) and b) 1 month sample

The image of the sample produced after a synthesis time of 3 hours shows that it is made up of larger grains (~75 μm length) with a microtexture of smaller needle-like crystallites on their surface. The EDS spectrum of the area indicated by the red box on the images shows that it contains calcium, aluminium and oxygen, with no selenium detected. This means that the larger smooth grains are the starting material, C3A. The EDS spectrum measured on the area shown by the green box on the image, identified the presence of calcium, aluminium, oxygen and selenium. So, this image shows that, as was found for the chromate equivalent sample, the ettringite crystallites are growing on the surface of the C3A grains. All EDS spectra are presented in Appendix 2.

The image of the 1 month sample shows a complex and intricate morphology. The sample is made up of many connected hexagonal plates. The hexagonal plates vary in size, with some having diameters as large as 100 μm. This observed morphology matches the hexagonal plates that have been previously observed for the monochromate sample in Figure 4.10 b) but this monoselenate sample has more defined and perfectly hexagonal platelets. EDS spectra were measured for various points on this sample and all showed the presence of calcium, aluminium, oxygen and selenium, so this image can be used to confirm the morphology of the monoselenate phases formed.

4.5.2 Reaction of C3A with Solutions of Na_2SeO_4 with Lower Concentrations

The solution concentration was lowered to 0.1 M, 0.02 M, and 0.01 M but the same experimental procedures as the 0.2 M Na_2SeO_4 experiment were used. This section will determine differences in reaction pathways as the solutions get less concentrated and therefore closer to realistic waste-water concentrations.

4.5.2.1 PXRD

The phases identified from the PXRD analysis (collected on a laboratory D8 diffractometer) are summarised in Table 4.8. The chemical formulae of the phases identified in this experiment are:

- C3A: $Ca_3Al_2O_6$
- Selenate ettringite: $Ca_6[Al(OH)_6]_2(SeO_4)_3.26H_2O$
- Monoselenate $14H_2O$: $3CaO.Al_2O_3.CaSeO_4.14H_2O$
- Monoselenate $9H_2O$: $3CaO.Al_2O_3.CaSeO_4.9H_2O$
- Gypsum analogue: $CaSeO_4.2H_2O$
- Monoselenate $12H_2O$: $3CaO.Al_2O_3.CaSeO_4.12H_2O$
- Monocarbonate: $3CaO.Al_2O_3.CaCO_3.11H_2O$
- Hemiselenate 14H2O: $3CaO.Al_2O_3.½CaSeO_4.$ $½Ca(OH)_2.14H_2O$

Throughout this section, the above names for compounds will be used in place of their chemical formulae. The PXRD patterns are plotted in Figure 4.21 a), b) and c) and larger sizes of these are available in Appendix 2.

Table 4.8: Summary of reaction times and phases identified in the solid products from experiments "0.1 M Na_2SeO_4" "0.02 M Na_2SeO_4" and "0.01 M Na_2SeO_4"

Time from C3A Addition	**Phases Identified by PXRD 0.1 M**	**Phases Identified by PXRD 0.02 M**	**Phases Identified by PXRD 0.01 M**
1 hour	C3A, selenate ettringite	C3A, selenate ettringite	
3 hours	C3A, selenate ettringite	C3A, selenate ettringite	
6 hours	C3A, selenate ettringite	C3A, selenate ettringite	
24 hours	C3A, selenate ettringite	C3A, selenate ettringite	C3A, monoselenate $12H_2O$, monocarbonate, amorphous content
3 days			monoselenate $12H_2O$, monocarbonate, amorphous content
5 days			monoselenate $12H_2O$, monocarbonate, hemiselenate $14H_2O$, amorphous content
1 week	monoselenate $14H_2O$, monoselenate $9H_2O$, gypsum analogue	monoselenate $12H_2O$	monoselenate $12H_2O$, monocarbonate, hemiselenate $14H_2O$, amorphous content
1 month	monoselenate $14H_2O$, monoselenate $9H_2O$, gypsum analogue	monoselenate $12H_2O$	

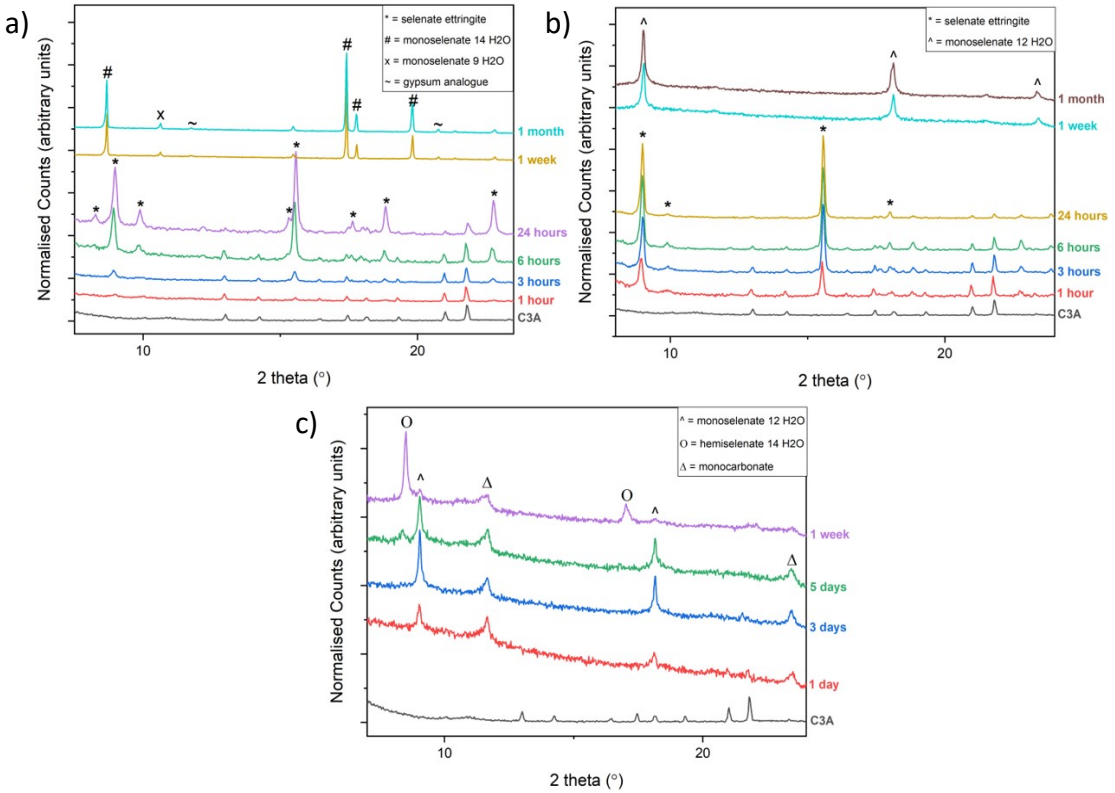

Figure 4.21 a) b) and c): Powder X-ray diffraction patterns of the solid samples collected at various time points during the experiments a) "0.1 M Na_2SeO_4" b) "0.02 M Na_2SeO_4" and c) "0.01 M Na_2SeO_4" (data collected on laboratory Bruker D8, λ = 1.5406 Å)

Analysis of the PXRD patterns measured for the 0.1 M and 0.02 M Na_2SeO_4 experiments show a similar reaction pathway to the 0.2 M set. Selenate ettringite can be observed after 1 hour and continues to exist as the main phase in the solid samples until over 24 hours of reaction time. The 1 week and 1 month samples contain no ettringite, no C3A starting material and are comprised of monoselenate phases of different hydration levels ($3CaO.Al_2O_3.CaSeO_4.nH_2O$, n = 9, 12, 14). This result is significantly different from the 0.1 M and 0.02 M K_2CrO_4 samples, where no ettringite type phases were formed in the early stages of the reaction and instead monochromate phases were the only products. So, there is a difference in the ability of chromate ettringite and selenate ettringite to form from solution, with selenate ettringite shown to be more stable.

Selenate ettringite is not identified in any of the PXRD patterns for the 0.01 M samples and monoselenate $12H_2O$ is the main selenium containing phase that can be identified for the 1 day, 3 day and 5 day samples. The lack of selenate ettringite in these samples was attributed to the excess of C3A (4:1, molar ratio C3A:selenate) making selenate ettringite formation unfavourable. All PXRD patterns for the 0.01 M experiment contain reflections assigned to monocarbonate which accounts for what the excess C3A has formed, through reaction with CO_2 from the air in the reaction vessel. At reaction times 5 days and 7 days, a new phase hemiselenate $14H_2O$ is identified by the presence of a reflection at 8.5° 2θ. The phase hemichromate ($3CaO.Al_2O_3.½CaCrO_4$. $½Ca(OH)_2.14H_4O$) is known and its main reflection is assigned to this position (8.5° 2θ) by Göske, König and Pöllmann[8]. Hemiselenate has the same structure as the monoselenate phases but also contains hydroxyl ions along with the selenate ions between the layers giving it a different layer spacing and therefore different characteristic reflection positions. The formation of this phase with a lower total selenate content is another way this system has adapted to the very low selenate concentration in solution.

4.5.2.2 FTIR

FTIR spectra were measured to confirm the presence of selenate in the samples and identify if any carbonate had been absorbed. The spectra are plotted in Figure 4.22 a) b) and c).

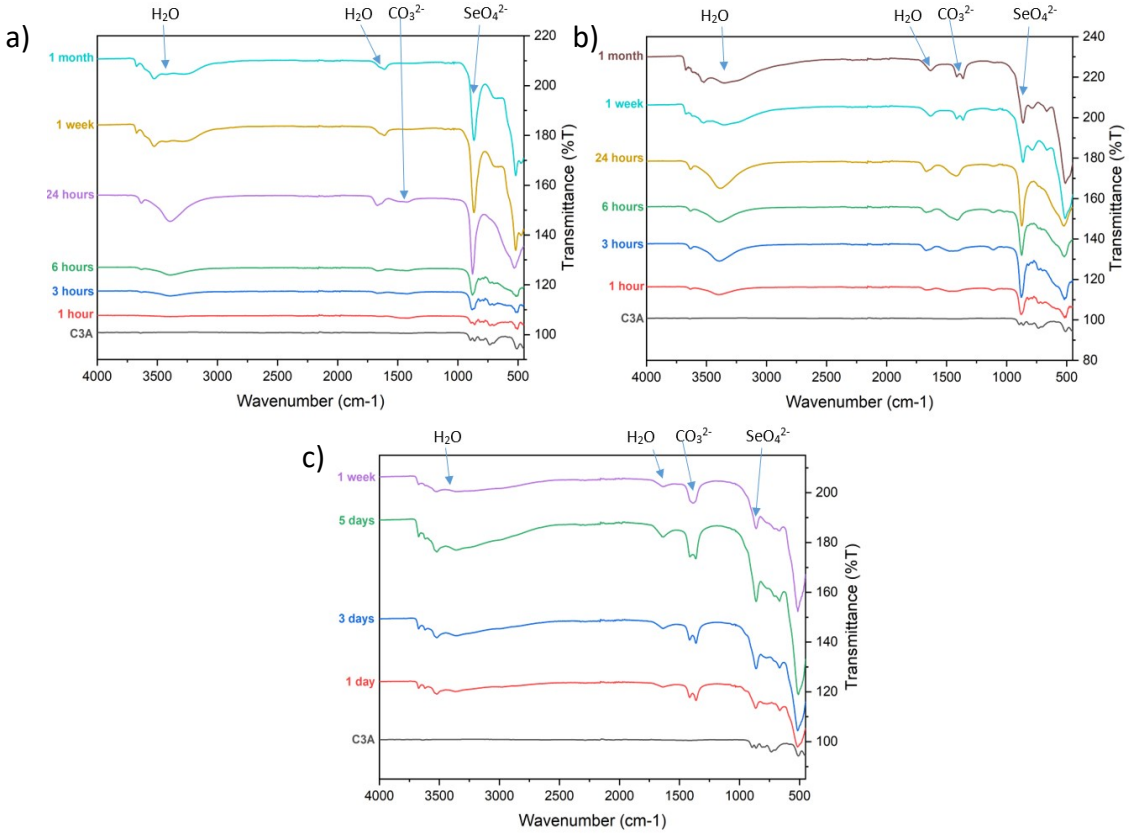

Figure 4.22 a) b) and c): FTIR spectra of the solid samples collected at various time points during the experiments a) "0.1 M Na_2SeO_4" b) "0.02 M Na_2SeO_4" and c) "0.01 M Na_2SeO_4", with bands for key functional groups indicated by arrows and labels

The spectra for the 0.1 M samples contain strong bands for selenate from 3 hours reaction time. There are no carbonate bands that are strongly present in any of the spectra. This could be the reason for the slower formation of monoselenate, it was hypothesised in the previous section that absorption of CO_2 and the incorporation of it into "mono" phases was aiding the overall formation of monochromate phases. The sodium selenate solutions appear to incorporate less carbonate in the early stages of reaction, as shown by the FTIR, and also produce solid selenate ettringite phases that convert more slowly to monoselenate, so this lends credibility to the previous assumption. The lack of absorbed carbonate has stopped any carbonate containing mono phases from forming and instead, selenate ettringite has been able to form and be the dominant product in reaction times up to 1 week.

Compared to this result for the 0.1 M experiment, the spectra for the 0.02 M and 0.01 M samples show significant carbonate bands. For the 0.01 M experiment, monocarbonate was identified by PXRD, with splitting of the FTIR band at ~1450 cm^{-1} showing that there is also carbonate incorporated into the monoselenate products. No carbonate containing phases were identified in the PXRD data for the 0.02 M experiment, which means that there must be carbonate incorporated into the selenate ettringite and monoselenate products identified by PXRD. The solutions with lower concentrations of sodium selenate are absorbing more CO_2 from the air and this further suggests that it is the solution that is inhibiting this absorption in the 0.2 M and 0.1 M solution experiments.

One of the reasons for this could be a difference in pH between the sodium selenate and previously tested potassium chromate solutions. The sodium selenate solutions had pH of ~8.5, while the potassium chromate solutions had pH of ~9.2. This is not a huge difference in pH so while this could be a contributing factor to why the potassium chromate solutions produce more carbonate containing products it is likely not the only reason. The other difference between the solutions is the cation present, Na^+ or K^+. These cations have been shown previously to have different affects on carbonate absorption and subsequent degradation of materials[14]. Solutions containing potassium have been found to absorb carbon dioxide and make the dissolved carbonate more soluble than solutions containing sodium. This means that in this study, the potassium chromate solutions would have more soluble carbonate present in solution which would be more available to react and incorporate into the products forming.

4.5.2.3 ICP-OES

ICP-OES was used to quantify how much selenium was in each solid sample and the elemental percentages of calcium, aluminium and selenium (relative to total Ca, Al,

Se content) are plotted in Figure 4.23 a) b) and c). The raw measured concentration data is given in Appendix 2.

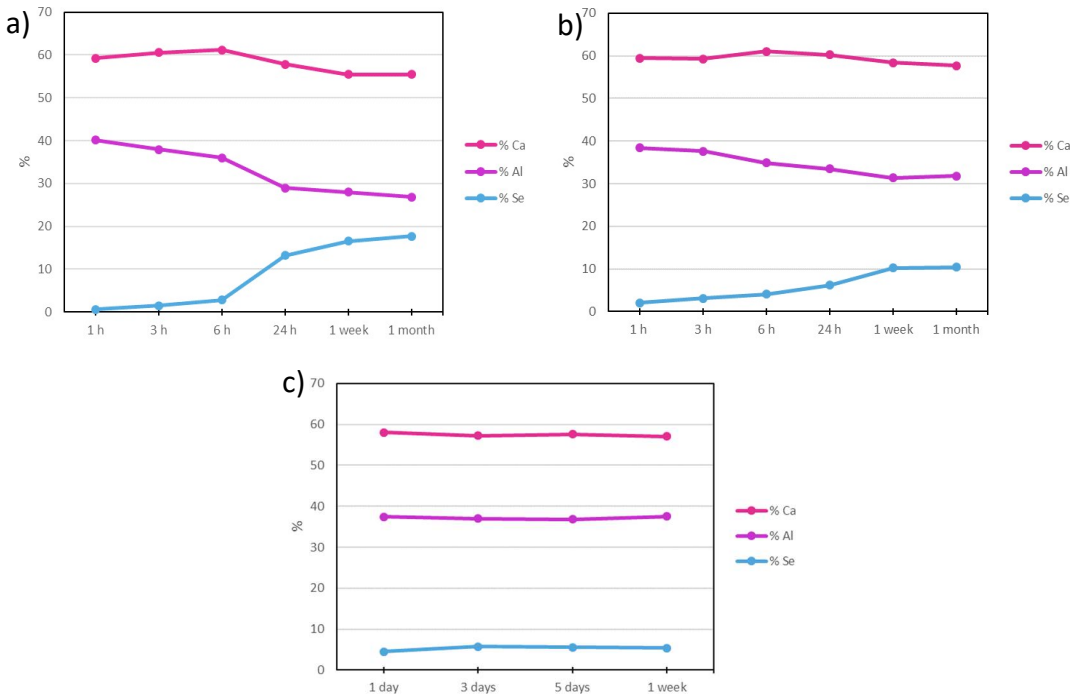

Figure 4.23 a) b) and c): ICP-OES results for the solid samples collected at various time points during the experiments a) "0.1 M Na_2SeO_4" b) "0.02 M Na_2SeO_4" and c) "0.01 M Na_2SeO_4" expressed as relative percentages (% Ca = pink, % Al = purple, % Se = blue)

The ICP-OES elemental analysis results for the selenium removal experiments are similar to those for the chromium removal experiments, despite major differences in which solid phases formed during the reactions. The 0.1 M results show an increasing selenium content as the reaction proceeds with a larger incorporation of selenium into the solid after 24 hours of reaction time. The 1 month sample (identified as being made up of monoselenate phases by PXRD), has the relative composition 55 % calcium, 27 % aluminium and 18 % selenium which is accurate for the formation of monoselenate as the ideal composition of $Ca_4Al_2O_6(SeO_4).14H_2O$ expressed as the same relative percentages of Ca, Al, and Se is 57 % calcium, 29 % aluminium and 14 % selenium.

The result for the 0.02 M Na_2SeO_4 1 month sample gave a relative composition of 58 % calcium, 32 % aluminium, 10 % selenium. This is a lower % of selenium than would be expected for a pure sample of monoselenate. No other crystalline phases were identified from the PXRD patterns, which indicates that the monoselenate phase identified in the PXRD data contains both carbonate and selenate ions between its layers. This strengthens the conclusions from the FTIR analysis, which identified carbonate in this and other samples.

The elemental analysis of the 0.02 M and 0.01 M samples shows the same trends as the chromium experiments using analogous solution concentrations, in that the selenium content increases but reaches a point in the reaction, after which, no more selenium incorporates into the solid products. For the 0.02 M Na_2SeO_4 experiment this is after 1 week of reaction time and for the 0.01 M Na_2SeO_4 experiment it is after 3 days, suggesting maximum selenium incorporation has been achieved. In this case the sodium selenate solution is colourless so there is no visual aid for identifying whether the selenium has been completely removed from the filtrate as was the case for the yellow potassium chromate solution. To determine if any of the experiments had removed all the selenium from the solutions the filtrates separated from the same samples as analysed for the chromate experiments were analysed by ICP-OES. The measured selenium concentrations of the solutions after reaction with C3A for various times are presented in Figure 4.24.

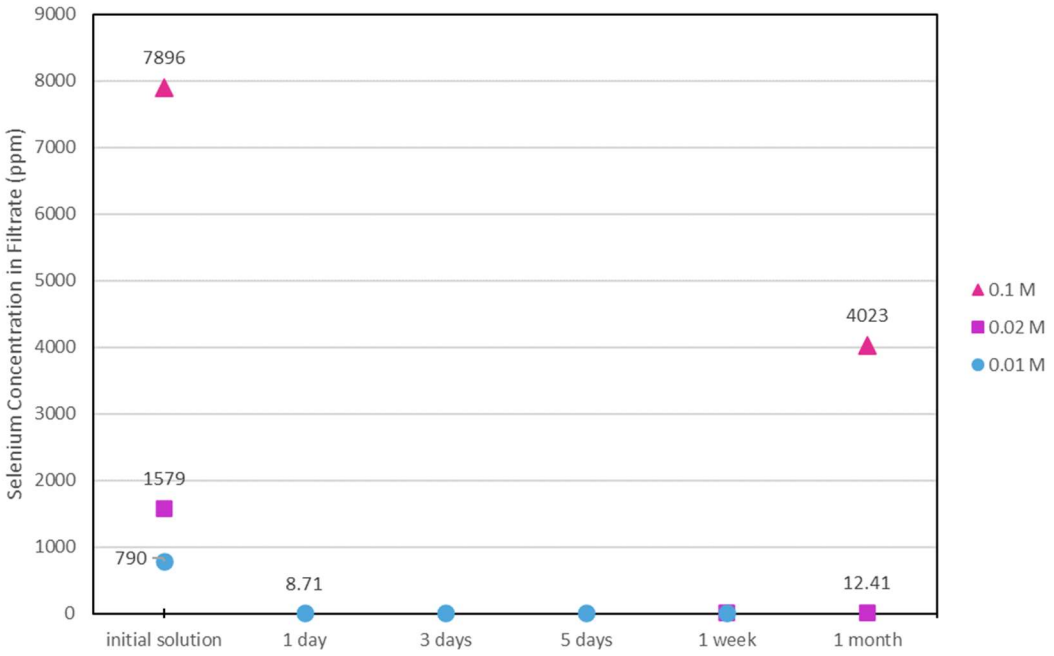

Figure 4.24: Selenium concentrations of the solutions after solid products separated, measured by ICP-OES

The elemental analysis of the solutions from these experiments show that the method is very effective at removing selenium from solution. For the 0.1 M solution, the concentration is reduced by ~4000 ppm, halving the selenium content of the initial solution after 1 months reaction with C3A. Both the 0.02 M and 0.01 M experiments have successfully removed almost all of the selenium, with the 0.02 M experiment reducing the selenium concentration from 1579 ppm to ~12 ppm after 1 week of reaction with C3A and the 0.01 M experiment reducing the selenium concentration from 790 ppm to 8.71 ppm after only 1 day of reaction with C3A.

This study, removing selenium from solution using C3A, has been successful, with selenium found to be incorporated in the solid products after a few hours. Compared to the previous section studying the removal of chromium, the formation of a selenate ettringite analogue phase was found to be stable up to reaction times of 24 hours in all solutions with a concentration greater than 0.01 M. Monoselenate phases were the final products in all of the experiments but the slower conversion of selenate ettringite to monoselenate was concluded to be due to the sodium selenate

solution inhibiting the absorption of carbon dioxide from the air in the reaction vessels.

4.6 CONCLUSIONS

A method to test the viability of ettringite precipitation to remove hexavalent chromium and selenium from solutions was set up using a single starting material, C3A ($Ca_3Al_2O_6$). C3A was added to solutions of either potassium chromate or sodium selenate and the time dependence of the phases formed, along with the extent to which the chromium or selenium was removed from solution, was tracked.

The concentration of the solutions were varied and it was shown that when solutions of either chromate or selenate were concentrated (0.2 M) an ettringite analogue phase ($Ca_6[Al(OH)_6]_2(XO_4)_3.26H_2O$, X = Cr, Se) would initially form after a few hours of reaction with the C3A. The ettringite analogue phase eventually converted to a "mono" phase ($3CaO.Al_2O_3.CaXO_4.nH_2O$, X = Cr, Se, n = 9-14) and up to reaction times of 1 month, the mono phases were the dominant reaction products.

When the concentrations of the solutions were decreased, the results for chromate and selenate containing solutions began to differ. The chromate containing solutions only produced monochromate phases and other related monocarbonate phases. Even though the chromate ettringite analogue phase was not formed, chromium was still successfully removed from all solutions. The tendency to form monochromate products instead of chromate ettringite was concluded to be related to the absorption of carbonate from the air in the reaction vessels, leading to the formation of layered monochromate phases with carbonate also incorporated between the layers. This was identified by the presence of carbonate bands in the FTIR spectra. In solutions with higher chromium concentrations all the carbonate was eventually replaced by chromate but in lower concentration solutions, carbonate remained incorporated at all measured reaction times.

The selenate containing solutions with concentrations of 0.1 M and 0.02 M still produced the selenate ettringite analogue phase for reaction times up to 24 hours with no carbonate being incorporated. A conversion to the monoselenate phase occurred when the reaction time was greater than 1 day. When the solution concentration was 0.01 M and the C3A was in great excess of the selenate in solution, monoselenate and monocarbonate phases formed at all reaction times measured, with even this experiment removing selenium successfully from the solution. The inhibition of carbonate absorption and subsequent stabilisation of selenate ettringite occurred in solutions with higher sodium selenate concentrations leading to the conclusion that the sodium selenate solution was responsible for inhibiting the absorption of carbonate from the air. There were no major differences in pH between the chromate and selenate containing solutions, so the fact that the sodium selenate solution inhibited carbonate absorption more than the potassium chromate solution must be due to other factors. The difference between the solutions in containing either potassium or sodium in the solution was the most likely cause of this.

Overall, the method of using C3A to remediate chromium and selenium waste waters was found to be effective at removing both hexavalent chromium and selenium from solution and could therefore be taken forward for further study into implementing them as remediation materials. Future work would include testing the stability of the formed phases with respect to leaching out the waste ions. The complexity of the solutions would need to be increased, for example, by adding in competing ions, to test whether this method would still remove chromium/ selenium from a solution that is more comparable to a real contaminated water sample.

4.7 REFERENCES

1 A. D. Lemly, *Ecotoxicol. Environ. Saf.*, 2004, **59**, 44–56.

2 K. Salnikow and A. Zhitkovich, *Chem. Res. Toxicol.*, 2008, **21**, 28–44.

3 C. Pellerin and S. M. Booker, *Environ. Health Perspect.*, 2000, **108,** 402–407.

4 A. Broadway, M. R. Cave, J. Wragg, F. M. Fordyce, R. J. F. Bewley, M. C. Graham, B. T. Ngwenya and J. G. Farmer, *Sci. Total Environ.*, 2010, **409**, 267–277.

5 H. F. W. Taylor, *Cement chemistry 2nd Edition*, Thomas Telford, London, 2nd edn., 1997.

6 H. J. Kuzel, *Cem. Concr. Compos.*, 1996, **18**, 195–203.

7 S. M. Leisinger, B. Lothenbach, G. Le Saout and C. A. Johnson, *Cem. Concr. Res.*, 2012, **42**, 158–165.

8 J. Göske, U. König and H. Pöllmann, *Mater. Sci. Forum*, 2004, **443–444**, 299–302.

9 J.-P. Rapin, Universite Henri Poincare, 2001.

10 R. Segni, Universite Blaise Pascal, 2005.

11 R. J. Myers, G. Geng, E. D. Rodriguez, P. da Rosa, A. P. Kirchheim and P. J. M. Monteiro, *Cem. Concr. Res.*, 2017, **100**, 176–185.

12 P. Mondal and J. W. Jeffery, *Acta Crystallogr. Sect. B Struct. Crystallogr. Cryst. Chem.*, 1975, **31**, 689–696.

13 S. Joseph, J. Skibsted and Ö. Cizer, *Cem. Concr. Res.*, 2019, **115**, 145–159.

14 F. M Maia Neto, T. W. C. O. Andrade, R. M. Gomes, A. F. Leal, A. N. F. Almeida, M. R. F. Lima Filho and S. M. Torres, *Constr Build Mater,* 2021, **299**, 123848.

CHAPTER 5 SOLID SOLUTIONS BETWEEN CHROMATE AND SULFATE ETTRINGITE AND BETWEEN SELENATE AND SULFATE ETTRINGITE

5.1 INTRODUCTION

The crystal structure of ettringite ($Ca_6[Al(OH)_6]_2(SO_4)_3.26H_2O$) has been shown to accommodate a variety of different elements in its crystal structure[1–5]. This has been discussed in the introduction and previous chapters including the replacement of the sulfate anion with chromate or selenate in chapter 3. Different ions can be tolerated by the ettringite structure as long as they are similar in size and structure to the ion they are replacing.

This study is focussed on the partial replacement of the sulfate anion with either chromate or selenate. Previously in chapter 3 of this work, synthesis of a chromate-ettringite analogue phase and a selenate-ettringite analogue phase were successfully completed. These analogue phases have no sulfate content and all of the original sulfate sites are occupied by either chromate or selenate ions. This is possible as sulfate, chromate and selenate ions are all divalent polyanions, tetrahedral in geometry and have similar thermochemical radii (sulfate = 2.18 Å, chromate = 2.29 Å and selenate = 2.29 Å)[6,7]. Since full substitution of the sulfate for chromate or selenate is possible, it should be possible to synthesise a phase where there is a partial substitution of the sulfate. This would be called a substitutional solid solution phase.

A solid solution series is a set of solid phases, which have variable compositions, between two pure end member phases. Each targeted composition is a single homogeneous product, rather than a simple mechanical mixture of two phases. In

this study, solid solution series were set up where a specific crystallographic sites' occupancy is being varied. For example: in the case of a solid solution between the end members ettringite ($Ca_6[Al(OH)_6]_2(SO_4)_3.26H_2O$) and chromate ettringite ($Ca_6[Al(OH)_6]_2(CrO_4)_3.26H_2O$) it is the S/Cr sites which are varying in occupancy, to give a solid solution series: $Ca_6[Al(OH)_6]_2(SO_4)_{3-x}(CrO_4)_x.26H_2O$. These sites are labelled in Figure 5.1.

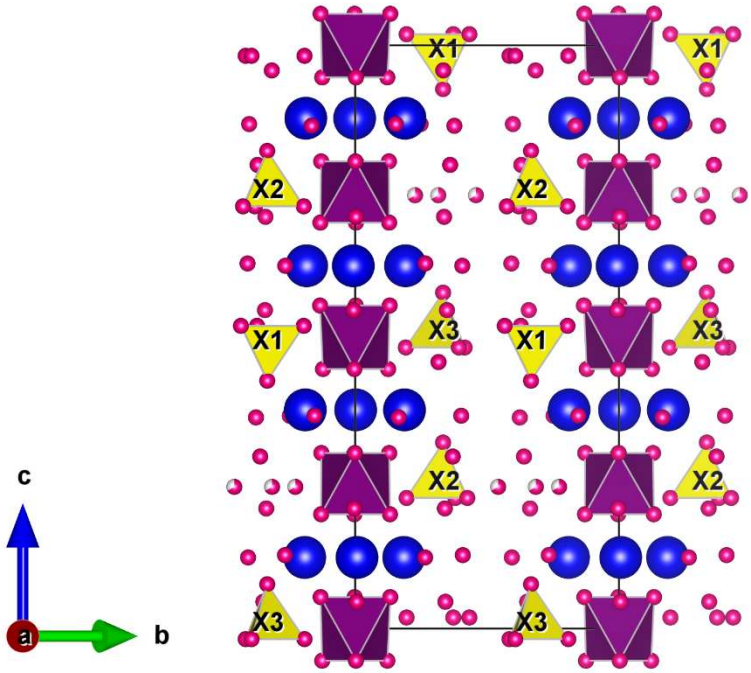

Figure 5.1: Projection of the ettringite crystal structure with the c axis vertical and the sulfur sites labelled X

According to Gibbs' condensed phase rule where F = C – P + 1 (F = number of degrees of freedom, C = number of components, P = number of phases). A solid solution is a binary system with two components (C = 2) so F = 3 – P. For a complete solid solution (P = 1), the degrees of freedom are temperature and composition of each phase. During synthesis of a targeted composition of a solid solution phase it can occur that two separate phases are formed which are more similar to the end member phases, rather than a single solid solution phase which is a true mixture. In this case P = 2 and phase composition is no longer a degree of freedom as the two components are now

directly making two phases. If the series is partitioning into two phases over a specific range of compositions then this region of the solid solution series is called a miscibility gap and two phases are forming. Figure 5.2 shows example phase diagrams for both cases.

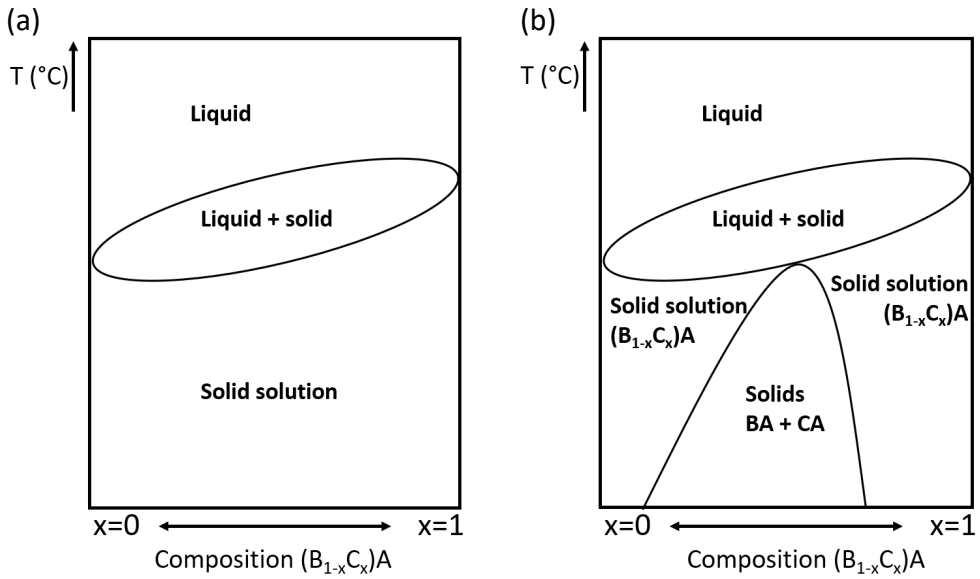

Figure 5.2: Example binary phase diagrams displaying solid solutions ($(B_{1-x}C_x)A$) over a range of compositions: (a) shows a continuous solid solution with P=1 for all compositions, (b) shows a solid solution series with a miscibility gap where P=2 for a range of compositions

This study investigated solid solution formations between chromate ettringite and sulfate ettringite $Ca_6[Al(OH)_6]_2(SO_4)_{3-x}(CrO_4)_x.26H_2O$, and selenate ettringite and sulfate ettringite $Ca_6[Al(OH)_6]_2(SO_4)_{3-x}(SeO_4)_x.26H_2O$. Different molar ratios of starting materials were used to target synthesis of different compositions of the solid solution series'. Analysis of the products formed allowed identification of any miscibility gaps in the solid solution series. If no miscibility gaps were identified then a complete solid solution series had been successfully synthesised and could be described as fully miscible. A specific synthesis method known as the "saccharate method" (described in Chapter 2.1.3) was used and the synthesis time varied to investigate the effect of different equilibration times.

Solid solutions between ettringite and ettringite analogue phases have been found occurring naturally[8,9] and can also been synthesised[5,10,11]. Solid solutions of ettringite have also been found occurring in concrete that was contaminated with chromate[12]. This was discovered where chromium had spilled onto the floor of a chrom plating facility and chromate containing ettringite crystals were found along with chromate containing hydrocalumite crystals. This was an important discovery as there is interest in stabilising chromate waste in cement matrices.

One of the earliest studies of solid solutions of the ettringite structure where the sulfate is being substituted is that of Hassett *et al.* (1990)[5]. In Hassett's study a solid solution was synthesised between end members sulfate-ettringite and selenate-ettringite ($Ca_6[Al(OH)_6]_2(SO_4)_{3-x}(SeO_4)_x.26H_2O$). They used the "saccharate method" and a synthesis time of 24 hours, to synthesise a range of compositions and concluded that they had successfully synthesised a complete solid solution with no phase partitioning. Using PXRD, they confirmed that each synthesised composition had the ettringite structure. However, their chemical analyses indicate that the maximum amount of sulfate substituted by selenate was 54 %, and they had not synthesised any samples with a higher selenate content. Also, their synthesis time (24 hours) is relatively short.

Using the same "saccharate method" as Hassett *et al.* this study attempted to synthesise a complete solid solution between sulfate-ettringite and selenate-ettringite. A larger number of compositions between the end members was targeted to obtain a more complete picture of the solid solution. Also, variation in the synthesis time was investigated, with periods of 24 hours and 7 days used in order to compare and assess how a longer synthesis time affected the solid solution formation.

Another early study into the partial replacement of sulfate in the ettringite structure is that of Pöllmann *et al.* (1993)[11]. In Pöllmann's study, solid solutions were synthesised between end members sulfate-ettringite and borate-ettringite ($Ca_6[Al(OH)_6]_2(SO_4)_{3-3x}(OH)_{2x}B(OH)_4)_{4x}.26H_2O$) and sulfate-ettringite and chromate-

ettringite ($Ca_6[Al(OH)_6]_2(SO_4)_{3-x}(CrO_4)_x.26H_2O$). This study used two different and commonly used ettringite synthesis methods in order to compare them. The two methods used were the previously mentioned “saccharate method” in addition to the “paste method”. The difference in these two methods is that the “paste method” uses all calcium salts and the “saccharate method” uses addition of sodium salts to a calcium oxide/ sugar solution. For the chromate-sulfate ettringite solid solution series they found that a completely miscible solid solution series was synthesised when using the paste method but when using the saccharate method there was a miscibility gap when chromate substitution for sulfate exceeded 33 % e.g. they could not synthesise any solid solutions with $Ca_6[Al(OH)_6]_2(SO_4)_{3-x}(CrO_4)_x.26H_2O$, $x > 1$. In the case of the borate-sulfate ettringite solid solution they found a miscibility gap when using the paste method and that both methods resulted in extra hydroxyl groups being incorporated, forming products with the general formula $Ca_6[Al(OH)_6]_2(SO_4)_{3-3x}(OH)_{2x}(B(OH)_4)_{4x}.26H_2O$ $0 \leq x \leq 1$.

Perkins (2000) also studied the chromate-sulfate ettringite solid solution[10]. They used tricalcium aluminate as a precursor and added this to calcium sulfate and calcium chromate in water, mixing the samples for 72 hours. They claim to have formed a complete solid solution where every composition is single phase, however, on inspection of the provided PXRD patterns, there appears to be peak splitting (Figure 5.3), which is an indication of a two phase ($P = 2$) system instead of a solid solution. This splitting occurred in samples where the chromate substitution was 10 % and 30 %.

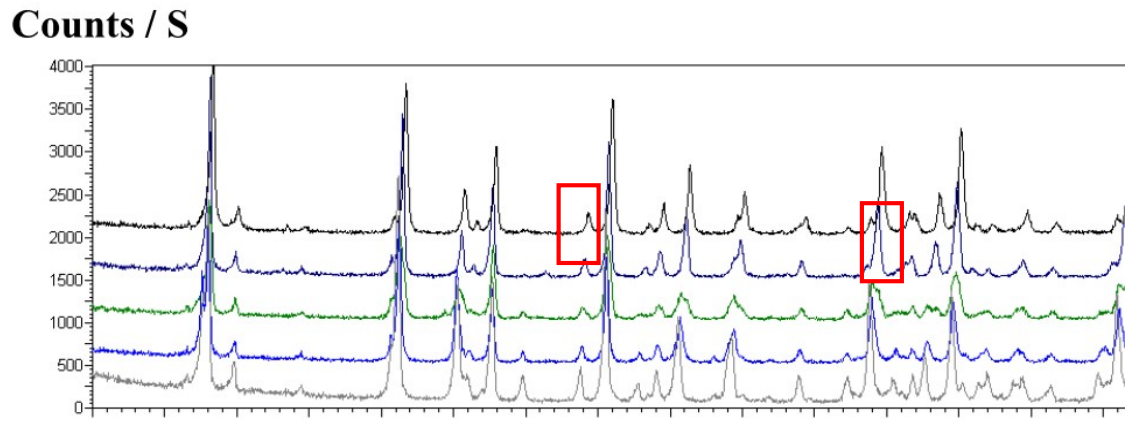

Figure 5.3: PXRD patterns for synthesised samples with chromate substitution of 0 % (top), 10 %, 30 %, 73 %, and 100 % (bottom). Figure 6-1 from Perkins (2000)[10]. Examples of split peaks highlighted with red boxes

A more recent study into the chromate-sulfate ettringite solid solution is that of Leisinger *et al.* (2010)[13]. Like Perkins, they used the addition of tricalcium aluminate, calcium sulfate and calcium chromate to water. The equilibration time was 90 days. They found that all the samples they synthesised contained a higher sulfate: chromate ratio than the solutions from which they were formed e.g. there was a preference for sulfate incorporation into the product. They also identified, through PXRD, that there was a miscibility gap when the incorporation of chromate, substituting the sulfate, exceeded 30 %.

This study attempted to synthesise a solid solution between sulfate-ettringite and chromate-ettringite. The saccharate method was employed for a large number of compositions and the results were compared to the previous studies. This study also utilised two different synthesis times for the solid solution to investigate whether this has an effect on the products formed.

One reason why studying the formation of solid solutions of the ettringite structure with chromate or selenate partially incorporated is important, is that they can be used to guide remediation methods. Chromate and selenate are hazardous in their hexavalent oxidation state and being able to incorporate these hazardous ions into the stable ettringite structure would be one way to stabilize these waste ions. Formation of a solid solution would lower the concentration of soluble chromate and

selenate in wastewater but before these materials could be implemented as remediation tools, the solid solution behaviour needs to be fully understood. The maximum amount of chromate / selenate that can be substituted for sulfate needs to be determined, as the tolerance for waste ions will determine the amount of waste ions that can be removed, the mass of precursors that would be needed to perform the remediation, and how viable, overall, the remediation process would be.

5.2 AIMS

The aim of this study was to synthesise two solid solutions; one between end member phases chromate ettringite and sulfate ettringite, and one between selenate ettringite and sulfate ettringite ($Ca_6[Al(OH)_6]_2(XO_4)_x(SO_4)_{3-x}.26H_2O$, X=Cr or Se). The purpose of this was to identify any unit cell variations across these solid solution series, if there were any miscibility gaps and therefore determine the solid solution limits. Previous work has been carried out on the chromate-sulfate ettringite solid solution[13] and the selenate-sulfate ettringite solid solution[5] so comparisons have been made between this and the previous studies.

Samples were prepared and analysed using the methods described in Chapter 2.1.3 and Chapter 2.2.

5.3 THE CHROMATE-SULFATE ETTRINGITE SOLID SOLUTION

Table 5.1 shows the target compositions used for investigations into the solid solution formation of the $Ca_6[Al(OH)_6]_2(CrO_4)_x(SO_4)_{3-x}.26H_2O$ (x = 0, 0.3, 0.6, 0.9, 1.2, 1.5, 1.8, 2.1, 2.4, 2.7 and 3.0) system. Two different ageing periods were used. As the ratio of chromate increased the sample colour visually changed from white to yellow.

Table 5.1: Targeted compositions of the chromate-sulfate ettringite solid solution ($Ca_6[Al(OH)_6]_2(CrO_4)_x(SO_4)_{3-x}.26H_2O$) samples

Sample Name	Target Composition	x CrO_4^{2-} in Targeted Formula
sulfate ettringite	$Ca_6[Al(OH)_6]_2(SO_4)_3.26H_2O$	0
chromate 0.3 sulfate 2.7	$Ca_6[Al(OH)_6]_2(CrO_4)_{0.3}(SO_4)_{2.7}.26H_2O$	0.3
chromate 0.6 sulfate 2.4	$Ca_6[Al(OH)_6]_2(CrO_4)_{0.6}(SO_4)_{2.4}.26H_2O$	0.6
chromate 0.9 sulfate 2.1	$Ca_6[Al(OH)_6]_2(CrO_4)_{0.9}(SO_4)_{2.1}.26H_2O$	0.9
chromate 1.2 sulfate 1.8	$Ca_6[Al(OH)_6]_2(CrO_4)_{1.2}(SO_4)_{1.8}.26H_2O$	1.2
chromate 1.5 sulfate 1.5	$Ca_6[Al(OH)_6]_2(CrO_4)_{1.5}(SO_4)_{1.5}.26H_2O$	1.5
chromate 1.8 sulfate 1.2	$Ca_6[Al(OH)_6]_2(CrO_4)_{1.8}(SO_4)_{1.2}.26H_2O$	1.8
chromate 2.1 sulfate 0.9	$Ca_6[Al(OH)_6]_2(CrO_4)_{2.1}(SO_4)_{0.9}.26H_2O$	2.1
chromate 2.4 sulfate 0.6	$Ca_6[Al(OH)_6]_2(CrO_4)_{2.4}(SO_4)_{0.6}.26H_2O$	2.4
chromate 2.7 sulfate 0.3	$Ca_6[Al(OH)_6]_2(CrO_4)_{2.7}(SO_4)_{0.3}.26H_2O$	2.7
chromate ettringite	$Ca_6[Al(OH)_6]_2(CrO_4)_3.26H_2O$	3.0

The samples have all been named according to their targeted composition (the value of x from the formula $Ca_6[Al(OH)_6]_2(CrO_4)_x(SO_4)_{3-x}.26H_2O$). This x CrO_4^{2-} will be used to discuss trends across the solid solution. It is important to note that this may not be the same as the actual measured composition of the solid phase produced. The concentrations of each element in the solid products were measured using ICP-OES, which allowed the actual composition and therefore the x CrO_4^{2-} value of the solid samples to be calculated. These data will be shown in Section 5.3.4.

5.3.1 PXRD

The PXRD patterns for the 1 day synthesised samples are plotted in Figure 5.4. Analysis of the powder diffraction data allows identification of the phases present,

including any impurities. Comparison of the PXRD patterns of the different compositions, will allow any shifts in peak position or changes in peak shape to be monitored and investigated.

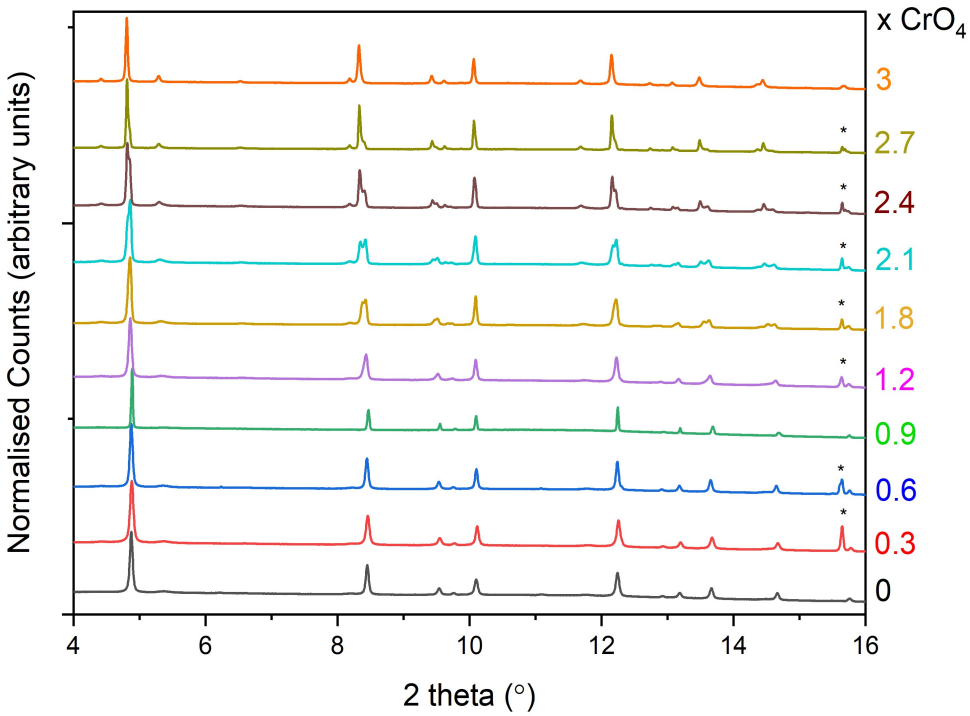

*Figure 5.4: Powder X-ray diffraction patterns for the 1 day synthesised chromate-sulfate solid solution samples (data collected on I11 at the Diamond Light Source Synchrotron, λ = 0.82661 Å). Calcite reflections = *(ICSD: 18164), all other reflections = ettringite (ICSD: 251756)*

All samples were found to have the ettringite structure but an impurity phase, identified as calcite ($CaCO_3$), was found to be present in some of the samples. The reflection at 15.64 °, marked with an asterisk in Figure 5.4 is the 104 reflection of calcite. The presence of calcite is normally caused by the absorption of carbon dioxide from the air while the synthesis is taking place. Its formation could be inhibited by carrying out the experiment in an inert atmosphere e.g. in a glove box. However, its formation in small amounts, as in this case, is not a problem for the work presented here as it can be modelled for during Pawley refinements of the data and will not impact the accuracy of the refined unit cell parameters of the ettringite phases.

The first observation that can be made is that there is a shift in peak positions for the ettringite phase between the samples with x = 0 to x = 3. This can be seen clearly in the 100 reflection at ~4.9 º (Figure 5.5). The peak position is shifting to lower 2θ values as the ratio of chromate to sulfate increases. This is because the chromate ion has a thermochemical radius of 2.29 Å and so is larger than the sulfate ion which has a thermochemical radius of 2.18 Å[6,7]. The larger radius will lead to larger d spacing in the crystal structure and therefore a smaller 2θ value of the reflections as per Bragg's law.

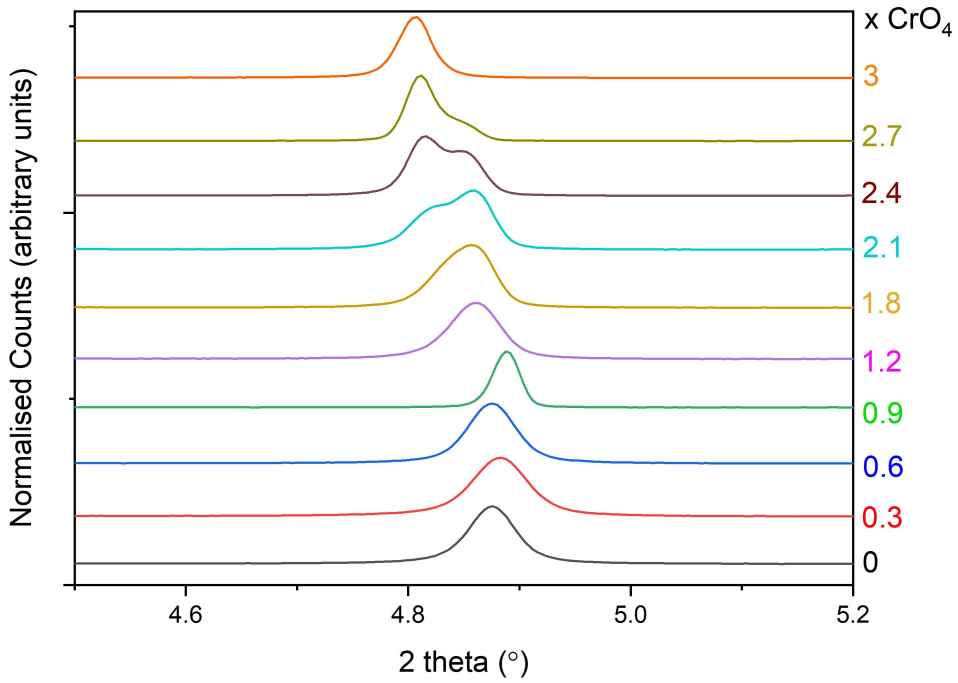

Figure 5.5: Expanded 2ϑ region between 4.5 – 5.2º 2ϑ from Figure 5.4, highlighting the 100 reflection of ettringite

For the samples to be members of the solid solution, $Ca_6[Al(OH)_6]_2(CrO_4)_x(SO_4)_{3-x}.26H_2O$, they must be single phase (P = 1). The samples with x = 0 – 1.2 can be confirmed as single phase as every reflection assigned to the ettringite phase shows no sign of splitting or peak broadening. These would be the indications that there may be more than one phase present which are isostructural but not identical. Fitting of the data to the standard ettringite pattern (ICSD: 251756) also showed no evidence

for the presence of more than one phase or the splitting of peaks. The results of the Pawley refinements will be discussed in more detail in Section 5.3.2.

However, analysis of the PXRD patterns of the samples where $1.8 \leq x < 3$, shows that each reflection is now either split into two reflections or has a distorted/ asymmetrical peak shape. Figure 5.6 shows an expanded 2θ region (7.8 - 9.0 º 2θ) highlighting the 110 reflection which splits at $x > 1.2$.

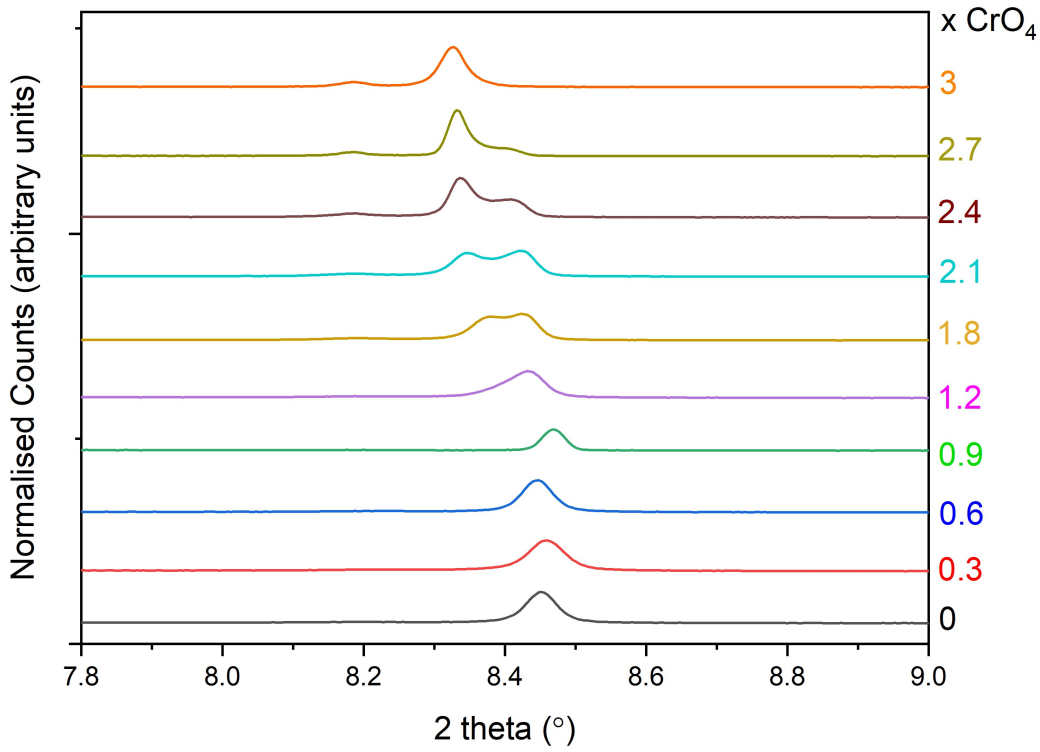

Figure 5.6: Expanded 2ϑ region between 7.8 – 9.0º 2ϑ from Figure 5.4, highlighting the 110 reflection of ettringite

The 2θ region shown in Figure 5.6 allows the peak splitting to be seen more clearly than in Figure 5.4. For the samples with x = 1.8 and 2.1 there are two observed peaks which could correspond to two ettringite phases with different compositions. The 2θ positions for these reflections are in between those of the end members (x = 0 and x = 3). This means that each of the coexisting ettringite phases are themselves

"secondary solid solutions" which is the name for solid solutions within the miscibility gap of a solid solution series[13].

A miscibility gap is a region in the phase diagram of a solid solution series where there is a mixture of two phases in a binary system (P = 2) instead of there being only one phase present (P = 1). This occurs because solid solutions often have limits based on the chemical composition and thus certain targeted compositions are outside that range and will instead produce a two phase product. Figure 5.2 b) shows an example of a phase diagram where the regions labelled "solid solution $(B_{1-x}C_x)A$" represent the compositional ranges where P = 1 and there is also a region labelled "solids BA + CA" which represents the range of compositions where P = 2.

Analysis of the PXRD patterns show that the solid solution presents as single phase P = 1 in the range $0.3 \leq x \leq 1.2$, and that the miscibility gap, where P = 2, is $1.2 < x \leq 2.7$.

The synthesis of the solid solution series was repeated using a reaction time of 7 days. These samples were not analysed using high resolution synchrotron X-ray diffraction, as they were prepared later in the project. The data presented here (Figure 5.7) were collected on a laboratory D8 Advanced powder X-ray diffractometer (λ = 1.54056 Å).

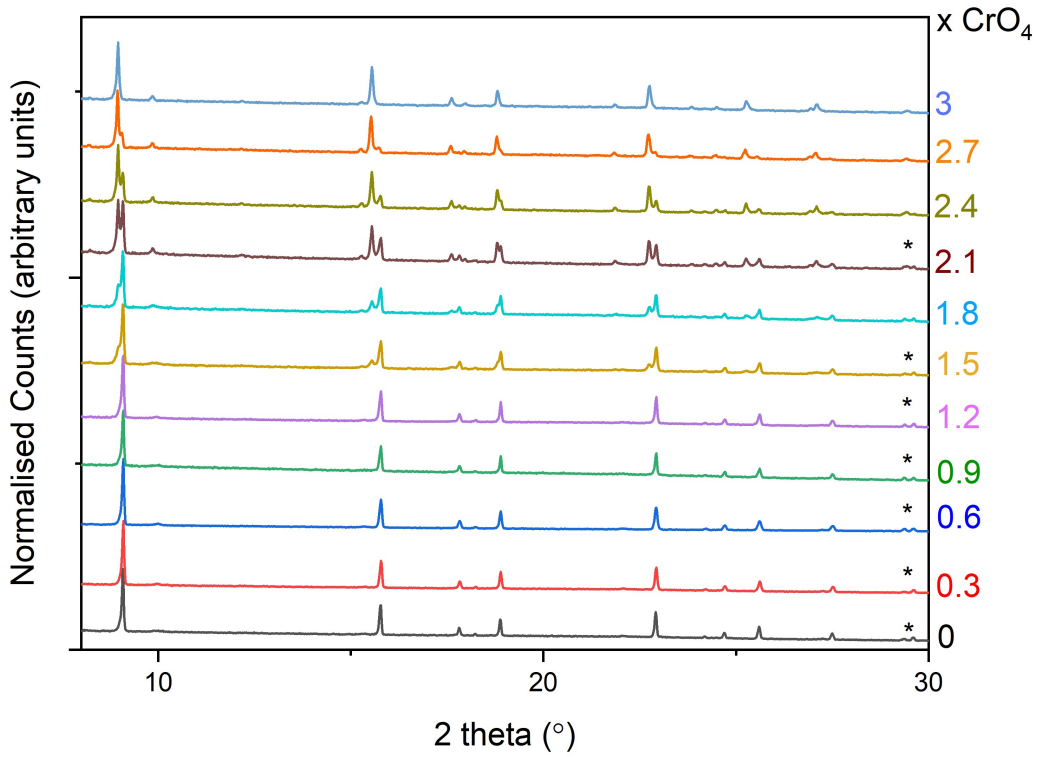

*Figure 5.7: Powder X-ray diffraction patterns for the 7 day synthesised chromate-sulfate solid solution samples (data collected on laboratory Bruker D8, λ = 1.5406 Å). Calcite reflections = *(ICSD: 18164), all other reflections = ettringite (ICSD: 251756)*

The 7 day samples were all found to be ettringite type phases, with the same observations as found in the 1 day synthesised samples. The samples with $0.3 \leq x \leq 1.2$ are single phase (P = 1) and samples with $1.2 < x \leq 2.7$ have P = 2 and therefore lie outside the compositional limit of the solid solution series.

The longer synthesis time resulted in a change in crystallinity as the peaks in the diffraction patterns are sharper. In the multiphase samples with a higher ratio of chromate the split in peaks between the two ettringite phases is more defined (Figure 5.8), meaning that the longer equilibration time has resulted in a more crystalline two phase product when $1.2 < x < 3$ in the $Ca_6[Al(OH)_6]_2(CrO_4)_x(SO_4)_{3-x}.26H_2O$ system.

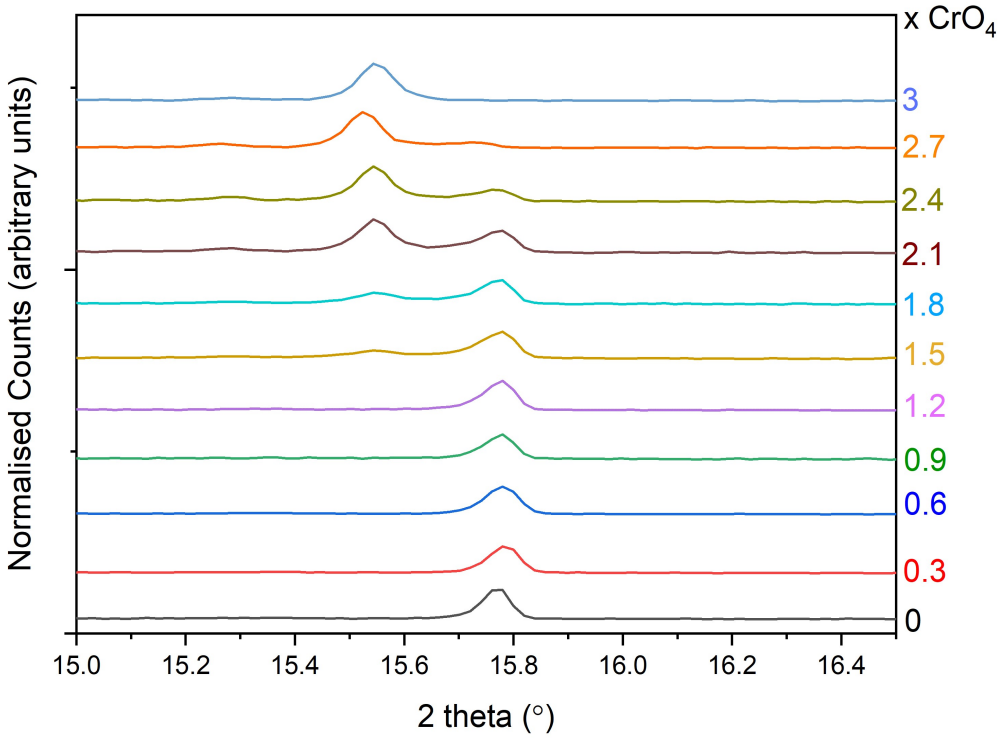

Figure 5.8: Expanded 2ϑ region between 15 – 16.5° 2ϑ from Figure 5.7, highlighting the 110 reflection of ettringite

5.3.2 Refinement of the PXRD Data

To examine the solid solution limits in more detail and refine the unit cell parameters of the different ettringite phases contained in the samples, Pawley refinements of the datasets were carried out.

If the samples were observed to be single phase from the powder X ray diffraction patterns (x = 0, 0.3, 0.6, 0.9, 1.2 and 3 for both the 1 day and 7 day samples) they were refined against starting parameters of a standard sulfate ettringite phase, a = 11.223345 Å, c = 21.45413 Å and space group = $P31c^2$. If calcite was observed to be present then it was included in the refinement. Refined unit cell parameters are given in Table 5.2.

Where samples had P = 2 and contained two different ettringite phases (x = 1.5, 1.8, 2.1, 2.4 and 2.7 for both 1 day and 7 day samples), they were refined against two different starting phases, in order to get unit cell values for both of the ettringite phases present in each sample. The two phases modelled were sulfate ettringite and chromate ettringite. Starting parameters for the sulfate ettringite phase were as above and starting parameters used for the chromate-ettringite phase were *a* = 11.3976 Å, *c* = 21.4713 Å and space group = P31c. These values are from Chapter 3.3 where Pawley refinement of data collected on a synthetic sample of pure chromate ettringite, was carried out. These samples will be referred to as "multiphase" as they contain multiple ettringite phases, this naming convention only applies to multiple ettringite phases and doesn't take into account the presence of calcite in several of the samples.

Table 5.2: Unit cell parameter values, refined using a Pawley refinement, for the chromate-sulfate solid solution (1 day and 7 day synthesis samples)

Targeted x CrO_4^{2-}	**Single or multiple ettringite phases**	***a* (1 day) Å**	***c* (1 day) Å**	***a* (7 days) Å**	***c* (7 days) Å**
0	Single	11.2243 (8)	21.4568 (2)	11.2300 (2)	21.4531 (5)
0.3	Single	11.2198 (9)	21.4294 (3)	11.2232 (1)	21.4454 (4)
0.6	Single	11.2372 (8)	21.4543 (2)	11.2267 (1)	21.4485 (3)
0.9	Single	11.2073 (1)	21.4800 (3)	11.2266 (2)	21.4440 (6)
1.2	Single	11.2514 (1)	21.4535 (4)	11.2252 (2)	21.4369 (5)
1.8	Multiple	11.2567	21.4527	11.2260 (3)	21.4312 (8)
		11.3288	21.4540	11.3890 (1)	21.4688 (3)
2.1	Multiple	11.2635 (2)	21.4507 (5)	11.2256 (4)	21.4267 (9)

		11.3677 (4)	21.4607 (1)	11.3935 (4)	21.4779 (9)
2.4	Multiple	11.2864 (2)	21.4563 (7)	11.2148 (6)	21.4133 (2)
		11.3855 (9)	21.4650 (2)	11.3846 (4)	21.4603 (9)
2.7	Multiple	11.3220	21.4715	11.2629 (1)	21.4148 (5)
		11.3902	21.4687	11.4058 (3)	21.4841 (1)
3	Single	11.3977 (7)	21.4720 (2)	11.3822 (3)	21.4524 (9)

The refined unit cell *a* parameters shown in Table 5.2 for the 1 day samples, are plotted against the targeted chromate content (x CrO_4^{2-}) in Figure 5.9.

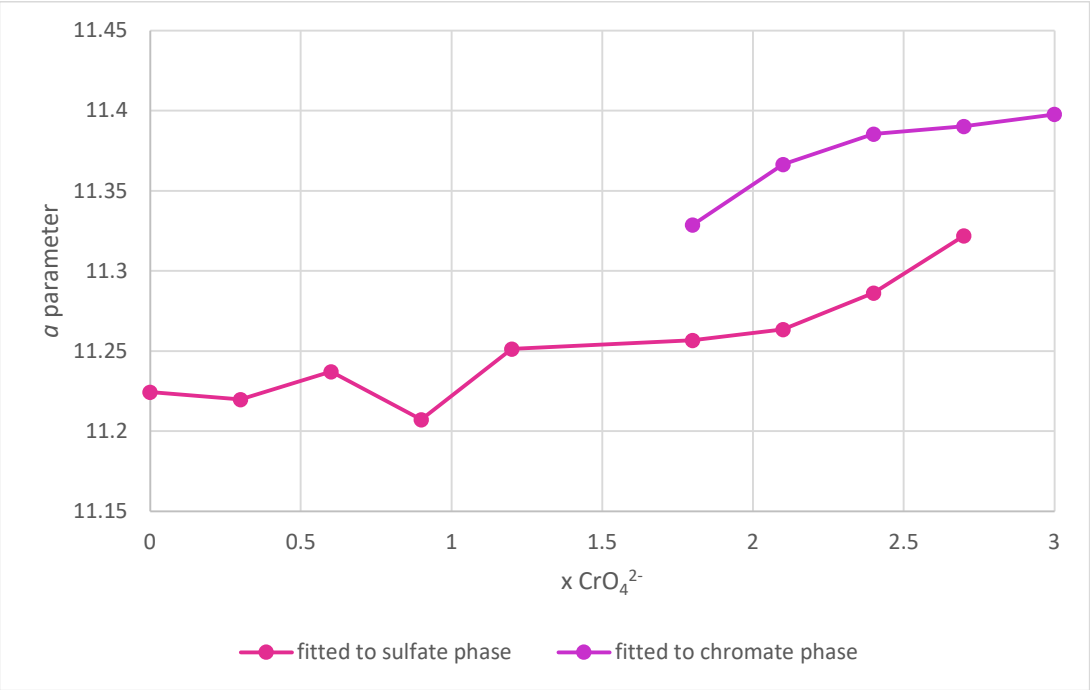

Figure 5.9: Refined a parameter for 1 day samples of the chromate-sulfate solid solution plotted against the targeted chromate ratio with error bars (too small to observe on this plot)

Figure 5.9 shows the difference in the unit cell parameter *a* as a function of increasing the chromate content in the solid phase and highlights the targeted compositions

that partition into multiple ettringite phases within one sample. The *a* unit cell parameter for the sulfate ettringite end member is 11.22 Å and for the chromate ettringite is 11.40 Å. Samples which have a composition between the end members should have an *a* unit cell parameter between these values. The *a* parameter doesn't change significantly across the single phase region ($0 < x < 1.8$) as the ratio of chromate increases and indicates that a sulfate ettringite phase has likely been formed which is not a solid solution phase. When the samples are multiphase the refined unit cell *a* parameters are in between the values for the end member phases and suggest that both coexisting phases contain different amounts of both sulfate and chromate, with one phase being sulfate rich and the other chromate rich.

There is less correlation between the *c* parameter and the chromium content of the sample, due to the similar values for the end member phases (21.46 Å for sulfate ettringite and 21.47 Å for chromate ettringite). This is due to the XO_4^{2-} anions being located in the channels between the columns of the crystal structure (Figure 5.10). In the *c* direction there is enough space between the oxyanions that the change in size from a sulfate ion (2.18 Å) to a chromate ion (2.29 Å) doesn't affect the overall unit cell size in this direction. The average distance between the X sites in the *c* direction is 5.23 Å (X1-X2 = 4.4 Å, X2-X3 = 3.8 Å, X1-X3 = 7.5 Å). However, in the *a* direction the XO_4^{2-} tetrahedra are closer to one another (the distance between the two highlighted on the projection is 3.88 Å) and so the change in size from sulfate to chromate will change the overall unit cell in this direction as the amount of chromate increases. Thus, the *a* parameter is affected by a change in anion XO_4^{2-} while the *c* is not and as such the refined *c* parameters plotted against the chromate content will not be shown (values are still shown in Table 5.2).

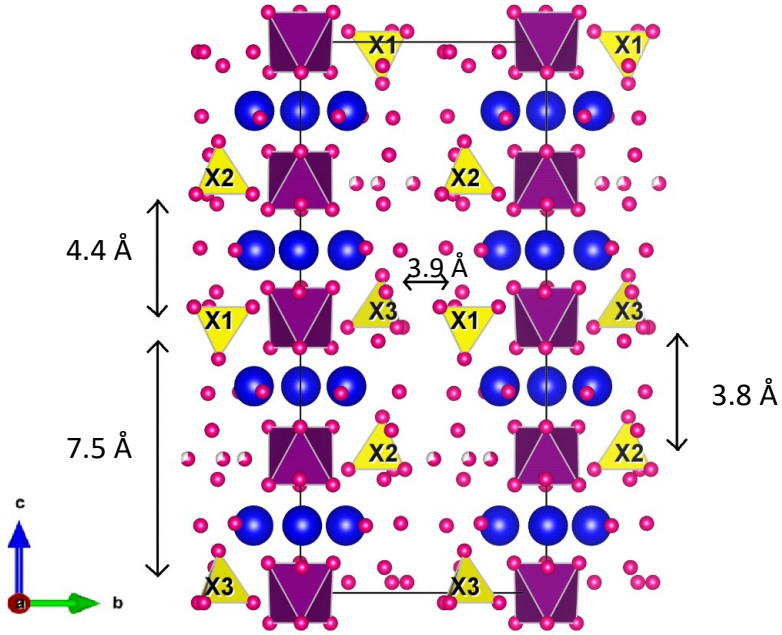

Figure 5.10: [11-20] projection of the ettringite crystal structure parallel to the c axis. Yellow tetrahedra = XO_4^{2-}, X = S^{6+} or Cr^{6+}. Arrows highlight the proximity of the XO_4^{2-} anions in different directions

The refined *a* unit cell parameters from Table 5.2 for the 7 day samples are plotted against the targeted ratio of chromate (x CrO_4^{2-}) in Figure 5.11.

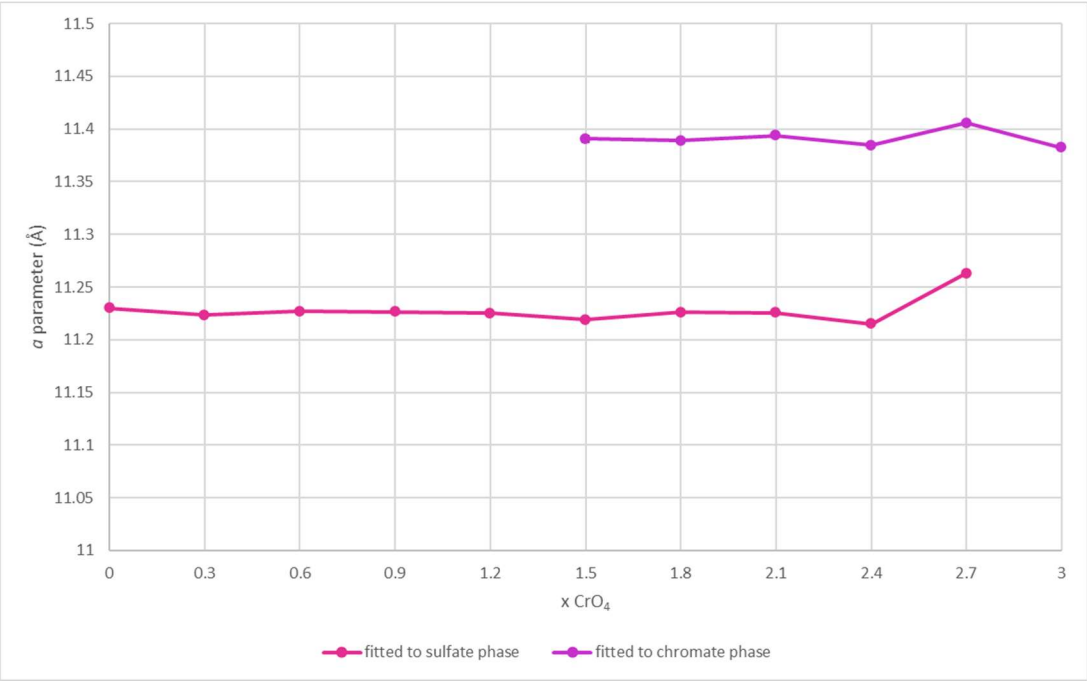

Figure 5.11: Refined a parameter for 7 day samples of the chromate-sulfate solid solution plotted against the targeted chromate ratio with error bars

The results from refinement of the 7 day samples differ from those of the 1 day samples as the *a* parameter stays constant (within error) at the starting sulfate ettringite value as the chromate content increases even for the compositions where a partitioning of phases occurs (x CrO_4^{2-} > 1.2). The *a* parameters for each ettringite phase within the multiphase samples were refined to the values for the pure end members sulfate ettringite and chromate ettringite. These phases within the multiphase samples were therefore not likely to be members of a secondary solid solution and were more likely to have split into a sulfate ettringite phase and a chromate ettringite phase. The *a* parameter staying constant for the single phase samples suggests that the product forming is sulfate-ettringite and not a member of the solid solution. The results of the elemental analysis (Chapter 5.3.4) will show whether these samples have any chromium incorporated.

Leaving the mixtures to equilibrate for longer during the synthesis time resulted in more crystalline products. A single phase was still produced when 0 < x CrO_4^{2-} ≤ 1.2 but likely with limited incorporation of the chromium into the ettringite phase. Where the chromate content is higher than this there was a separation of phases and the two end members were produced with no detectable secondary solid solutions being formed. ICP-OES will be used to measure the concentrations of chromium and sulfur in the products and provide the measured compositions of the formed products. (Chapter 5.3.4)

This suggests that when the synthesis was targeting a higher chromate content, the most stable phases were the end member compositions and the solid solution cannot tolerate chromate with x > 1.2.

Overall, these results correlate well with the results acquired by Leisinger and Lothenbach[13] even though they were using a different synthesis method and longer reaction time. They found a miscibility gap at values of x ≥ 1.2. This corroborates that there is a compositional limit to the solid solution $Ca_6[Al(OH)_6]_2(CrO_4)_x(SO_4)_{3-x}.26H_2O$.

5.3.3 FTIR

Fourier transform infrared spectroscopy was used to identify the presence of sulfate and chromate in the solid solution samples. The presence of carbonate impurities can also be detected in the samples by looking for the carbonate stretch.

FTIR data were collected on all samples from the solid solution and the results are plotted below (1 day synthesis samples in Figure 5.12 and 7 day samples in Figure 5.13).

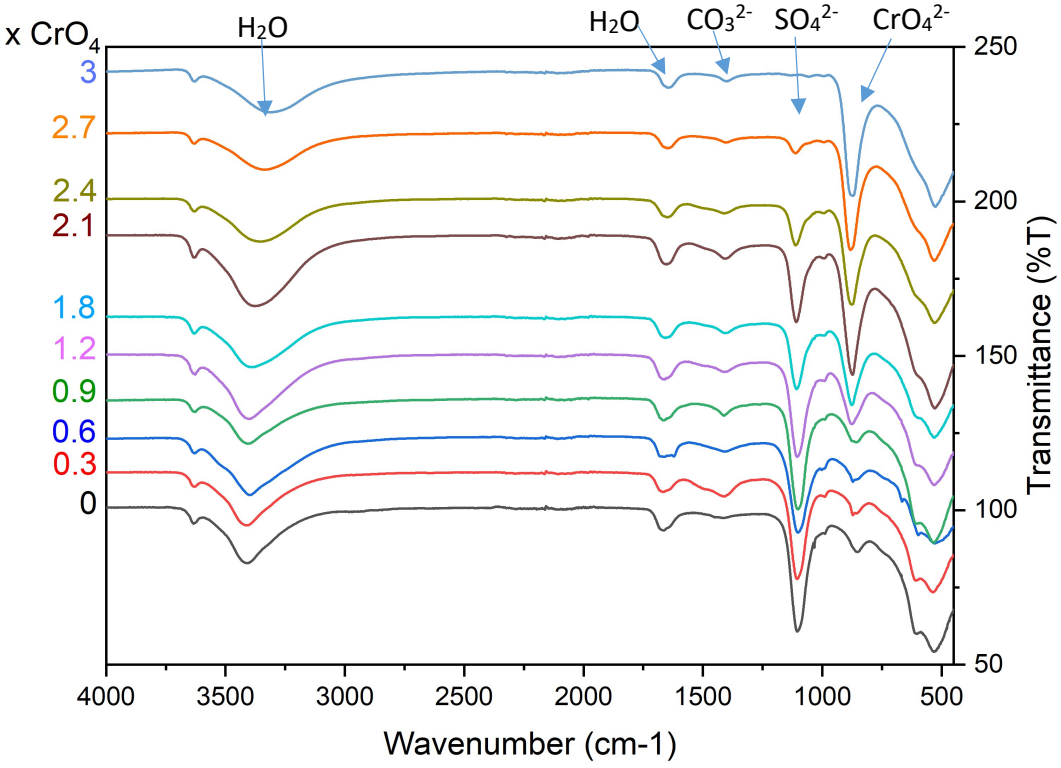

Figure 5.12: FTIR data for the 1 day synthesis samples (chromate-sulfate solid solution), with bands for key functional groups indicated by arrows and labels

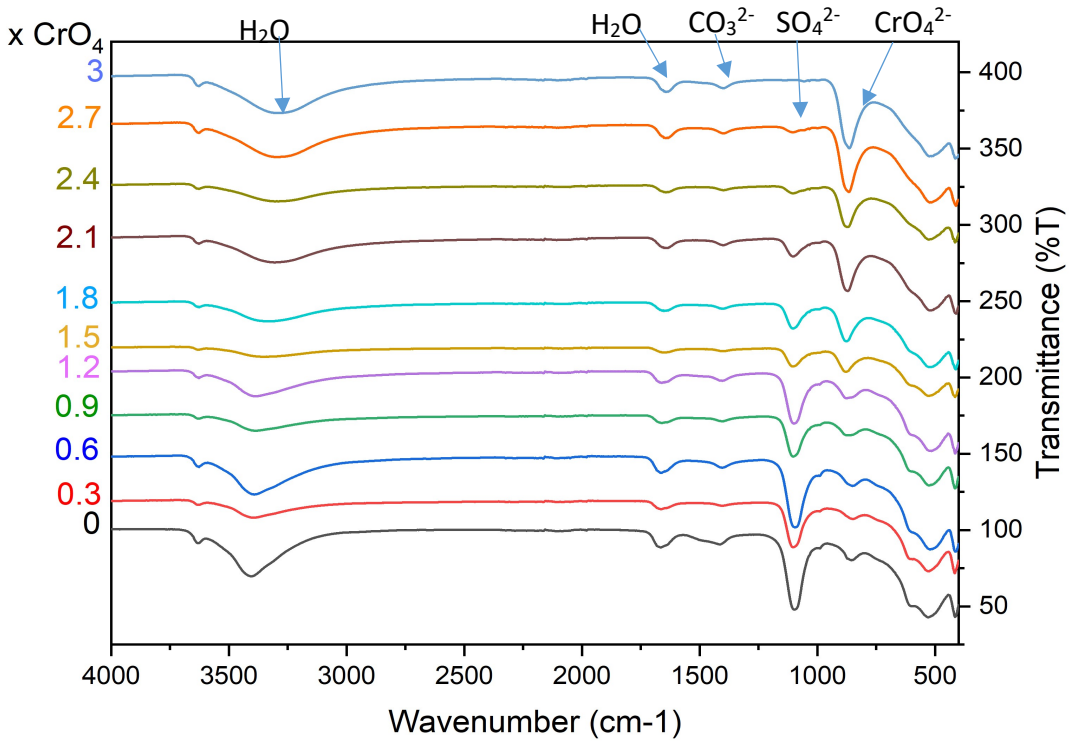

Figure 5.13: FTIR data for the 7 day synthesis samples (chromate-sulfate solid solution) with bands for key functional groups indicated by arrows and labels

The key functional groups of ettringite are all present in the IR spectra. The water stretch is the broad peak at ~3400 cm^{-1} and the water bend is the peak at ~1650 cm^{-1}. The sulfate stretch is identified by presence of a band at 1108 cm^{-1} and the chromate stretch is at 875 cm^{-1}. Unfortunately, the chromate band lies in an area with many overlapping bands, the AlOH band is present at 851 cm^{-1} so will also be present in all of the ettringite phase spectra. The presence of any calcite impurities in the samples or incorporated carbonate will be identified by the presence of a carbonate stretch at 1400 cm^{-1}.

All the spectra have a carbonate band with a small intensity which correlates with the PXRD results where calcite was identified in all samples apart from those with x = 1, 0.9 and 3 for the 1 day samples and x = 2.4, 2.7 and 3 for the 7 day samples. The presence of a carbonate peak in the IR spectrum but no observed calcite in the PXRD

patterns for these samples, could be due to the presence of such a small amount of calcite that it could not be detected by PXRD.

As the targeted ratio of chromate increases the intensity of the chromate peak increases relative to the intensity of the sulfate stretch. However, the FTIR analysis was not carried out quantitatively and so to confirm exact quantities of ions in the solid samples, elemental analysis using the ICP-OES technique was carried out and the results of this will be discussed in Section 5.3.4.

5.3.4 ICP-OES

The solid samples were dissolved in nitric acid and the resulting solutions were analysed using ICP-OES, to measure the concentration of each element present in each solution. Specific information on this procedure is given in Chapter 2.2.4.

For these samples, the elements analysed were calcium, aluminium, sulfur and chromium. Oxygen and hydrogen concentrations cannot be determined by ICP-OES due to the nitric acid matrix and carbon cannot be detected due to its small number of electrons, causing it to be difficult to ionise.

The raw data obtained from the ICP-OES analysis is given in milligrams per litre for each element. These values were used along with the molar masses of the elements to calculate a molar concentration for each element in the ettringite phase. The ideal stoichiometry for the solid solution phases is $Ca_6[Al(OH)_6]_2(CrO_4)_x(SO_4)_{3-x}.26H_2O$ and in terms of the cations and anions the molar ratio is 6Ca: 2Al: 3(CrO_4^{2-} + SO_4^{2-}). The concentration of aluminium detected in the solid digests was normalised to 2 and this allowed the molar ratios of calcium, chromate and sulfate to be calculated. An accurate x CrO_4^{2-} could then be calculated using the ratio of CrO_4^{2-}:SO_4^{2-} normalised to a total of 3. The results are given in Table 5.3 for the 1 day samples and Table 5.4 for the 7 day samples.

Table 5.3: ICP-OES results for solid digests of 1 day chromate-sulfate ettringite samples (= single phase)*

Targeted x CrO_4^{2-}		**Measured concentrations (mM)**						**Molar ratios Ca:Al:(CrO_4^{2-} + SO_4^{2-}) normalised to 6 Ca^{2+} (Ideal would be 6:2:3)**						**Measured x CrO_4^{2-}**
		Ca^{2+}	Al^{3+}	SO_4^{2-}	CrO_4^{2-}	SO_4^{2-} + CrO_4^{2-}		Ca^{2+}	Al^{3+}	SO_4^{2-} + CrO_4^{2-}	SO_4^{2-}	CrO_4^{2-}		
0 *		8.04	2.87	3.50	0.00	3.50		5.61	2.00	2.44	2.44	0.00		**0.00**
0.3 *		8.77	2.73	3.26	0.06	3.32		6.42	2.00	2.43	2.39	0.04		**0.05**
0.6 *		8.51	2.71	3.30	0.28	3.58		6.28	2.00	2.64	2.43	0.21		**0.24**
0.9 *		8.86	2.99	3.06	0.65	3.70		5.93	2.00	2.48	2.05	0.43		**0.52**
1.2 *		7.99	2.58	2.58	0.94	3.52		6.18	2.00	2.73	2.00	0.73		**0.80**
1.8		9.13	3.01	1.94	2.16	4.09		6.06	2.00	2.72	1.29	1.43		**1.58**
2.1		8.25	2.72	1.37	2.44	3.82		6.06	2.00	2.80	1.01	1.80		**1.92**
2.4		8.63	2.85	0.88	3.11	3.99		6.06	2.00	2.81	0.62	2.19		**2.34**
2.7		8.24	2.78	0.36	3.58	3.94		5.93	2.00	2.83	0.26	2.57		**2.72**
3 *		8.12	2.65	0.00	3.85	3.85		6.14	2.00	2.91	0.00	2.91		**3.00**

Table 5.4: ICP-OES results for solid digests of 7 day chromate-sulfate ettringite samples (= single phase)*

Targeted x CrO_4^{2-}		**Measured concentrations (mM)**						**Molar ratios Ca:Al:(CrO_4^{2-} + SO_4^{2-}) normalised to 6 Ca^{2+} (Ideal would be 6:2:3)**						**Measured x CrO_4^{2-}**
		Ca^{2+}	Al^{3+}	SO_4^{2-}	CrO_4^{2-}	CrO_4^{2-} + SO_4^{2-}		Ca^{2+}	Al^{3+}	CrO_4^{2-} + SO_4^{2-}	SO_4^{2-}	CrO_4^{2-}		
0 *		9.01	2.77	3.56	0.00	3.56		6.51	2.00	2.57	2.57	0.00		**0.00**
0.3 *		8.61	2.99	3.69	0.03	3.72		5.77	2.00	2.49	2.47	0.02		**0.02**
0.6 *		8.48	2.92	3.44	0.09	3.52		5.81	2.00	2.41	2.35	0.06		**0.07**
0.9 *		8.11	2.80	3.09	0.37	3.46		5.79	2.00	2.47	2.21	0.26		**0.32**
1.2 *		8.17	2.87	2.90	0.50	3.40		5.69	2.00	2.37	2.02	0.35		**0.44**
1.5		8.17	2.83	2.23	1.26	3.49		5.79	2.00	2.47	1.58	0.89		**1.08**
1.8		8.15	2.76	1.91	1.53	3.44		5.90	2.00	2.49	1.38	1.11		**1.33**
2.1		8.36	2.90	1.31	2.35	3.66		5.76	2.00	2.52	0.90	1.62		**1.92**
2.4		8.03	2.75	0.84	2.74	3.58		5.84	2.00	2.60	0.61	1.99		**2.30**
2.7		8.36	2.86	0.42	3.36	3.78		5.84	2.00	2.64	0.29	2.35		**2.67**
3 *		8.12	2.72	0.00	3.68	3.68		5.97	2.00	2.71	0.00	2.71		**3.00**

The ideal molar ratio for ettringite in terms of the cations and anions is $6Ca^{2+}$: $2Al^{3+}$: $3SO_4^{2-}$, so for the solid solution the stoichiometry should ideally be Ca^{2+}:Al^{3+}:(CrO_4^{2-} + SO_4^{2-}) 6:2:3. After normalisation of the aluminium to 2 the ratio of calcium for all of the samples was 6 ± 0.51, and the ratio of the anions (CrO_4^{2-} + SO_4^{2-}) was mostly between 2.5 and 3. The value of the anions was lower than ideal and this is because there is often larger errors on the determination of sulfur using ICP-OES, due to the difficulty in ionising sulfur. Despite this, the values obtained can still be used to determine the chromium content of the samples. The ratios obtained confirm, along with the PXRD and FTIR data, that ettringite-type phases have formed.

The individual chromate and sulfate values were combined and normalised to 3 to give an accurate, measured x CrO_4^{2-} which was found to be different to the targeted x CrO_4^{2-}. For every sample the measured x CrO_4^{2-} was lower than targeted, indicating that there was a preference for the ettringite structure to incorporate the sulfate over the chromate. This effect was more pronounced in the single phase samples (0 < targeted x CrO_4^{2-} ≤ 1.2) where the measured x CrO_4^{2-} was much lower than the target.

The samples with a targeted x CrO_4^{2-} > 1.2 were found to be multiphase by PXRD and therefore not part of the solid solution series. The ICP-OES results for these samples had measured x CrO_4^{2-} values which were closer to their targets. This was because when there was the partitioning of phases to form sulfate rich and chromate rich ettringite phases more of the sulfate and chromate containing reagents were able to be converted to the solid products.

The graphs of the refined unit cell parameters plotted against the targeted x CrO_4^{2-} from section 5.3.2 can now be replotted against the measured x CrO_4^{2-} values and these are shown in Figure 5.14 and Figure 5.15.

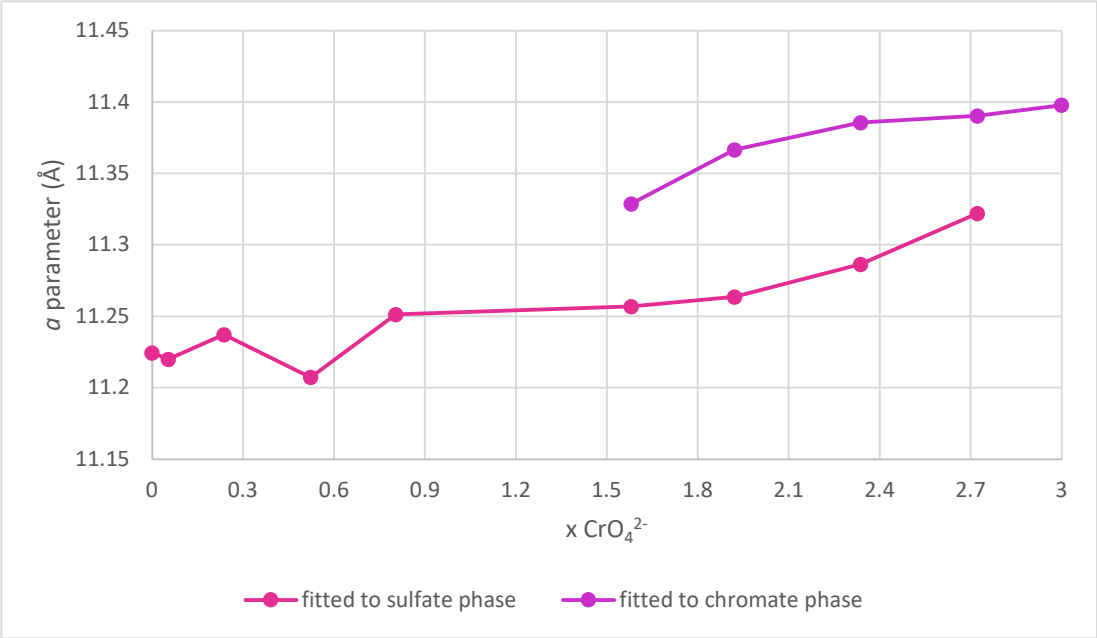

Figure 5.14: Accurate x CrO_4^{2-} plot of the refined a parameter for 1 day samples of the chromate-sulfate solid solution (the targeted x CrO_4^{2-} values are the increments on the x axis) with error bars

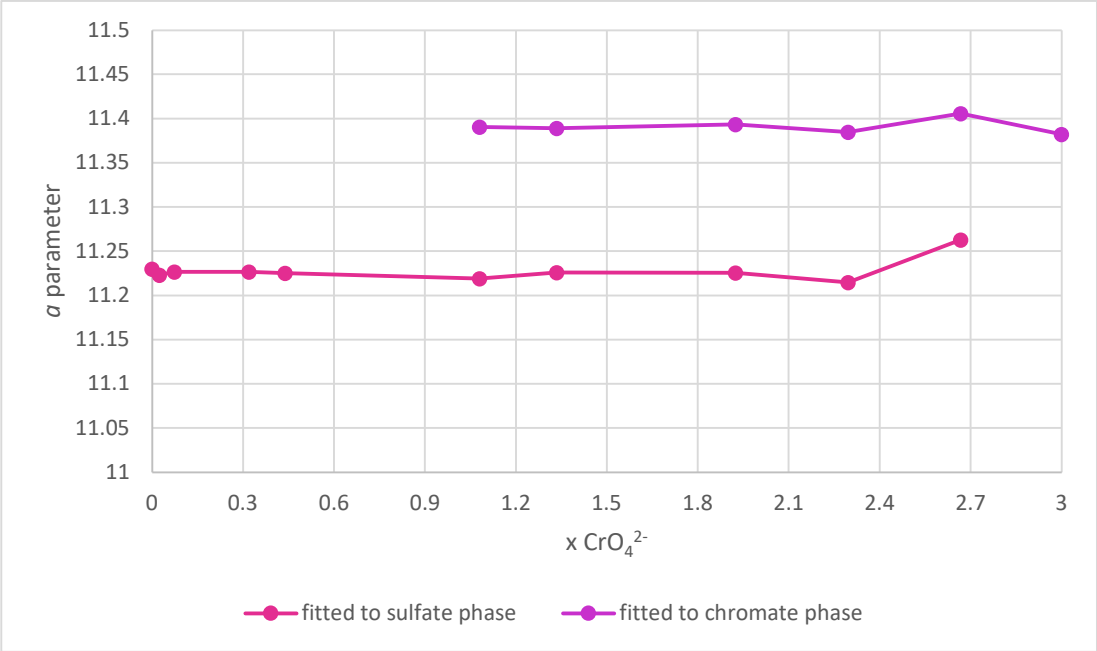

Figure 5.15: Accurate x CrO_4^{2-} plot of the refined a parameter for 7 day samples of the chromate-sulfate solid solution (the targeted x CrO_4^{2-} values are the increments on the x axis) with error bars

These corrected plots show the change in unit cell parameter *a* as a function of the measured amount of chromate in the solid phase. They show the true amount of chromate that the solid solution can tolerate before splitting into two phases.

For the 1 day samples, x CrO_4^{2-} = 0.8 was the highest amount of chromate that could be incorporated into a single ettringite-type phase before there was a partitioning of phases. This compares to a value of x CrO_4^{2-} = 0.44 for the 7 day samples. This shows that when the samples have longer to equilibrate the structure prefers to displace the chromate in favour of a higher ratio of sulfate.

However, the fact still remains that the unit cell *a* parameter is not changing significantly between the single phase samples, even though the ICP-OES results have shown that chromium is present in these samples. This means that these samples are likely not true members of the solid solution, and that any chromium incorporated is either just absorbed onto the surfaces of the ettringite grains, or is forming structures in domains so small that there is no effect on the crystal structure as a whole.

The paper by Leisinger and Lothenbach found a maximum x CrO_4^{2-} of 0.9 for the solid solution[13], which is similar to the results found in this study for the 1 day samples even though their study had a different synthesis procedure and a 90 day synthesis time. Their use of all calcium containing start materials resulted in the formation of gypsum ($CaSO_4.2H_2O$) as a secondary phase for the samples targeting higher sulfate contents.

5.3.5 SEM and EDS

SEM images were acquired for a selection of samples, synthesised for both 1 day and 7 days, to confirm the results from other analysis techniques and analyse the samples morphology. For the chromate-sulfate system the samples analysed by SEM/EDS were the 1 day and 7 day samples with targeted x = 1.2 (Figure 5.16 a and b) and 2.1 (Figure 5.17 a and b).

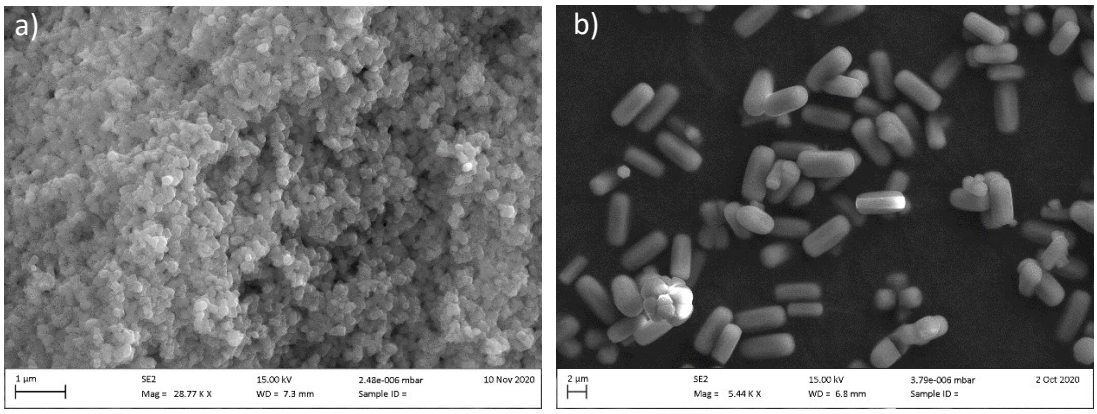

Figure 5.16 a) and b): SEM images for the samples chromate 1.2 sulfate 1.8 synthesised for a) 1 day and b) 7 days

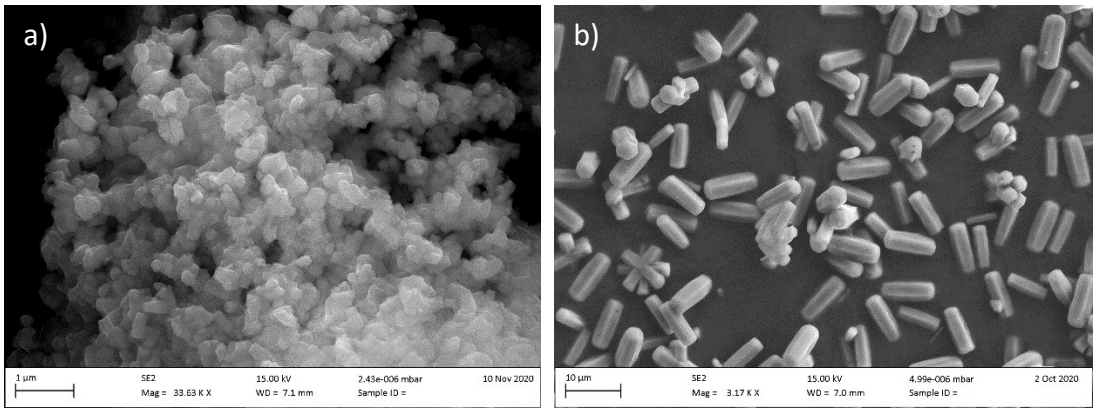

Figure 5.17 a) and b): SEM images for the samples chromate 2.1 sulfate 0.9 synthesised for a) 1 day and b) 7 days

These images show the differences in crystallite morphology when the same compositions are targeted with different synthesis times. The “chromate 1.2 sulfate 1.8” samples (Figure 5.16) were both identified as single phase from the PXRD data, and EDS analysis shows that all areas contain small amounts of Cr and larger amounts of S. The EDS spectra for these samples are given in Appendix 3. The difference in synthesis time caused the crystallites to grow in size from agglomerates of very small crystallites for the 1 day sample, to larger, distinct hexagonal prismatic crystallites for the 7 day sample.

The “chromate 2.1 sulfate 0.9” samples (Figure 5.17) were both identified as being multiphase from the PXRD data. EDS analysis of the 1 day sample shows all areas

containing small amounts of Cr and larger amounts of S. The SEM images again show that the crystallites grow larger with longer synthesis time, and EDS analysis of the 7 day sample shows that the larger crystals exhibit zoning with the middle of the crystallites being shown to contain S and no Cr, and the ends of the crystallites are shown to contain Cr and no S.

Overall, we see that this system has a very limited ability to form a solid solution series, and only small amounts of chromate ions, as measured by ICP-OES, were able to incorporate into the samples resulting in single phase products. These single phase products are also thought not to be true solid solution members due to the unit cell parameters remaining constant. When the targeted amount of chromate was increased beyond a certain value, multiphase products were formed which were able to incorporate the larger amounts of chromium detected by ICP-OES into the chromate rich phase that was formed alongside a sulfate rich phase.

Determining the limits of the solid solution is important for waste removal purposes as it helps develop remediation methods that maximise chromium removal. Knowledge of the solid solution can indicate the amounts of precursors that will be needed to target the precipitation of specific compositions when other ions are also present in the wastewater.

5.4 The Selenate-Sulfate Ettringite Solid Solution

Table 5.5 shows the target compositions used for investigations into the solid solution formation of the $Ca_6[Al(OH)_6]_2(SeO_4)_x(SO_4)_{3-x}.26H_2O$ (x = 0, 0.3, 0.6, 0.9, 1.2, 1.5, 1.8, 2.1, 2.4, 2.7 and 3.0) system. As with the chromate-sulfate system, two different ageing periods were used, 1 day and 7 days, with targeted compositions being the same for both. Each synthesised sample was given a sample name based on the value of x SeO_4^{2-} being targeted.

Table 5.5: Targeted compositions of the selenate-sulfate ettringite solid solution ($Ca_6[Al(OH)_6]_2(SeO_4)_x(SO_4)_{3-x}.26H_2O$) samples

Sample Name	Target Composition	Targeted x SeO_4^{2-}
sulfate ettringite	$Ca_6[Al(OH)_6]_2(SO_4)_3.26H_2O$	0
selenate 0.3 sulfate 2.7	$Ca_6[Al(OH)_6]_2(SeO_4)_{0.3}(SO_4)_{2.7}.26H_2O$	0.3
selenate 0.6 sulfate 2.4	$Ca_6[Al(OH)_6]_2(SeO_4)_{0.6}(SO_4)_{2.4}.26H_2O$	0.6
selenate 0.9 sulfate 2.1	$Ca_6[Al(OH)_6]_2(SeO_4)_{0.9}(SO_4)_{2.1}.26H_2O$	0.9
selenate 1.2 sulfate 1.8	$Ca_6[Al(OH)_6]_2(SeO_4)_{1.2}(SO_4)_{1.8}.26H_2O$	1.2
selenate 1.5 sulfate 1.5	$Ca_6[Al(OH)_6]_2(SeO_4)_{1.5}(SO_4)_{1.5}.26H_2O$	1.5
selenate 1.8 sulfate 1.2	$Ca_6[Al(OH)_6]_2(SeO_4)_{1.8}(SO_4)_{1.2}.26H_2O$	1.8
selenate 2.1 sulfate 0.9	$Ca_6[Al(OH)_6]_2(SeO_4)_{2.1}(SO_4)_{0.9}.26H_2O$	2.1
selenate 2.4 sulfate 0.6	$Ca_6[Al(OH)_6]_2(SeO_4)_{2.4}(SO_4)_{0.6}.26H_2O$	2.4
selenate 2.7 sulfate 0.3	$Ca_6[Al(OH)_6]_2(SeO_4)_{2.7}(SO_4)_{0.3}.26H_2O$	2.7
selenate ettringite	$Ca_6[Al(OH)_6]_2(SeO_4)_3.26H_2O$	3.0

5.4.1 PXRD

The PXRD patterns for the 1 day synthesis samples are plotted in Figure 5.18. All samples were found to be ettringite type phases and the impurity phase calcite was identified as present in the patterns of some samples (marked with an asterisk on the relevant patterns).

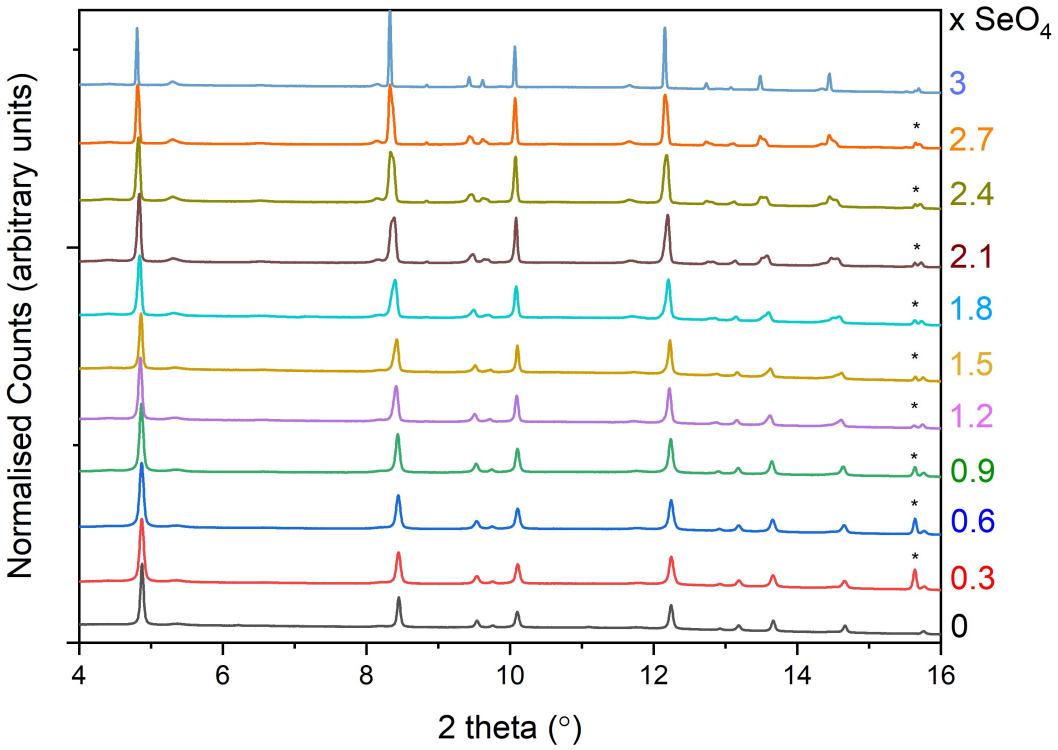

*Figure 5.18: Powder X-ray diffraction patterns for the 1 day synthesised selenate-sulfate solid solution samples (data collected on I11 at the Diamond Light Source Synchrotron, λ = 0.82661 Å). Calcite reflections = *(ICSD: 18164), all other reflections = ettringite (ICSD: 251756)*

Comparing the position of the reflection at ~4.85° 2θ (the 100 reflection of ettringite, highlighted in Figure 5.19) between the samples with x = 0 and x = 3 shows a shift to a lower 2θ angle. This is because the selenate ion has a thermochemical radius of 2.29 Å[6,7] which is larger than that of the sulfate anion (2.18 Å).

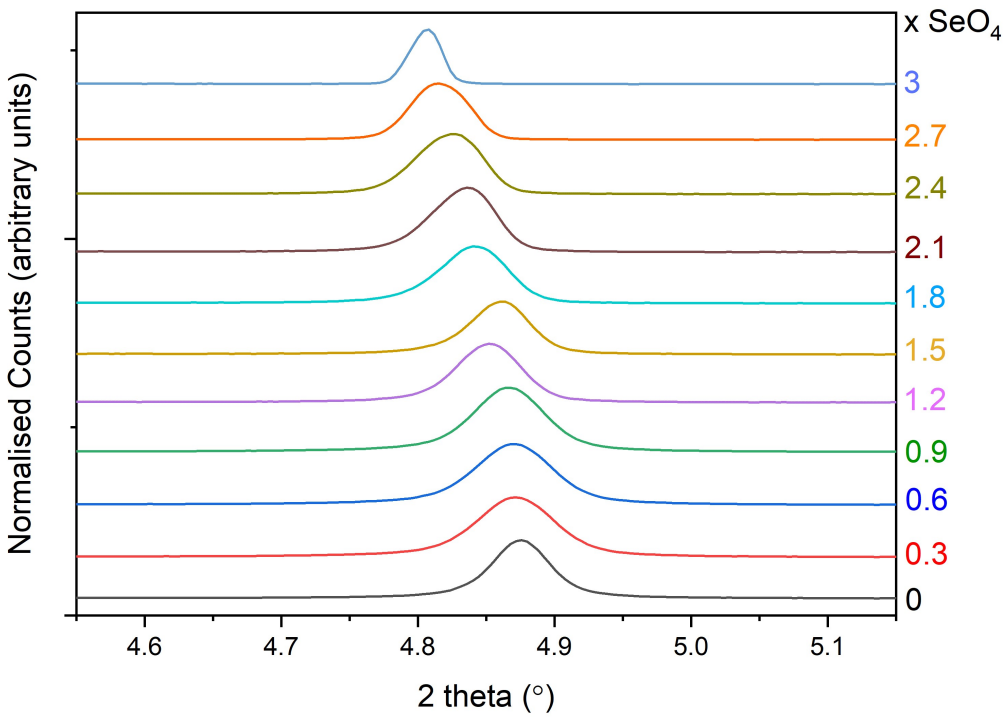

Figure 5.19: Expanded 2ϑ region between 4.55 – 5.15° 2ϑ from Figure 5.18, highlighting the 100 reflection of ettringite

The first sign that a complete solid solution had been successfully produced would be no splitting or broadening of the observed peaks in the PXRD patterns (indicating that P = 1 for all samples). However, the samples with x = 1.8 , 2.1, 2.4 and 2.7 show peak splitting. Figure 5.20 shows an expanded 2θ region in order to see these effects more clearly.

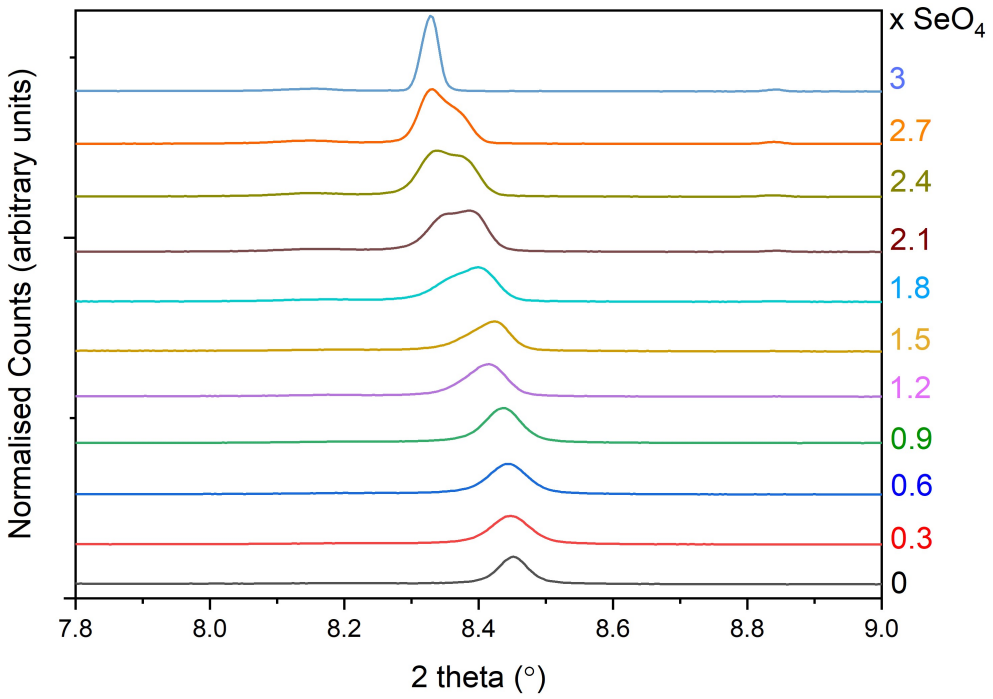

Figure 5.20: Expanded 2ϑ region between 7.8 – 9.0° 2ϑ from Figure 5.18, highlighting the 110 reflection of ettringite

The PXRD patterns confirm that the samples with x = 0 - 1.5 and 3 have all reflections assigned to either a single ettringite type phase or calcite where the impurity is present. The other patterns, with observable peak asymmetry, were assigned as multiphase samples (P = 2) as they contained more than one ettringite type phase. Pawley refinements of the unit cell parameters were carried out on all the datasets and the results of these will be presented and discussed in section 5.4.2.

PXRD data for the samples synthesised for 7 days were collected on a laboratory D8 Advanced powder X-ray diffractometer (λ = 1.54056 Å) and the results are shown in Figure 5.21.

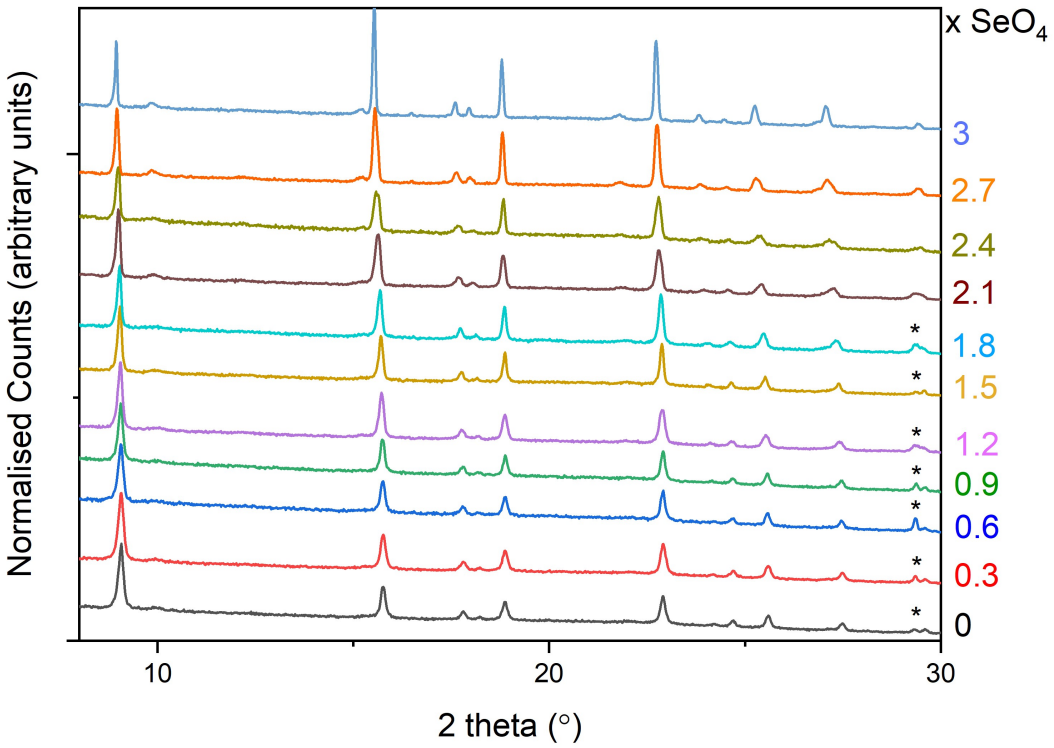

*Figure 5.21: Powder X-ray diffraction patterns for the 7 day synthesised selenate-sulfate solid solution samples (data collected on laboratory Bruker D8, λ = 1.5406 Å). Calcite reflections = *(ICSD: 18164), all other reflections = ettringite (ICSD: 251756)*

The longer synthesis time has resulted in all samples presenting as single phase in the PXRD patterns. An expanded 2θ range shows this in greater clarity in Figure 5.22. Although some of the samples contained calcite as an impurity (x = 0 – 1.8) the main phase present was a single ettringite type phase.

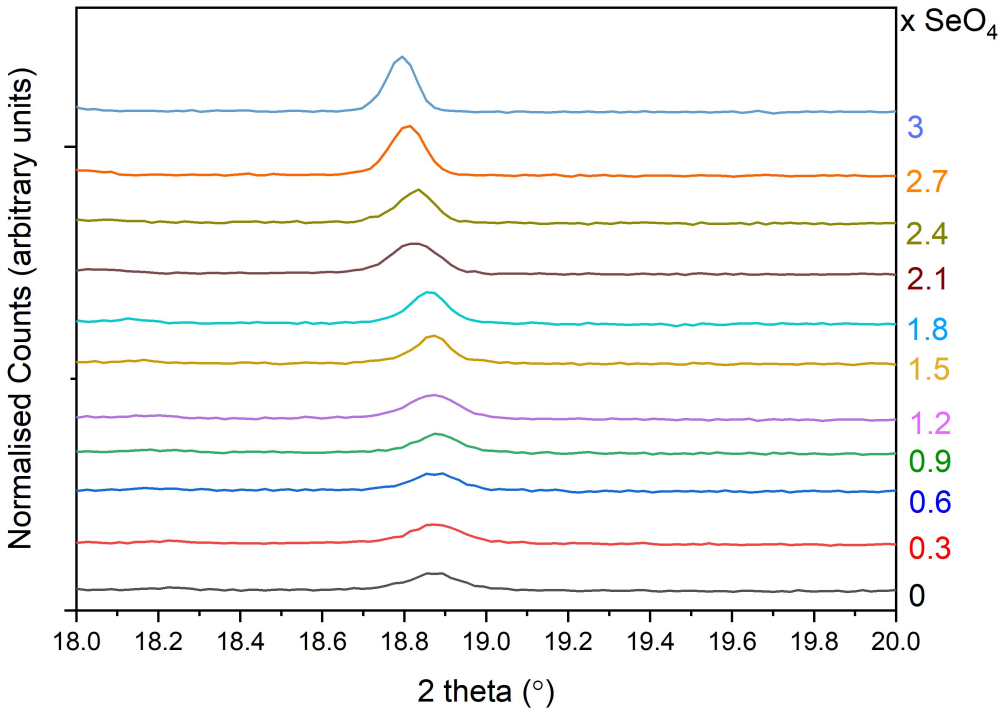

Figure 5.22: Expanded 2ϑ region between 18 – 20° 2ϑ from Figure 5.21 highlighting the 104 reflection of ettringite

Since all the samples were single phase (P = 1) it could be concluded from the PXRD data that a complete solid solution has been formed for the series $Ca_6[Al(OH)_6]_2(SeO_4)_x(SO_4)_{3-x}.26H_2O$ (x = 0, 0.3, 0.6, 0.9, 1.2, 1.5, 1.8, 2.1, 2.4, 2.7 and 3.0). The results of Pawley refinement of the data will now be discussed in order to observe any trends in unit cell parameters across this solid solution series which will aid confirmation that this is a complete solid solution.

5.4.2 Refinement of the PXRD Data

The unit cell parameters of the ettringite type phases were refined using the Pawley method. This was done against standard sulfate ettringite parameters from ICSD card 251756, *a* = 11.223345 Å, *c* = 21.45413 Å and space group = $P31c^2$ when the patterns

had been determined to be single phase (P = 1). When the samples were identified as multiphase (P = 2) two sets of starting parameters were used, the first being the standard sulfate ettringite parameters as before and the other being selenate ettringite unit cell parameters. These were determined by Pawley refinement of data collected on a synthetic sample of pure selenate ettringite (Chapter 3.3), to be *a* = 11.3870 Å, *c* = 21.4530 Å, space group P31c. If calcite was observed in the PXRD pattern it was included in the refinement of that sample. Table 5.6 shows the refined parameters for the samples.

Table 5.6: Unit cell parameter values, refined using a Pawley refinement, for the selenate-sulfate solid solution (1 day and 7 day synthesis samples)

Targeted x SeO_4^{2-}	**Single or multiple ettringite phases**	***a* (1 day) Å**	***c* (1 day) Å**	***a* (7 days) Å**	***c* (7 days) Å**
0	Single	11.2243 (8)	21.4568 (2)	11.2249 (3)	21.4453 (8)
0.3	Single	11.2279 (7)	21.4352 (2)	11.2262 (3)	21.4387 (8)
0.6	Single	11.2341 (2)	21.4366 (5)	11.2348 (3)	21.4398 (9)
0.9	Single	11.2446 (9)	21.4405 (2)	11.2377 (3)	21.4271 (8)
1.2	Single	11.2725 (1)	21.4454 (4)	11.2563 (6)	21.4344 (1)
1.5	Single	11.2688 (1)	21.4378 (4)	11.2646 (4)	21.4287 (9)
1.8	Multiple for 1 day sample	11.2736	21.4470	11.2866 (5)	21.4367 (1)
		11.3379	21.4590		
2.1	Multiple for 1 day sample	11.2924	21.4457	11.2941 (5)	21.4377 (1)
		11.3565	21.4574		
2.4		11.3136	21.4662	11.3424 (6)	21.4487 (1)

	Multiple for 1 day sample	11.3862	21.4806		
2.7	Multiple for 1 day sample	11.3402	21.4918	11.3699 (7)	21.4539 (1)
		11.3988	21.4620		
3	Single	11.3935 (6)	21.4626 (2)	11.3921 (3)	21.4726 (7)

The refined unit cell parameters can be plotted against the targeted x SeO_4^{2-} to allow observation of any trends. For the reasons explained in section 5.3.2, the *c* parameter does not change significantly between the end members, x = 0 and 3, and so plots of the varying *c* parameter will not be shown. The refined *a* parameters are shown plotted against the targeted x SeO_4^{2-} in Figure 5.23 and Figure 5.24 for the 1 day and 7 day synthesised samples respectively.

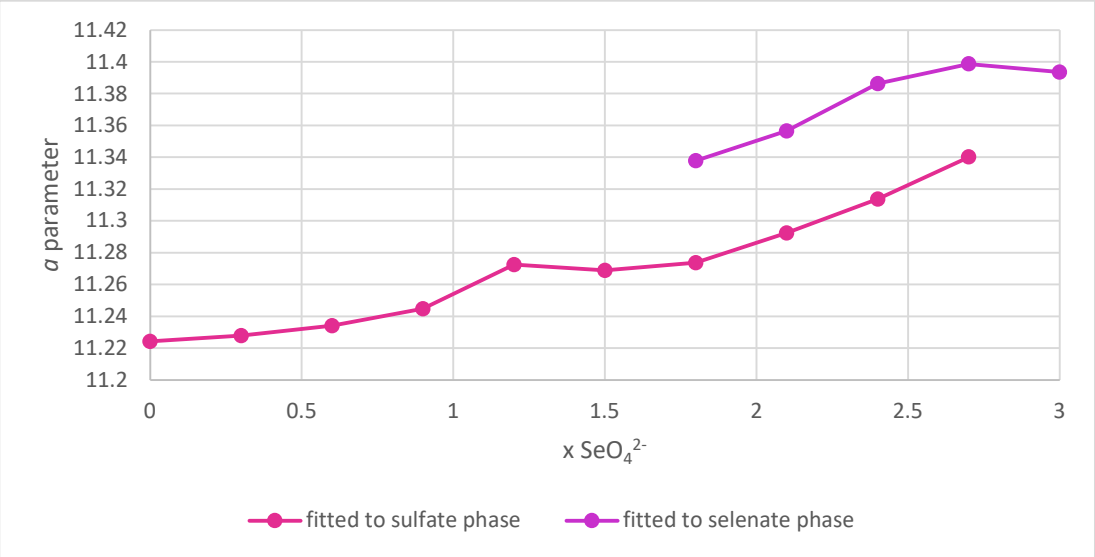

Figure 5.23: Refined a parameter for 1 day samples of the selenate-sulfate solid solution plotted against the targeted selenate ratio with error bars (too small to be observed on this plot)

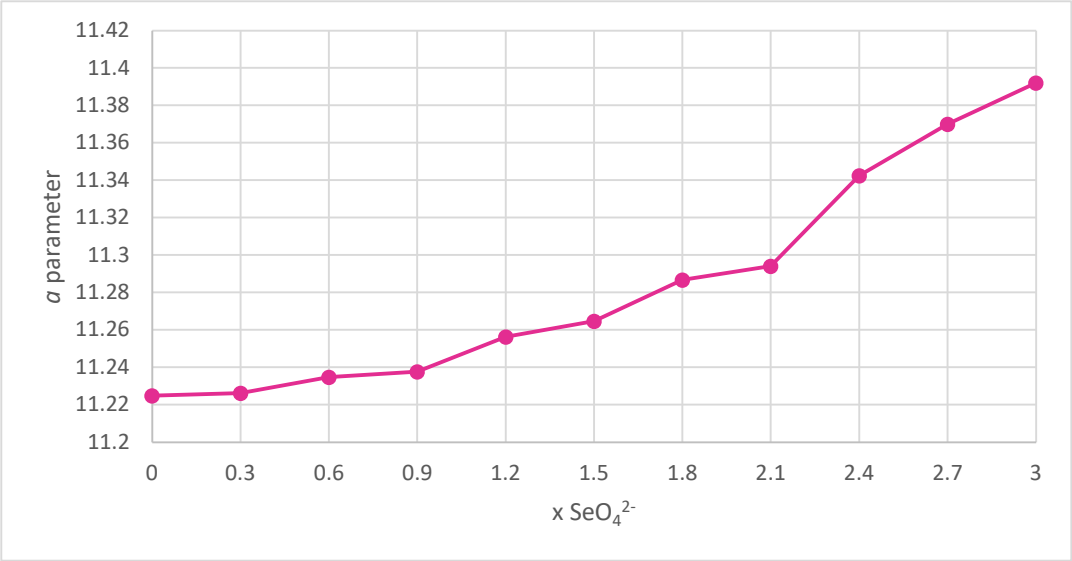

Figure 5.24: Refined a parameter for 7 day samples of the selenate-sulfate solid solution plotted against the targeted selenate ratio with error bars

These plots allow comparison between the 1 day and 7 day synthesised solid solution series. The main difference is that after only 1 day of synthesis some multiphase samples were produced but after 7 days all samples were single phase. When the samples were left to equilibrate for longer the result was a complete solid solution with a gradual increase in the *a* parameter as the targeted x SeO_4^{2-} was increased.

When the samples were synthesised for only 1 day those with x SeO_4^{2-} < 1.8 were single phase (P = 1) and the *a* parameter was increasing as x SeO_4^{2-} increases, suggesting that increasing amounts of selenate were incorporating into the structure. However, when x ≥ 1.8 there was a partitioning of phases and the samples presented as P = 2. The individual *a* parameters of each of the two coexisting ettringite type phases in the P = 2 samples (x = 1.8, 2.1 and 2.4) were in between the values for the end members. So, the samples had not simply split into a sulfate ettringite phase and a selenate ettringite phase, but rather a sulfate rich phase still containing some selenate, and a selenate rich phase still containing some sulfate. In the case of the sample where x = 2.7 the unit cell *a* parameter suggests that the two coexisting phases that have formed were a pure selenate ettringite end member phase and a selenate rich phase still containing some sulfate.

FTIR data and ICP-OES results will now be used to confirm that there is indeed a complete solid solution series with no miscibility gap for the 7 day samples and that increasing amounts of selenate are being incorporated into the solid products for both series.

5.4.3 FTIR

Fourier transform infrared spectroscopy was used to determine whether selenate and sulfate were present in the samples by identifying their characteristic bands in the spectra. The collected spectra for both sets of samples (1 day and 7 day) are shown in Figure 5.25 and Figure 5.26.

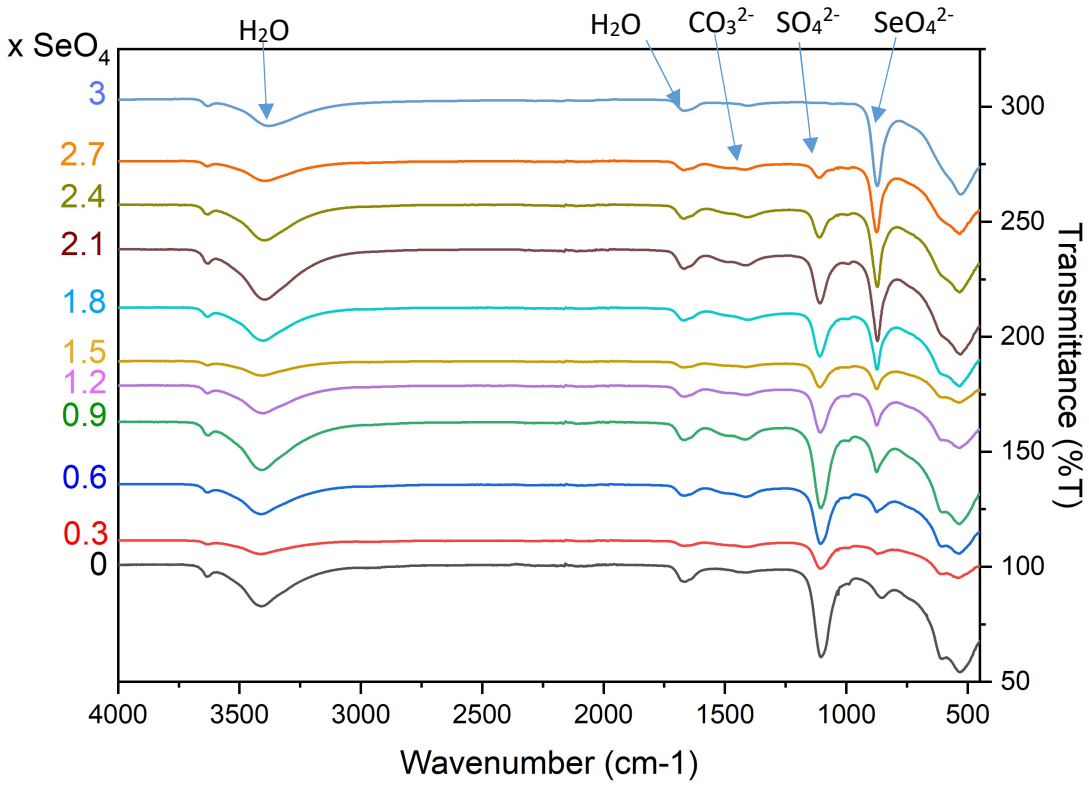

Figure 5.25: FTIR data for the 1 day synthesis samples (selenate-sulfate solid solution), with bands for key functional groups indicated by arrows and labels

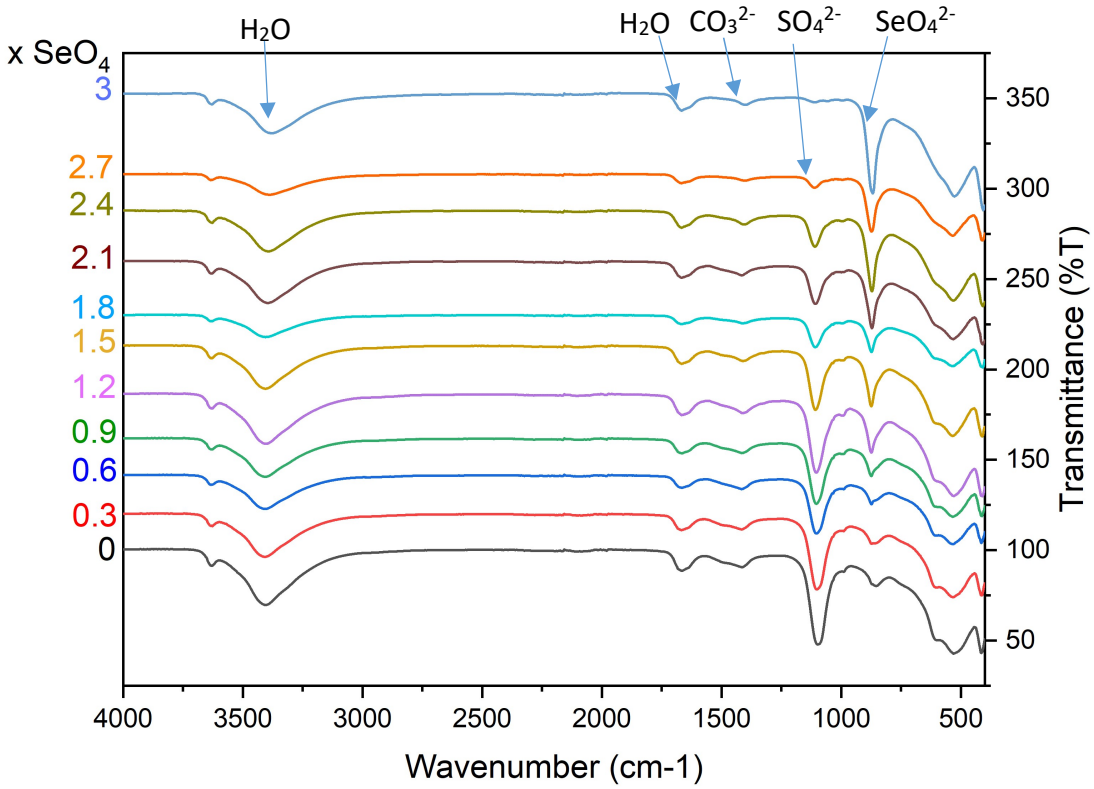

Figure 5.26: FTIR data for the 7 day synthesis samples (selenate-sulfate solid solution), with bands for key functional groups indicated by arrows and labels

All the spectra collected contain the bands for the key functional groups of ettringite, their positions are indicated on the figures by the labels and arrows. The selenate band is at 870 cm^{-1} which is close to the band for AlOH (850 cm^{-1}). This is why there appears to be a small intensity ~850 cm^{-1} in the x = 0 sample where there should be no selenate present in this sample.

The presence of a carbonate band at ~1400 cm^{-1} indicates the presence of the impurity calcite. For the 1 day samples this band was present for samples where $0 < x < 3$ which corresponds to the samples where calcite was identified by PXRD. For the 7 day samples, the carbonate band is present in every spectrum. Calcite was not identified by PXRD in the samples with $x > 1.8$ so the amount present in these sample must be too low to be picked up by PXRD.

Selenate can be identified on all the spectra except for those with x = 0 for both 1 day and 7 day samples. This confirms that selenate has incorporated into the solid samples. The spectra for all samples except for those with x = 3 contain the band for sulfate. This means that all the intermediate samples contained a mixture of selenate and sulfate and so have not simply formed the end member phases. To obtain numerical values for the amounts of sulfate and selenate in each of the samples elemental analysis was carried out using the technique ICP-OES and the results will now be discussed.

5.4.4 ICP-OES

The samples were prepared and analysed using the same method as described in section 5.3.4 and Chapter 2.2.4. Selenium was included in the analysis instead of chromium in this case. The ideal stoichiometry for these solid solution phases is $Ca_6[Al(OH)_6]_2(SeO_4)_x(SO_4)_{3-x}.26H_2O$ and in terms of the cations and anions the molar ratio is 6Ca: 2Al: 3(SeO_4^{2-} + SO_4^{2-}). The measured concentrations of the elements along with the molar ratios after the aluminium has been normalised to 2 are presented in Table 5.7 for the 1 day samples and Table 5.8 for the 7 day samples. Normalising the total molar ratio of SeO_4^{2-} + SO_4^{2-} to 3 allowed an accurate x SeO_4^{2-} to be calculated and this is also included in the results tables (measured x SeO_4^{2-}).

Table 5.7: ICP-OES results for solid digests of 1 day selenate-sulfate ettringite samples (= single phase)*

Targeted x SeO_4^{2-}		**Measured solid digest concentrations in mM**						**Molar ratios Ca:Al:(SeO_4^{2-} + SO_4^{2-}) normalised to 6 Ca^{2+} (Ideal would be 6:2:3)**						**Measured x SeO_4^{2-}**
		Ca^{2+}	Al^{3+}	SO_4^{2-}	SeO_4^{2-}	SeO_4^{2-} + SO_4^{2-}		Ca^{2+}	Al^{3+}	SeO_4^{2-} + SO_4^{2-}	SO_4^{2-}	SeO_4^{2-}		
0 *		8.04	2.87	3.50	0.00	3.50		5.61	2.00	2.44	2.44	0.00		**0.00**
0.3 *		10.95	3.24	2.36	0.17	2.53		6.77	2.00	1.56	1.46	0.10		**0.20**
0.6 *		13.11	3.79	4.55	0.44	4.99		6.91	2.00	2.63	2.40	0.23		**0.26**
0.9 *		9.16	2.76	2.67	0.62	3.30		6.63	2.00	2.38	1.94	0.45		**0.57**
1.2 *		9.37	2.92	2.37	1.32	3.69		6.41	2.00	2.53	1.62	0.91		**1.08**
1.5 *		8.68	2.66	1.86	1.57	3.43		6.52	2.00	2.57	1.40	1.18		**1.37**
1.8		8.47	2.61	1.38	1.90	3.28		6.48	2.00	2.51	1.06	1.45		**1.74**
2.1		9.48	2.96	0.98	2.69	3.66		6.40	2.00	2.47	0.66	1.82		**2.20**
2.4		9.12	2.91	0.50	3.12	3.63		6.28	2.00	2.49	0.35	2.15		**2.58**
2.7		9.43	2.99	0.09	3.62	3.70		6.30	2.00	2.48	0.06	2.42		**2.93**
3 *		10.50	3.19	0.00	4.38	4.38		6.57	2.00	2.74	0.00	2.74		**3.00**

Table 5.8: ICP-OES results for solid digests of 7 day selenate-sulfate ettringite samples (all are single phase)

Targeted x SeO_4^{2-}		**Measured solid digest concentrations in mM**						**Molar ratios Ca:Al:(SeO_4^{2-} + SO_4^{2-}) normalised to 6 Ca^{2+} (Ideal would be 6:2:3)**						**Measured x SeO_4^{2-}**
		Ca^{2+}	Al^{3+}	SO_4^{2-}	SeO_4^{2-}	SeO_4^{2-} + SO_4^{2-}		Ca^{2+}	Al^{3+}	SeO_4^{2-} + SO_4^{2-}	SO_4^{2-}	SeO_4^{2-}		
0		9.01	2.77	3.56	0.00	3.56		6.51	2.00	2.57	2.57	0.00		**0.00**
0.3		9.51	2.93	3.47	0.12	3.59		6.49	2.00	2.45	2.37	0.08		**0.10**
0.6		9.48	2.89	3.05	0.27	3.33		6.56	2.00	2.30	2.11	0.19		**0.25**
0.9		8.80	2.63	2.58	0.48	3.06		6.70	2.00	2.33	1.96	0.36		**0.47**
1.2		8.59	2.61	2.07	0.81	2.88		6.58	2.00	2.21	1.59	0.62		**0.84**
1.5		14.44	4.00	3.16	1.99	5.15		7.23	2.00	2.58	1.58	1.00		**1.16**
1.8		9.23	2.75	1.52	1.55	3.07		6.71	2.00	2.23	1.11	1.13		**1.51**
2.1		8.83	2.66	1.02	2.18	3.19		6.65	2.00	2.40	0.77	1.64		**2.04**
2.4		9.14	2.65	0.46	2.60	3.06		6.90	2.00	2.31	0.35	1.96		**2.55**
2.7		8.56	2.59	0.11	3.10	3.21		6.62	2.00	2.48	0.09	2.40		**2.90**
3		8.04	2.48	0.00	3.40	3.40		6.48	2.00	2.74	0.00	2.74		**3.00**

The ideal molar ratio in terms of the cations and anions would be Ca^{2+}:Al^{3+}:(SeO_4^{2-} + SO_4^{2-}) = 6:2:3. After the normalisation of the aluminium molar ratio to 2 the calcium ratio was between 5.61 and 7.23, with almost all samples having a calcium ratio of over 6. This is due to the presence of calcite ($CaCO_3$) in most of the samples, which means that the amount of calcium measured in the solid products is not all attributed to the ettringite phases. The total molar ratio of the anions XO_4 (SeO_4^{2-} + SO_4^{2-}) should be 3 and again the results were lower than this, ranging from 1.56 to 2.74. The 1 day sample with a targeted x SeO_4^{2-} of 0.3 was the only sample where the XO_4 ratio was as low as 1.56. This indicates that the measurement was inaccurate. Excluding this result, the total molar ratio of XO_4 in the samples ranged between 2.21 to 2.74, which is closer to the target. As with the chromate-sulfate ettringite solid solution results, this is probably caused by the detection of sulfur by ICP-OES having larger errors. Overall, the molar ratio of selenate was usually lower than was targeted.

Using the molar ratios of sulfate and selenate to calculate a measured x SeO_4^{2-} allows the plots (Figure 5.23 and Figure 5.24) to be updated to show the change in the *a* unit cell parameter as a function of the measured x SeO_4^{2-}. These updated plots are shown in Figure 5.27 and Figure 5.28 for the 1 day and 7 day samples.

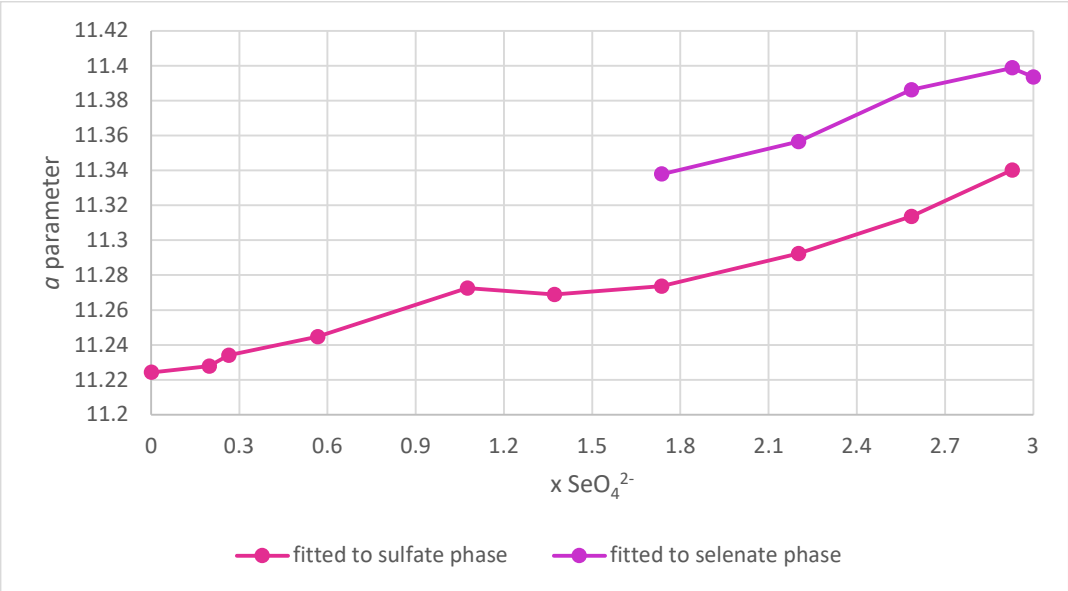

Figure 5.27: Accurate x SeO_4^{2-} plot of the refined a parameter for 1 day samples of the selenate-sulfate solid solution (the targeted x SeO_4^{2-} values are the increments on the x axis)

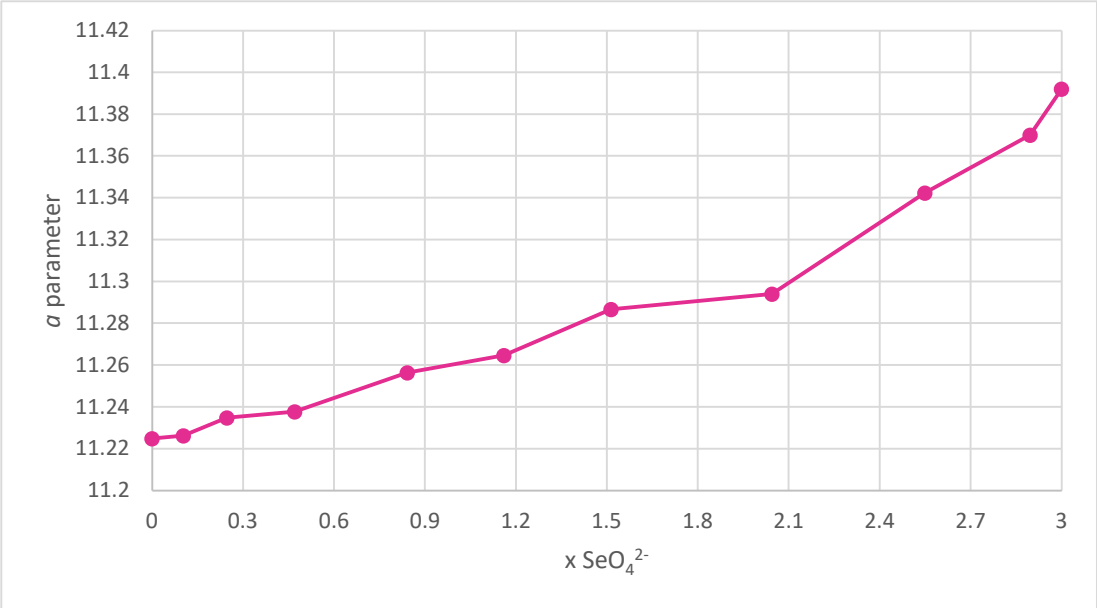

Figure 5.28: Accurate x SeO_4^{2-} plot of the refined a parameter for 7 day samples of the selenate-sulfate solid solution (the targeted x SeO_4^{2-} values are the increments on the x axis)

These plots show the actual amounts of selenate that is being incorporated into the solid products. Results from the 1 day samples shows that x SeO_4^{2-} = 1.37 was the largest amount of selenate that can be incorporated before a partitioning of phases occurred. In the samples where the amount of selenate targeted was x < 1.5, the actual amount of selenate measured in the samples was much lower than this. After the partitioning of phases (targeted x > 1.8) the amount of selenate that was incorporated was measured to be closer to the target and overall a lot more selenate was detected in the solid phase. This means that when the samples were single phase with low amounts of selenate being targeted the system preferred to produce a very sulfate rich ettringite phase. But as higher ratios of selenate were targeted, the phases partitioned into two and allowed greater selenate incorporation into a selenate rich phase.

For the set of samples aged for 7 days they are all single phase so there was no maximum amount of selenate that could be incorporated before partitioning of phases occurred. When the targeted amount of selenate was below x = 1.2 the actual amount incorporated was much lower, again suggesting a preference to form a

sulfate rich ettringite phase. However, for this set of samples, as the targeted amount of selenate increased the incorporated amount also increased and got closer to the target, but this time without the need to partition into two phases.

5.4.5 SEM and EDS

SEM images were acquired for a selection of samples, synthesised for both 1 day and 7 days, to confirm the results from other analysis techniques and analyse the samples morphology. For the selenate-sulfate ettringite system the samples analysed by SEM/EDS were the 1 day and 7 day samples with targeted x = 0.9 (Figure 5.29 a and b) and x = 2.1 (Figure 5.30 a and b).

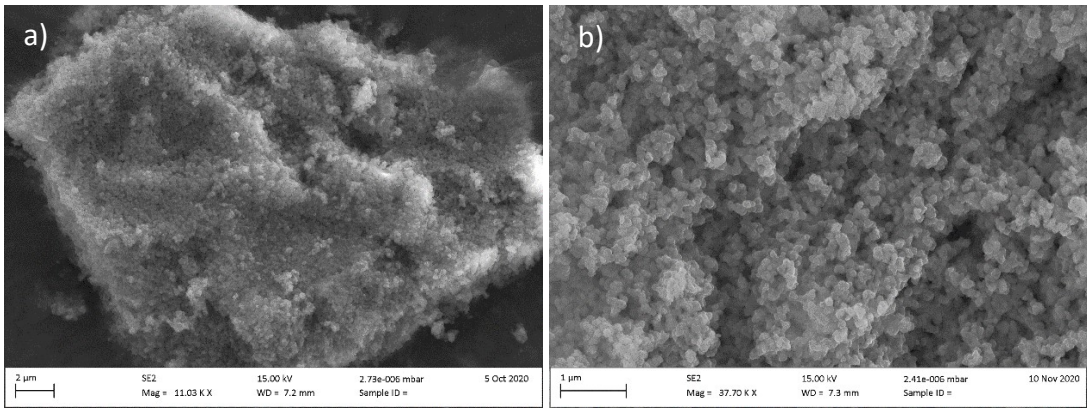

Figure 5.29 a) and b): SEM images for the samples selenate 0.9 sulfate 2.1 synthesised for a) 1 day and b) 7 days

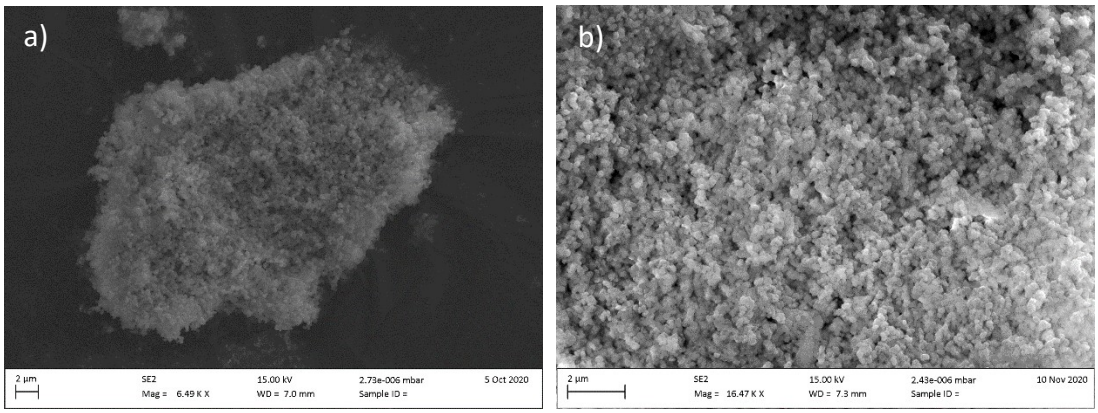

Figure 5.30 a) and b): SEM images for the samples selenate 2.1 sulfate 0.9 synthesised for a) 1 day and b) 7 days

SEM images of all the samples from the selenate-sulfate system showed that they all possessed a morphology where very small crystallites had agglomerated. Due to the small size of the crystallites, differences in composition across individual crystallites could not be measured by EDS. EDS spectra for each sample are in Appendix 4 and all show the presence of both Se and S in the samples.

All of the analytical techniques used here have shown that the selenate sulfate ettringite solid solution series ($Ca_6[Al(OH)_6]_2(SeO_4)_x(SO_4)_{3-x}.26H_2O$) is fully miscible when synthesised using the saccharate method and left to equilibrate for 7 days. A wide range of compositions have been synthesised and had their compositions verified by ICP-OES. Pawley refinement of PXRD data has shown that there is a trend in the unit cell parameter *a* as x SeO_4^{2-} increases.

The study by Hassett *et al.*[5] is the only comparable study in the literature as they used the same synthesis method but a synthesis time of only 1 day. They synthesised a smaller number of samples compared to this study and claim to have produced a system with complete miscibility. However, the sample they produced with the highest amount of selenate incorporated had x SeO_4^{2-} of only 1.64. This study has both targeted and successfully synthesised more compositions whilst also investigating the phase formation under different conditions of time and is therefore a more complete study of this system.

5.5 CONCLUSIONS

The solid solutions between chromate ettringite and sulfate ettringite, and selenate ettringite and sulfate ettringite were investigated in this study. Two different ageing times, 1 day and 7 days, were used to study what effect synthesis time had on the series. The solid solution limits for the targeted compositions were identified using PXRD analysis and the amounts of either chromate or selenate that had been incorporated into any solid solution members was measured using ICP-OES.

The series between chromate ettringite and sulfate ettringite ($Ca_6[Al(OH)_6]_2(CrO_4)_x(SO_4)_{3-x}.26H_2O$) was found to have very limited solid solubility, with a range of $0 < x < 0.8$ for the 1 day samples and $0 < x < 0.44$ for the 7 day samples. Within these ranges the unit cell parameters do not change, suggesting the chromium is not actually incorporated into a solid solution structure, but is simply absorbed to the surface of the grains, or is present in very small domains of the crystallites. Any samples produced with a larger value of x were found to be multiphase and therefore definitely not members of a solid solution. ICP-OES analysis showed that when the targeted ratio of chromate was low, the actual amount incorporated was lower, indicating a preference for sulfate incorporation. As higher amounts of chromate were targeted multiphase samples were produced which could incorporate higher amounts of chromate into either chromate rich ettringite phases still containing some sulfate in the case of the 1 day samples, or a chromate ettringite end member phase, coexisting with a sulfate ettringite end member phase, for the 7 day samples.

The series between selenate ettringite and sulfate ettringite ($Ca_6[Al(OH)_6]_2(SeO_4)_x(SO_4)_{3-x}.26H_2O$) was found to have a miscibility gap when $x > 1.37$ for samples aged for 1 day, but when the samples were aged for 7 days a complete solid solution series was produced. ICP-OES identified that targeting lower amounts of selenate led to a strong preference for sulfate incorporation while targeting higher amounts of selenate led to greater selenate incorporation. For the 1 day samples this was due to partitioning of phases into a selenate rich phase and sulfate rich phase,

but for the 7 day samples, higher amounts of selenate were able to be incorporated into a single solid solution phase with a maximum x = 2.9.

5.6 References

1 H. Pöllmann, H. J. Kuzel and R. Wenda, *Neues Jahrb. Miner. Abh.*, 1989, **160**, 133–158.

2 R. L. Norman, S. E. Dann, S. C. Hogg and C. A. Kirk, *Solid State Sci.*, 2013, **25**, 110–117.

3 R. B. Perkins and C. D. Palmer, *Appl. Geochemistry*, 2000, **15**, 1203–1218.

4 P. Kumarathasan, G. J. McCarthy, D. J. Hassett and D. F. Pflughoeft-Hassett, *Mater. Res. Soc. Symp. Proc.*, 1990, **178**, 83–104.

5 D. J. Hassett, G. J. McCarthy, P. Kumarathasan and D. Pflughoeft-Hassett, *Mater. Res. Bull.*, 1990, **25**, 1347–1354.

6 M. C. Simoes, K. J. Hughes, D. B. Ingham, L. Ma and M. Pourkashanian, *Inorg. Chem.*, 2017, **56**, 7566–7573.

7 H. K. Roobottom, H. Donald, B. Jenkins, J. Passmore and L. Glasser, *Thermochemical Radii of Complex Ions*, 1999, vol. 76.

8 D. R. Peacor, P. J. Dunn and M. Duggan, *Can. Mineral.*, 1983, **21**, 705–709.

9 S. Gross, *Isr. J. Earth Sci.*, 1980, **29**, 81–84.

10 R. B. Perkins, Portland State University, 2000.

11 H. Pöllmann, S. Auer, H.-J. Kuzel and R. Wenda, *Cem. Concr. Res.*, 1993, **23**, 422–430.

12 C. D. Palmer, *Environ. Sci. Technol.*, 2000, **34**, 4185–4192.

13 S. M. Leisinger, B. Lothenbach, G. Le Saout, R. Kägi, B. Wehrli and C. A. Johnson, *Environ. Sci. Technol.*, 2010, **44**, 8983–8988.

CHAPTER 6 INVESTIGATING THE SYNTHESIS OF ETTRINGITE AND ITS IRON AND GALLIUM CONTAINING ANALOGUE PHASES

6.1 INTRODUCTION

This study is focussed on optimising the synthesis of aluminium-, iron-, and gallium-ettringite ($Ca_6[X(OH)_6]_2(SO_4)_3.26H_2O$, X = Al, Fe, Ga). The mineral ettringite has the ideal composition $Ca_6[Al(OH)_6]_2(SO_4)_3.26H_2O$ and this will be referred to as aluminium-ettringite in this chapter. When occurring naturally, ettringite can have a variable composition, and as mentioned in Chapter 1 the mineral sturmanite ($Ca_6(Fe^{3+},Al^{3+},Mn^{3+})_2(OH)_{12}(SO_4)_{2.5}[B(OH)_4].25H_2O$) can contain iron, aluminium and manganese and crystallises with the ettringite structure. Ettringite containing only iron will be referred to as iron-ettringite ($Ca_6[Fe(OH)_6]_2(SO_4)_3.26H_2O$) in this chapter and is a phase that is sometimes present in cement as part of the Aft group of phases. The general composition for the AFt phases is given as: $[Ca_3(Al,Fe)(OH)_6.12H_2O]_2X_3.nH_2O$, where X is a doubly charged anion (e.g. SO_4^{2-}) and $n \geq 2$.[1] Purely aluminium containing ettringite is the most common example of an AFt phase in cement systems but iron-ettringite can also be present along with a variety of intermediate compositions with both aluminium and iron in the structure. When aluminium and iron are both present in the ettringite crystal structure this is known as a solid solution phase.

The IUPAC definition of a solid solution is “a solid in which components are compatible and form a unique phase”. The solid solutions discussed in this thesis are binary systems with two different ettringite phases as end members and there will be investigations into the solid solution formation between the end members. The solid solution series between end members aluminium-ettringite and iron-ettringite is a substitutional solid solution as the occupancy of the aluminium site is reducing as

more iron is incorporated. According to the Hume-Rothery rules a solid solution will be able to readily form if the two end members have the same crystal structure and the substituting ions have similar atomic radii, electronegativity and valency[2,3]. By these rules, it should be possible to set up complete solid solutions between any ettringite analogue phases that can be synthesised as long as the ions being varied have similar radii.

The solid solution between aluminium-ettringite and iron-ettringite ($Ca_6[Al_xFe_{1-x}(OH)_6]_2(SO_4)_3.26H_2O$, $0 \leq x \leq 1$) has been investigated by Möschner *et al* (2009)[4]. To synthesise the members of the solid solution, they combined solutions containing CaO, $Fe_2(SO_4)_3.5.3H_2O$ and / or $Al_2(SO_4)_3.16.2H_2O$ and added them to a KOH solution. In order to produce a range of compositions, where x varied between 0 and 1, they varied the starting amounts of the aluminium and iron containing reagents.

Investigations into replacement of Al in the ettringite series were carried out by Norman et al using the saccharate method[5]. They showed the iron-ettringite end member ($Ca_6[Fe(OH)_6]_2(SO_4)_3.26H_2O$) formed, but with the impurity phases gypsum ($CaSO_4.2H_2O$) and hemihydrate ($CaSO_4.0.5H_2O$) also present. The gallium-ettringite end member ($Ca_6[Ga(OH)_6]_2(SO_4)_3.26H_2O$) phase was also synthesised using the saccharate method and was found to be phase pure. Currently, no other studies have investigated further the formation of the gallium-ettringite analogue phase. This study investigated the synthesis of this end member phase and the solid solution behaviour between the end members aluminium-ettringite and gallium-ettringite ($Ca_6[Al_xGa_{1-x}(OH)_6]_2(SO_4)_3.26H_2O$). Structural analysis of phases in this system was carried out using Rietveld refinement of high resolution synchrotron powder X-ray diffraction data. Refinement of the crystal structure allowed determination of the site occupancies for the cation site and calculation of bond lengths. The calculated bond lengths were used to carry out bond valence sum analysis.

The bond valence model is derived from Pauling's second rule (the electrostatic valence rule), which states that the sum of the bond strengths of the ions coordinated

to a central ion is equal to the charge of the central ion[6,7]. After X-ray diffraction became widely available, experimental bond lengths were able to be calculated. If these bond lengths are used instead of bond strength then Pauling's second rule becomes quantitatively exact and the experimental bond valence can be calculated using Equation 1[8].

Equation 1: Equation for the calculation of experimental bond valence Sij

$$S_{ij} = \exp\left(\frac{R_o - R_{ij}}{B}\right)$$

S_{ij} : experimental bond valence, R_o : length of the bond of unit valence, R_{ij} : bond length between atoms i and j, B : a constant close to 0.37 Å.

The atomic valence (V_i) is equal to the sum of the experimental bond valences around the atom and so can be calculated using Equation 2. Calculating atomic valences for the members of the solid solution will allow trends across the solid solution series to be identified.

Equation 2: Equation for the calculation of atomic valence

$$V_i = \sum_j S_{ij}$$

The synthesis of iron- and gallium- ettringite analogue phases could be useful for waste remediation. For example, gallium is identified as being a critical element[9] and is used in the manufacture of semiconductors, LEDs, photovoltaics, and other electronic devices[10]. It is currently produced as a by-product of the mining of zinc, copper and aluminium. The current market is relatively small, and the price of gallium is high[11]. As such the refiners have little incentive to increase the recovery of gallium.

However, the electronics markets, especially photovoltaics, is expected to increase and this could put pressure on the gallium supply[9]. For this reason it will become more important in the future, to find new ways to recover gallium that has been deposited in waste streams. Gallium is present in the ash produced by the combustion of coal and it is estimated that gallium concentrations in bottom ash and fly ash are 0.001 – 0.3 %[12] and there have already been studies into the recovery of gallium from fly ash[11,13].

Understanding the range of conditions that ettringite and its analogue phases can form under, is critical to determining whether its formation could be used to remove waste ions from the environment. Some previous investigations into waste remediation using ettringite precipitation have been carried out. Álvarez-Ayuso *et al* used the precipitation of ettringite to simultaneously remove aluminium and sulfate from wastewaters that result from the aluminium anodizing industry[14]. They achieved this by adding CaO and $Ca_{12}Al_{14}O_{33}$ to the acidic wastewater, using NaOH to raise the pH. Sulfate removal from wastewater was also investigated by Dou *et al*. They added $CaCl_2$ and $AlCl_3$.$6H_2O$ to synthetic wastewater, resulting in the precipitation of ettringite[15].

Iron/arsenic containing ettringite phases have been studied as materials for arsenic encapsulation[16]. Choi *et al* added CaO and $FeCl_3$ to a synthetic arsenic-containing wastewater and proved that an ettringite type phase precipitated, removing the arsenic from the water.

Utilising the precipitation of ettringite or any of its analogues as a method for waste removal requires that the formation time be short and the conditions for formation are well known. For these reasons, the time dependence of the ettringite formation using the adapted saccharate methods was examined in this study.

6.2 AIMS

The aims of this study were to determine an optimum set of conditions for the synthesis of ettringite and its iron and gallium analogue phases ($Ca_6[X(OH)_6]_2(SO_4)_3.26H_2O$, X = Al^{3+}, Fe^{3+}, Ga^{3+}). The saccharate method was used and the experimental conditions such as the presence of sugar and whether or not the reaction mixture was stirred were varied to determine the optimal conditions for synthesis of a phase pure product.

The solid solution behaviour between aluminium and gallium ettringite ($Ca_6[Al_xGa_{1-x}(OH)_6]_2(SO_4)_3.26H_2O$, $0 \leq x \leq 1$) was also investigated along with the site occupancy and bond valence sums of this system.

6.3 INVESTIGATING THE SYNTHESIS OF ETTRINGITE

6.3.1 Aluminium-ettringite Synthesis under Different Experimental Conditions

The synthesis of ettringite ($Ca_6[Al(OH)_6]_2(SO_4)_3.26H_2O$) was investigated using variations of the saccharate method described in Section 2.1.4. Reaction conditions were changed systematically, in order to find an optimal set of synthesis conditions. The different synthesis conditions are summarised in Table 6.1. All samples produced were analysed using PXRD and FTIR with the results plotted in Figure 6.1 and Figure 6.2 respectively and summarised in Table 6.1.

Table 6.1: Summary of conditions for the synthesis of ettringite

Conditions of Synthesis	Phases identified by PXRD	Functional groups identified in FTIR	Unit cell parameters	
			***a* (Å)**	***c* (Å)**
Sugar and stirring	ettringite	water, sulfate, carbonate	11.224 (1)	21.456 (2)
No sugar and stirring	ettringite	water, sulfate, carbonate	11.220 (1)	21.445 (1)
Sugar and no stirring	ettringite	water, sulfate, carbonate	11.194 (1)	21.443 (2)
Sodium salts used in synthesis	ettringite	water, sulfate, carbonate	11.222 (2)	21.433 (3)

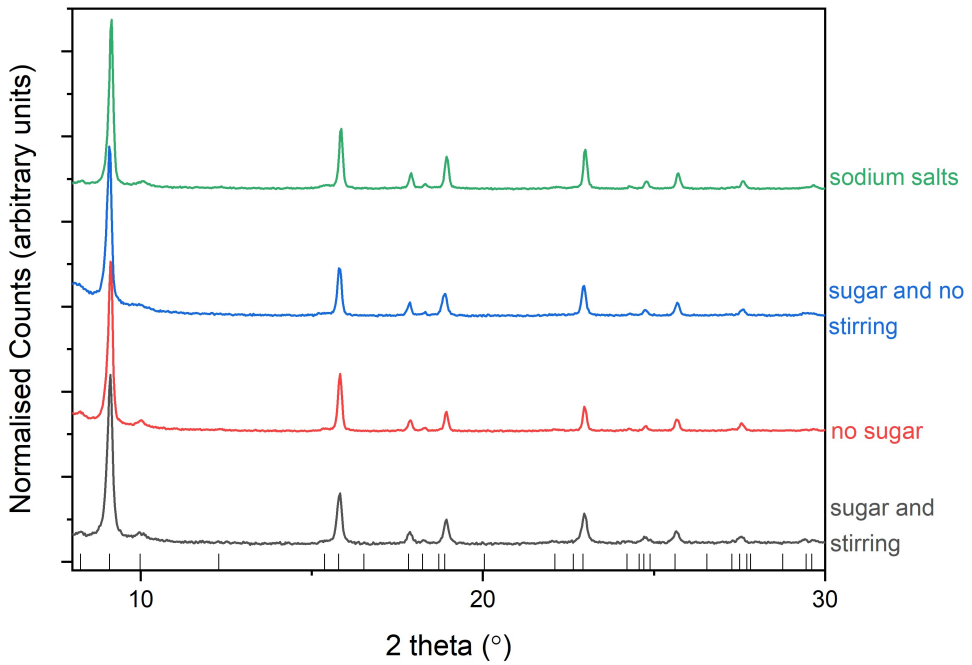

Figure 6.1: Powder X-ray diffraction patterns for ettringite synthesised under different conditions (data collected on laboratory Bruker D2, λ = 1.541 Å) All reflections assigned to ettringite with tick marks from ICSD: 251756

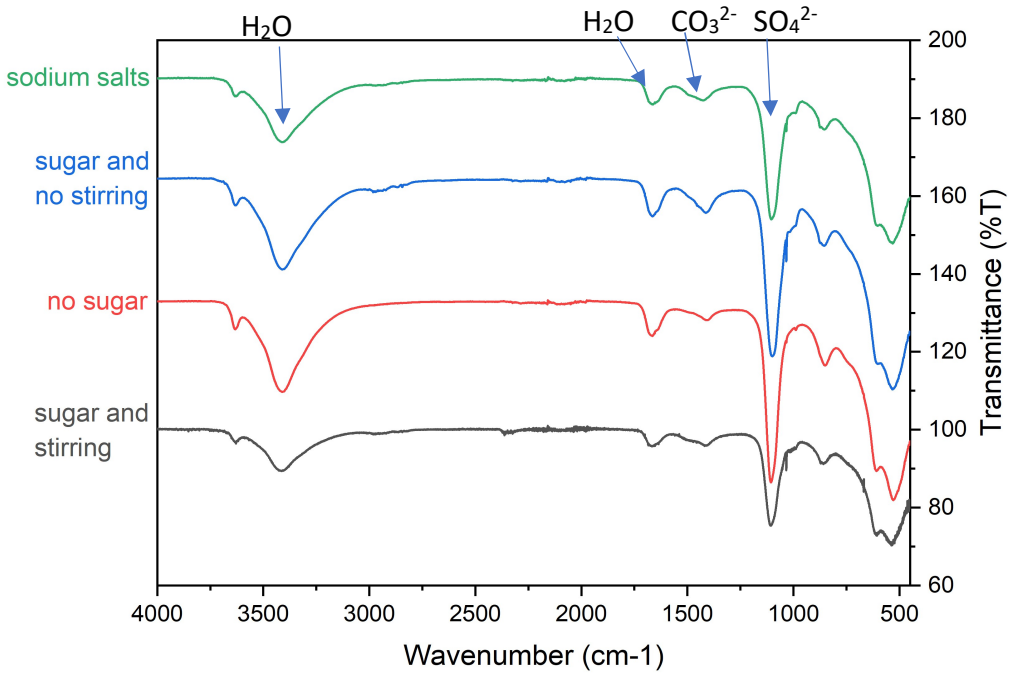

Figure 6.2: FTIR data for ettringite synthesised under different conditions with bands for key functional groups indicated by arrows and labels

These results show that aluminium ettringite is able to form under a variety of conditions. The PXRD patterns for samples produced by all of the conditions used, show that a crystalline ettringite phase forms. Some common impurities that can form when using these synthesis methods are calcite ($CaCO_3$) and gypsum ($CaSO_4.2H_2O$), however, the PXRD data (Figure 6.1) show no presence of any impurity peaks that can be attributed to either of these phases. All observed reflections can be assigned to ettringite and the unit cell parameters were refined using a Pawley fitting method, and the results confirmed that the structures were ettringite.

The IR spectra (Figure 6.2) of these samples contain bands for water (3400 cm^{-1}) and sulfate (1100 cm^{-1}), which would be present in ettringite. However, the band at ~1420 cm^{-1} is assigned as a carbonate stretch. This could mean that there is a small amount of impurity calcite present that is either very poorly crystalline or in too small quantities to be detected by PXRD. Carbonate containing impurities usually form due to absorption of carbonate from the air during synthesis, a way to reduce this could

be to carry out the reaction in an air free environment, such as a glove box, or a sealed container such as a closed bottle rather than a beaker.

6.3.2 Time Dependence of the Synthesis of Aluminium-ettringite

The samples of aluminium-ettringite ($Ca_6[Al(OH)_6]_2(SO_4)_3.26H_2O$) produced in the previous section (Section 6.3.1) were synthesised using a reaction time of 48 hours and all were found to be phase pure. The time dependence of the formation of aluminium-ettringite was investigated to determine whether this reaction time could be reduced while still producing a pure and crystalline ettringite phase. A shorter reaction time would make for a more efficient synthesis process and this is important if the precipitation of ettringite phases were to be used for waste remediation purposes.

The time dependence of the synthesis of aluminium-ettringite was tested for both the sugar and stirring, and no sugar and stirring methods. To test this, a solution containing calcium oxide and aluminium sulfate (with or without sugar) was stirred for a certain amount of time before filtering to quench the reaction, and this was repeated for various reaction times.

6.3.2.1 Time Dependence of the Synthesis of Aluminium Ettringite using the Sugar and Stirring Method

Samples were made where the total reaction times before separation of the products by filtration were as follows: instant, 10 minutes, 20 minutes, 30 minutes, 40 minutes, 50 minutes, 1 hour, 4 hours, 8 hours, 1 day and 7 days. The reaction time labelled “instant” refers to a sample produced by the combination of the calcium oxide / sugar solution and the aluminium sulfate solution with a minimal reaction time. This was achieved by pouring the two solutions simultaneously into a Buchner funnel and thus

"instantly" separating any products from the filtrate. The total time the reagents were in the funnel was < 30 s. The products were analysed using PXRD and FTIR and the results are shown below in Figure 6.3 and Figure 6.4 respectively.

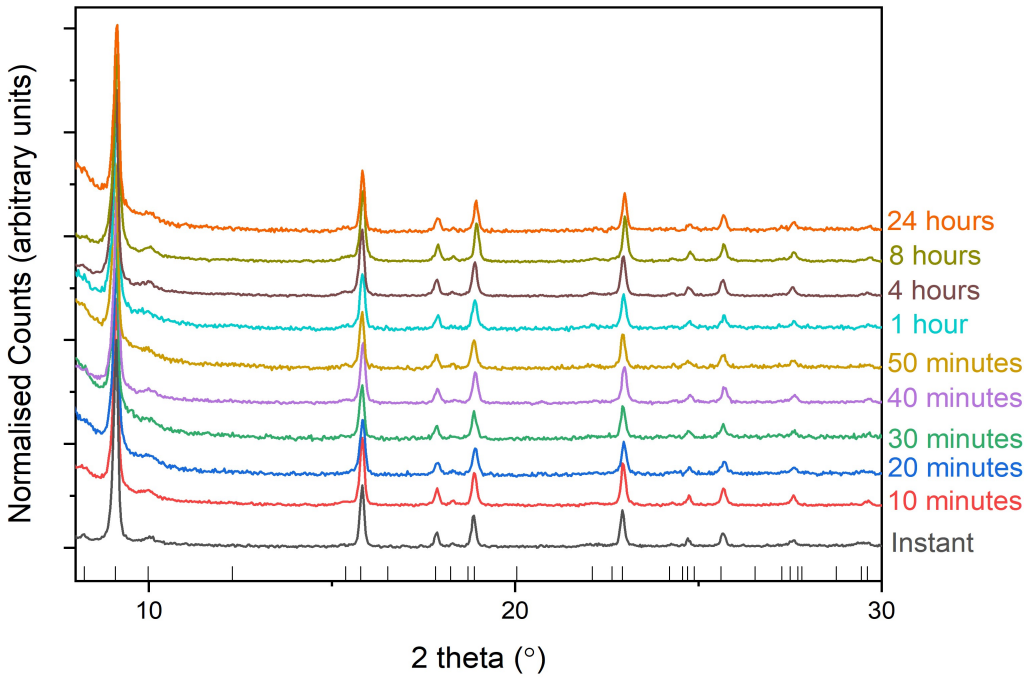

Figure 6.3: Powder X-ray diffraction patterns for ettringite synthesised with the sugar and stirring method for various time periods (data collected on laboratory Bruker D2, λ = 1.541 Å) All reflections assigned to ettringite with tick marks from ICSD: 251756

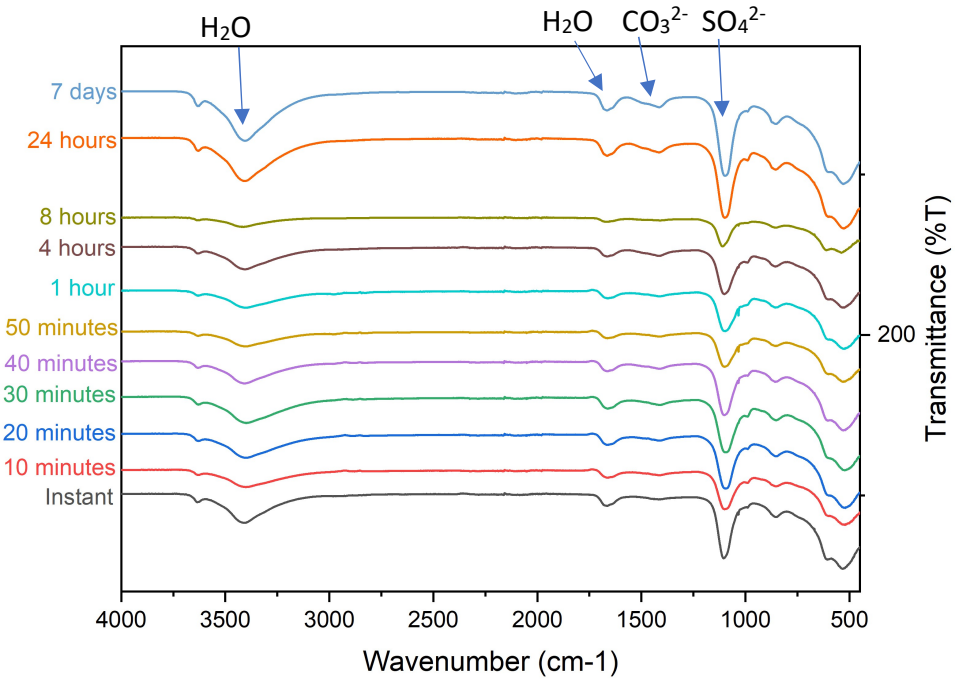

Figure 6.4: FTIR data for ettringite synthesised with the sugar and stirring method for various time periods (bands for key functional groups indicated by arrows and labels)

Ettringite was the only phase identified in all of the PXRD patterns, even the sample synthesised "instantly". The FTIR spectra confirm the synthesis of ettringite, with the water and sulfate stretches present for all samples. No impurity phases were identified in the PXRD patterns and the FTIR spectra showed only low intensity carbonate bands for some of the samples. The spectra for the samples synthesised with lower reaction times have less intense carbonate bands, indicating that lowering the reaction time gives less time for the CO_2 to dissolve into the solution and subsequently incorporate into the ettringite structure. These results show that the formation of ettringite using this synthesis method (sugar and stirring saccharate method) does not have a time dependence and that phase pure aluminium ettringite can be produced with minimal reaction times.

6.3.2.2 *Time Dependence of the Synthesis of Aluminium Ettringite using the No Sugar and Stirring Method*

The time dependence of the reaction was also investigated for the same synthesis procedure but without sugar present in the CaO solution. In this case, samples were only synthesised at the following times intervals: 1 hour, 4 hours, 8 hours, 1 day and 2 days. The products were again analysed using PXRD and FTIR and the results are shown below in Figure 6.5 and Figure 6.6.

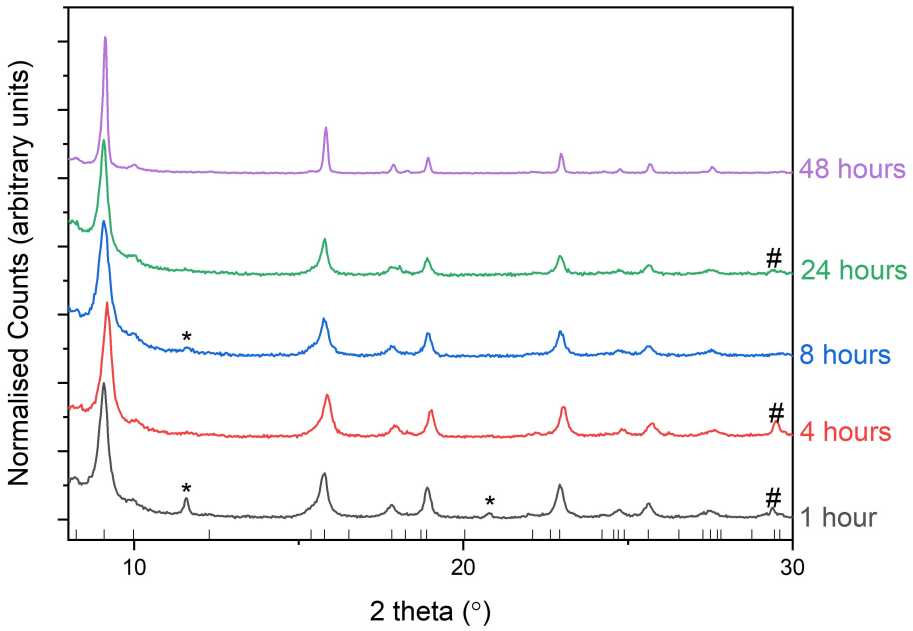

*Figure 6.5: Powder X-ray diffraction patterns for ettringite synthesised with the no sugar and stirring method for various time periods (data collected on laboratory Bruker D2, λ = 1.541 Å) * = gypsum (ICSD: 2058), # = calcite (ICSD: 18166), all other reflections = ettringite with tick marks from ICSD: 251756*

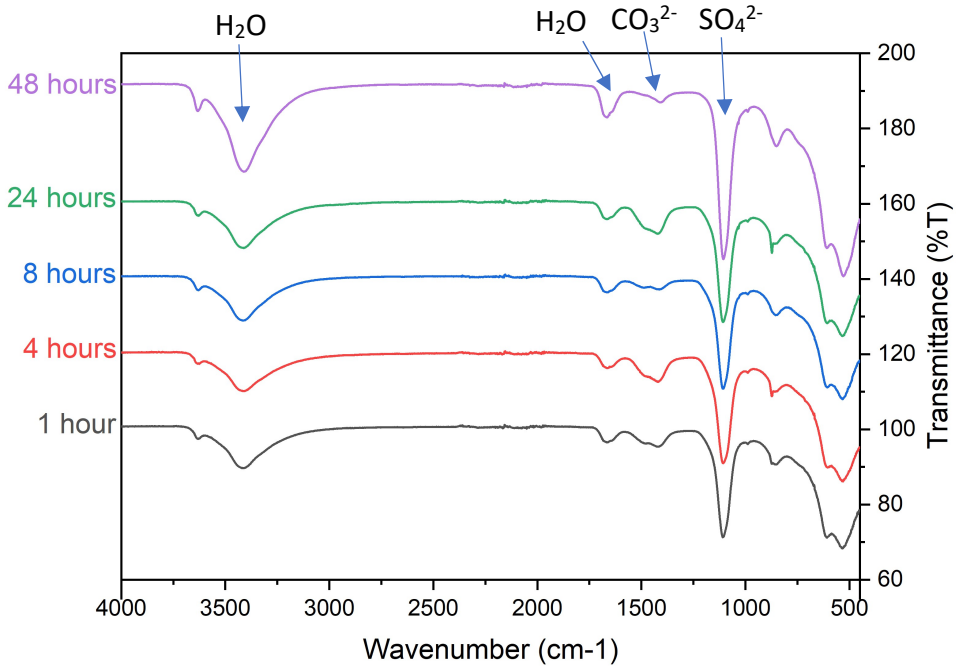

Figure 6.6: FTIR data for ettringite synthesised with the no sugar and stirring method for various time periods (bands for key functional groups indicated by arrows and labels)

Ettringite is identified in all of the PXRD patterns, however, the impurity phase gypsum ($CaSO_4.2H_2O$, reflections indicated by a *) is identified as present in the PXRD patterns for the 1 hour and 8 hours samples, and calcite ($CaCO_3$, reflections indicated by a #) is identified in the PXRD patterns for the 1 hour, 4 hours and 24 hours samples. The FTIR spectra contain the stretches for water and sulfate but also significant carbonate stretches for all samples. The carbonate bands are most intense for the 1 hour, 4 hours and 24 hours samples which fits well with the observation that calcite is present in the PXRD patterns for these samples. The carbonate bands observed for these samples also show peak splitting, meaning that there are two distinct carbonate environments, and so along with calcite formation there is likely carbonate incorporated into the ettringite structure.

These results show that excluding sugar from the reaction makes impurity formation more likely, and as such, impurities are identified in samples synthesised with different reaction times. The sugar is used in the synthesis to increase the solubility

of the calcium oxide, so the exclusion of the sugar will lead to a certain amount of solid calcium oxide present in the starting solution and therefore calcium containing impurities are more likely to form, as is found in these experiments. The sugar also has an added benefit of inhibiting the absorption of carbon dioxide from the air, therefore, with no sugar in the system, the likelihood of formation of carbonate containing impurities is increased[17]. The ideal conditions for synthesis of aluminium-ettringite phase have been found to be the stirring and sugar saccharate method with no time dependence for the production of a phase pure product found.

6.4 Synthesis of Iron and Gallium Containing Ettringite Analogue Phases

Analogue phases of the ettringite structure where the aluminium cation has been replaced by other metal ions are well known and this has been discussed in Chapter 1.2. This section aims to investigate the formation of iron-ettringite and gallium-ettringite analogue phases and to identify the synthesis conditions required to produce phase pure samples.

6.4.1 Iron-ettringite Synthesis Method Optimisation

Iron-ettringite was synthesised using the different synthesis methods from Section 6.3.1 for the synthesis of aluminium-ettringite. The different synthesis methods are given in Table 6.2. The products were analysed by PXRD and FTIR and the results are shown in Figure 6.7, Figure 6.8 and summarised in Table 6.2.

Table 6.2: Summary of conditions for the synthesis of iron-ettringite

Conditions of Synthesis	**Phases identified by PXRD**	**Functional groups identified in FTIR**
Sugar and stirring	iron-ettringite	water, sulfate, carbonate
Sugar and no stirring	iron-ettringite	water, sulfate, carbonate
No sugar and stirring	Calcium carbonate hydrate, calcite, unknown phase	sulfate, carbonate

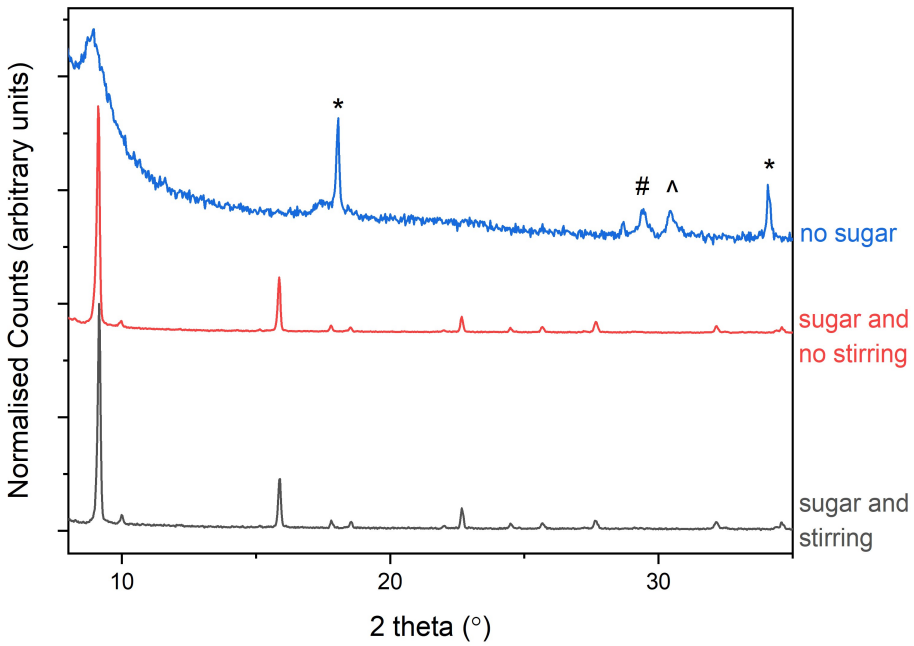

*Figure 6.7: Powder X-ray diffraction patterns for iron-ettringite synthesised under different conditions (data collected on laboratory Bruker D2, λ = 1.541 Å), *=$CaCO_3.6H_2O$ (ICSD: 16070), #=calcite (ICSD: 18166), ^= unknown impurity phase, all other reflections = ettringite (ICSD: 251756)*

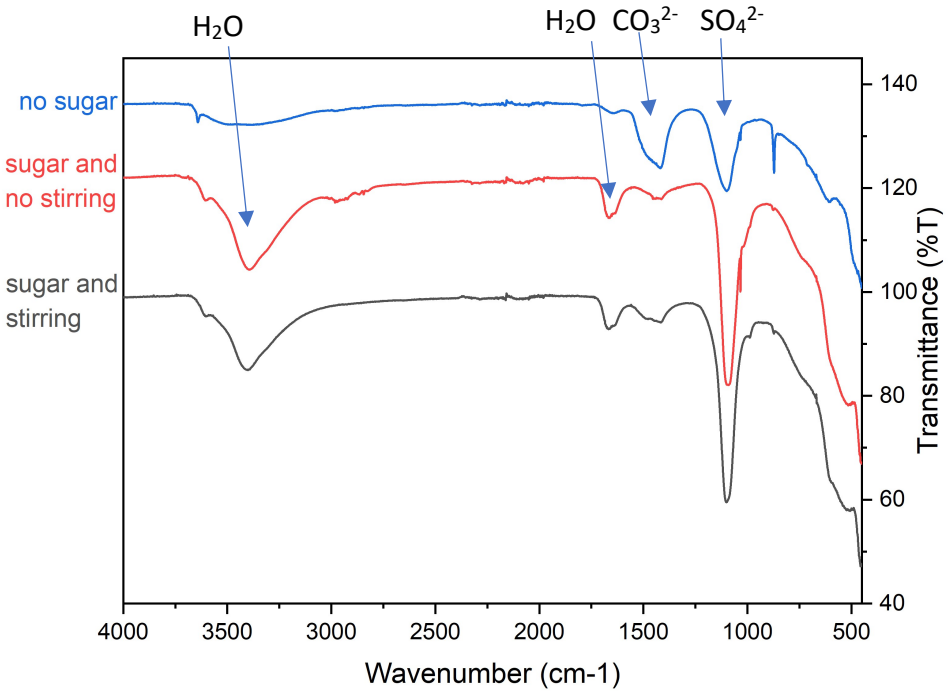

Figure 6.8: FTIR data for iron-ettringite phases synthesised under different conditions (bands for key functional groups indicated by arrows and labels)

The PXRD patterns show that when the synthesis includes sugar all the reflections can be assigned to an ettringite type phase with no impurity phases identified. There is no difference in the patterns for the product synthesised with stirring and the one without stirring. However, when sugar is excluded from the reaction, a phase pure ettringite phase does not form, instead there are reflections for calcite ($CaCO_3$) and the hydrated form of calcium carbonate ($CaCO_3.6H_2O$). There is a broad reflection at ~8.9 ^{o} which could indicate the presence of an ettringite type phase which has poor crystallinity or a very small particle size. Overall, when synthesising iron-ettringite, sugar must be included in order to produce the ettringite phase and inhibit impurity formation. This is similar to the observations of the aluminium ettringite system, where the inclusion of sugar inhibited the absorption of CO_2 from the air. For iron-ettringite, the effect of CO_2 absorption is more pronounced, with no crystalline ettringite analogue phase being produced. This indicates that the iron-ettringite is

less stable and the formation of impurity phases is favoured when sugar is excluded from the reaction.

The FTIR spectra confirm these results, with the spectra for both the 'sugar and stirring' method, and the 'sugar and no stirring' method, containing the stretches for water and sulfate, characteristic to ettringite. The spectrum for the sample was produced using the synthesis method where sugar was excluded contains very weak water stretches, the sulfate stretch and a much larger carbonate stretch than the spectra for the other samples. This complements the PXRD results which showed the presence of carbonate containing impurity phases and a potentially poorly crystalline ettringite phase.

The optimal experimental method was chosen to be the 'sugar and stirring' method and the unit cell parameters of the sample produced using this method were refined in space group P31c using the Pawley method to a = 11.182 (8) Å, c = 22.05 (2) Å with R_{wp} = 5.873. These compare well to published unit cell parameters for iron-ettringite: a = 11.162 (3) Å, c = 22.04 (1) Å[5]. The observed, calculated and difference profiles are shown in Figure 6.9.

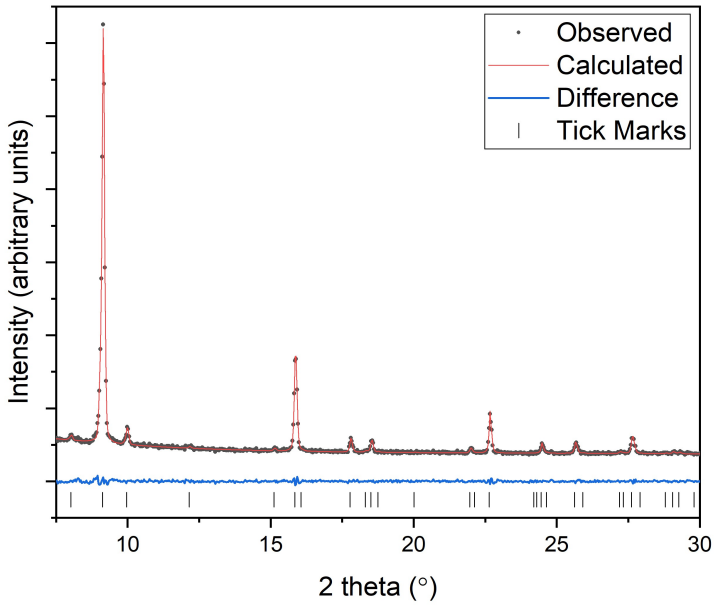

Figure 6.9: Observed, calculated and difference profiles from data collected on an iron-ettringite sample synthesised using the sugar and stirring method and a synthesis time of 48 hours (data collected on laboratory Bruker D2, λ = 1.541 Å) refined using the Pawley method

Comparison of the refined unit cell parameters for the aluminium ettringite phase (Section 6.3.1, *a* = 11.224 Å, *c* = 21.456 Å) with the iron-ettringite phase (*a* = 11.182 Å, *c* = 22.05 Å) shows that the value of the *a* parameter hasn't changed by a significant amount. However, the value of the *c* parameter increases from 21.456 Å for the aluminium ettringite to 22.05 Å for iron ettringite. This increase in unit cell size is due to the increased size of the Fe^{3+} cation (0.645 Å) relative to the Al^{3+} cation (0.535 Å)[18]. This increase in cation size influences the length of the *c* axis of the ettringite crystal structure more significantly than the *a* axis as the metal cations are positioned in the columns which run parallel to the *c* axis (shown in Figure 6.10). The aluminium / iron (M) cations are closer to one another in the *c* direction with an M-M distance of 5.364 Å, compared to an M-M distance of 11.223 Å in the *a* direction. Therefore, changing the cation on the M site from Al^{3+} to the larger Fe^{3+} will result in a lengthening of the *c* axis.

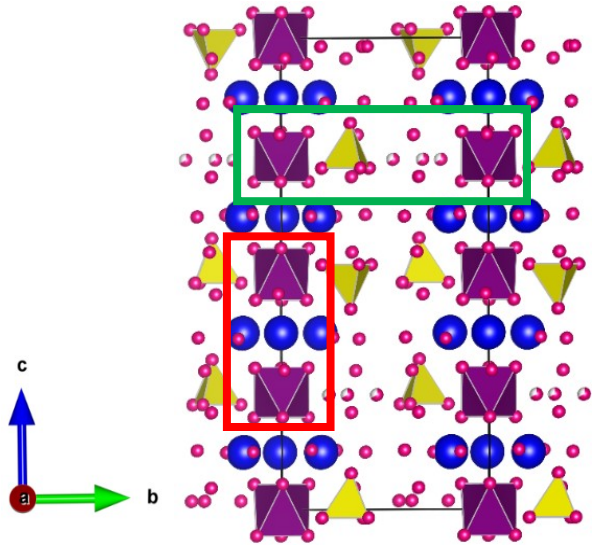

Figure 6.10: [11-20] projection of the ettringite crystal structure parallel to the c axis. Purple octahedral = $M(OH)_6$, M = Al^{3+} or Fe^{3+}. Boxes highlight the proximity of the M atoms in different directions

6.4.2 Gallium-ettringite Synthesis Method Optimisation

Gallium-ettringite was synthesised using the different synthesis methods used previously in Section 6.3.1 for the synthesis of aluminium-ettringite. The different synthesis methods are given in Table 6.3. The products were analysed by PXRD and FTIR and the results are shown in Figure 6.11 and Figure 6.12 and are summarised in Table 6.3.

Table 6.3: Summary of conditions for the synthesis of gallium-ettringite

Conditions of Synthesis	**Phases identified by PXRD**	**Functional groups identified in FT-IR**
Sugar and stirring	gallium-ettringite	water, sulfate
10 minute synthesis	gallium-ettringite	water, sulfate
Sugar and no stirring	gallium-ettringite with preferred orientation	water, sulfate
No sugar and stirring	gallium-ettringite, calcium carbonate hydrate, calcite	water, sulfate, carbonate

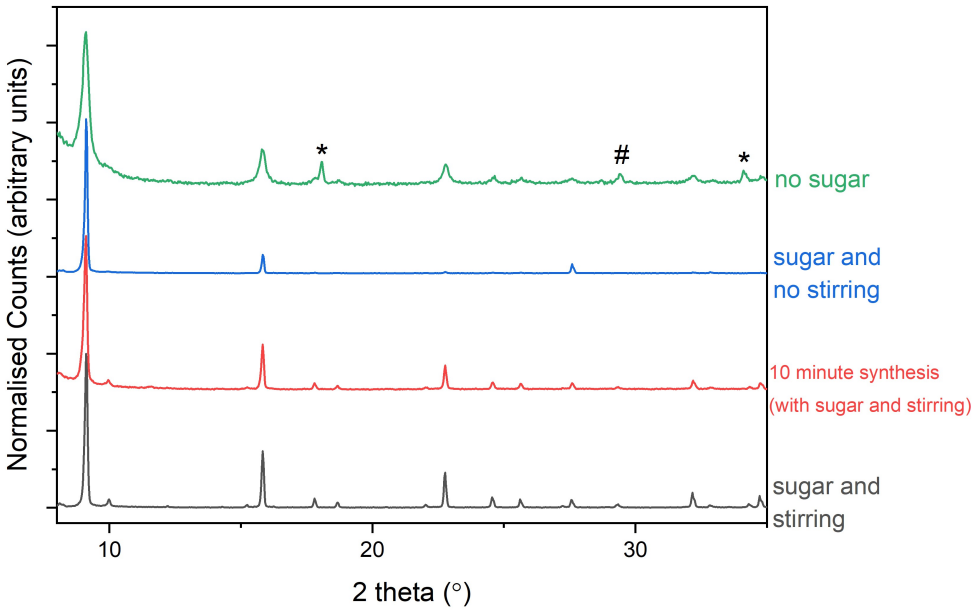

*Figure 6.11: Powder X-ray diffraction patterns for gallium-ettringite phases synthesised under different conditions (data collected on laboratory Bruker D2, λ = 1.541 Å) *=$CaCO_3.6H_2O$ (ICSD: 16070), #=calcite (ICSD: 18166), all other reflections assigned to ettringite (ICSD: 251756)*

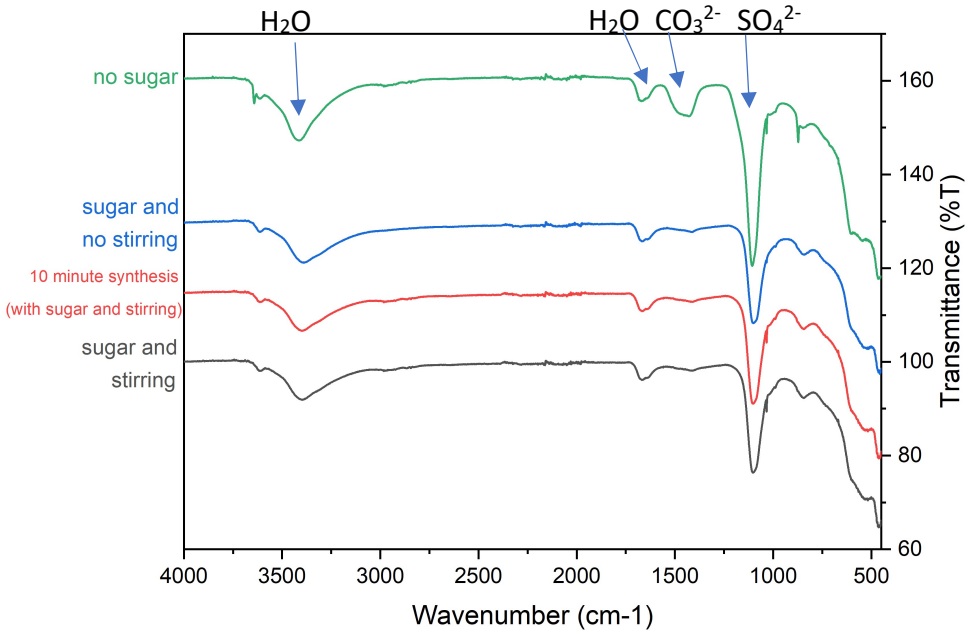

Figure 6.12: FTIR data for gallium-ettringite phases synthesised under different conditions (bands for key functional groups indicated by arrows and labels)

Ettringite reflections are present in the PXRD patterns for all the samples. When the reaction mixture was not stirred the PXRD pattern contains some reflections (100, 110, 300) that are disproportionately intense. This could be the result of the sample preparation technique used for PXRD analysis. The samples are prepared as smears on Si substrates which could induce the preferred orientation of a sample. In this case, the reflections present in the PXRD pattern suggest a tabular morphology which is in contrast to the needle morphology expected for ettringite phases, and so the lack of agitation of the sample has resulted in an atypical morphology for this phase. The pattern for the sample where sugar had been excluded contained reflections for the impurity phases calcite and calcium carbonate hydrate, again emphasising the importance of sugar for inhibiting the absorption of CO_2 to avoid carbonate containing impurities forming. The IR spectra confirm these results with spectrum for the 'no sugar' method sample containing a large carbonate stretch.

The 'sugar and stirring' method was found to be the optimum method and the time dependence of the formation of gallium ettringite using this method was investigated with a phase pure ettringite being found to form after only 10 minutes. The unit cell parameters of a sample of gallium ettringite synthesised using the 'sugar and stirring' method were refined in the space group P31c using the Pawley method to a = 11.177 (1) Å, c = 21.812 (5) Å, R_{wp}= 9.940. These compare well to published unit cell parameters for gallium ettringite: a = 11.202 (2) Å, c = 22.797 (3) Å[5]. The observed, calculated and difference profiles are shown in Figure 6.13.

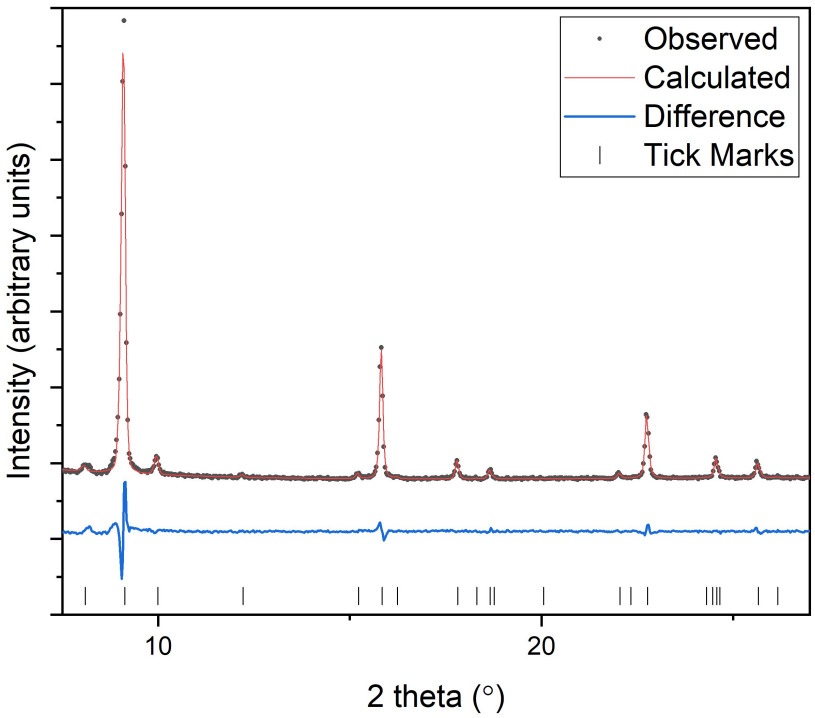

Figure 6.13: Observed, calculated and difference profiles from data collected on an gallium ettringite sample synthesised using the sugar and stirring method and a synthesis time of 48 hours (data collected on laboratory Bruker D2, λ = 1.541 Å) refined using the Pawley method

The results of this refinement confirm that an ettringite phase has been successfully synthesised. Comparison of the refined unit cell parameters for the aluminium ettringite phase (Section 6.3.1, *a* = 11.224 Å, *c* = 21.456 Å) with the gallium-ettringite phase (*a* = 11.177 Å, *c* = 21.812 Å) show that the unit cell is larger for the gallium analogue. This is because of the larger size of the Ga^{3+} cation (0.62 Å) compared to the Al^{3+} cation (0.535 Å). The change in size is directed along the *c* axis (as with the iron-ettringite analogue refined in section 6.4.1) due to the position of the Al^{3+} / Ga^{3+} cations causing a change in unit cell *c* parameter from 21.456 Å for aluminium-ettringite to 21.812 Å for the gallium-ettringite. The *a* unit cell parameter decreases in size, but on a much smaller scale than the *c* parameter increase.

6.5 Synthesis of a Solid Solution Between Aluminium- and Gallium-ettringite

From the previous investigations into the formation of structural analogues of ettringite, it was found that, along with aluminium-ettringite, the gallium analogue was also able to form with no impurities over a wide range of conditions and also in a short amount of time. For this reason, solid solution formation between these two analogues was investigated.

Samples were made with the general formula $Ca_6[Al_xGa_{1-x}(OH)_6]_2(SO_4)_3.26H_2O$ by altering the ratios of $Al_2(SO_4)_3.16H_2O$ and $Ga_2(SO_4)_3.13H_2O$ used during the synthesis to target different compositions (x = 0, 0.1, 0.2, 0.3, 0.4, 0.5, 0.6, 0.7, 0.8, 0.9, 1). PXRD patterns were collected using an internal silicon standard to allow accurate refinement of the unit cell parameters. The PXRD results are shown in Figure 6.14.

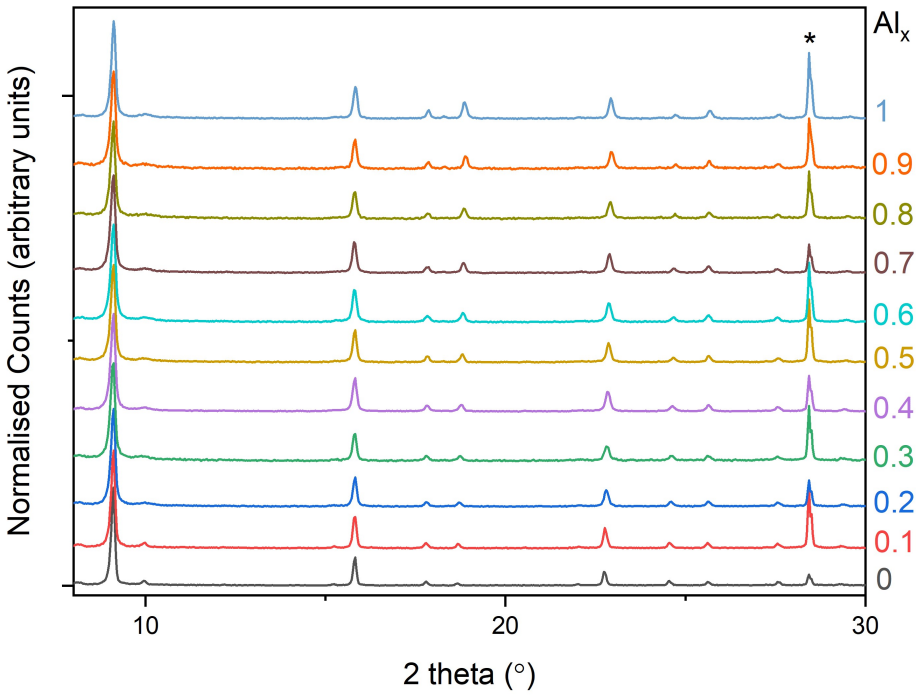

*Figure 6.14: Powder X-ray diffraction patterns for the aluminium-gallium ettringite solid solution (data collected on laboratory Bruker D2, λ = 1.541 Å) *= 111 reflection of the silicon internal standard used to calibrate data, all other reflections assigned to ettringite (ICSD: 251756)*

The PXRD patterns for all members of the solid solution contain the reflections associated to the ettringite structure and no impurity phases are identified. As has been previously discussed, there is an increase in the size of the unit cell (caused by an increase in the size of the *c* unit cell parameter) when the aluminium is replaced with gallium. The intermediate members of the solid solution series have varying ratios of Al^{3+}:Ga^{3+}, and according to Vegard's rule the lattice parameters between two end members of a solid solution series will change linearly with composition[19]. This means that there should be a change in certain peak positions as the larger *c* unit cell parameter will lead to a larger d spacing for reflections with a (00l) component. Therefore, those peaks will appear at lower 2θ positions on the PXRD patterns of samples with increasing gallium content. Expanded 2θ regions of Figure 6.14 are shown below in Figure 6.15 a) and b) to highlight this. The reflections highlighted in Figure 6.15 a) and b) are the 110 and 114 reflections respectively. The position of the 110 reflection doesn't change with composition as this has no *c* contribution, but the position of the 114 reflection does change and moves to a lower 2θ position as more gallium is incorporated, and this is because this reflection has a *c* parameter contribution.

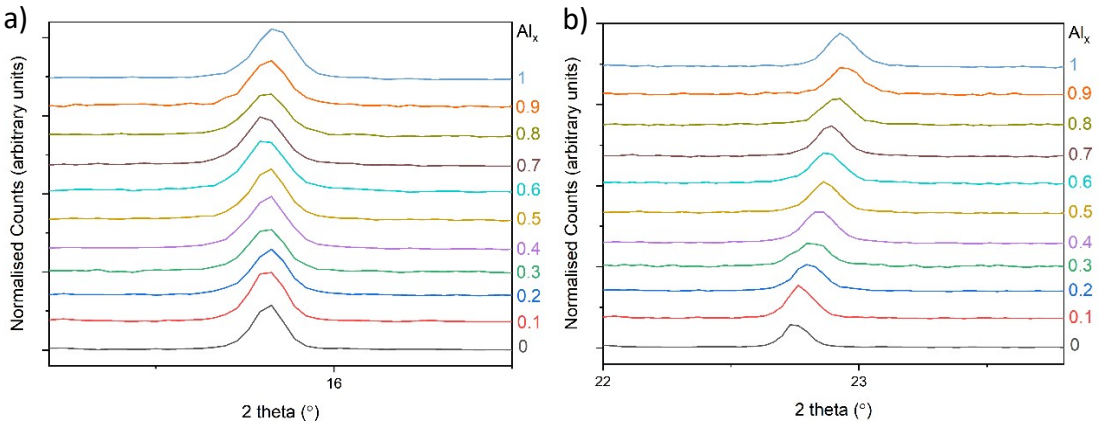

Figure 6.15 a) and b): Expanded 2ϑ region between a) 15.2-16.5 ° 2ϑ and b) 22-23.8 ° 2ϑ from Figure 6.14, highlighting the a) 110 and b) 114 reflection of ettringite

Refinements of the data collected on each sample were carried out. First the silicon was refined along with the zero point error, to take into account any experimental errors, then the unit cell parameters of the sample were refined using the Pawley method. The refined unit cell parameters (all in space group P31c) are given in Table 6.4, and are plotted against the aluminium content in Figure 6.16, Figure 6.17, and Figure 6.18.

Table 6.4: Unit cell parameter values, refined using a Pawley refinement, for the aluminium-gallium ettringite solid solution members

x in Al_xGa_{1-x}	***a* (Å)**	***c* (Å)**	**Volume (Å^3)**
0	11.184 (1)	21.810 (4)	2362 (1)
0.1	11.199 (2)	21.772 (7)	2364 (1)
0.2	11.197 (2)	21.700 (8)	2356 (1)
0.3	11.190 (3)	21.64 (1)	2346 (2)
0.4	11.197 (2)	21.615 (6)	2346 (1)
0.5	11.195 (2)	21.564 (7)	2340 (1)
0.6	11.212 (3)	21.562 (7)	2347 (1)
0.7	11.202 (2)	21.540 (5)	2340 (1)
0.8	11.186 (3)	21.504 (9)	2330 (1)
0.9	11.190 (2)	21.465 (8)	2327 (1)
1.0	11.183 (2)	21.495 (5)	2328 (1)

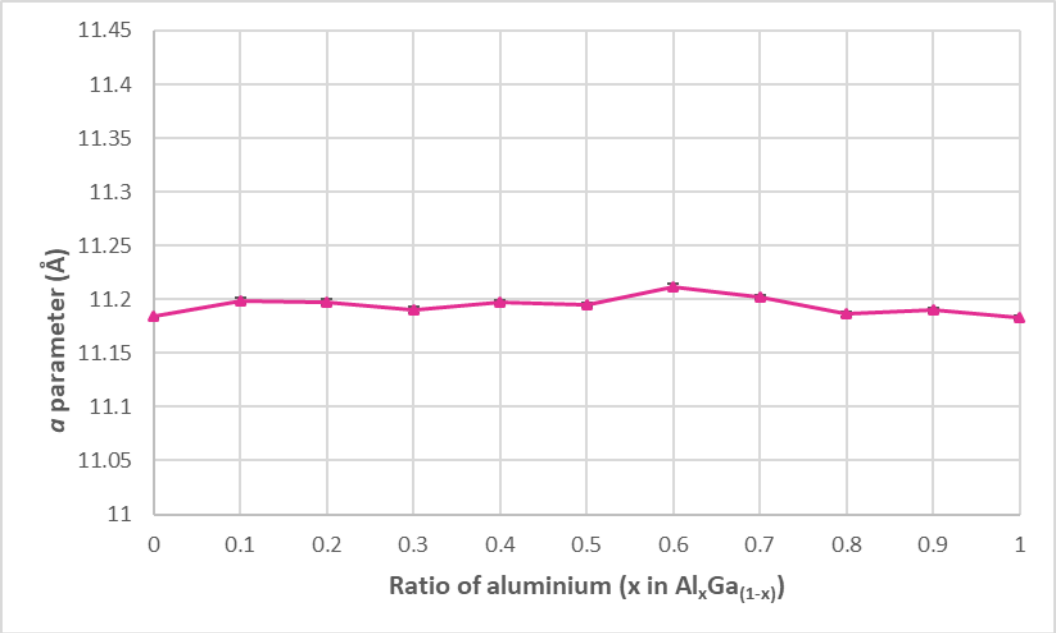

*Figure 6.16: Graph displaying the Pawley refined **a** parameters of members of the aluminium-gallium solid solution with error bars*

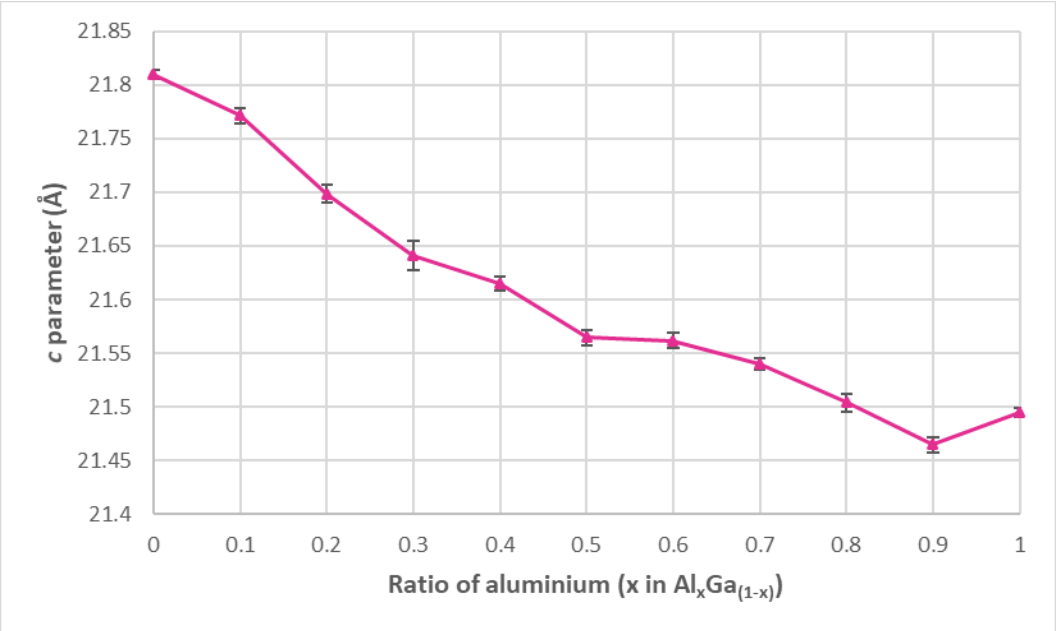

*Figure 6.17: Graph displaying the Pawley refined **c** parameters of members of the aluminium-gallium solid solution with error bars*

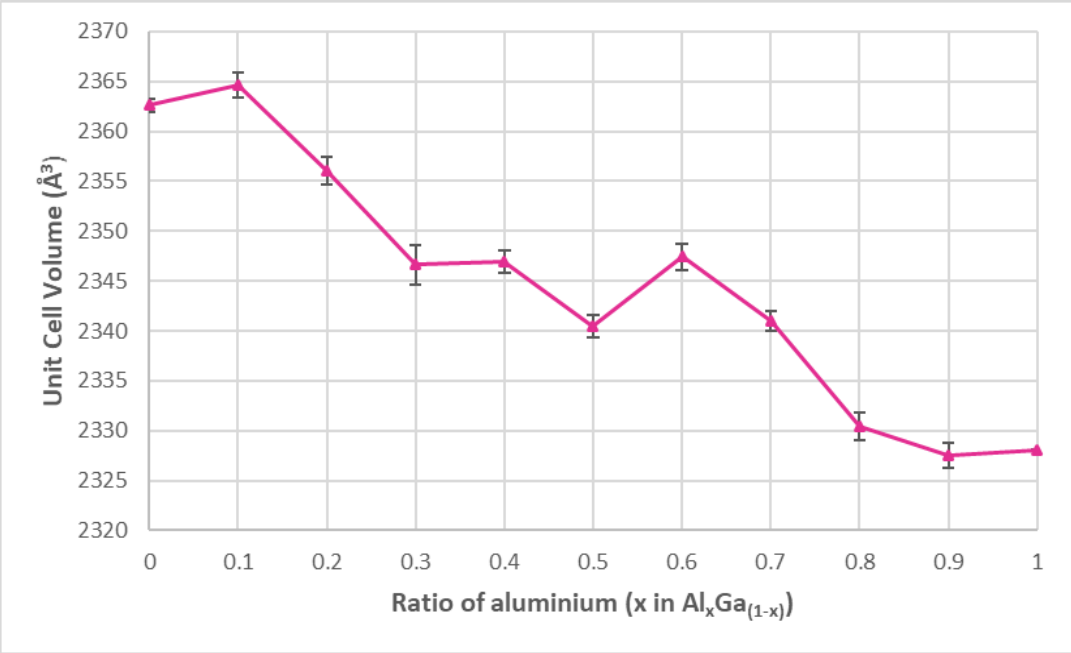

Figure 6.18: Graph displaying the Pawley refined unit cell volumes of members of the aluminium-gallium solid solution with error bars

From the above data the expected trend is found showing that the volume of the unit cell decreases as the amount of aluminium increases, which is due to the smaller ionic radius of Al^{3+} (0.535 Å) compared to Ga^{3+} (0.62 Å). The same trend can also be observed for changes in the *c* parameter as a function of aluminium content, with the difference between largest and smallest *c* parameter = 0.345 Å. However, any changes in the *a* parameter between members of the solid solution are very small, with the difference between smallest and largest *a* = 0.028 Å. Using these results, a complete solid solution can be confirmed to form between the two end members aluminium-ettringite and gallium-ettringite.

6.5.1 Bond Valence Sum Analysis of Synchrotron Data

The investigation into the aluminium-gallium ettringite solid solution series in the above Section 6.5 was carried out using samples synthesised during this project and PXRD data collected on these samples using a laboratory Bruker D2 powder X-ray

diffractometer. This section will now deal with the analysis of samples prepared by Dr Rachel Norman in 2010[5]. They were synthesised using the same method as the previous samples, however, a smaller number of members of the solid solution series were prepared: $Ca_6([Al_xGa_{1-x}]OH_6)_2(SO_4)_3.26H_2O$, x = 0, 0.25, 0.5, 0.75, 1. PXRD data on these samples were collected in 2010 on beamline I11 at the Diamond Light Source synchrotron, and the improved data quality of the synchrotron data means that more information can be extracted from the data and more in-depth analysis can be carried out. Rietveld refinements of these data were performed, as part of this study in 2018-2020, to refine the atomic positions, occupancy of sites and bond lengths. The PXRD data are plotted below in Figure 6.19, with expanded regions to highlight the change in position of certain reflections as the ratio of Al^{3+}:Ga^{3+} changes, shown in Figure 6.20 a) and b).

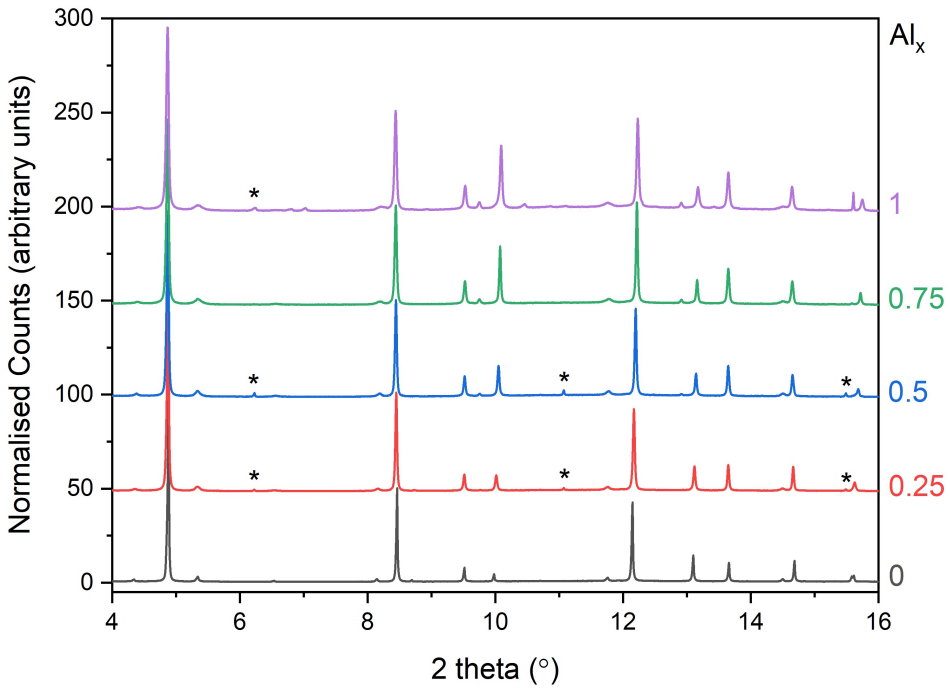

*Figure 6.19: Powder X-ray diffraction patterns for the aluminium-gallium ettringite solid solution synthesised by Rachel Norman (data collected on I11 at the Diamond Light Source Synchrotron, λ = 0.82626 Å) * = gypsum (ICSD: 2058), all other reflections assigned to ettringite (ICSD: 251756)*

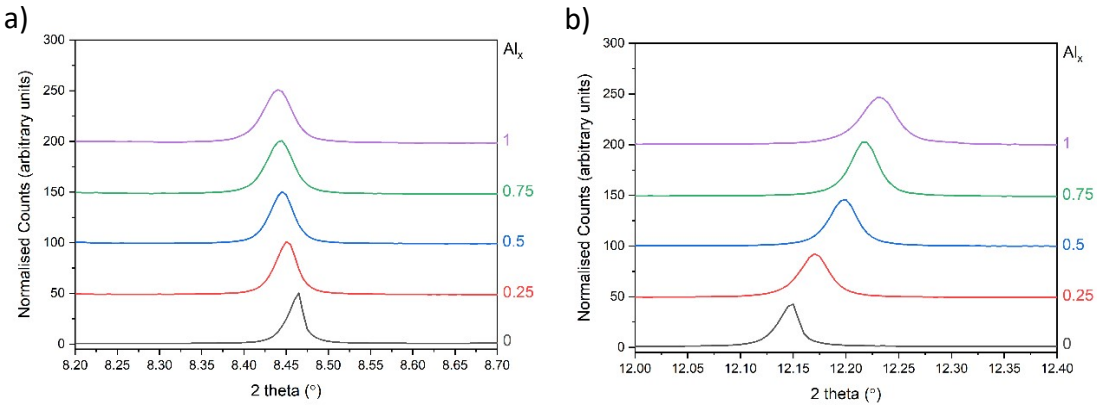

Figure 6.20 a) and b): Expanded 2ϑ region between a) 8.2-8.7 and b) 12-12.4 ° 2ϑ from Figure 6.19, highlighting the a) 110 and b) 114 reflection of ettringite

Table 6.5, Figure 6.21 and Figure 6.22 show the refined unit cell parameters from Rietveld refinement of the data and are compared to the refined unit cell parameters obtained from analysis of laboratory PXRD data collected on samples synthesised and discussed in section 6.5. There is good correlation between the two sets of samples refined unit cell parameters. The unit cell *a* parameter remains relatively unchanged across the series of compositions, and the unit cell *c* parameter decreases linearly as the amount of aluminium is increased, with this resulting in the unit cell volume also decreasing linearly.

Table 6.5: Refined unit cell parameters and site occupancies for the aluminium-gallium ettringite solid solution members analysed at the Diamond Light Source Synchrotron (beamline I11)

x in Al_xGa_{1-x}	***a* (Å)**	***c* (Å)**	**Volume (Å^3)**
0	11.19595 (4)	21.79383 (1)	2365.84 (3)
0.25	11.21209 (5)	21.6862 (2)	2360.95 (3)
0.5	11.21884 (6)	21.5777 (2)	2351.97 (3)
0.75	11.22227 (6)	21.5054 (2)	2345.53 (3)
1.0	11.22335 (8)	21.4541 (2)	2340.38 (3)

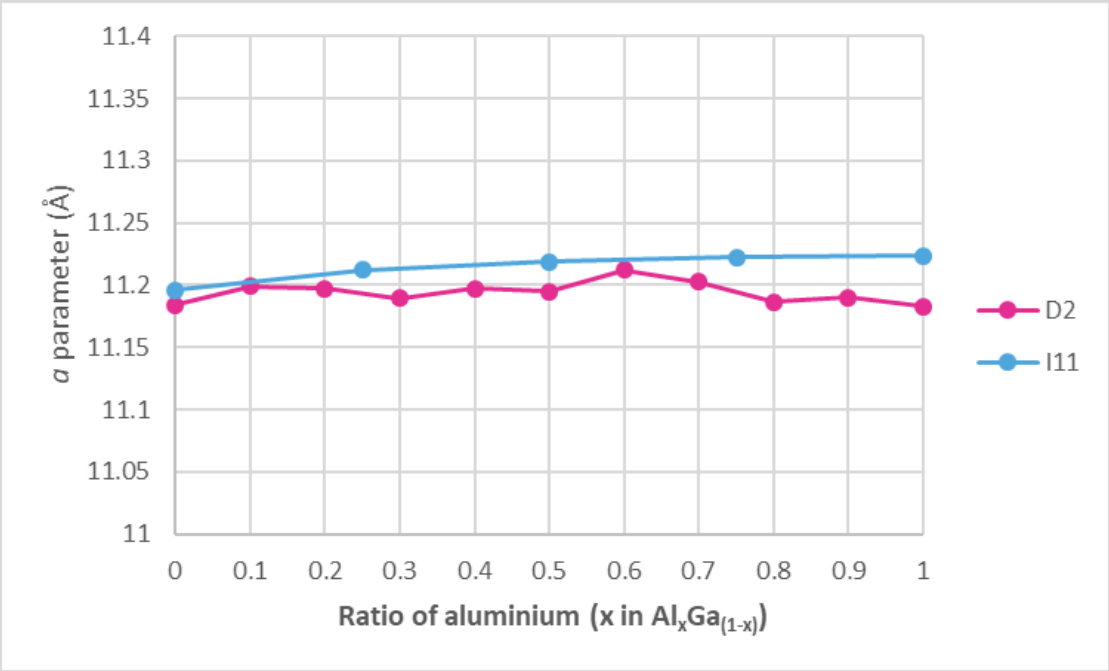

*Figure 6.21: Graph comparing the refined **a** parameters of members of the aluminium-gallium solid solution collected on beamline I11 and a laboratory D2 (with error bars)*

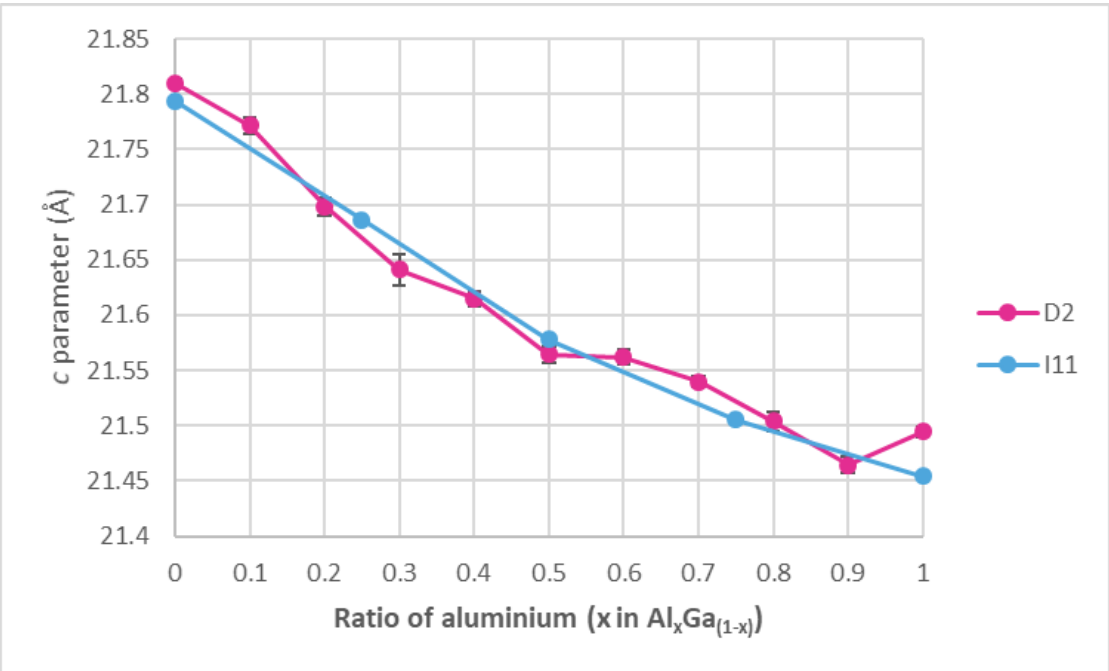

*Figure 6.22: Graph comparing the refined **c** parameters of members of the aluminium-gallium solid solution collected on beamline I11 and a laboratory D2 (with error bars)*

The occupancy of the aluminium sites of the ettringite structure (called ‘Al1’ and ‘Al2’) were refined to determine the relative occupancies of aluminium and gallium on each site. The bond lengths were calculated and using these, along with the site occupancies, allowed the valence of the aluminium sites to be calculated using the bond valence sum method. These results are given in Table 6.6.

The thermal parameters were fixed at different values and were found to be correlated to the site occupancies. However, allowing the thermal parameters to refine from any starting value resulted in the same occupancy values and bond lengths being calculated for each member. The table below contains these refined values. The calculated bond lengths are presented in Appendix 4.

Table 6.6: Calculated site occupancies, bond lengths and valences of the aluminium-gallium ettringite solid solution members

x in Al_xGa_{1-x}	**Site 'Al1'**						**Site 'Al2'**					
	$Al_{occupancy}$	$Ga_{occupancy}$	Thermal parameter	Bond length Al1:O1 (x3)	Bond length Al1:O2 (x3)	Valence	$Al_{occupancy}$	$Ga_{occupancy}$	Thermal parameter	Bond length Al2:O3 (x3)	Bond length Al2:O4 (x3)	Valence
0	0	1	1.4 (2)	1.98 (5)	1.95 (5)	3.18	0	1	1.0 (2)	1.97 (5)	1.96 (5)	3.18
0.25	0.27 (2)	0.73 (2)	2.4 (2)	1.99 (3)	1.89 (4)	3.19	0.25 (2)	0.75 (2)	1.2 (2)	1.96 (3)	1.99 (3)	2.90
0.5	0.51 (2)	0.49 (2)	2.7 (3)	1.96 (3)	2.00 (3)	2.65	0.67 (2)	0.33 (2)	0.1 (2)	1.95 (3)	1.83 (3)	3.26
0.75	0.72 (2)	0.28 (2)	3.7 (4)	1.93 (3)	1.98 (3)	2.67	0.86 (1)	0.14 (1)	0.5 (3)	1.90 (3)	1.87 (3)	3.08
1	1	0	1.1 (5)	1.95 (4)	1.85 (4)	2.84	1	0	2.6 (6)	2.02 (3)	1.81 (4)	2.81

Using the refined occupancies given in Table 6.6, the total stoichiometry of the solid solution members can be calculated and are given in Table 6.7. As the targeted aluminium content of the series increases there is a stronger preference for aluminium to incorporate in the structure compared to gallium, and in particular there is also a site preference for aluminium to occupy site Al2. This results in there being a higher aluminium content than was targeted for the members above the 50:50 composition. This is likely due to the stability of the aluminium-ettringite end member being greater than that of the gallium-ettringite end member. An excess of aluminium containing reagents will cause the aluminium to preferentially incorporate into the ettringite structure to form a more aluminium rich product than was targeted. There is the potential that this preference for aluminium incorporation could have led to zoning of the crystallites, but this cannot be identified using XRD alone. SEM imaging with EDS analysis could be used to acquire images of the crystallites and determine the elemental composition of different points and zones. The calculated valences of the aluminium sites should ideally be 3, the end members and the $Al_{0.25}Ga_{0.75}$ sample gave appropriate values close to 3. The valences of both sites for the $Al_{0.5}Ga_{0.5}$ sample are off, with site Al1 having a low valence (2.65) and site Al2 having a high valence (3.26) indicating that site Al2 is overbonded and the bonds from cation to oxygen are shorter than they should be. The same observations of valence can be made for the $Al_{0.75}Ga_{0.25}$ sample and this corresponds to the Al2 site being preferentially occupied by aluminium rather than gallium.

Table 6.7: Calculated aluminium and gallium stoichiometry for members of the aluminium-gallium ettringite solid solution

Targeted stoichiometry	**Calculated aluminium stoichiometry**	**Calculated gallium stoichiometry**
Al 0 Ga 1	0	1
Al 0.25 Ga 0.75	0.2602	0.7398
Al 0.5 Ga 0.5	0.5938	0.4062
Al 0.75 Ga 0.25	0.7891	0.2109
Al 1 Ga 1	1	0

6.6 CONCLUSIONS

This study focussed on optimising the reaction conditions for the synthesis of ettringite and its structural analogue phases where the aluminium was replaced by iron or gallium ($Ca_6[X(OH)_6]_2(SO_4)_3.26H_2O$, X = Al^{3+}, Fe^{3+}, Ga^{3+}). The synthesis method chosen was the saccharate method and conditions such as the presence of sugar and whether or not the reaction mixture was stirred were varied to determine the optimal conditions for synthesis of a phase pure product.

It was found that aluminium-ettringite formed instantaneously with no impurity phases present. The pure aluminium ettringite was the most tolerant to changes in synthesis methods and could also form under conditions with no sugar present in the synthesis and when the reaction mixture was not stirred. This ability to form under a range of different conditions, along with the speed of formation means that this synthesis method would be easy to scale up and implement for aluminium or sulfate remediation.

The analogue phases containing iron and gallium were found to form without impurities only when sugar was present in the reaction mixture, with carbonate containing impurities forming when sugar was excluded. The study into iron-ettringite formation by Möschner et al[4] used a different synthesis method with no sugar but took care to exclude air from the reaction vessel. Even with these controls they identified calcite ($CaCO_3$) in the solid products confirming that synthesis of iron-ettringite is highly susceptible to forming carbonate containing impurities. Gallium ettringite was found to form with no impurities after 10 minutes when using the 'sugar and stirring' method, however, formation of iron-ettringite using the same method required a synthesis time of 48 hours. The unit cell parameters for the iron-ettringite and gallium-ettringite were refined using the Pawley method and both were found to have larger unit cells due to iron and gallium cations being larger than aluminium. The refined unit cell parameters for both correlated well to those published previously.

A complete solid solution between aluminium-ettringite and gallium-ettringite was shown to exist ($Ca_6([Al_xGa_{1-x}](OH)_6)_2(SO_4)_3.26H_2O$). Unit cell parameters were refined, and the unit cell volume was shown to decrease linearly as the gallium content of the phase decreased. High resolution synchrotron PXRD data from a previous study were analysed and the occupancy of sites shared between Al^{3+} and Ga^{3+} were refined, confirming the synthesis of specific compositions of the solid solution series. It was found that when targeting compositions (Al_xGa_{1-x}) where $x \geq 0.5$, aluminium preferentially incorporated forming Al-rich ettringite phases, with an even higher aluminium content than was targeted. It was also discovered that the aluminium had a preference for one of the two Al sites.

6.7 REFERENCES

1 H. F. W. Taylor, *Cement chemistry 2nd Edition*, Thomas Telford, London, 2nd edn., 1997.

2 W. Hume-Rothery and H. M. Powell, *Zeitschrift für Krist. - Cryst. Mater.*, 1935, **91**, 23–47.

3 W. Hume-Rothery, *The Structure of Metals and Alloys*, 2nd edn., 1950.

4 G. Möschner, B. Lothenbach, F. Winnefeld, A. Ulrich, R. Figi and R. Kretzschmar, *Cem. Concr. Res.*, 2009, **39**, 482–489.

5 R. L. Norman, S. E. Dann, S. C. Hogg and C. A. Kirk, *Solid State Sci.*, 2013, **25**, 110–117.

6 L. Pauling, *J. Am. Chem. Soc.*, 1929, **51**, 1010–1026.

7 L. Pauling, *The nature of the chemical bond and the structure of molecules and crystals : an introduction to modern structural chemistry*, Cornell University Press, Ithaca, 1960.

8 I. D. Brown, *The Chemical Bond in Inorganic Chemistry: The Bond Valence Model*, Oxford University Press, 2002, vol. 1.

9 N. K. Foley, B. W. Jaskula, B. E. Kimball and R. F. Schulte, *Gallium*, 2017.

10 R. R. Moskalyk, *Miner. Eng.*, 2003, **16**, 921–929.

11 B. Gutiérrez, C. Pazos and J. Coca, *Waste Manag. Res.*, 1997, **15**, 371–382.

12 D. H. Klein, A. W. Andren, J. A. Carter, J. F. Emery, C. Feldman, W. Fulkerson, W. S. Lyon, J. C. Ogle, Y. Talmi, R. I. Van Hook and N. Bolton, *Environ. Sci. Technol.*, 1975, **9**, 973–979.

13 O. Font, X. Querol, R. Juan, R. Casado, C. R. Ruiz, Á. López-Soler, P. Coca and F. G. Peña, *J. Hazard. Mater.*, 2007, **139**, 413–423.

14 E. Álvarez-Ayuso and H. W. Nugteren, *Water Res.*, 2005, **39**, 65–72.

15 W. Dou, Z. Zhou, L. M. Jiang, A. Jiang, R. Huang, X. Tian, W. Zhang and D. Chen, *J. Environ. Manage.*, 2017, **196**, 518–526.

16 W.-H. Choi, J.-H. Shim, P. A. Ghorpade and J.-Y. Park, *Desalin. Water Treat.*, 2014, **52**, 712–718.

17 E. T. Carlson and H. A. Berman, *J. Res. Natl. Bur. Stand. - A Phys. Chem.*, 1960, **64A**, 333–341.

18 R. D. Shannon, *Acta Crystallogr. Sect. A*, 1976, **32**, 751–767.

19 L. Vegard, *Zeitschrift fur Phys.*, 1921, **5**, 17–26.

CHAPTER 7 CONCLUSIONS AND FURTHER WORK

This thesis presents investigations into the synthesis of the mineral ettringite, its structural analogues, and their use as waste remediation materials. Overall, this work has confirmed the successful synthesis of many different ettringite analogue phases ($Ca_6[M(OH)_6]_2(XO_4)_3.26H_2O$; M = Al^{3+}, Fe^{3+}, Ga^{3+}; X = S^{6+}, Cr^{6+}, Se^{6+}) and has investigated how the structure changes with the replacement of different ions. The ability of this system to form solid solutions between ettringite and the chromate and selenate containing analogue phases produced was also investigated. The analogue phases of the mineral monosulfate ($3CaO.Al_2O_3.CaXO_4.14H_2O$, X = S^{6+}, Cr^{6+}) were also investigated as under certain reaction conditions, ettringite can further react and convert to monosulfate[1]. A novel method of remediating the potentially toxic elements hexavalent chromium and selenium, was shown to successfully remove them from solution and encapsulate them in solid mineral phases. Various solid state characterisation techniques were employed to analyse the phases formed in this study, including synchrotron powder X-ray diffraction, powder neutron diffraction, fourier transform infrared spectroscopy, scanning electron microscopy and inductively coupled plasma-optical emission spectroscopy. The combination of all these techniques allowed the crystal structures and elemental compositions of all products to be determined and thus synthesis methods and remediation processes could be compared, and the optimum conditions could be established.

The mineral ettringite and its chromium and selenium containing analogues ($Ca_6[Al(OH)_6]_2(XO_4)_3.26H_2O$, X = S^{6+}, Cr^{6+}, Se^{6+}) were successfully synthesised in Chapter 3 using the saccharate method, and reaction times of only 24 hours. Refinement of the unit cell parameters using synchrotron powder X-ray diffraction data showed that the ettringite phases containing the larger CrO_4^{2-} and SeO_4^{2-} anions had larger *a* unit cell parameters than ettringite containing SO_4^{2-} anions (*a* = 11.224 Å for sulfate ettringite, 11.398 Å for chromate ettringite, 11.387 Å for selenate ettringite). Synchrotron powder X-ray diffraction data also allowed the analysis of a

synthesised sample of monochromate ($3CaO.Al_2O_3.CaCrO_4.14H_2O$) and a model of its crystal structure was determined. The crystal structure of monochromate is debated in literature[2–5], but this study determined that a sample synthesised by reaction of tricalcium aluminate ($Ca_3Al_2O_6$, C3A) with potassium chromate (K_2CrO_4) for 1 month crystallised with a layered structure in the space group P3c1. The model produced for this structure was only an approximation as the exact positions of the oxygens in the interlayer could not be determined. In order to fully characterise the interlayer region and determine the oxygen positions, low temperature neutron diffraction would need to be carried out in the future.

A novel method of removing chromium and selenium from solution was developed and tested in Chapter 4. It involved adding C3A ($Ca_3Al_2O_6$) to solutions of either potassium chromate (K_2CrO_4), or sodium selenate (Na_2SeO_4). The concentration of the PTE (potentially toxic element, Cr^{6+} or Se^{6+}) in the solutions was varied and solid samples were taken at various time points after the addition of C3A. This was done to track how much of the PTE had been removed from solution, and what solid phases were forming. Overall, the method was shown to be effective, as all of the solutions tested showed a reduction in the concentration of either chromium or selenium, as a result of reaction with C3A.

For the solutions containing chromium, when the concentration was high (0.2 M, K_2CrO_4), chromate ettringite ($Ca_6[Al(OH)_6]_2(CrO_4)_3.26H_2O$) and monochromate ($3CaO.Al_2O_3.CaCrO_4.14H_2O$) were the solid products that formed initially, with any chromate ettringite converting to monochromate at times of over 1 week. When the concentration of the potassium chromate solution was lower (0.1 M, 0.02 M, 0.01 M) only mono phases were formed including monochromate and monocarbonate ($3CaO.Al_2O_3.CaCO_3.11H_2O$). The solutions with initial concentrations of 0.02 M and 0.01 M were almost fully remediated using this method, with the chromium concentration in solution reducing to 2.4 ppm after 1 week of reaction with C3A for the 0.02 M solution and 0.26 ppm after only 1 day of reaction with the 0.01 M solution.

The sodium selenate solutions with concentration 0.2 M, 0.1 M and 0.02 M followed a similar reaction pathway to the 0.2 M potassium chromate solution, with selenate ettringite ($Ca_6[Al(OH)_6]_2(SeO_4)_3.26H_2O$) forming initially, and monoselenate ($3CaO.Al_2O_3.CaCrO_4.14H_2O$) being the final product at times of over 1 week. It was only when the concentration of the initial solution was reduced to 0.01 M that no selenate ettringite was formed and all the products were mono phases. The same success in total PTE removal was observed for the sodium selenate solutions as was for the potassium chromate solutions. The selenium concentration of the 0.02 M solution was reduced to 12 ppm after 1 week of reaction with C3A and the concentration of the 0.01 M solution reduced to 8.7 ppm after only 1 day of reaction with C3A. The differences in the results for the set of chromate experiments and selenate experiments was concluded to be related to the amount of carbon dioxide absorbed from the air into the reaction vessels. FTIR analysis showed that the chromium containing products contained more carbonate than the selenium containing products and the chromium products were predominantly mono phases. It is concluded that carbonate is more easily able to absorb into the potassium chromate solutions and that the presence of carbonate stabilises the formation of mono phases. With no significant differences in the pH of the potassium chromate and sodium selenate solutions, it is not fully understood how the sodium selenate solution is less susceptible to absorption of carbonate, and so this would be an area for further study.

With the removal of chromium and selenium from solution being shown to be successful using this method, it can be taken forward for further study into implementing it as a remediation method. This further work would include increasing the complexity of the solutions and testing the stability of the solid products. In real wastewater, other ions would be present so the complexity of the PTE containing solution would need to be increased and the method tested again to determine whether it could still remove the chromium and selenium with competing ions present. The stability of the ettringite and mono phases would need to be tested to

determine whether the chromium and selenium is stable in the solid phases and will not leach back out into the environment.

The solid solution behaviour for the systems between sulfate ettringite and chromate ettringite ($Ca_6[Al(OH)_6]_2(CrO_4)_x(SO_4)_{3-x}.26H_2O$) and between sulfate ettringite and selenate ettringite ($Ca_6[Al(OH)_6]_2(SeO_4)_x(SO_4)_{3-x}.26H_2O$) were investigated in Chapter 5. ICP-OES elemental analysis along with powder X-ray diffraction data were used to determine the solid solution limits of both series. The series between sulfate ettringite and chromate ettringite was found to have very limited solid solution behaviour, with a range of $0 < x < 0.8$ when a synthesis time of 1 day was used, and a range of only $0 < x < 0.44$ when a synthesis time of 7 days was used. Any samples where x was out with this range, presented as multiphase, with both the sulfate ettringite and chromate ettringite end members being produced. The series between sulfate ettringite and selenate ettringite had a solid solution range of $0 < x < 1.37$ when using a synthesis time of 1 day, but when a synthesis time of 7 days was used a complete solid solution was produced with no miscibility gaps found. This information, acquired on the solid solution behaviour of these phases, is important when aiming to use ettringite type phases as waste remediation materials. This study provided valuable information into the phases that are produced when sulfate anions are present in solution along with chromate or selenate anions in different ratios.

This PhD project also investigated the synthesis of ettringite analogue phases where the Al^{3+} cation was replaced with either Fe^{3+} or Ga^{3+} ($Ca_6[X(OH)_6]_2(SO_4)_3.26H_2O$, X = Al^{3+}, Fe^{3+}, Ga^{3+}), and the reaction conditions were optimised in Chapter 6. It was found for all three phases that the “saccharate method”, where sugar was added to the reaction mixture and the mixture was stirred, was the best method for synthesis. In particular, the addition of sugar was important to inhibit the formation of carbonate containing impurity phases. A complete solid solution was synthesised between the end members, aluminium ettringite and gallium ettringite ($Ca_6[Al_xGa_{1-x}(OH)_6]_2(SO_4)_3.26H_2O$). Synchrotron powder X-ray diffraction data was used to refine the occupancy of the Al/Ga sites, and it was found that targeting compositions with $x > 0.5$ preferentially incorporated aluminium. This resulted in the

formation of Al-rich phases where the aluminium showed a preference for one of the aluminium sites in the crystal structure.

Overall, the work presented in this thesis is a comprehensive investigation into the synthesis and structures of ettringite and monosulfate analogue phases. The investigations into the structures of analogue phases and solid solution series members have greatly added to the knowledge of these phases in this field. The results from the study conducted in Chapter 4, exploring the potential for removing chromium and selenium from solution using tricalcium aluminate, were very promising and can be used as a proof of concept for taking this work forward. In the future, this work could be expanded and eventually implemented into polluted environments, in order to remediate the waste. The extent of the study presented in this thesis, means that the full reaction pathways have been identified and the reaction products can be predicted and therefore targeted when using this remediation method.

This work could have real consequences for water treatment in the future, as it shows that using this simple method, requiring only one starting material, can effectively remove large quantities of potentially toxic elements in short periods of time. The starting material, tricalcium aluminate, is non-hazardous, and the products of the reaction are known phases which have been fully characterised in this thesis. Encapsulating waste ions in known materials, which are products of the cement industry, means that there is also the potential for the waste to be stabilised fully in a cement matrix, which would allow long term stabilisation and no further threat to the environment.

All of the positive aspects of the work discussed here, mean that this remediation method will be very attractive to industry. It would be easy to implement in contaminated rivers, and also directly into industries where toxic waste is being produced. The immediate future work to progress this remediation technology should involve further testing, using more complex solutions that first mimic the natural environment, then the testing should progress to using water samples

collected from polluted environments. Longer term, the products of the remediation reaction could be incorporated into cement matrices and the effects studied to assess the viability of ultimately stabilising the waste in this way.

7.1 References

1 H. J. Kuzel, *Cem. Concr. Compos.*, 1996, **18**, 195–203.

2 J.-P. Rapin, Universite Henri Poincare, 2001.

3 R. Segni, Universite Blaise Pascal, 2005.

4 J. Göske, U. König and H. Pöllmann, *Mater. Sci. Forum*, 2004, **443**–**444**, 299–302.

5 S. M. Leisinger, B. Lothenbach, G. Le Saout and C. A. Johnson, *Cem. Concr. Res.*, 2012, **42**, 158–165.

APPENDIX 1: CHAPTER 3 SUPPLEMENTARY INFORMATION

Table A.1.1: Atomic positions and thermal parameters for a synthesised sample of ettringite, refined using the Rietveld method against ICSD structure 251756

Atomic Position	x	y	z	Thermal parameter (Beq Å^3)
Al1	0	0	0	0.3 (3)
Al2	0	0	0.25	0.09
Ca1	0.002	0.8116	0.8697	0.7 (3)
Ca2	1.001 (1)	0.1910 (6)	0.1197 (6)	1.5 (3)
O1	1.004 (3)	0.133 (3)	0.938 (1)	0.3 (1)
O2	0.001 (3)	0.882 (2)	0.0489 (9)	0.3 (1)
O3	1.001	0.1263	0.7971	0.3 (1)
O4	0.000 (2)	0.859 (2)	0.1944 (8)	0.3 (1)
O5	1.010 (2)	0.347 (2)	0.048 (1)	1.2 (1)
O6	0.004 (3)	0.680 (2)	0.9688 (9)	1.2 (1)
O7	0.019 (3)	0.371 (3)	0.2077 (9)	1.2 (1)
O8	0.992 (3)	0.640 (3)	0.7913 (9)	1.2 (1)
O9	0.230 (2)	0.394 (2)	0.621 (1)	1.2 (1)
O10	0.720 (2)	0.613 (2)	0.366 (1)	1.2 (1)
O11	0.244 (2)	0.406 (2)	0.136 (1)	1.2 (1)
O12	0.736 (2)	0.580 (2)	0.859 (1)	1.2 (1)
O13	0.333	0.666	0.425	12.5 (3)
O14	0.333	0.666	0.819	12.5 (3)
O15	0.333	0.666	0.076	12.5 (3)
O16	0.195	0.628	0.519	12.5 (3)
O17	0.195	0.620	0.724	12.5 (3)

O18	0.192	0.585	0.982	12.5 (3)
O19	0.227	0.685	0.243	0.3 (6)
S1	0.333	0.666	0.492	3.2 (1)
S2	0.333	0.666	0.751	3.2 (1)
S3	0.333	0.666	0.009	3.2 (1)

Table A.1.2: Atomic positions and thermal parameters for a synthesised sample of chromate ettringite, refined using the Rietveld method against an adapted model from ICSD structure 251756

Atomic Position	**x**	**y**	**z**	**Thermal parameter (Beq Å^3)**
Al1	0	0	0	1.35
Al2	0	0	0.25	0.9
Ca1	0.0035 (9)	0.8207 (7)	0.8702 (7)	1.2 (2)
Ca2	0.9848 (6)	0.1834 (6)	0.1174 (6)	0.7 (2)
O1	1.011	0.1427	0.9402	0.62 (9)
O2	0.0033	0.8671	0.0473	0.62 (9)
O3	1.001	0.1263	0.7971	0.62 (9)
O4	0.0028	0.8653	0.1896	0.62 (9)
O5	1.019 (2)	0.358 (2)	0.047 (1)	1.7 (1)
O6	0.021 (2)	0.688 (2)	0.960 (1)	1.7 (1)
O7	0.004 (3)	0.359 (3)	0.204 (1)	1.7 (1)
O8	0.976 (3)	0.635 (3)	0.784 (1)	1.7 (1)
O9	0.242 (1)	0.404 (2)	0.620 (1)	1.7 (1)
O10	0.718 (2)	0.617 (2)	0.365 (1)	1.7 (1)
O11	0.217 (1)	0.371 (2)	0.134 (1)	1.7 (1)
O12	0.734 (2)	0.583 (2)	0.861 (1)	1.7 (1)
O13	0.333	0.666	0.415	12.8 (4)
O14	0.333	0.666	0.829 (1)	12.8 (4)
O15	0.333	0.666	0.09	12.8 (4)

O16	0.182 (3)	0.639 (3)	0.506 (2)	12.8 (4)
O17	0.175 (2)	0.661 (3)	0.726 (1)	12.8 (4)
O18	0.169 (2)	0.591 (3)	0.972 (2)	12.8 (4)
O19	0.227	0.685	0.243	0.6 (6)
Cr1	0.333	0.666	0.492	2.46 (8)
Cr2	0.333	0.666	0.751	2.46 (8)
Cr3	0.333	0.666	0.009	2.46 (8)

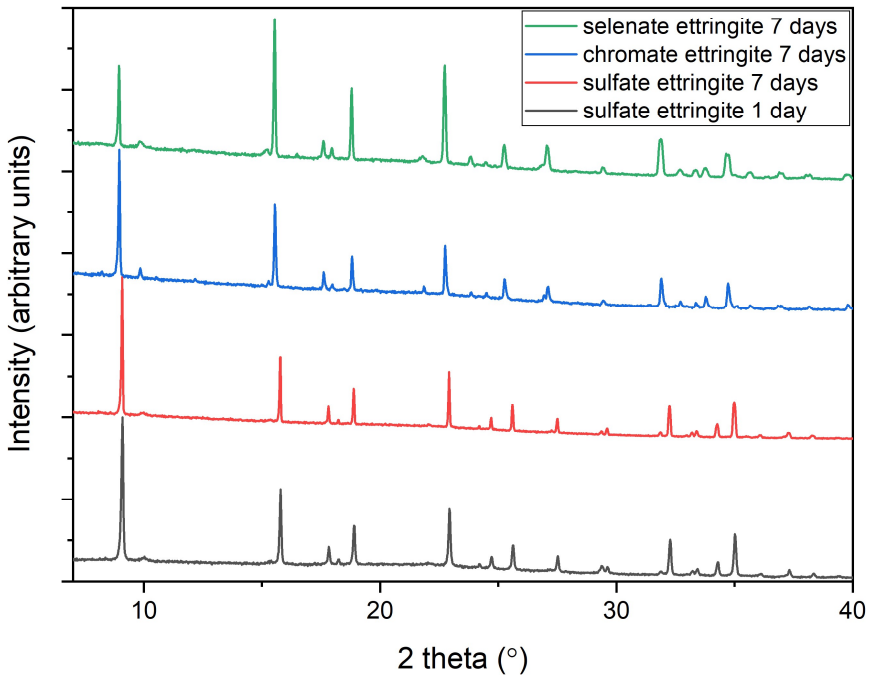

Figure A.1.1: Powder X-ray diffraction patterns of sulfate ettringite, chromate ettringite and selenate ettringite, synthesised with a reaction time of 7 days (all data collected on laboratory Bruker D8, λ = 1.5406 Å)

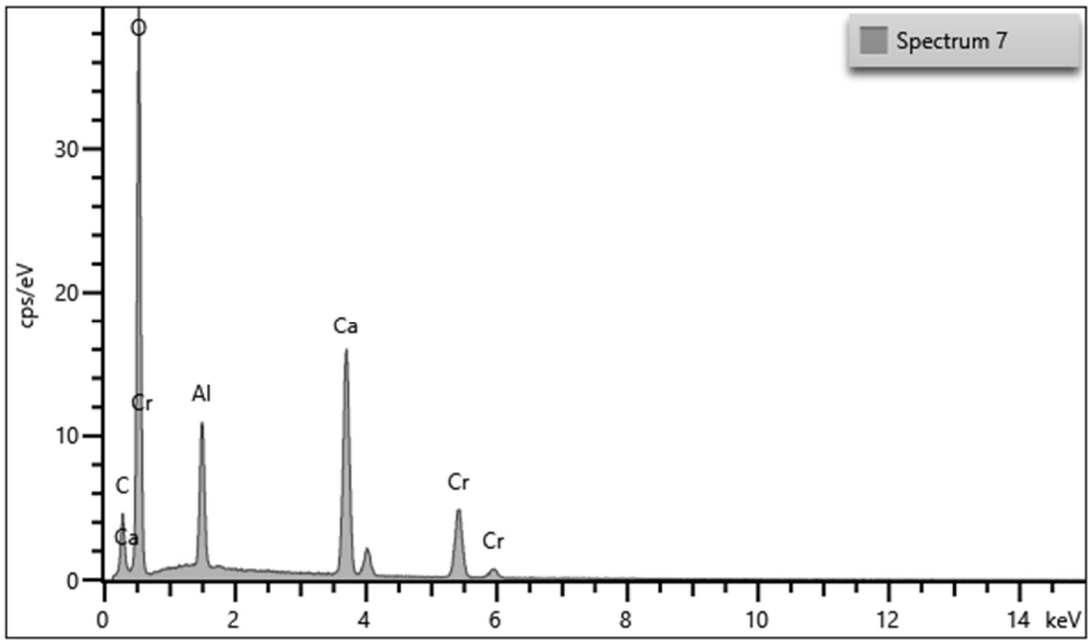

Figure A.1.2: EDS spectrum of a face of a chromate ettringite crystallite (shown in chapter 3 figure 3.7b)

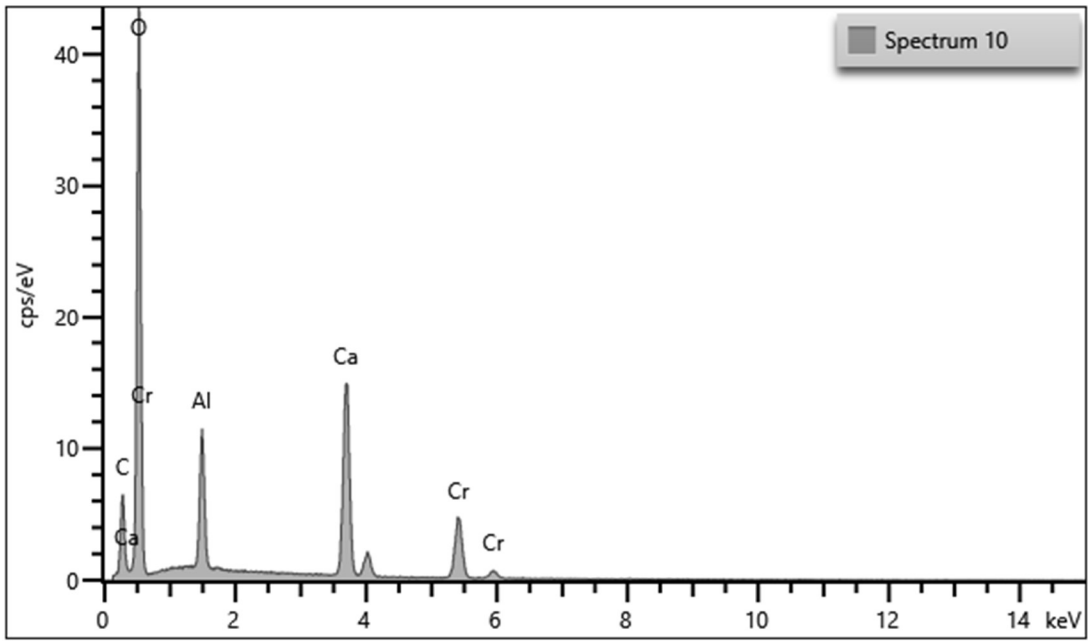

Figure A.1.3: EDS spectrum of an edge of a chromate ettringite crystallite (shown in chapter 3 figure 3.7b)

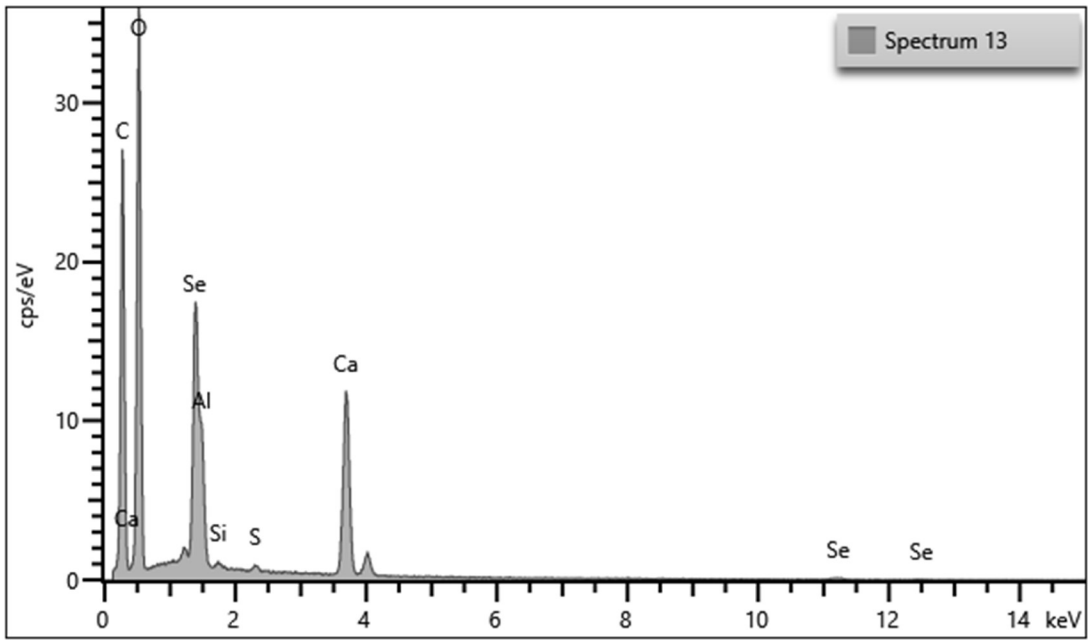

Figure A.1.4: EDS spectrum of a selenate ettringite crystallite (shown in chapter 3 figure 3.7c)

APPENDIX 2: CHAPTER 4 SUPPLEMENTARY INFORMATION

THE STRUCTURE OF TRICALCIUM ALUMINATE (C3A, $Ca_3Al_2O_6$)

Table A.2.1: Comparison of bond lengths refined by PXRD and PND on a sample of C3A

Bond	**PXRD refined length (Å)**	**PND refined length (Å)**
Ca1-O6	2.304 (5) x6	2.348 (6)
Ca2-O5	2.396 (5) x6	2.364 (6)
Ca3-O3	2.361 (6) x3	2.359 (5)
Ca3-O4	2.368 (5) x3	2.359 (6)
Ca4-O1	2.516 (5) x3	2.537 (5)
Ca4-O4	2.503 (6) x3	2.530 (5)
Ca5-O1	2.479 (5)	2.444 (9)
Ca5-O2	2.368 (6)	2.425 (9)
Ca5-O3	2.422 (6)	2.452 (9)
Ca5-O4	2.977 (7)	2.99 (1)
Ca5-O5	2.243 (6) 2.545 (6)	2.268 (9) 2.57 (1)
Ca6-O2	2.465 (6)	2.436 (9)
Ca6-O3	2.336 (6)	2.329 (9)
Ca6-O4	2.244 (6)	2.251 (8)
Ca6-O6 x3	2.268 (6) 2.472 (6) 2.772 (6)	2.285 (8) 2.485 (9) 2.762 (8)
Al1-O1	1.717 (8)	1.71 (1)
Al1-O2	1.786 (8)	1.78 (1)
Al1-O5	1.795 (6)	1.76 (1)
Al1-O6	1.795 (6)	1.74 (1)
Al2-O1	1.749 (8)	1.75 (1)
Al2-O2	1.743 (8)	1.75 (1)
Al2-O3	1.725 (7)	1.73 (1)
Al2-O4	1.800 (6)	1.81 (1)

Table A.2.2: ICP-OES data analysis for the solid samples collected at various time points during the experiment "0.2 M K_2CrO_4"

Time	Ca concentration (mM)	Al concentration (mM)	Cr concentration (mM)	% Ca	% Al	% Cr
1 hour	18.839	13.131	0.390	58.2	40.6	1.2
3 hours	17.833	11.801	0.920	58.4	38.6	3.0
6 hours	15.854	9.880	1.605	58.0	36.1	5.9
24 hours	9.440	5.086	1.905	57.5	31.0	11.5
1 week	10.819	5.643	3.241	54.9	28.6	16.5
1 month	10.105	5.027	3.478	54.3	27.0	18.7

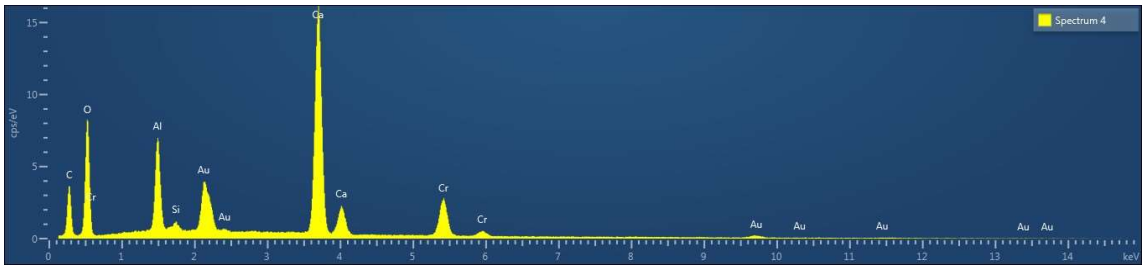

Figure A.2.1: EDS spectrum of red box on Figure 4.10 a)

Figure A.2.2: EDS spectrum of green box on Figure 4.10 a)

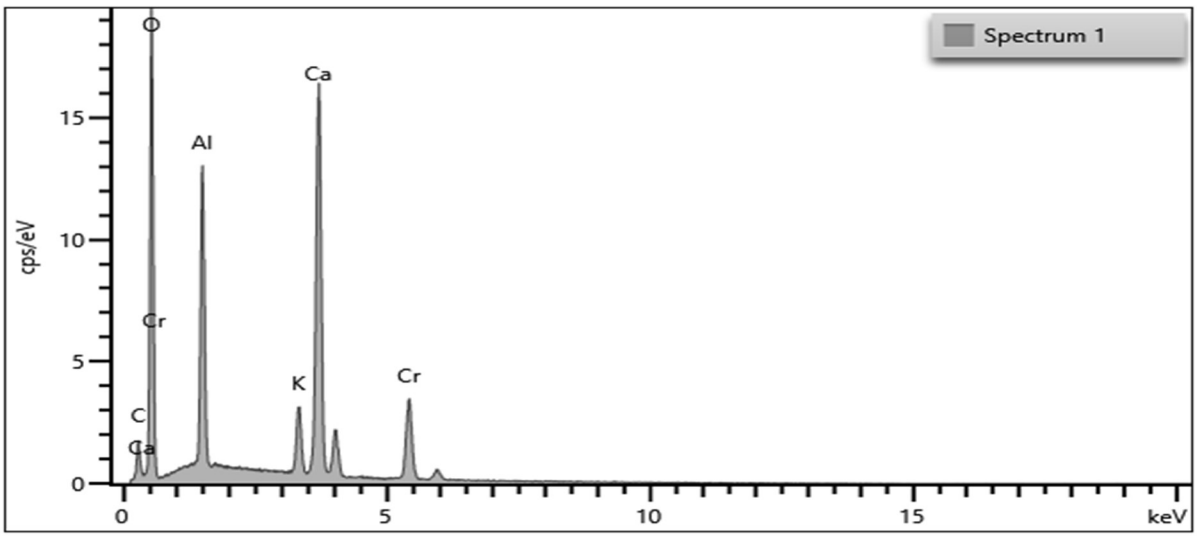

Figure A.2.3: EDS spectrum from Figure 4.10 b)

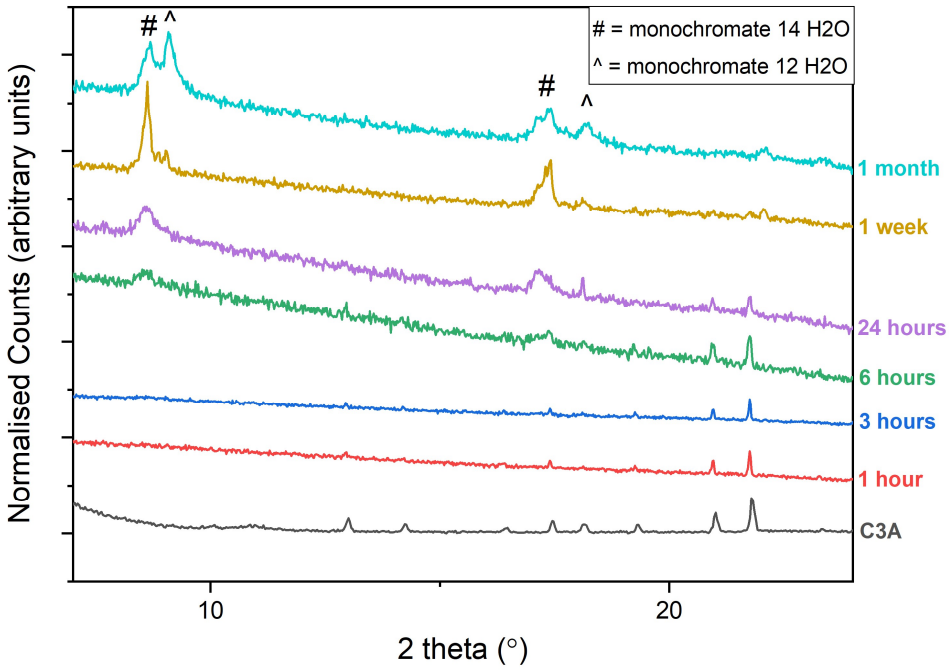

Figure A.2.4: Powder X-ray diffraction patterns of the solid samples collected at various time points during the experiment "0.1 M K_2CrO_4" (data collected on laboratory Bruker D8, λ = 1.5406 Å)

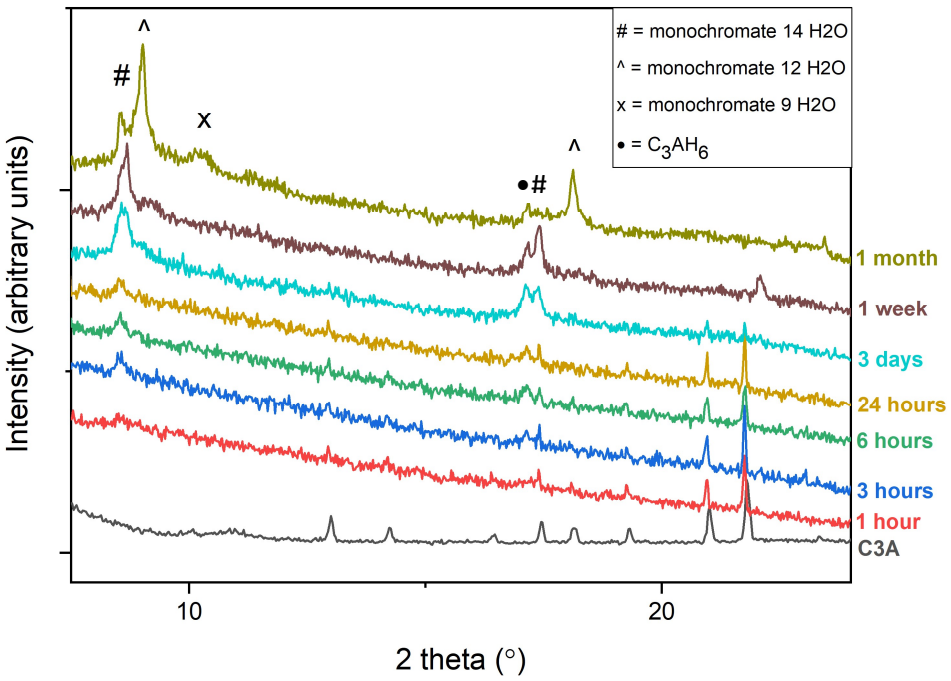

Figure A.2.5: Powder X-ray diffraction patterns of the solid samples collected at various time points during the experiment "0.02 M K_2CrO_4" (data collected on laboratory Bruker D8, λ = 1.5406 Å)

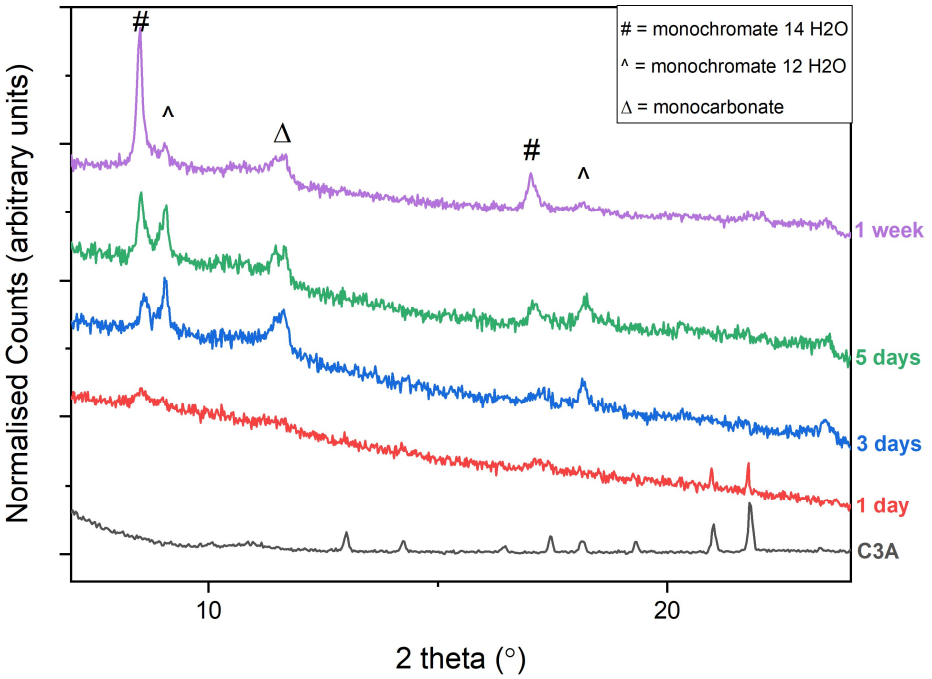

Figure A.2.6: Powder X-ray diffraction patterns of the solid samples collected at various time points during the experiment "0.01 M K_2CrO_4" (data collected on laboratory Bruker D8, λ = 1.5406 Å)

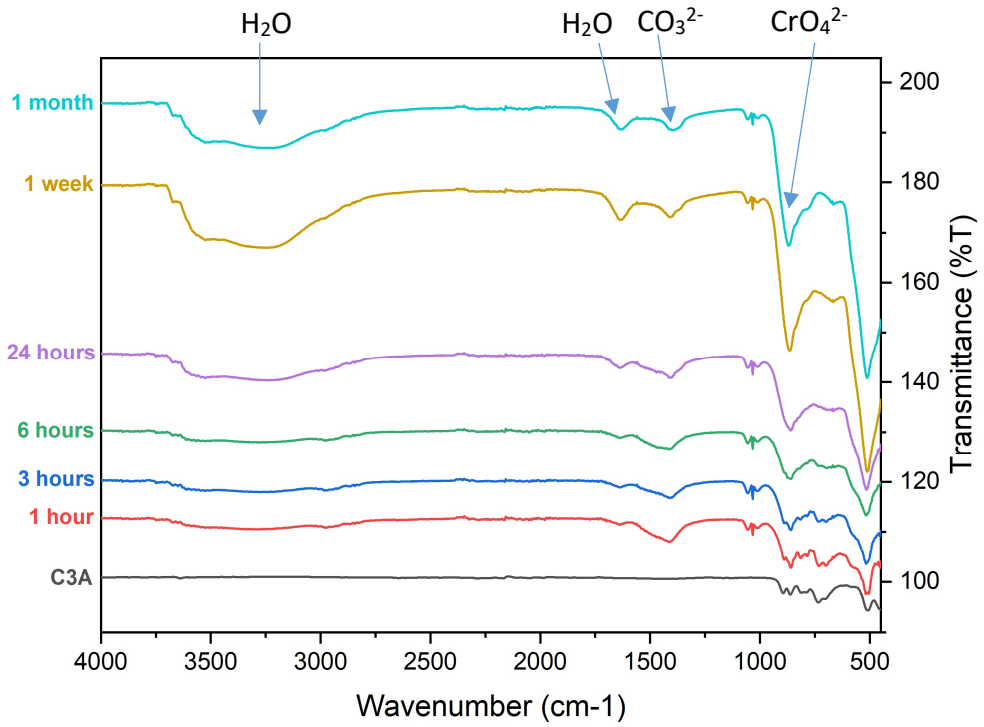

Figure A.2.7: FTIR spectra of the solid samples collected at various time points during the experiment "0.1 M K_2CrO_4", with bands for key functional groups indicated by arrows and labels

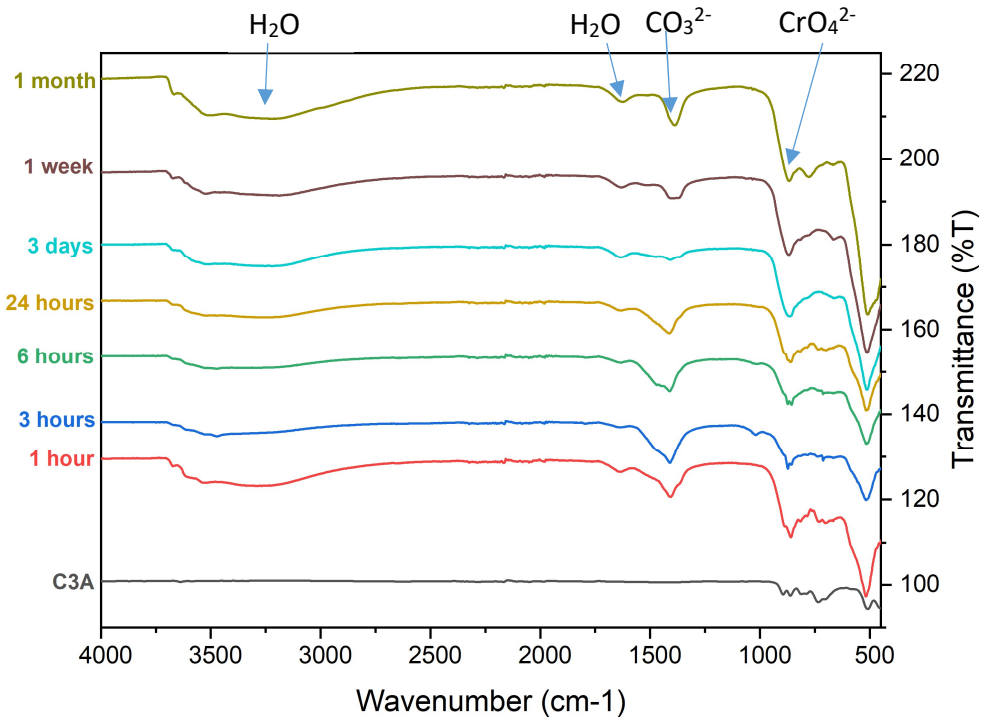

Figure A.2.8: FTIR spectra of the solid samples collected at various time points during the experiment "0.02 M K_2CrO_4", with bands for key functional groups indicated by arrows and labels

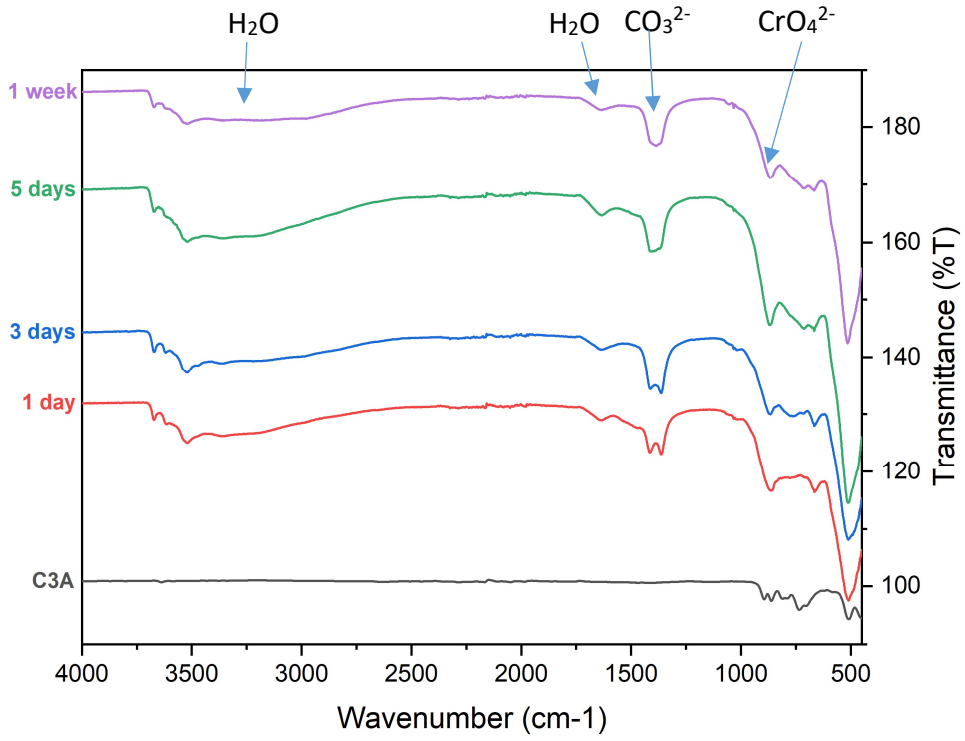

Figure A.2.9: FTIR spectra of the solid samples collected at various time points during the experiment "0.01 M K_2CrO_4", with bands for key functional groups indicated by arrows and labels

Table A.2.3: ICP-OES data analysis for the solid samples collected at various time points during the experiment "0.1 M K_2CrO_4"

Time	Ca concentration (mM)	Al concentration (mM)	Cr concentration (mM)	% Ca	% Al	% Cr
1 hour	18.405	12.593	0.470	58.5	40.0	1.5
3 hours	17.867	11.827	0.644	58.9	39.0	2.1
6 hours	17.356	11.069	1.000	59.0	37.6	3.4
24 hours	13.816	8.715	1.563	57.3	36.2	6.5
1 week	12.0122	6.682	2.422	56.9	31.6	11.5
1 month	11.0143	5.584	2.802	56.8	28.8	14.4

Table A.2.4: ICP-OES data analysis for the solid samples collected at various time points during the experiment "0.02 M K_2CrO_4"

Time	Ca concentration (mM)	Al concentration (mM)	Cr concentration (mM)	% Ca	% Al	% Cr
1 hour	16.614	10.961	0.952	58.2	38.4	3.4
3 hours	16.992	11.189	1.000	58.2	38.3	3.5
6 hours	16.504	10.605	0.887	59.0	37.9	3.1
24 hours	17.464	10.932	1.047	59.3	37.1	3.6
3 days	14.572	8.564	2.071	57.8	34.0	8.2
1 week	11.284	6.478	2.141	56.7	32.5	10.8
1 month	10.807	6.438	2.152	55.7	33.2	11.1

Table A.2.5: ICP-OES data analysis for the solid samples collected at various time points during the experiment "0.01 M K_2CrO_4"

Time	Ca concentration (mM)	Al concentration (mM)	Cr concentration (mM)	% Ca	% Al	% Cr
1 day	13.396	8.705	1.230	57.4	37.3	5.3
3 days	12.548	8.302	1.288	56.7	37.5	5.8
5 days	10.705	7.389	1.141	55.7	38.4	5.9
1 week	10.097	6.974	1.024	55.8	38.5	5.7

Table A.2.6: ICP-OES data analysis for the solid samples collected at various time points during the experiment "0.2 M Na_2SeO_4"

Time	Ca concentration (mM)	Al concentration (mM)	Se concentration (mM)	% Ca	% Al	% Se
1 hour	21.155	13.958	0.530	59.4	39.2	1.4
3 hours	17.999	10.799	1.469	59.5	35.7	4.8
6 hours	15.943	9.235	2.102	58.4	33.9	7.7
24 hours	12.036	5.969	2.996	57.3	28.4	14.3
1 week	10.372	5.043	3.263	55.5	27.0	17.5
1 month	13.936	6.656	4.240	56.1	26.8	17.1

Figure A.2.10: EDS spectrum of red box on Figure 4.20 a)

Figure A.2.11: EDS spectrum of green box on Figure 4.20 a)

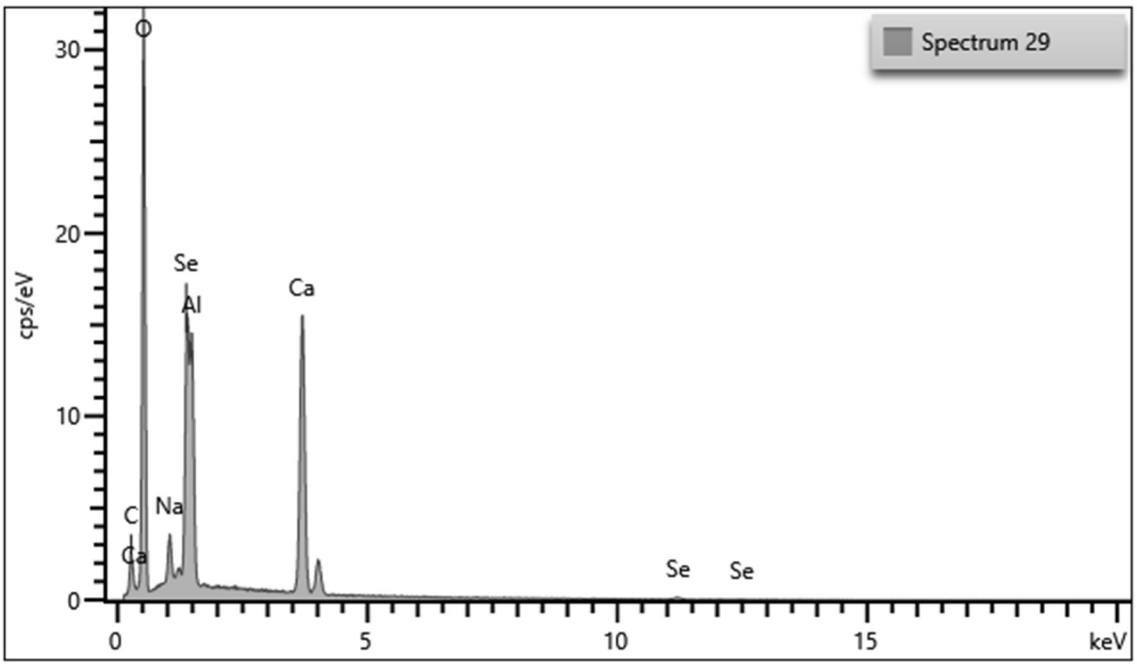

Figure A.2.12: EDS spectrum of Figure 4.20 b)

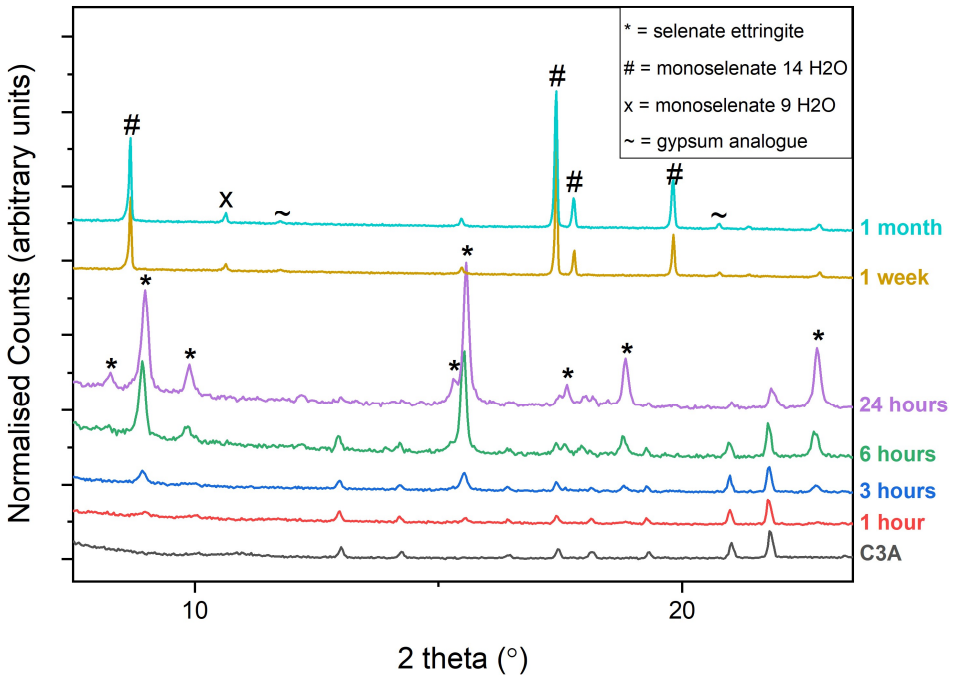

Figure A.2.13: Powder X-ray diffraction patterns of the solid samples collected at various time points during the experiment "0.1 M Na_2SeO_4" (data collected on laboratory Bruker D8, λ = 1.5406 Å)

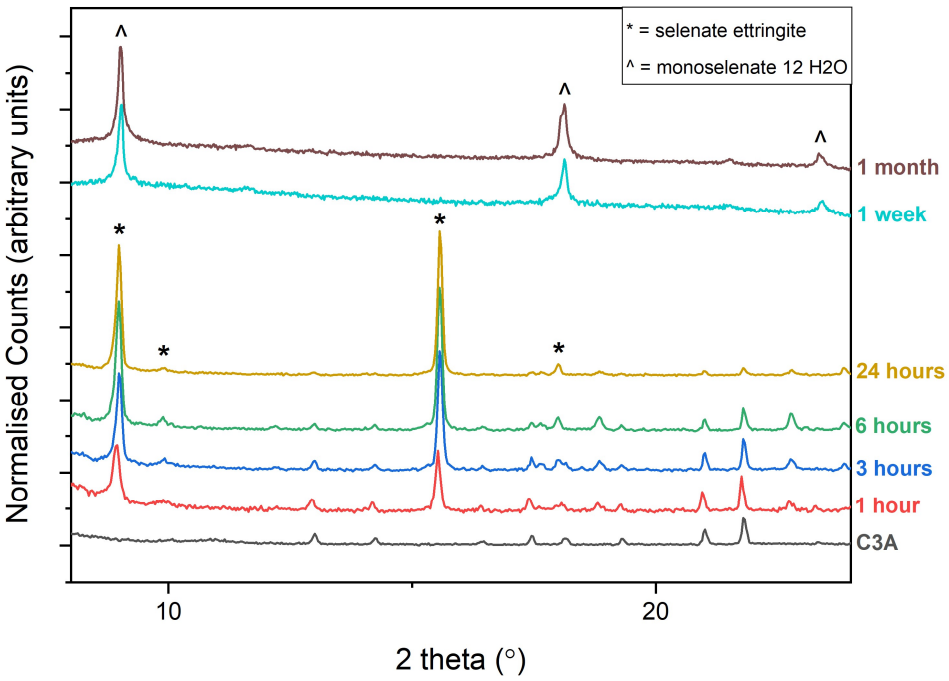

Figure A.2.14: Powder X-ray diffraction patterns of the solid samples collected at various time points during the experiment "0.02 M Na_2SeO_4" (data collected on laboratory Bruker D8, λ = 1.5406 Å)

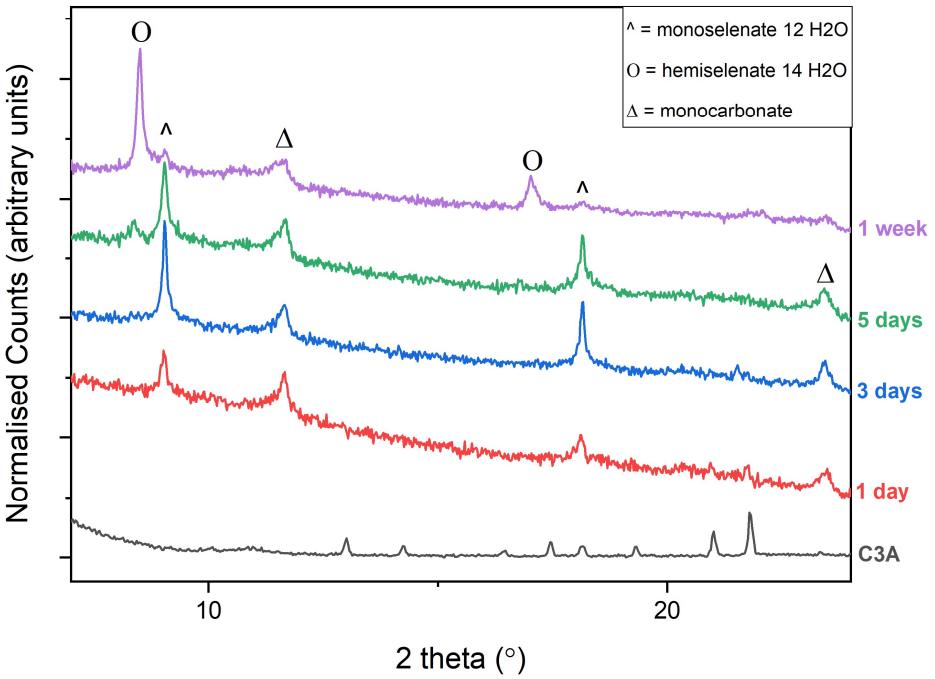

Figure A.2.15: Powder X-ray diffraction patterns of the solid samples collected at various time points during the experiment "0.01 M Na_2SeO_4" (data collected on laboratory Bruker D8, λ = 1.5406 Å)

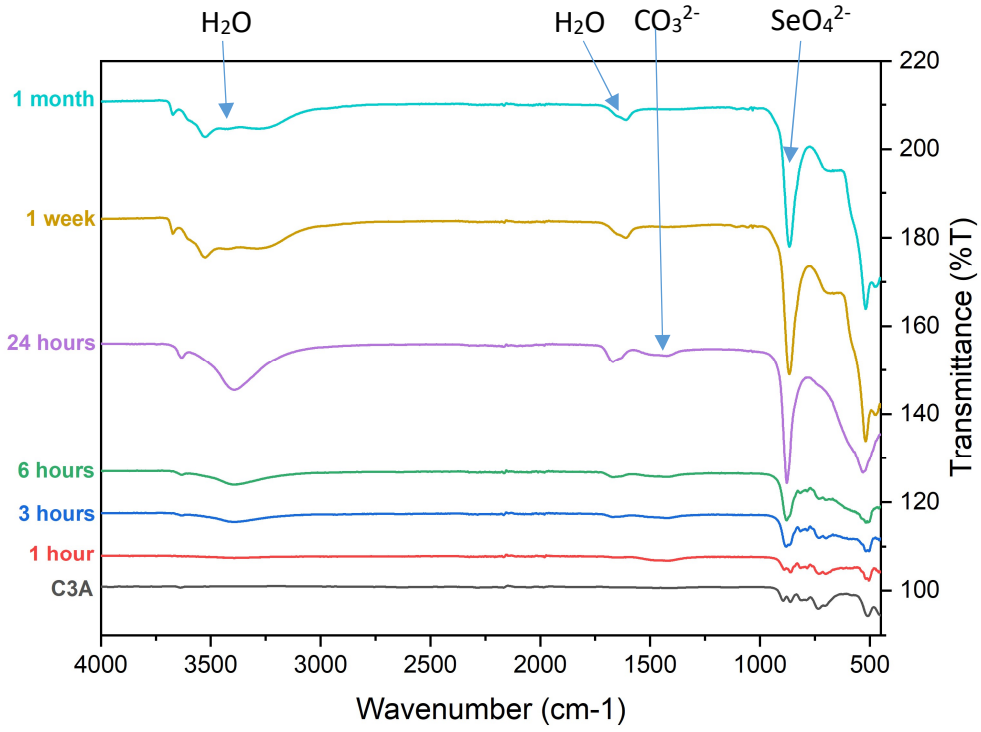

Figure A.2.16: FTIR spectra of the solid samples collected at various time points during the experiment "0.1 M Na_2SeO_4", with bands for key functional groups indicated by arrows and labels

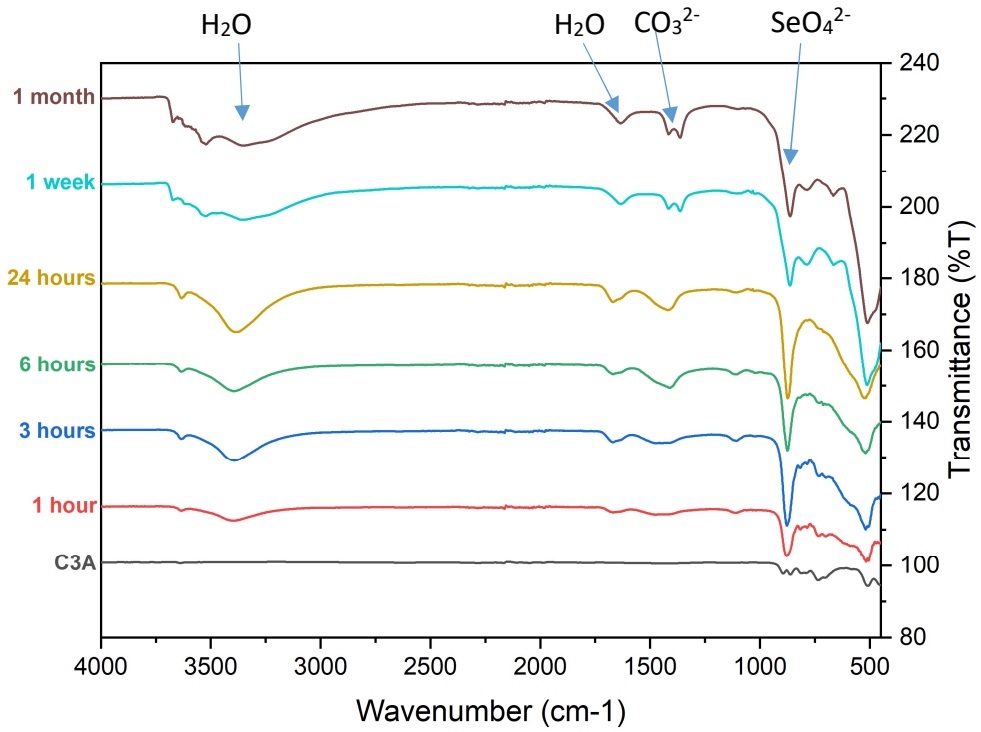

Figure A.2.17: FTIR spectra of the solid samples collected at various time points during the experiment "0.02 M Na_2SeO_4", with bands for key functional groups indicated by arrows and labels

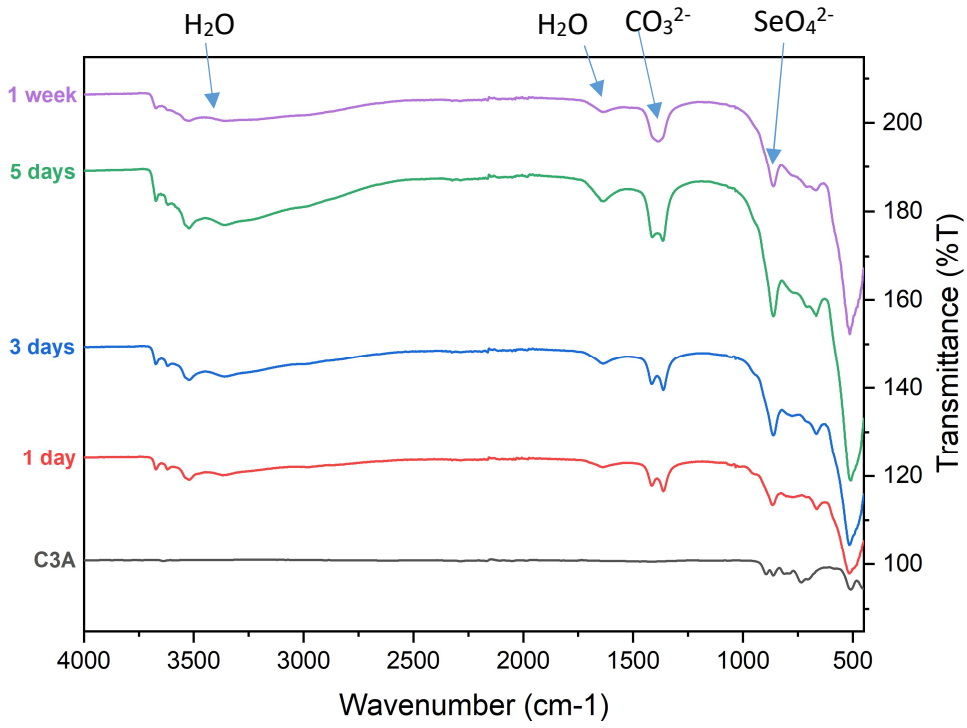

Figure A.2.18: FTIR spectra of the solid samples collected at various time points during the experiment "0.01 M Na_2SeO_4", with bands for key functional groups indicated by arrows and labels

Table A.2.7: ICP-OES data analysis for the solid samples collected at various time points during the experiment "0.1 M Na_2SeO_4"

Time	Ca concentration (mM)	Al concentration (mM)	Se concentration (mM)	% Ca	% Al	% Se
1 hour	20.996	14.222	0.221	59.2	40.1	0.7
3 hours	20.747	12.986	0.506	60.6	37.9	1.5
6 hours	16.366	9.629	0.749	61.2	36.0	2.8
24 hours	11.859	5.929	2.714	57.8	28.9	13.3
1 week	11.024	5.557	3.288	55.5	28.0	16.5
1 month	11.125	5.377	3.544	55.5	26.8	17.7

Table A.2.8: ICP-OES data analysis for the solid samples collected at various time points during the experiment "0.02 M Na_2SeO_4"

Time	Ca concentration (mM)	Al concentration (mM)	Se concentration (mM)	% Ca	% Al	% Se
1 hour	19.602	12.673	0.690	59.5	38.4	2.1
3 hours	18.536	11.752	0.974	59.3	37.6	3.1
6 hours	15.852	9.061	1.049	61.1	34.9	4.0
24 hours	20.756	11.531	2.139	60.3	33.5	6.2
1 week	15.458	8.308	2.716	58.4	31.4	10.2
1 month	12.012	6.628	2.164	57.7	31.9	10.4

Table A.2.9: ICP-OES data analysis for the solid samples collected at various time points during the experiment "0.01 M Na_2SeO_4"

Time	Ca concentration (mM)	Al concentration (mM)	Se concentration (mM)	% Ca	% Al	% Se
1 day	13.733	8.868	1.065	58.0	37.5	4.5
3 days	12.697	8.197	1.279	57.3	36.9	5.8
5 days	12.920	8.249	1.246	57.6	36.8	5.6
1 week	11.965	7.875	1.134	57.0	37.5	5.5

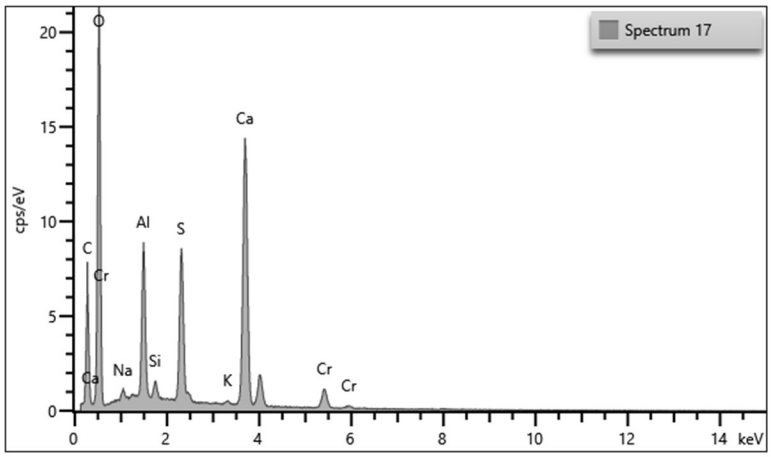

Figure A.3.1: EDS spectrum for Figure 5.17 a)

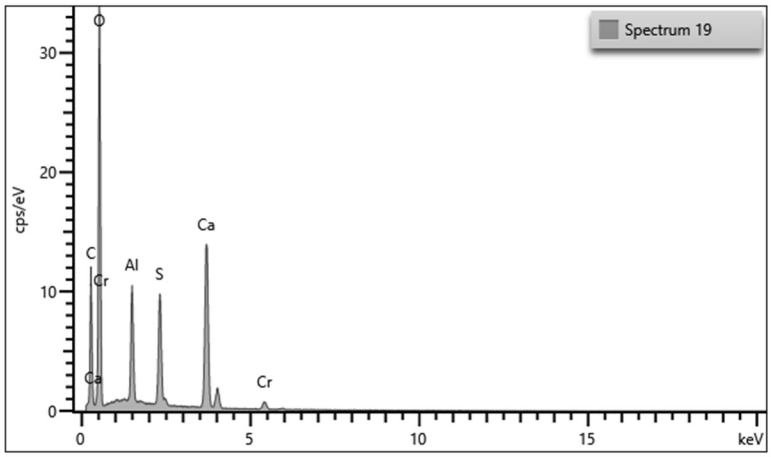

Figure A.3.2: EDS spectrum for Figure 5.17 b)

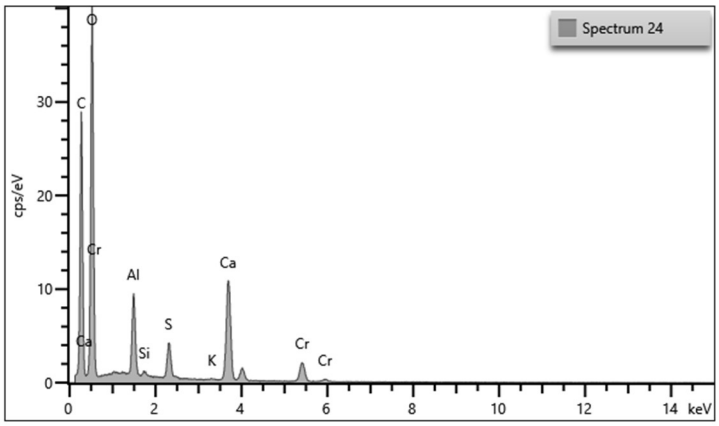

Figure A.3.3: EDS spectrum for Figure 5.18 a)

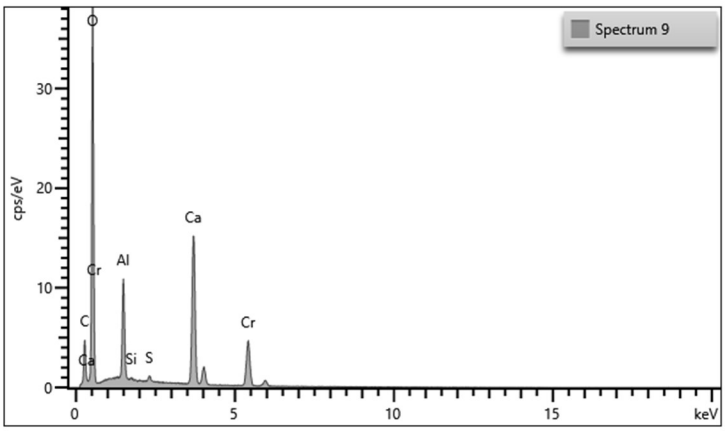

Figure A.3.4: EDS spectrum for the ends of the crystallites from Figure 5.18 b)

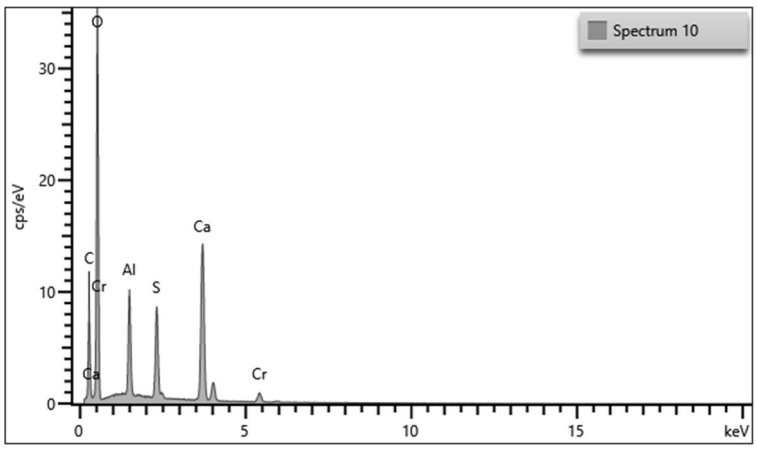

Figure A.3.5: EDS spectrum for the centres of the crystallites from Figure 5.18 b)

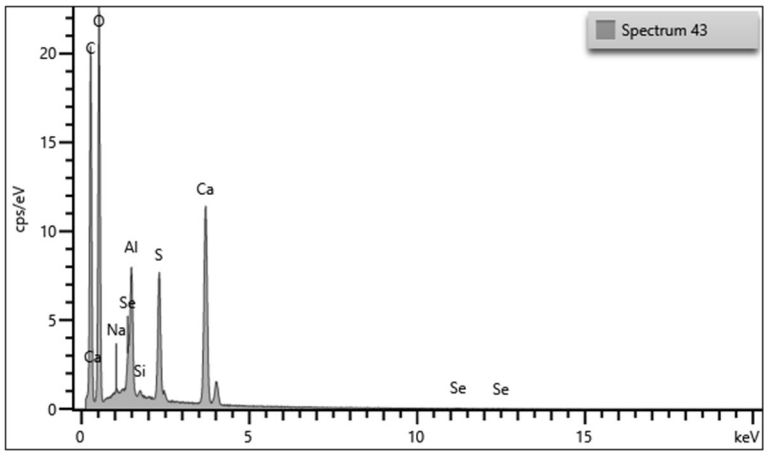

Figure A.3.6: EDS spectrum for Figure 5.30 a)

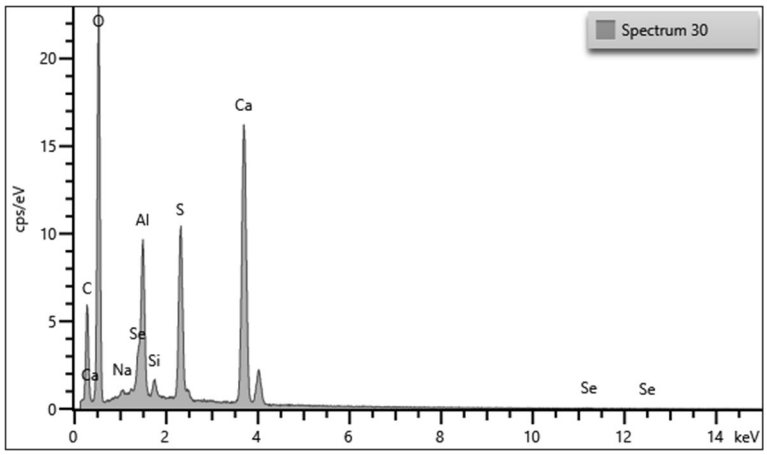

Figure A.3.7: EDS spectrum for Figure 5.30 b)

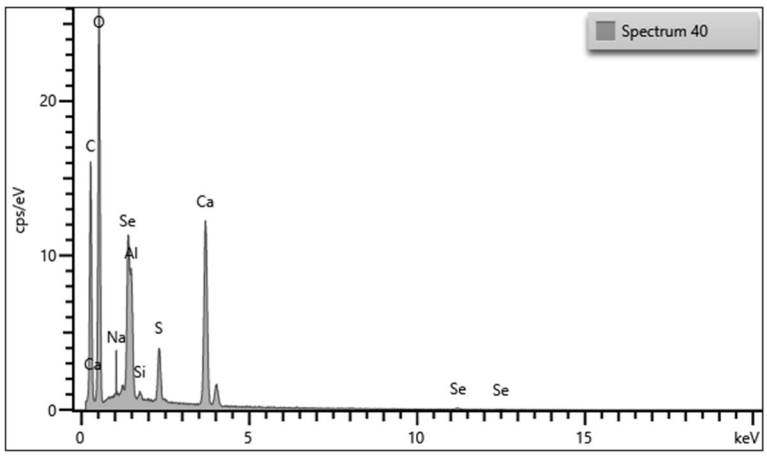

Figure A.3.8: EDS spectrum for Figure 5.31 a)

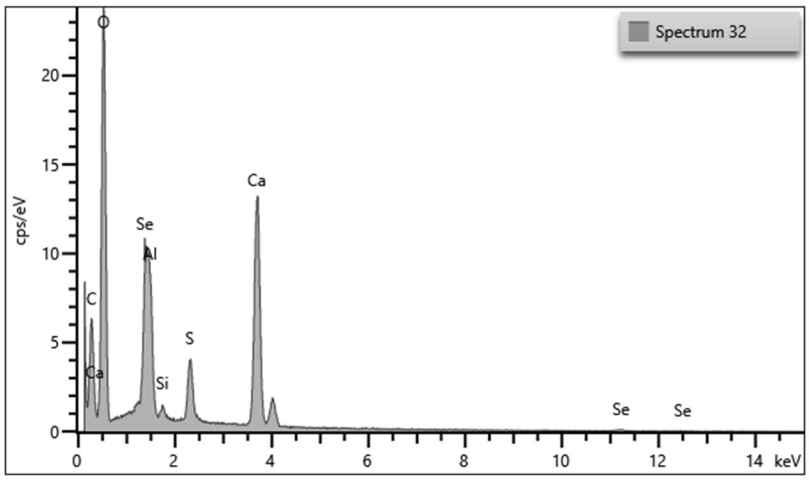

Figure A.3.9: EDS spectrum for Figure 5.31 b)

APPENDIX 4: CHAPTER 6 SUPPLEMENTARY INFORMATION

Table A.4.1: Table of calculated bond lengths for the aluminium-gallium ettringite solid solution

Bond Length (Å)	Al_0Ga_1	$Al_{0.25}Ga_{0.75}$	$Al_{0.5}Ga_{0.5}$	$Al_{0.75}Ga_{0.25}$	Al_1Ga_0
Al1-O1 (x3)	1.98	1.99	1.96	1.93	1.95
Al1-O2 (x3)	1.95	1.89	2.00	1.98	1.85
Al2-O3 (x3)	1.97	1.96	1.95	1.90	2.02
Al2-O4 (x3)	1.96	1.99	1.83	1.87	1.81
Ca1-O1:1	2.41	2.43	2.44	2.36	2.45
Ca1-O1:2	2.50	2.47	2.53	2.48	2.46
Ca1-O3:2	2.49	2.47	2.40	2.35	2.37
Ca1-O3:1	2.42	2.55	2.49	2.47	2.51
Ca1-O6	2.42	2.30	2.44	2.47	2.49
Ca1-O8	2.52	2.73	2.61	2.61	2.40
Ca1-O10	2.46	2.69	2.69	2.70	2.56
Ca1-O12	2.69	2.84	2.81	2.82	2.53
Ca2-O2:1	2.36	2.44	2.40	2.45	2.47
Ca2-O2:2	2.47	2.49	2.50	2.48	2.47
Ca2-O4:1	2.51	2.36	2.41	2.48	2.44
Ca2-O4:2	2.47	2.38	2.39	2.45	2.46
Ca2-O5	2.28	2.38	2.28	2.31	2.58
Ca2-O7	2.63	2.55	2.62	2.58	2.45
Ca2-O9	2.75	2.55	2.55	2.53	2.71
Ca2-O11	2.71	2.64	2.63	2.63	2.76
S1-O13	1.49	1.62	1.58	1.63	1.70
S1-O16 (x3)	1.54	1.53	1.46	1.48	1.56
S2-O14	1.42	1.41	1.38	1.63	1.43
S2-O17 (x3)	1.67	1.73	1.75	1.63	1.84
S3-O15	1.58	1.33	1.38	1.51	1.68
S3-O19 (x3)	1.51	1.65	1.66	1.58	1.41